Wireline Communications in a Wireless World

Yezi Huang

LUND UNIVERSITY

Yezi Huang
Department of Electrical and Information Technology
Lund University
Box 118, SE-221 00 LUND
SWEDEN

To my family ♡

Abstract

The whole society is digitalizing, filled with streaming services, cloud computing and an ambition of ubiquitous connectivity. To address the data demand, ultra-fast broadband, at the speeds of 1 Gbps and more, is developed and deployed. Optical fibers have been long viewed as a future-proof carrier for the ultra-fast broadband. However, the physical deployment of fiber networks, including digging, burying, rewiring, drilling, etc., is still an expensive and disruptive process. The economic concern repeatedly defers the delivery of end-to-end fiber connections to every premise while the 5G development cannot wait any longer. This dilemma motivates the industry to use the readily in-place copper-based network to deliver the last-mile communication which is the most expensive segment for fiber roll-outs. The challenge is: are the copper cables capable of offering a fiber-like experience?

This thesis supports the answer: Yes. Focusing on the network side, where centralized cooperative processing is available, the potential of copper networks is explored in three subparts: evolution, maintenance and extension.

The first subpart, devoted to digital subscriber line (DSL) evolution, continues extracting available resources to increase network capacity. The main concept of the fourth generation broadband (4GBB) is to further broaden bandwidth over shorter cables for loading more data. However, its effectiveness gets saturated after around 200 MHz due to severe data channel attenuation and strong interference level. To cut this Gordian knot, a new precoding scheme combining beamforming and crosstalk mitigation is presented, improving the bit-loading capability at high frequencies via constructive crosstalk from adjacent twisted pairs.

The second subpart addresses a newly observed disruption of the evolved broadband network to maintain the stability of services. The disruption, caused by sudden termination changes at user premises, significantly degrades performances at high frequencies, which are the key for the DSL evolution. A low-cost precoder updating procedure is proposed and applied to two types of common-used precoders. It enables quick retrieving of the normal opera-

tion state without the end-users experiencing any impairment on the quality of service.

The third subpart extends the application from providing fixed access to fronthauling 4G and 5G mobile networks. In order to coordinate power and spectrum usage, the mobile network has its baseband units (BBUs) centralized, while pushing the radio units (RUs) closer to end-users with fronthaul links connected in between. Those links are then normally served by the fixed access network. In this regard, this thesis firstly sketches and analyzes the feasibility of an LTE-over-copper system considering the crosstalk issue. When it comes to 5G where the number of antennas scales up to be "massive", strategies of beneficial functional split are discussed to lessen the dramatically growing traffic on the fronthaul links.

Preface

This doctorate dissertation is comprised of two parts. The first part gives an overview of the research field in which I have been working during my Ph.D. studies and a brief summary of my contributions to it. The second part is composed of the following published or submitted journal papers, technical report, and conference contributions:

I. Yezi Huang, Thomas Magesacher, Eduardo Medeiros, Chenguang Lu, Per-Erik Eriksson, and Per Ödling, "Rate-Boosting Using Strong Crosstalk in Next Generation Wireline Systems," in *Proc. 2015 IEEE Global Communications Conference (GLOBECOM)*, San Diego, CA, December 2015, pp. 1-6.

II. Yezi Huang, Anas F. Al Rawi, Thomas Magesacher, and Per Ödling, "Rate-Boosting via Beamforming for Multi-Pair Copper Channels," *Technical Report*, June 2017.

III. Yezi Huang, Thomas Magesacher, Eduardo Medeiros, Chenguang Lu, Per-Erik Eriksson, and Per Ödling, "Mitigating Disorderly Leaving Events in G.fast," in *Proc. 2015 IEEE International Conference on Communications (ICC)*, London, U.K., June 2015, pp. 939-944.

IV. Yezi Huang, Thomas Magesacher, Chenguang Lu and Per Ödling, "Fast Mitigation of Sudden Termination Changes in Wideband Wireline Systems," in *IEEE Transactions on Communications*, vol. 64, no. 6, pp. 2610-2621, June 2016.

V. Eduardo Medeiros, Yezi Huang, Thomas Magesacher, Stefan Höst, Per-Erik Eriksson, Chenguang Lu, Per Ödling, and Per Ola Börjesson, "Crosstalk Mitigation for LTE-Over-Copper in Downlink Direction," in *IEEE Communications Letters*, vol. 20, no. 7, pp. 1425-1428, July 2016.

VI. Yezi Huang, Eduardo Medeiros, Thomas Magesacher, Stefan Höst, Chenguang Lu, Per-Erik Eriksson, Per Ödling, and Per Ola Börjesson, "Time-Domain Precoding for LTE-over-Copper Systems," in *Proc. 2016 IEEE International Conference on Communications (ICC)*, Kuala Lumpur, Malaysia, pp. 1-6.

VII. Yezi Huang, Chenguang Lu, Miguel Berg, and Per Ödling, "Functional Split of Zero-Forcing Based Massive MIMO for Fronthaul Load Reduction," submitted to *IEEE Transactions on Wireless Communications*, 2017.

Paper III and Paper V include the corresponding patent applications:

[A] Yezi Huang, Thomas Magesacher, Eduardo Medeiros, Chenguang Lu, and Per-Erik Eriksson, "Method and Arrangement in a DSL Vectoring System," *Patent application*, US15509210, filed 30 September 2014, US20170250731A1, publication date 31 August 2017.

[B] Eduardo Medeiros, Per-Erik Eriksson, Yezi Huang, and Chenguang Lu, "Methods and Nodes of a Wireless Communication Network for Mitigating Crosstalk in a Base Station System," *Patent application*, PCT/EP2015/052888, filed 11 February 2015, WO2016128045A1, publication date 18 August 2016.

During my Ph.D. studies, I have also (co)authored the following conference contributions and patent applications, which are related to but not included in the thesis:

VIII. Yezi Huang, Eduardo Medeiros, Stefan Höst, Thomas Magesacher, Per-Erik Eriksson, Chenguang Lu, Per Ödling, and Per Ola Börjesson, "Enabling DSL and Radio on the Same Copper Pair," in *Proc. 2015 IEEE International Conference on Communications (ICC)*, London, U.K., June 2015, pp. 1031-1035.

IX. Yezi Huang, Eduardo Medeiros, Nilma Fonseca, Stefan Höst, Thomas Magesacher, Per-Erik Eriksson, Chenguang Lu, Per Ödling, and Per Ola Börjesson, "LTE over Copper – Potential and Limitations," in *Proc. IEEE 26th Annual International Symposium on Personal, Indoor and Mobile Radio Communications (PIMRC)*, Hong Kong, China, September 2015, pp. 1339-1343.

X.   Chenguang Lu, Yezi Huang, and Miguel Berg, "Methods and Devices for Processing Uplink Signals," *Patent application*, filed June 2017.

Acknowledgements

Before coming to Sweden, I had never thought about adding a doctorate degree to my resume. Shortly after approving my master's thesis, Thomas Magesacher, who later became my Ph.D. supervisor, brought up this possibility of pursuing an academic Ph.D. stationed inside Ericsson. The special combination of academic and industrial competence sounded too exciting to be missed. Four years fly by, and now I am filled with gratitude to all the people that made the decision right. Doing research is fascinating!

My deep gratitude goes first to Thomas who is knowledgable and encouraging. Thomas introduced me to the world of optimization, which became my key to extricate many mazes. Those inspiring discussions, from candidate algorithms to subtle abnormalities in simulation curves, developed me to think actively and work precisely.

I am indebted to my co-supervisor Per Ödling who grants me the privilege to travel around the world, attending, giving presentations and discussing directly with professionals at many international conferences and European project meetings. His authority and charisma attract experts and entrepreneurs from numerous industries, whom are also invited over to the smörgåstårta lunch seminar *Verticals to ICT*. The "exotic" talks largely broaden my vision.

I appreciate Per Ola Börjesson, also my co-supervisor and role model, for generously sharing his expertise. Irrespective of occasions, he always has ideas sparked with a cigar and has problems solved on a tissue—this is what I admire the most.

I am particularly grateful to Henrik Almeida and his team at Ericsson Research. Thanks for the open environment that allows me to work closely with top-notch researchers and projects. I should express my special thanks to Chenguang, Pelle and Miguel for the insights in DSL techniques and 5G designs. Thanks Boris for the patient instructions in the lab, and thanks Neiva, Gemma, Elmar, Daniel, and Patryk for sharing knowledge and information with genuine kindness.

Special thanks are devoted to Jochen Maes and Björn Landfeldt for the

inspiring discussions during my Licentiate seminar. It is also a great honor to cooperate with Anas Mohsin and Les Humphrey from British Telecom (BT) as well as Lajos Hanzo, Jiankang Zhang and Rong Zhang from University of Southampton. Thanks for sharing thoughts, data, and profound comments to make our cooperation accomplished with fruitful results. I am grateful to Ian Cooper from BT, Rob van den Brink from TNO, Martin Kuipers and Torsten Kunz from ADTRAN, and all the experts in the GOLD consortium. From them, I have kept learning both theoretical and practical perspectives, which develop my research to be more industrially relevant.

My appreciation is also extended to my dear LTH colleagues. I would like to thank my doctoral comrade Eduardo for trekking towards the light at the end of the tunnel together, thank William for collaborating in the Arduino project, and thank Pernilla, Antoni, Adriana and Kaan for always being helping and for encouraging me to speak Swedish. Being the teaching assistant for Stefan and Jens were great experiences—thanks for the tutoring and trust. Since I am mostly working from Stockholm, those 200 trips between Stockholm and Lund as well as the special working needs would not have been possible without the administrative assistance from Pia Bruhn and Anne Andersson. Thank you for the time and great patience.

I owe immeasurable gratitude to my parents, who are always caring and supportive. I acknowledge my beloved husband Ruoyang for his understanding and support. Thanks for all the warm and joyful days even in Sweden's Novembers.

Yezi Huang
Stockholm, October 14, 2017

List of Acronyms and Abbreviations

3GPP   third generation partnership project

4GBB   fourth generation broadband

ADSL   asymmetric digital subscriber line

AFE   analog front-end

AoA   angle of arrival

ASIC   application-specific integrated circuitry

ATM   asynchronous transfer mode

AWGN   additive white Gaussian noise

BBU   baseband unit

CDF   cumulative distribution function

CEE   channel estimation error

CIR   channel impulse response

CNR   channel-to-noise power ratio

CO   central office

CP   customer premise

CPE   customer-premises equipment

CPRI   common public radio interface

CPU   central processing unit

C-RAN   centralized radio access network

CRS   cell-specific reference signal

CSI   channel state information

CWDD   column-wise diagonal dominant

DFT   discrete Fourier transform

DLE   disorderly leaving event

DMT   discrete multi-tone modulation

DP   distribution point

DPC   dirty paper coding

DS   direction-selection

DSE   disorderly shutdown event

DSL   digital subscriber line

DSLAM   DSL access multiplexer

DSP   digital signal processor

DTA   dynamic time allocation

EEPROM   electrical erasable programmable read-only memory (ROM)

EGT   equal gain transmission

eoc   embedded operations channel

EVM   error vector magnitude

FDD   frequency-division duplex

FEXT   far-end crosstalk

FFT   fast Fourier transform

FH	fronthaul
FIR	finite impulse response
FRN	FEXT-reflected-NEXT
FTTH	fiber-to-the-home
I/O	input/output
IF	intermediate frequency
IFFT	inverse fast Fourier transform
IIR	infinite impulse response
IQ	in-phase and quadrature
IRS	impulse response shortening
IRU	intermediate radio unit
ISI	inter-symbol interference
ITU	international telecommunication union
ITU-T	telecommunication standardization sector of the international telecommunication union
KKT	Karush-Kuhn-Tucker
LAN	local area network
LMS	least mean square
LoC	LTE-over-copper
LoS	line-of-sight
los	loss of signal
LP	linear precoder
LS	least square
LTE	long term evolution

MIP	mixed integer programming
MMSE	minimum mean square error
MRC	maximum ratio combining
MRT	maximum ratio transmission
MU-MIMO	multi-user MIMO
NEXT	near-end crosstalk
OFDM	orthogonal frequency-division multiplexing
OLE	orderly leaving event
PDSCH	physical downlink shared channel
PLD	programmable logic device
PSD	power spectrum density
QAM	quadrature amplitude modulation
RAM	random-access memory
RB	resource block
RDS	radio dot system
RE	resource element
RF	radio frequency
RFI	radio frequency interference
RH	radio head
RMC	robust management channel
RN	reflected-NEXT
ROC	robust embedded operations channel
ROM	read-only memory
RRH	remote radio head

RRU	remote radio unit
RU	radio unit
RWDD	row-wise diagonally dominant
sEGT	single-selective-destination EGT
SINR	signal-to-interference-and-noise ratio
sMRC	selective MRC
SNR	signal-to-noise ratio
SoC	system-on-a-chip
SSNR	shortening SNR
STC	sudden termination change
SVD	singular value decomposition
TCO	total-cost-of-ownership
TDD	time-division duplex
TDIM	time-division inverse multiplexing
THP	Tomlinson-Harashima precoder
UE	user equipment
ULA	uniform linear array
VCE	vectoring control entity
VDSL	very-high-bit-rate digital subscriber line
VHF	very high frequency
ZF	zero-forcing
ZFP	zero-forcing precoder

Contents

Part I

Overview of the Field of Research

Chapter 1

Introduction

One may have heard the following conversations:

- How to get an ultra-fast broadband connection?

- Pull a fiber to your home.

- How to back up the densified small cells in 5G?

- Pull a load of fibers to the radio heads.

The fiber, short for optical fiber, provides Internet connection by light signals. The transmission provides higher bit rates, on a scale of Gigabits per second (Gbps) in both downlink and uplink, than other connection types over a long hop. Despite of its rate advantage, the long-discussed fiber-to-the-home (FTTH) concept is still far from being a ubiquitous reality. One of the major obstacles lies in the cost, which is not driven by the optic-fiber cables or equipment per se but rather by its installation including trenching, digging, drilling, rewiring, etc. Estimation gives that the fiber installation costs 3 000 to 4 000 US dollars per home on an average which sum up to 4 trillion US dollars globally. This largely limits the availability of fiber-optics, which are usually deployed in densely-populated urban areas. Distant rural areas may not have access to the fiber connections at all. When it comes to fronthauling and backhauling the mobile networks over fiber, expenses are again an obstacle. Just for Europe alone, the new fiber installation for 5G deployment is estimated to be another 400 billion Euros [1].

To cut the cost, copper network operators complement FTTH with a hybrid fiber-copper architecture in which fiber is brought to some intermediate points (*e.g.,* central office (CO), street cabinet or the "last" distribution point (DP))

in the distribution network, and digital subscriber line (DSL) technology is used for the last mile communication [2]. This hybrid deployment makes FTTH more flexible by deferring the cost of rolling out fibers to every premises but still offering an FTTH-like experience to the end-users. This thesis mainly focuses on the analysis and improvement of the copper-based segment of hybrid access networks.

1.1   Overview of DSL Technology

The origin of DSL technology can be tracked back to Alexander Graham Bell's invention of the telephone in 1876 [3], followed by a patent of improvement in 1881 [4] to use shielded twisted copper pairs. Since then, the twisted copper cables have been deployed all around the world. Up to now, there have been 1.3 billion telephone lines installed globally, providing telephony services to almost every business and residential subscriber in most of the world [5]. Although there are other broadband access technologies that serve the same purpose as DSL, none of them reaches the same level of deployment as DSL does.

DSL services are designed to be delivered together with the wired telephone services on the same telephone lines but over different frequency bands. While the transmission of speech occupies the frequencies below 3.4 kHz, the DSL techniques make use of higher frequencies for data transmission. The delivered data rates range from several Mbps to multiple Gbps depending on the applied DSL techniques, operational bandwidth, loop length, cable type, deployment configuration, etc. For instance, the asymmetric digital subscriber line (ADSL) technology [6] appearing in the 1990s provides up to 8 Mbps in the downstream and up to 896 kbps in the upstream direction utilizing frequencies below 1.104 MHz with a loop length of about 2 kilometers. Its evolved version ADSL2plus [7] further explores frequencies up to 2.2 MHz to increase the downstream data rates to 20 Mbps over 1 kilometer. The widely adopted very-high-bit-rate digital subscriber line (VDSL) technology [8,9] explores frequencies up to 35 MHz to provide data rates exceeding 100 Mbps simultaneously in both the upstream and downstream directions as loop length shortens. The emerging G.fast standard [10–12] delivers several Mbps to Gbps throughput with loop-lengths shorter than 500 meters. In 2016, Nokia (previously Alcatel-Lucent) Bell Lab announced their new XG-FAST concept [13] which expands the signal bandwidth up to 500 MHz to deliver 10 Gbps net rates over short distances (*i.e.,* < 100 meters). The latest contribution to the standardization body ITU [14] claims Terabit-speed DSLs by using the *"long-dormant waveguide modes of those existing billion-plus twisted-pair phone lines"*.
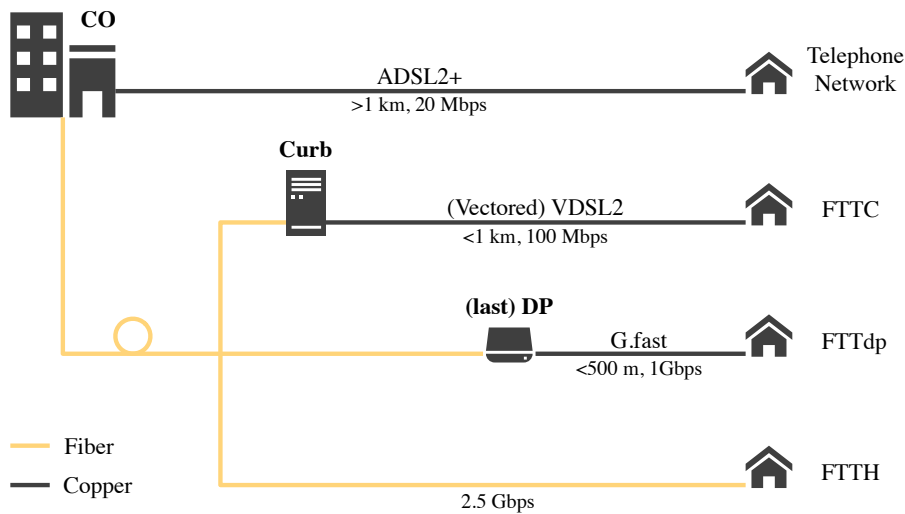
1.2 DSL Development

Fig. 1.1: Examples of the hybrid deployment of fiber and copper cables. The presented data rates are some typical values achieved in downstream direction.

The arising fiber technology drives the network speed up to the Gbps era, but it does not rule out DSL. Built upon the extensively available telephone lines, DSL technologies largely accelerate the roll-outs of ultra-broadband. Over the years, fibers have been gradually pulled closer to the customer premises, and correspondingly the distance served by DSL is reduced, as illustrated in Fig. 1.1, improving the achievable rates since shorter DSL cable length means lower signal attenuation. The latest DSL standard G.fast is able to deliver a fiber-like Internet speed over short loop length while using fiber as backbone network, *i.e.,* the existing copper-based infrastructure complements the fiber network by saving the cost for having fibers in the last mile transmission, which is the most expensive part to deploy. As claimed by Sckipio, an Israeli chipmaker, a single phone company could roll G.fast out to the entire country of United States in four years [15]. As a comparison, the nation-wide fiber coverage in the US just reaches 25% after several years' effort of big providers like Google and Verizon [16]. Additionally, the DSL technology enables ultra-broadband to almost everywhere even for places where installing new fiber cables is difficult or too costly, such as for historical architectures.

In the development of DSL technologies by exploiting broader bandwidth

over shorter loop lengths, however, several aspects need to be taken care of. For example, the channel properties change significantly at high frequencies compared to lower frequencies due to the frequency dependent electromagnetic behaviour. Also, the whole system becomes more sensitive to environmental variations which were not causing troubles when operating at lower frequencies, for example, the channel variation noted in [17−19].

The new use cases to reuse the in-place copper-based infrastructure with DSL techniques in the context of 4G and 5G mobile networks also have great economical benefits. For future cellular networks, centralized radio access network (C-RAN) is proposed to enhance the performance of base-station coordination and reduce the total-cost-of-ownership (TCO). The C-RAN architecture includes two geographically separated units: remote radio unit (RRU) and baseband unit (BBU). The RRUs are located at the network edge to bring the access points closer to the end-users, while BBUs are centralized to benefit from cooperative processing. The fronthaul links, which connect RRUs and BBUs, can be carried by the fixed access networks [21−25]. Using the more readily available telephone lines to complement the fiber connections will assist the mobile network evolution to better comply with its ambitious time plan.

The aforementioned demands and challenges motivate a continuation of exploring the potential of telephone lines and improving the capability of DSL techniques, so as to match the growing needs for fast and ubiquitous connectivity.

1.3   Thesis Structure

This thesis investigates aspects of the fourth generation broadband (4GBB) development itself as well as its potential to serve the next generation mobile networks. Part I introduces the background of the research field, including the conducted channel measurements and channel properties, the most common DSL techniques, the featured MIMO processing, and the specific contribution of this thesis. Part II follows with seven technical papers on the related research findings.

Chapter 2

Wireline Channel

Unlike the wireless channel where the transmission medium is in essence the free-space, the wireline channel is confined to cables, which is less time-variant compared to the wireless environment. The signaling from and to the end-users is supposed to be carried by direct paths along the connecting twisted pairs. Compared to the signal strength, the background noise in the cable is normally low. The dominant impairment of wireline channels is mutual interference, termed crosstalk, due to electromagnetic couplings between adjacent pairs within the same cable binder. The crosstalk is further divided into near-end crosstalk (NEXT) and far-end crosstalk (FEXT), as exemplified in Fig. 2.1, according to the different directions of transmitting and receiving.
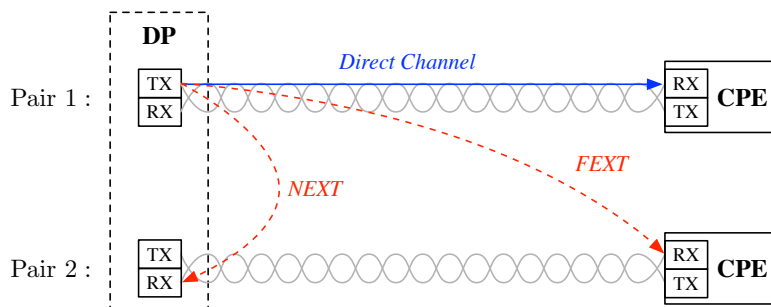

Fig. 2.1: Illustration of the twisted pair channel couplings.

NEXT appears when one pair is transmitting while the neighboring pair is receiving on the same frequency at the same side of a cable. It can be largely suppressed by applying multiplexing techniques, such as frequency-division du-

plex (FDD) or synchronized time-division duplex (TDD), so that the adjacent terminations transmit or receive simultaneously. FEXT happens when one pair is transmitting while the neighboring pair is receiving on the same frequency at the opposite side of a cable. This is the major crosstalk source this thesis will process. Thanks to the co-located transceivers at the operator side (*e.g.,* in the CO or DP), the FEXT can be effectively handled by cooperative MIMO processing, named vectoring [26–28] in the DSL context.

2.1   Channel Measurements

Although there are several empirical cable models available for both direct paths (*i.e.,* insertion loss) and crosstalk paths *e.g.,* [29–35] and the references herein, the studies in this thesis are mostly based on channel measurements of cables in the lab to make more relevant performance evaluations.

This thesis employs two groups of measurement data: one is acquired at Ericsson measuring an Ericsson cable [36] and one at BT (formerly British Telecom) measuring a BT cable.

2.1.1   Measurements at Ericsson

Fig. 2.2 shows the cable measurement setup at the small cell transport lab of Ericsson Research in Stockholm. To measure the insertion loss of a direct path, both ends of a twisted pair are connected to the network analyzer as the input and output, respectively. The network analyzer is set to measure at frequency points within a predefined frequency range separated by a constant tone spacing (*e.g.,* 4.3125 kHz for VDSL2 or 51.75 kHz for G.fast). The complex S_{21} values in frequency domain correspond to the channel coupling coefficients for each frequency point. To measure FEXT, a similar set-up is used except that one end of the source pair and the opposite end of the victim pair are connected to the network analyzer as input and output, respectively. The cable under test is stored on a cable drum. Connector-ports are mounted to go from the cable ends to the switch-port (see Fig. 2.3a) to avoid changing the pair and connected ports manually every time after completing a measurement of a single path. Once the desired frequency range and pair indices are settled, the measurement can run automatically until all channel data is obtained.

Additionally, two connection boards (see Fig. 2.3b) are assembled to simulate different termination behaviors at the cable ends. For example, it is used to simulate the influence of sudden termination changes (STCs) on the perceived showtime channel.

Due to the equipment imperfection and impact from the set-up between
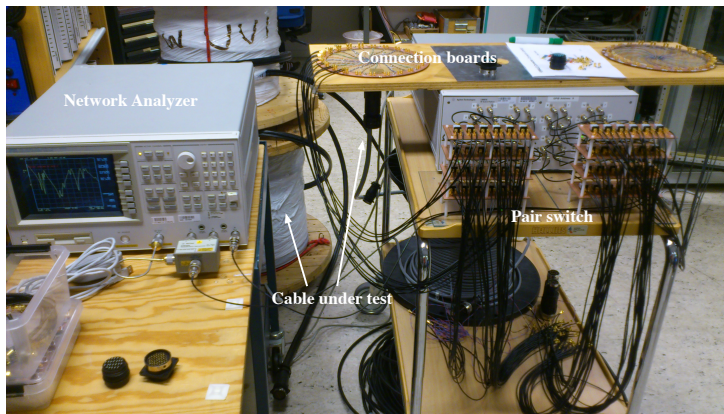
Fig. 2.2: Set-up overview of the measurements conducted at Ericsson.

(a) Switch   **(b)** Connection board (one side)
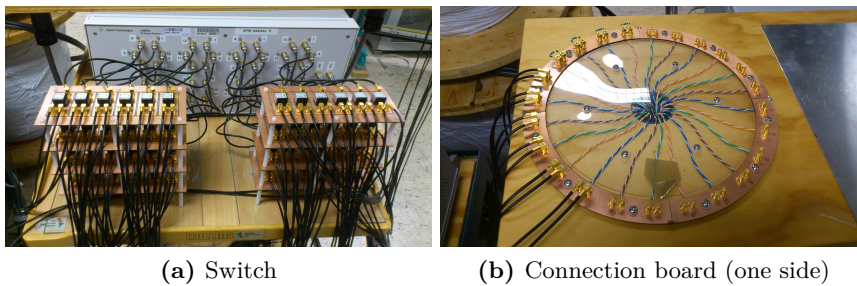
Fig. 2.3: Some more details about the measurement set-up.

the balun close to network interface and the connection boards, systematic errors exist in the cable measurement. The assumption is that those errors are repeatable and time-invariant. Accordingly, calibration is conducted following the regular cable measurements to measure the set-up itself without the cable under test, so as to identify the measurement setup errors. S_{21} and S_{11} parameters at the same frequency points as the cable measurements are measured when the two cable connectors below the connection boards are set to be short/open/load/thru (SOLT method), respectively. The measured data is then used to solve the full 2-port twelve-term error model [37–39], and thereby compensate the measured cable data.
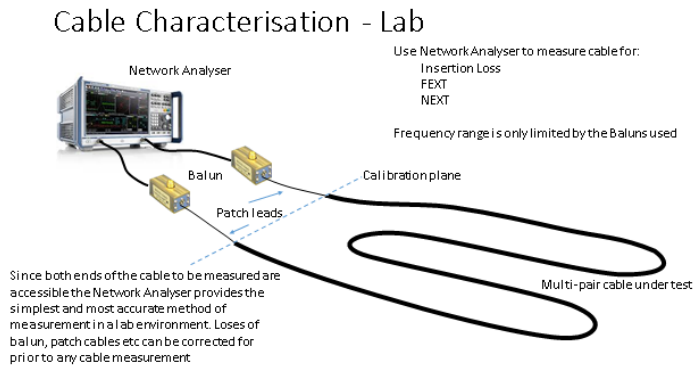
Fig. 2.4: An example of BT's measurement set-up.

2.1.2   Measurements at BT

Fig. 2.4 shows an example of the measurement set-up at BT, which is used to conduct cable measurements in a similar manner to what is described above. There are fewer components between the network analyzer and the cable under test compared to the Ericsson set-up. It requires to change the pair ends manually after each channel path measurement. To reduce possible reflections along the pair and unexpected environmental disturbance, all unconnected ends of the remaining pairs are terminated with 100 Ohm resistors. Baluns are used to match impedances between the 50 Ohm coaxial cables, which connect to the 50 Ohm-input of the network analyzer, and the cables under test with about 100 Ohm characteristic impedance. Calibration is carried out to minimize the influence of the components between network analyzer and the multi-pair cable under test.

Since this set-up is to measure channel behaviors at very high frequencies (*e.g.,* 300 MHz and above), the cable under test is unrolled to avoid potential extra couplings between close-by segments of the cable.

2.2   Wideband Channel Characteristics

One measurement result from the BT set-up is exemplified in Fig. 2.5 in terms of channel coupling strength in dB scale. As summarized in Section 1.1, one of the major differences among various DSL technologies is the operational bandwidth, which is illustrated in Fig. 2.5. The VDSL standard defines several
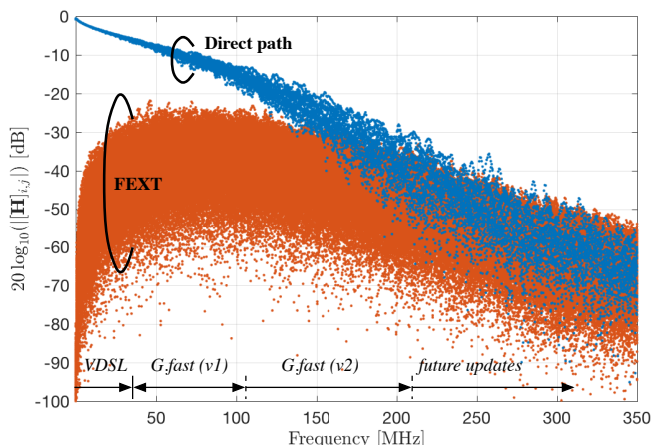
Fig. 2.5: Wideband channel coupling of a measured 50 meters BT cable consisting of 20 pairs of 0.5 mm twisted copper wires.

profiles to make use of different bandwidth regarding different deployment architecture, in which the profile 17a employs bandwidths up to 17 MHz and the latest profile 35b uses up to 35 MHz. The G.fast standard commits to co-exist with ADSL and the various profiles of VDSL standards. Thus, it starts operating beyond the VDSL frequency, and the first version runs up to 106 MHz over shorter loop lengths compared to the VDSL technology. The 212 MHz profile is planned for the second version, with possible higher bandwidth in future updates.

One obvious trend observed in Fig. 2.5 is that the strength difference between the direct and FEXT paths changes along the frequency. This behavior influences the property of the corresponding MIMO channel matrix. Let $\mathbf{H}$ denote an $N \times N$ matrix representing the MIMO channel on one tone (*i.e.,* one frequency point) for an N pair cable binder. The diagonal entry $[\mathbf{H}]_{i,i}$ denotes the direct path for pair i, and the off-diagonal entry $[\mathbf{H}]_{i,j}$ for $i \neq j$ denotes the FEXT from pair j to pair i, where $i, j \in [1, \ldots, N]$. Within the VDSL bandwidth where the direct path is prominently stronger than the FEXT paths, the channel matrix on each tone is diagonal-dominant. For G.fast frequencies, the strength difference between direct and FEXT paths reduces gradually. At the high end of the studied spectrum, the FEXT turns out to be as strong as, sometimes even stronger than, the direct couplings. As a result, channel matrices on those frequencies become non-diagonal-dominant, which is ill-conditioned for matrix inversion.

The changed channel property influences the DSL operation in many aspects. For example, it has a strong impact on precoding schemes presented in Chapter 4.

Chapter 3

DSL Aspects

Compared to VDSL2, the emerging G.fast standard improves both speed and reach by combining multiple technologies. This chapter gives a brief overview of the most common techniques for next generation wideband wireline communications. Among them, vectoring is of particular importance to this thesis, and will be further sketched out in the next chapter.

3.1 Duplex

Before G.fast, the legacy DSL technologies have been using frequency-division duplex (FDD) to allocate upstream and downstream signals within the operational bandwidth which is also exemplified in Fig. 2.5. An instance of the VDSL2 17a profile band plan with the regulated power spectrum density (PSD) mask is shown in Fig. 3.1.

   The G.fast standard adopts time-division duplex (TDD). One of the advantages of the TDD scheme is that the channel information obtained in the upstream direction can be exploited for downstream transmission, which facilitates vectoring. Another advantage is that the resource assignment regarding upstream and downstream becomes more flexible compared to the FDD scheme, where the asymmetry of the two transmission directions is fixed based on the allocated bands. For example, a new capability of G.fast deployment termed dynamic time allocation (DTA) allows dynamic adjustment of the connection asymmetry based on the specific application needs. Also, a discontinuous operation can be exploited in the TDD mode to allow a trade-off between rate and power consumption [40].

   In the XG-FAST concept, full-duplex mode is explored to further boost the
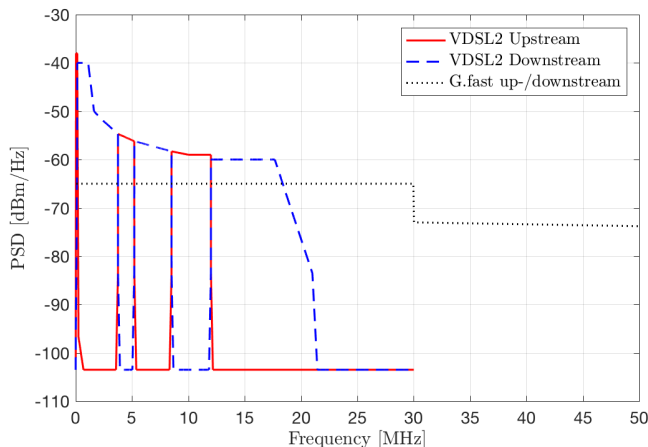
Fig. 3.1: Instance of VDSL2 and G.fast frequency plan. Regarding VDSL2, plan 998ADE17 [8] is shown where the maximum frequency point is at 17.664 MHz. The starting point of G.fast depends on the required coexistence with other DSL services.

throughput [13]. Sine XG-FAST is used as a single-subscriber technology, simultaneous upstream and downstream on the same frequency is feasible without particularly dealing with NEXT between customer-premises equipments (CPEs). In this case, the spectral efficiency is doubled compared to the FDD or TDD counterparts.

3.2 Modulation

The underlying modulation technique of most DSL flavors is discrete multitone modulation (DMT). The DMT frequency carriers are equally spaced and are mutually orthogonal. The corresponding MIMO channel on each tone can therefore be treated independently. In ADSL and VDSL profiles, the tone spacing is defined to be 4.3125 kHz, while G.fast uses 51.75 kHz tone spacing.

To limit the corresponding constellation size, there is a *bit-cap* defined to upper-bound the maximum number of bits that can be loaded on one tone. The VDSL2 standard allows constellations up to 15 bits, whereas the number is reduced to 12 bits in G.fast to keep a manageable implementation complexity.

3.3   Multi-pair Bonding

In some deployment scenarios, additional throughput is required for a given loop length. One option is to connect multiple DSL lines to a single user, across which the data stream is multiplexed and bonded at the receiving end to generate a single pipe with higher rates. In particular, three bonding methods are defined by ITU-T: asynchronous transfer mode (ATM)-based bonding [41], Ethernet-based bonding [42], and time-division inverse multiplexing (TDIM) [43]. When vectoring is implemented, the rate gain is proportional to the number of bonded channels.

3.4   Phantom Mode

Besides the pair-bonding technique which bonds physical DSL lines together, another technique called phantom-mode transmission creates additional virtual pairs between copper pairs [44]. In short, if there are two pairs available connecting to one CPE, they can be viewed as two virtual wires composing the third virtual pair. The two physical pairs operate in differential mode, while the difference between their common-mode signals constitutes the differential signal of the phantom mode. Again, the three data streams are bonded at the receiving CPE, which potentially triples the throughput compared to the single-pair case. Extra hardware elements are required both at the network side and at the CPE side to enable the phantom mode.

3.5   Vectoring

Vectoring is a transmission technique that requires coordination of a group of DSL lines to cancel FEXT, specifically self-FEXT, in downstream and upstream directions [26, 27]. It is particularly beneficial for short cable lengths with relatively strong self-FEXT, given limited NEXT, background noise, and alien noise (*i.e.,* the crosstalk from lines outside the vectored group). The maximum crosstalk-cancellation gain of vectoring is achieved when the cancelling module has access to the channel state information (CSI) of all the pairs that generate crosstalk.

In a vectored system, the vectoring control entity (VCE) of the vectored group acquires and manages the per-tone CSI. Based on this information, a precoder is calculated for the downstream signals or an equalizer is calculated for the upstream signals to compensate the FEXT from the adjacent lines in

the same group. The system keeps on tracking and maintaining the CSI via the pilot sequences carried by the sync symbols to preserve the system performance.

Chapter 4

Precoding

As introduced in Section 3.5, vectoring is used to mitigate FEXT and improve system performance via cooperative processing at the co-located network side. Particularly in the downstream direction, precoding is implemented to transmit both data and anti-crosstalk signals from each pair. At the geographically distributed receivers in CPEs, FEXT is cancelled out by the received anti-crosstalk signals and only the desired data signal is forwarded.

Both linear and non-linear precoding schemes are considered for DSL systems. For some precoding schemes, such as the singular value decomposition (SVD)-based method [45], cooperative decomposition at the remote user side is also required. This thesis only investigates the scenario that cooperative processing operates at the operator side but not at the user side.

In [26], it is shown that a decision-feedback precoding scheme based on the non-linear Tomlinson-Harashima precoder (THP) [46] is theoretically optimum and can achieve a performance close to the single-user bound. It outperforms the lower complexity linear zero-forcing precoder (ZFP) [47], especially at higher frequencies when the channel matrices become non-diagonal-dominant [48]. However, THP has a high run-time complexity and contains a modulo operation, which makes it incompatible with legacy CPEs [49, 50]. Recent studies [18–20] also show that THP is more sensitive to the accuracy of the estimated CSI than ZFP, and therefore does not always perform better than ZFP in practice. To provide fair comparisons, both systems with ZFP and systems with THP are evaluated in this thesis.

4.1 Zero-Forcing Precoder (ZFP)

The linear ZFP $\mathbf{P}_{\text{ZF}}$ diagonalizes the channel matrix $\mathbf{H}$ on each tone as

$$\mathbf{P}_{\text{ZF}} = \mathbf{H}^{-1}\mathbf{H}_{\Sigma},$$

where $\mathbf{H}_{\Sigma}$ denote a diagonal matrix composed by the diagonal entries of $\mathbf{H}$. Let $\sqrt{\mathbf{G}} = \text{diag}([\sqrt{g_1}, ..., \sqrt{g_N}])$ denote a diagonal matrix containing gain-scaling factors that the transmitters assign to each pair on that tone. Let $\mathbf{x}, \mathbf{y}, \mathbf{n} \in \mathbb{C}^{N \times 1}$ denote the transmit and receive signals, as well as the additive background noise, respectively. The signal transmission with ZFP can be formulated as

$$\mathbf{y} = \mathbf{H}\mathbf{P}_{\text{ZF}}\sqrt{\mathbf{G}}\mathbf{x} + \mathbf{n}$$
$$= \mathbf{H}_{\Sigma}\sqrt{\mathbf{G}}\mathbf{x} + \mathbf{n}.$$

Since both $\mathbf{H}_{\Sigma}$ and $\sqrt{\mathbf{G}}$ are diagonal matrices, each element of $\mathbf{y}$ (*i.e.,* the received symbol on each pair) is a scaled version of the corresponding element in $\mathbf{x}$ corrupted by additive white Gaussian noise (AWGN). Thereby, crosstalk-free transmission is achieved, where each CPE receiver does not need to be aware of the existence of other CPEs.

To normalize any possible transmit power increase induced by the precoder $\mathbf{P}_{\text{ZF}}$, [47] proposed to divide the precoder by a scalar defined as

$$\beta = \max_{n} \|[\mathbf{H}^{-1}\mathbf{H}_{\Sigma}]_{\text{row } n}\|,$$

where $\| \cdot \|$ denotes the Euclidean norm. The authors also proved that this linear precoder is near-optimal in the sense of reaching similar performance as THP as long as the channel is row-wise diagonally dominant (RWDD). When the bandwidth extends to the G.fast regime, however, the RWDD condition is no longer fulfilled as described in Chapter 2. This scaling factor in turn causes large penalty to the system performance when ZFP is implemented. In [40, 48, 51], other methods of formulating the scaling factors are proposed to reduce the performance penalty at high frequencies.

4.2 Tomlinson-Harashima Precoder (THP)

The non-linear THP is based on the QR-decomposition of $\mathbf{H}^{\text{H}}$, or equivalently, $\mathbf{H} = \mathbf{R}^{\text{H}}\mathbf{Q}^{\text{H}}$, where $\mathbf{R}$ is an upper-triangular matrix and $\mathbf{Q}$ is a unitary matrix. Let $\mathbf{x}' = \mathbf{Q}\tilde{\mathbf{x}}$ denote the precoded transmit signal, where $\tilde{\mathbf{x}}$ is the output of the

non-linear part of the precoder. The signal transmission with THP is supposed to become crosstalk-free as

$$\mathbf{y} = \mathbf{R}^{\mathrm{H}}\mathbf{Q}^{\mathrm{H}}\mathbf{x}' + \mathbf{n}$$
$$= \mathbf{R}_{\Sigma}^{\mathrm{H}}\sqrt{\mathbf{G}}\mathbf{x} + \mathbf{n},$$

where $\mathbf{R}_{\Sigma}^{\mathrm{H}}$ denotes a diagonal matrix composed by the diagonal entries of $\mathbf{R}^{\mathrm{H}}$. Since $\mathbf{R}^{\mathrm{H}}\mathbf{Q}^{\mathrm{H}}\mathbf{x}' = \mathbf{R}^{\mathrm{H}}\tilde{\mathbf{x}}$, the above derivation implies that

$$\mathbf{R}^{\mathrm{H}}\tilde{\mathbf{x}} = \mathbf{R}_{\Sigma}^{\mathrm{H}}\sqrt{\mathbf{G}}\mathbf{x} \qquad (4.1)$$

or $\tilde{\mathbf{x}} = (\mathbf{R}^{\mathrm{H}})^{-1}\mathbf{R}_{\Sigma}^{\mathrm{H}}\sqrt{\mathbf{G}}\mathbf{x}$. Direct computation of $\tilde{\mathbf{x}}$ based on Eq. (4.1) will result in a significant increase of the transmit power. Therefore, THP implements non-linear modulo arithmetic when calculating $\tilde{\mathbf{x}}$ to fulfil Eq. (4.1) while suppressing the power increase as

$$\tilde{x}_1 = \sqrt{g_1}x_1$$
$$\tilde{x}_2 = \Gamma_{C_2}\left\{\sqrt{g_2}x_2 - \frac{r_{2,1}}{r_{2,2}}\tilde{x}_1\right\}$$
$$\vdots$$
$$\tilde{x}_N = \Gamma_{C_N}\left\{\sqrt{g_N}x_N - \sum_{i=1}^{N-1}\frac{r_{N,i}}{r_{N,N}}\tilde{x}_i\right\},$$

where $r_{k,i}$ is the element on the k-th row and i-th column of $\mathbf{R}^{\mathrm{H}}$, and the modulo operation $\Gamma_{C_i}\{\cdot\}$ is defined for C_i-QAM constellation as

$$\Gamma_{C_i}\{z\} = z - \sqrt{C_i}d_i\left\lfloor\frac{z}{\sqrt{C_i}d_i} + \frac{1}{2} + j\frac{1}{2}\right\rfloor,$$

where d_i is the corresponding spacing between two neighboring constellation points. One example of the modulo operation on a scaled 16-QAM signal $z = 9 + j6$ is illustrated in Fig. 4.1. The "new" constellation after implementing the modulo arithmetic is an integer multiple shift of the original constellation along the real (horizontal) and imaginary (vertical) axes to include the scaled symbol (marked by red-cross) to be within the range of a constellation map.

At the receiver side, the same modulo operation is applied prior to detection as

$$y_k' = \Gamma_{C_k}\left\{\frac{y_k}{r_{k,k}\sqrt{g_k}}\right\}.$$

Although the constellation-based modulo arithmetic of THP bounds the value of the precoded signal, there is still a moderate power increase, which
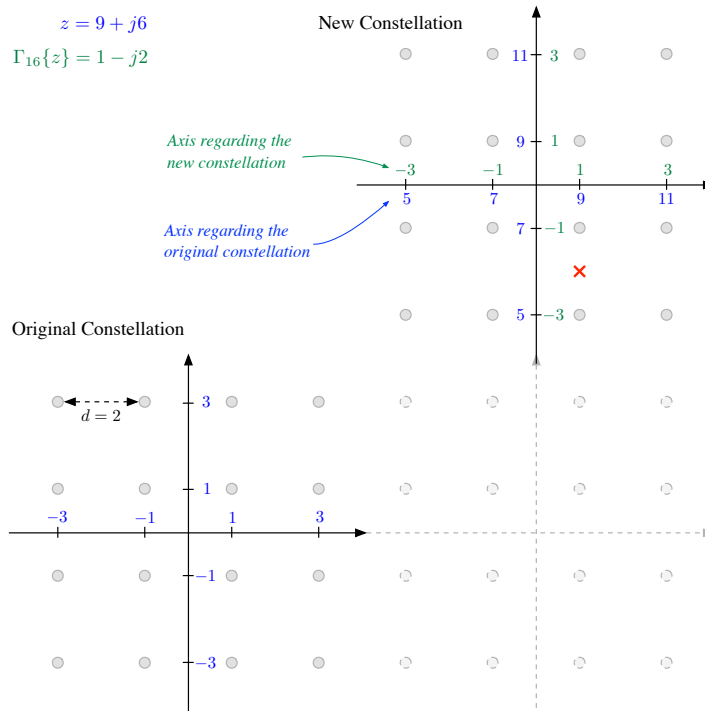
Fig. 4.1: Illustration of signal-power reduction through modulo arithmetic for a 16-QAM constellation. The scaled transmit signal z is marked by a red cross.

varies depending on the applied constellation sizes. This increase is negligible for large constellations, therefore only observed at high frequencies when the bit-loading is low. In [52], the power increase factors are calculated for all relevant QAM constellations.

The implementation of both ZFP and THP requires full knowledge of the frequency-domain channel $\mathbf{H}$ on each tone. In G.fast, for example, sync symbols are used to carry orthogonal sequences, such as Walsh-Hadamard sequences, for channel estimation [27]. When the channel condition, such as topology, temperature, etc., changes, the estimation coefficients should be updated timely to avoid generating residual crosstalk due to the out-dated precoder.

Chapter 5

Research Contributions

The contributions of this thesis are divided into three subparts, where the first two subparts are devoted to the development of 4GBB, and the third subpart focuses on its potential of supporting 4G and 5G mobile networks.

5.1 Rate-Boosting via Strong Crosstalk

The first subpart contributes to an essential and enduring issue in the development of broadband access networks: increasing data rates. The main idea is to use strong FEXT couplings as data channels via beamforming, since now the operational bandwidth of the 4GBB network has been extended so much that the wireline channel bears a certain resemblance to the wireless channel seen in LTE and 5G mobile communication. Regarding my research contribution to this subpart, I am the main author of both papers, conducting derivation, simulation, and results evaluation.

- Paper I designs an additional precoding component to boost data rates for target users. It performs as a complement to the traditional ZFP, and promises great theoretical potential of wireline rate-boosting. Given idle pairs available in a vectored group, there are more transmit ports than active receivers, which yields a channel matrix $\mathbf{H}_{\mathrm{sub}}$ (on one tone) with more columns than rows. The new precoder is thereby formulated as

$$\mathbf{P}_{\mathrm{sub}} = 1/\mu \mathbf{P}_{\mathrm{BF}} \mathbf{P}_{\mathrm{ZF}},$$

  where $\mathbf{P}_{\mathrm{BF}}$ enables coherent transmission via beamforming, $\mathbf{P}_{\mathrm{ZF}}$ zero-forces mutual interference between active users, and μ normalizes the power of

$\mathbf{P}_{\mathrm{sub}}$. Two beamforming schemes are proposed, based on maximum ratio combining (MRC) and convex optimization respectively, to enable additional signaling on the FEXT paths and thereby increase the deliverable data rates.

- Paper II extends the first work by allowing optimization of spectrum usage and addressing several aspects of practicality, which presents more realistic results. This paper exploits unused spectrum on active adjacent pairs whose dedicated services are still delivered, instead of relying on idle pairs only, and can therefore improve throughput depending on service demands. The signal transmission is formulated as

$$\mathbf{y} = \mathbf{H} \underbrace{\mathbf{P}_{\mathrm{BF}}\mathbf{P}_{\mathrm{C}}\sqrt{\mathbf{G}}\mathbf{x}}_{\text{transmitter}} + \mathbf{n},$$

where $\mathbf{P}_{\mathrm{C}}$ denotes the crosstalk-cancellation part of the precoder (either ZFP or THP), and $\sqrt{\mathbf{G}}$ is a diagonal matrix containing the overall gain-scaling coefficients for symbols destined to each target user. Specifically, the assignment of $\mathbf{G}$ counts in the transmit power increase invoked by both beamforming and crosstalk-cancellation parts of the precoder, meanwhile implements optimized transmit power allocation constrained by the aggregate transmit power limit, the regulated PSD mask, and the bit-cap. Three beamforming variants for constructing $\mathbf{P}_{\mathrm{BF}}$ are discussed, and their individual advantageous conditions are identified. Simulations with the measured BT and EAB cables show that the newly proposed coherent transmission is harmonized to complement the regular vectoring using both ZFP and THP, and provide various rate range for a group of users. The principle can also be applied to, for example, the network slicing concept in 5G.

5.2 Solution to Sudden Termination Changes

The second subpart of the thesis deals with performance maintenance problems when systems start operating on high frequencies (*i.e.,* >30 MHz), where new channel behaviors are observed which impact the delivered service quality. One identified problem, termed sudden termination changes or STC, disrupts the effectiveness of vectoring and causes service interruption to end-users over a noticeable period of time. Regarding my research contribution to this subpart, I am the main inventor of the included patent and wrote the two technical papers. I designed the whole procedure for minimizing disruption and updating precoders, as well as implemented it with lab cable measurements.
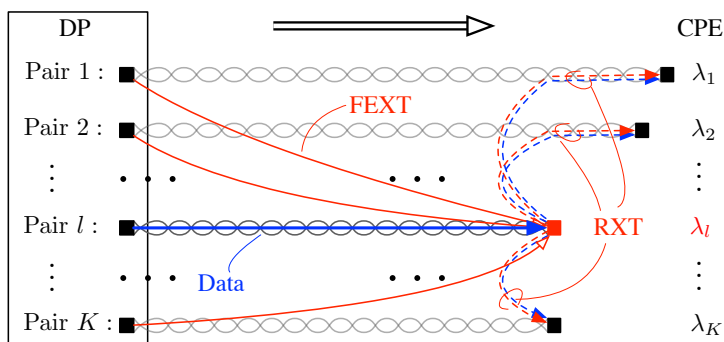
Fig. 5.1: Downstream FRN model in case of outdated vectoring operation.

- Paper III resolves a typical STC case, referred to as disorderly leaving event (DLE) for the frequency range from 30 MHz to 106 MHz. A FEXT-reflected-NEXT (FRN) model (depicted in Fig. 5.1) is described for DLE with an ideal initial status, where all CPEs are connected, *i.e.,* all terminations are perfectly matched. When DLE happens, the leaving line's termination becomes a reflective surface, forwarding both data and FEXT destined for this end to the other CPEs as NEXT and generating residual crosstalk that cannot be handled by the outdated precoder. The traditional way of shutting down the leaving line fails at eliminating all residual crosstalk, which was not observed for lower frequencies due to the weaker FEXT level. The solution is to keep the outdated precoder running, sending only the anti-crosstalk signal on the leaving line without data symbols. FEXT and anti-crosstalk signals cancel out before the reflective termination, therefore nothing will be reflected to the other CPEs.

  In addition, a parameterized channel estimation is proposed for systems using ZFP for precoder updating, which reduces the estimation effort from $\mathcal{O}(K^2)$ to $\mathcal{O}(K)$. Compared to the state-of-the-art method, the period during which active users are disturbed is significantly reduced to just the time it takes to detect the DLE.

- Paper IV extends the model to cover a general STC scenario, and proposes solutions for both deactivating and (re)activating STC events. Since the studied frequencies are also extended up to 180 MHz, the impact of an STC on both linear and non-linear precoding systems is analyzed. Low-complexity precoder-updating procedures are presented, which avoid

full matrix inversion for the linear precoder and avoid full matrix QR-decomposition for the non-linear precoder. The advantage of the minimized disturbed period for active users is also maintained for the extended scenarios. One example of the solution to a line-reactivation-caused STC is shown in Fig. 5.2.
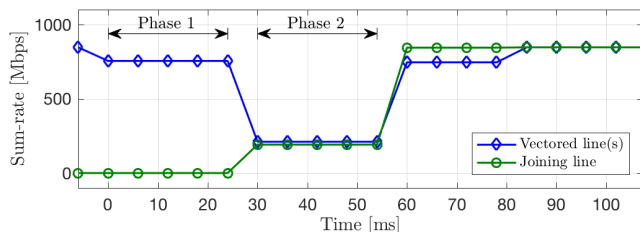
(a) Traditional procedure
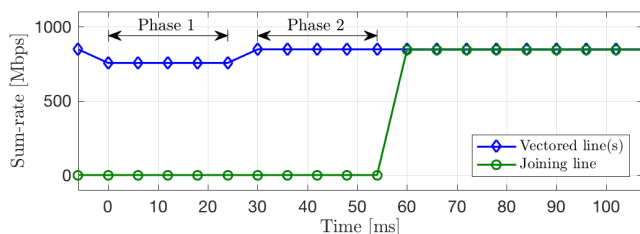
(b) Proposed procedure

Fig. 5.2: Sum-rate example over 30 MHz-106 MHz during the process of new line (re)activation. Activating STC occurs at time 0.

5.3   Efficient Fronthaul Interface

The third subpart focuses on a special role of the fixed access network: fronthauling for radio systems like 4G and 5G. It investigates the feasibility as well as proposes beneficial transmission schemes both from the wireline channel and from radio signal processing point of view. In particular, Paper V and Paper VI implement crosstalk cancellation with respect to an LTE-over-copper system in frequency-domain and time-domain, respectively. I took the lead in developing the time-domain approach and wrote Paper VI. Regarding Paper VII, I derived the fronthaul load reduction methods with the given system concern about massive MIMO, conducted simulations and wrote the paper.

- Paper V investigates the feasibility of crosstalk cancellation for LTE-over-copper systems in the downstream direction. The studied scenario considers the copper-based network as an analog fronthaul between RRU and remote radio head (RRH) for LTE signals. Channel estimation is conducted based on available LTE reference signals with a newly designed cell-ID assignment as illustrated in Eq. (5.1).

$$
\begin{aligned}
&N_{\text{ID}}^{\text{cell}}(1) \in \{0, 1, \dots, 503\} \\
&N_{\text{ID}}^{\text{cell}}(i) = \left(N_{\text{ID}}^{\text{cell}}(i-1) + 6\right) \bmod 504, \ i \in \{2, \dots, M\},
\end{aligned}
\tag{5.1}
$$

  where M denotes the number of users considered in the same vectored group. This design takes advantage of the cell-specific frequency shift of reference signal locations implied by cell ID $N_{\text{ID}}^{\text{cell}}$, and aligns reference signals of the involved users to end up on the same resource element (RE). It thereby enables a least-square based frequency-domain channel estimation, as well as the implementation of ZFP as in the traditional DSL systems.

- Paper VI deals with crosstalk cancellation in the same context as the previous work regarding analog fronthaul. Since the LTE signal is typically generated in time domain, this work develops a new scheme to keep both channel estimation and precoding to be conducted in time domain. The resulting time-domain precoder not only mitigates crosstalk but also creates effective direct paths of the wireline segment to be identical for all involved pairs as

$$
\begin{aligned}
\boldsymbol{\mathcal{Y}} &= \boldsymbol{\mathcal{H}} * \boldsymbol{\mathcal{P}}_{\text{D}} * \boldsymbol{\mathcal{X}} + \boldsymbol{\mathcal{N}} \\
&= \det(\boldsymbol{\mathcal{H}}) * \boldsymbol{\mathcal{I}} * \boldsymbol{\mathcal{X}} + \boldsymbol{\mathcal{N}},
\end{aligned}
$$

  where $*$ denotes the convolution operator, $\boldsymbol{\mathcal{H}}$ is a three-dimensional channel matrix having the third dimension denoting time-domain samples, $\boldsymbol{\mathcal{P}}_{\text{D}} = \text{adj}(\boldsymbol{\mathcal{H}})$ denotes the time-domain diagonalizing precoder, and $\boldsymbol{\mathcal{X}}$, $\boldsymbol{\mathcal{Y}}$, and $\boldsymbol{\mathcal{N}}$ denote the three-dimensional representation of time-domain transmit signal, receive signal and additive noise, respectively.

- Paper VII extends the view to the coming 5G when the RRUs support massive MIMO. In this scenario, intra-PHY split becomes a promising option to relieve the dramatically increased fronthaul traffic. This paper proposes a new uplink functional split alternative between RRU and BBU. Let $\mathbf{H}_{\text{A}}$ denote an $N \times K$ frequency-domain uplink channel matrix regarding the air interface, for example in antenna-element domain or direction domain, where N is the number of antennas and K is the number

of user-layers. For massive-MIMO systems, it is typical that $N \gg K$. Using the zero-forcing layer separation as an example, the equalization is implemented as the pseudo-inverse of $\mathbf{H}_{\mathrm{A}}$, *i.e.,*

$$\mathbf{H}_{\mathrm{A}}^{\dagger} = (\mathbf{H}_{\mathrm{A}}^{\mathrm{H}}\mathbf{H}_{\mathrm{A}})^{-1}\mathbf{H}_{\mathrm{A}}^{\mathrm{H}}.$$

This can be viewed as two steps: 1) $\mathbf{H}_{\mathrm{A}}^{\mathrm{H}}$ conducts MRC regarding $\mathbf{H}_{\mathrm{A}}$; 2) $(\mathbf{H}_{\mathrm{A}}^{\mathrm{H}}\mathbf{H}_{\mathrm{A}})^{-1}$ conducts zero-forcing regarding the equivalent channel of $\mathbf{H}_{\mathrm{A}}$ reshaped by $\mathbf{H}_{\mathrm{A}}^{\mathrm{H}}$. The proposition is to place the two steps in the RRU and the BBU respectively, which still maintains the performance of zero-forcing layer separation. More importantly, the MRC gives low RRU complexity while reducing the signal dimension from N to K, largely lightening the burden on the fronthaul link compared to the current common public radio interface (CPRI)-type fronthauling scheme. When $\mathbf{H}_{\mathrm{A}}$ is "sparse", an additional step of user-specific selection can be added before the MRC beamformer to further reduce the RRU complexity without compromising the post-processing performance.

References

[1] J. Cioffi, K. Kerpez, C. S. Hwang, and I. Kanellakopoulos, "Terabit DSL (TDSL): Use of a Copper Pair's Sub-millimeter Waveguide Modes," in *G.fast Summit (Keynote)*, Paris, May 2017. [Online]. Available: http://www.assia-inc.com/wp-content/uploads/2017/05/TDSL-presentation.pdf

[2] P. Ödling, T. Magesacher, S. Höst, P. O. Börjesson, M. Berg, and E. Areizaga, "The Fourth Generation Broadband Concept," in *IEEE Communications Magazine*, vol. 47, no. 1, pp. 62-69, January 2009.

[3] A. G. Bell, "Improvement in Telegraphy," Patent US174465 A, March, 1876. [Online]. Available: https://www.google.com/patents/US174465

[4] A. G. Bell, "Telephone-Circuit," Patent US244426 A, July, 1881. [Online]. Available: https://www.google.com/patents/US244426

[5] P. Golden, H. Dedieu, and K. S. Jacobsen, *Fundamentals of DSL Technology.* Auerbach Publications, 2006.

[6] ITU, "Asymmetric digital subscriber line (ADSL) transceivers," Recommendation ITU-T G.992.1, June 1999. [Online].
Available: https://www.itu.int/rec/T-REC-G.992.1/en

[7] ITU, "Asymmetric digital subscriber line transceivers 2 (ADSL2) – Extended bandwidth (ADSL2plus)," Recommendation ITU-T G.992.5, January 2009. [Online]. Available: https://www.itu.int/rec/T-REC-G.992.5-200901-I/en

[8] ITU, "Very High Speed Digital Subscriber Line Transceivers 2 (VDSL2)," Recommendation ITU-T G.993.2, January 2015. [Online]. Available: https://www.itu.int/rec/T-REC-G.993.2-201501-I/en

[9] P.-E. Eriksson and B. Odenhammar, "VDSL2: Next Important Broadband Technology," in *Ericsson Review*, no. 1, pp. 36-47, 2006.

[10] ITU, "Fast Access to Subscriber Terminals (G.fast) – Physical Layer Specification," Recommendation Draft ITU-T G.9701, 2014. [Online]. Available: https://www.itu.int/rec/T-REC-G.9701/en

[11] M. Timmers, M. Guenach, C. Nuzman, and J. Maes, "G.fast: Evolving the Copper Access Network," in *IEEE Communication Magazine*, vol. 51, no. 8, pp. 74–79, August 2013.

[12] V. Oksman, R. Strobel, X. Wang, D. Wei, R. Verbin, R. Goodson, and M. Sorbara, "The ITU-T's New G.fast Standard Brings DSL into the Gigabit Era," in *IEEE Communications Magazine*, vol. 54, no. 3, pp. 118-126, March 2016.

[13] W. Coomans, R. B. Moraes, K. Hooghe, A. Duque, J. Galaro, M. Timmers, A. J. van Wijngaarden, M. Guenach, and J. Maes, "XG-FAST: The 5th Generation Broadband," in *IEEE Communications Magazine*, vol. 53, no. 12, pp. 83-88, December 2015.

[14] ASSIA Inc., "G.mgfast: Waveguide Transmission for Extremely High Speed Copper Transmission," ITU-T Contribution SG15-C-0038R1, June 2017.

[15] D. Goldman, "Huge breakthrough in blazing fast internet speeds," [Online; posted May 16, 2016].
Available: http://money.cnn.com/2016/05/16/technology/gfast-internet-speeds

[16] BroadbandNow, "Fiber-Optic Internet in the United States," [Online]. Available: http://broadbandnow.com/Fiber (date visited: June 2017.)

[17] E. Medeiros, T. Magesacher, P.-E. Eriksson, C. Lu, and P. Ödling, "How Vectoring in G.fast May Cause Neighborhood Wars," in *Proc. 2014 IEEE International Conference on Communications (ICC)*, Sydney, NSW, 2014, pp. 3859-3864.

[18] Alcatel-Lucent, "G.fast: Perspectives on Nonlinear Precoding," ITU-T SG15 Contribution 2016-06-Q4-041, June 2016.

[19] J. Maes, C. Nuzman, and P. Tsiaflakis, "Sensitivity of Nonlinear Precoding to Imperfect Channel State Information in G.fast," in *Proc. 2016 24th European Signal Processing Conference (EUSIPCO)*, August 2016, pp. 290–294.

[20] Intel, "G.fast: On the Channel Estimation Accuracy of LP and NLP," ITU-T SG15 Contribution 2016-11-Q4-044, November 2016.

[21] J. Gambini and U. Spagnolini, "Radio over Telephone Lines in Femtocell Systems," in *Proc. 21st Annual IEEE International Symposium on Personal, Indoor and Mobile Radio Communications*, Instanbul, 2010, pp. 1544-1549.

[22] J. Gambini and U. Spagnolini, "Wireless over Cable for Femtocell Systems," in *IEEE Communications Magazine*, vol. 51, no. 5, pp. 178-185, May 2013.

[23] C. Lu, M. Berg, E. Trojer, P.-E. Eriksson, K. Laraqui, O. V. Tidblad, and H. Almeida, "Connecting the dots: small cells shape up for high-performance indoor radio," in *Ericsson Review*, vol. 91, December 2014. [Online]. Available: http://goo.gl/YvdY5N

[24] H. Niu, C. Li, A. Papathanassiou, and G. Wu, "RAN Architecture Options and Performance for 5G Network Evolution," in *Proc. 2014 IEEE Wireless Communications and Networking Conference Workshops (WCNCW)*, Istanbul, 2014, pp. 294-298.

[25] M. Peng, C. Wang, V. Lau, and H. V. Poor, "Fronthaul-Constrained Cloud Radio Access Networks: Insights and Challenges," in *IEEE Wireless Communications*, vol. 22, no. 2, pp. 152-160, April 2015.

[26] G. Ginis and J. Cioffi, "Vectored Transmission for Digital Subscriber Line Systems," in *IEEE Journal on Selected Areas in Communications*, vol, 20, no. 5, pp. 1085-1104, June 2002.

[27] ITU, "Self-FEXT cancellation (vectoring) for use with VDSL2 transceivers," Recommendation ITU-T G.993.5, April 2010. [Online]. Available: https://www.itu.int/rec/T-REC-G.993.5/en

[28] V. Oksman, H. Schenk, A. Clausen, J. M. Cioffi, M. Mohseni, G. Ginis, C. Nuzman, J. Maes, M. Peeters, K. Fisher, and P.-E. Eriksson, "The ITU-T's New G.vector Standard Proliferates 100 Mb/s DSL," in *IEEE Communications Magazine*, vol. 48, no. 10, pp. 140-148, October 2010.

[29] TNO, "G.fast: Wideband modeling of twisted pair cables as two-ports," ITU-T SG15 Contribution 11GS3-028, September 2011.

[30] Ericsson AB and TNO, "Improved Model for Shunt Admittance in G.fast Cable Mode," ITU-T SG15 Contribution 2012-05-4A-045, May 2012.

[31] D. Acatauassu, S. Höst, C. Lu, M. Berg, A. Klautau, and P. O. Börjesson, "Simple and Causal Copper Cable Model Suitable for G.fast Frequencies," in *IEEE Transactions on Communications*, vol. 62, no. 11, pp. 4040-4051, November 2014.

[32] E. Karipidis, N. Sidiropoulos, A. Leshem, L. Youming, R. Tarafi, and M. Ouzzif, "Crosstalk Models for Short VDSL2 Lines from Measured 30 MHz

Data," in *EURASIP Journal on Applied Signal Processing*, vol. 2006, no. 1, pp. 1-9, 2006.

[33] TNO, "G.fast: Far-end Crosstalk in Twisted Pair Cabling; Measurements and Modelling," ITU-T SG15 Contribution 11RV-022, November 2011.

[34] Deutsche Telekom AG, "G.fast: EL-FEXT Analysis," ITU-T SG15 Contribution 2012-06-4A-041, June 2012.

[35] R. F. M. van den Brink, "Modeling the Dual-Slope Behavior of in-Quad EL-FEXT in Twisted Pair Quad Cables," in *IEEE Transactions on Communications*, vol. 65, no. 5, pp. 2153-2163, May 2017.

[36] Ericsson AB, *Access Network Pair Cable, TEL 312*, 2010. [Online]. Available: http://goo.gl/4RdCXc

[37] D. K. Rytting, "Network Analyzer Error Models and Calibration Methods," Agilent Technology. [Online]. Available: https://goo.gl/R2s6HX

[38] Anritsu, "Understanding VNA Calibration," 2012. [Online]. Available: https://goo.gl/ni7UBR

[39] Keysight, "Specifying Calibration Standards and Kits for Keysight Vector Network Analyzers," Application Note, June 2016. [Online]. Available: http://literature.cdn.keysight.com/litweb/pdf/5989-4840EN.pdf

[40] J. Maes and C. Nuzman, "Energy Efficient Discontinuous Operation in Vectored G.fast," in *Proc. 2014 IEEE International Conference on Communications (ICC)*, Sydney, NSW, 2014, pp. 3854-3858.

[41] ITU, "ATM-Based Multi-pair Bonding," Recommendation ITU-T G.998.1, January 2005. [Online]. Available: https://www.itu.int/rec/T-REC-G.998.1-200501-I/en

[42] ITU, "Ethernet-based Multi-pair Bonding," Recommendation ITU-T G.998.2, January 2005. [Online]. Available: https://www.itu.int/rec/T-REC-G.998.2-200501-I/en

[43] ITU, "Multi-pair Bonding Using Time-Division Inverse Multiplexing," Recommendation ITU-T G.998.3, January 2005. [Online]. https://www.itu.int/rec/T-REC-G.998.3-200501-I/en

[44] W. Foubert, C. Neus, L. Van Biesen and Y. Rolain, "Exploiting the Phantom-Mode Signal in DSL Applications," in *IEEE Transactions on Instrumentation and Measurement*, vol. 61, no. 4, pp. 896-902, April 2012.

[45] V. L. Nir, M. Moonen, J. Verlinden, and M. Guenach, "Full Vectoring Optimal Power Allocation in xDSL Channels under Per-Modem Power Constraints and Spectral Mask Constraints," in *IEEE Transactions on Communications*, vol. 57, no. 1, pp. 194–202, January 2009.

[46] G. Ginis and J. Cioffi, "A Multi-User Precoding Scheme Achieving Crosstalk Cancellation with Application to DSL Systems," in *Proc. Conference Record of the Thirty-Fourth Asilomar Conference on Signals, Systems and Computers*, vol. 2, pp. 1627-1631, October 2000.

[47] R. Cendrillon, G. Ginis, E. Van den Bogaert, and M. Moonen, "A Near-Optimal Linear Crosstalk Precoder for Downstream VDSL," in *IEEE Transactions on Communications*, vol. 55, no. 5, pp. 860-863, May 2007.

[48] Alcatel-Lucent, "G.fast: Comparison of Linear and Non-linear Precoding," ITU-T SG15 Contribution 2013-01-Q4-046, January 2013.

[49] Intel, "G.fast: Use of Linear Precoding on Frequencies above 106 MHz," ITU-T SG15 Contribution 2016-05-11-Q4-023, May 2016.

[50] Intel, "G.fast: Rate-Reach Comparison for Linear and Non-Linear Precoding up to 212 MHz," ITU-T SG15 Contribution 2016-06-Q4-072R1, June 2016.

[51] F. Müller, C. Lu, P.-E. Eriksson, S. Höst, and A. Klautau, "Optimizing Power Normalization for G.fast Linear Precoder by Linear Programming," in *Proc. 2014 IEEE International Conference on Communications (ICC)*, Sydney, NSW, 2014, pp. 4160-4165.

[52] Ikanos, "G.fast: Constellations for Use with Non-linear Pre-coding," ITU-T SG15 Contribution 2013-01-Q4-028, January 2013.

Part II

Included Papers

Paper I

1 Rate-Boosting Using Strong Crosstalk in Wideband Wireline Systems

Abstract

Next-generation wireline systems may exploit frequencies up to several hundred MHz on short lines. Strong crosstalk coupling, comparable to the direct paths, is one of the main channel characteristics at high frequencies. Instead of fully canceling all crosstalk, we utilize strong crosstalk paths to boost data-rate for active users. Two linear precoding schemes, based on maximum ratio combining and convex optimization respectively, are proposed and applied to a common network topology. The precoding schemes exploit constructive crosstalk signals on unused lines or in unused parts of the spectrum on neighboring lines to boost data-rate while still complying with the regulated spectral power limits per line. More than $500\,\mathrm{Mbps}$ throughput gain per active user can be achieved compared to state-of-the-art linear precoding.

1.1   Introduction

Data-rate hungry services may soon push current wireline broadband networks to their limit. The fiber-to-the-home (FTTH) concept, which would conceivably satisfy the throughput demand, is still no ubiquitous reality since its installation requires large efforts in both time and money. The migration via a hybrid copper-fiber concept [1] bridges the gap by continuously using the copper wires to support the costly last-mile part. Recent standardization efforts have resulted in the emerging G.fast system [2, 3] capable of supporting in the order of 1 Gbps aggregate net data-rate on copper pairs. In its second version, even higher data-rates can be expected. Future efforts, such as [4−6], aim at providing multi-gigabit access via copper by exploring frequency ranges well beyond 100 MHz.

The first version of G.fast relies on linear precoding [7, 8] to mitigate crosstalk. Linear precoding is a well developed scheme and has been widely implemented in vectored digital subscriber line (DSL) systems for its effectiveness and low-complexity. In order to transmit below the regulated power spectrum density (PSD) mask on each line and each sub-carrier, power normalization is included in the linear precoder which, however, degrades the system performance at very high frequencies [9, 10]. In [11], the choice of the power normalization factor for linear precoding is posed as a linear programming problem, resulting in a moderate increase in delivered data-rate.

In practice, resources are still available for further data-rate boosting without additional hardware cost. For example, as part of the zero-touch philosophy, G.fast equipment could be pre-installed on a bundle basis regardless whether all customers have signed up or not. Thus, there could be more available lines than active users. Furthermore, users sharing the same binder may use either very-high-bit-rate digital subscriber line (VDSL) [12] equipment or G.fast equipment. The lines of VDSL users will be idle for frequencies beyond 35 MHz [13]. In both cases, idle lines are available and already connected to transceiver equipment at the distribution point (DP).

In this paper, we exploit strong crosstalk from idle lines in a constructive way to boost the data-rate of active users (see Fig. 1.1), while mitigating destructive crosstalk among active users and fully obeying the spectral power limits. The supporting lines can be unused lines or lines with unused spectrum in the cable, which allows for permanent boosting. Alternatively, lines connecting users that are temporarily idle or have no data to transmit at the moment can be used for peak-rate boosting. Two linear precoding schemes are introduced in the downstream direction. The first method is maximum ratio combining (MRC), which is frequently used in wireless multiple-input-single-output transmission to maximize the delivered energy to the active users. In order to
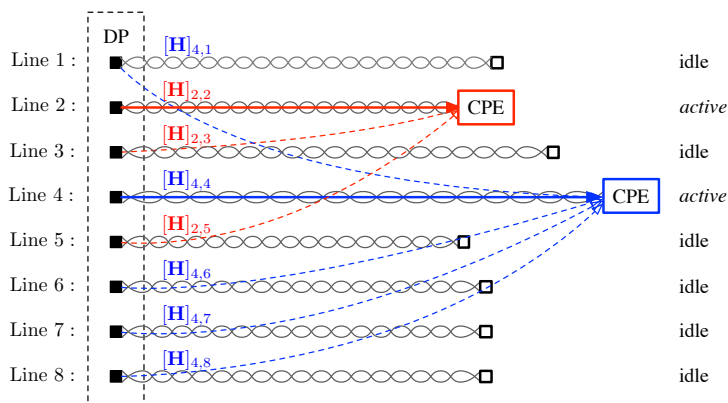
Fig. 1.1: Example scenario with two active CPEs and six idle lines contributing constructive FEXT. Line 2, 3 and 5 are chosen to support the CPE-2, and the other lines within the group are chosen to support CPE-4.

further exploit the rate-boosting potential via cooperative linear precoding, we formulate a convex feasibility problem resulting in the second precoder, which shows significant throughput gain at high frequencies.

1.2 Channel Characteristics at High Frequencies

In DSL systems, single line performance is defined as the throughput in an end-to-end transmission over a certain line with a fixed background-noise level. It can be viewed as an upper bound of the throughput on that line since no other interference or transmit power constraint is considered. Crosstalk among copper wires within a binder, classified into near-end crosstalk (NEXT) and far-end crosstalk (FEXT), is an inherent wireline channel property. In order to approach the single line performance for each line in the group, crosstalk cancellation is needed. NEXT can be mitigated by using duplexing methods such as frequency-division duplex (FDD) or time-division duplex (TDD), whereas FEXT can be mitigated by vectoring [14], as indicated in the VDSL [15] and G.fast [2] standards.

In the downstream direction, which is our main focus in this paper, a precoder in the DP enables cooperative data transmission. Consider a vectored group of size N. Let $\mathcal{N} = \{1, \ldots, N\}$ denote the set of line indices in the vectored group. Also, let $\mathbf{H} \in \mathbb{C}^{N \times N}$ denote the frequency-domain channel

matrix of the vectored group on a certain sub-carrier. The prevailing idea to cancel out crosstalk is to use a linear precoder which diagonalizes the channel matrix [8]. Mathematically, the nearly optimal linear precoder $\mathbf{P} \in \mathbb{C}^{N \times N}$ is given by

$$\mathbf{P} = 1/\mu \, \mathbf{H}^{-1} \mathbf{H}_\Sigma,$$

where $\mathbf{H}_\Sigma$ is a diagonal matrix carrying the diagonal elements of $\mathbf{H}$. The scalar μ is defined to make the overall precoded signal comply with the transmit power constraint, *i.e.,*

$$\mu = \max_{i \in \mathcal{N}} \left\| \left[\mathbf{H}^{-1} \mathbf{H}_\Sigma \right]_{\text{row } i} \right\|_2 . \tag{1.1}$$

When the frequency range is extended, new channel characteristics are observed. To demonstrate this, we take measurements for direct paths and FEXT paths from a 30 pairs, 100 m, 0.5 mm cable [16]. In this case study, 8 pairs are randomly chosen from a single binder. A sub-carrier spacing of 51.75 kHz has been used. Channel measurements are taken from 35 MHz up to 300 MHz (see Fig. 1.2a). The choice of 35 MHz yields a generous spectral margin with respect
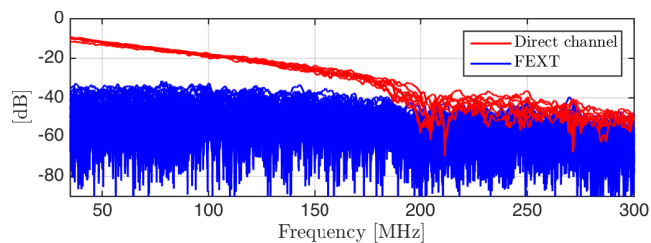
(a) Channel measurements
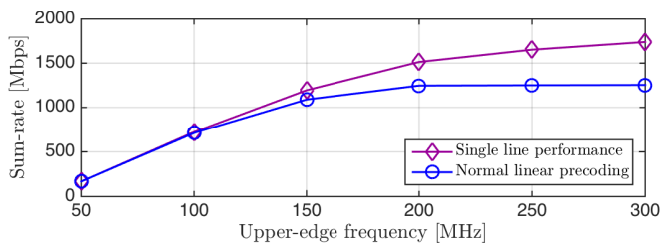
(b) Accumulated bit-rate in the band from 35 MHz to upper-edge frequency

Fig. 1.2: Channel measurements and average accumulated bit-rate per line for an 8-line vectored group.

to the VDSL 30 MHz profile. It can be observed that the FEXT becomes comparable to the direct channel as the frequency increases. As a consequence, the column-wise diagonal dominant (CWDD) property, which is the foundation of the near-optimal linear precoder, begins to diminish. Its influence on the system performance is illustrated in Fig. 1.2b.

In Fig. 1.2b, the average sum-rate for the 8 lines is shown versus available bandwidth, which is defined as upper-edge frequency minus 35 MHz. Although the bandwidth keeps increasing, the sum-rate of the linear precoding system diverges gradually from the single line performance and converges to a saturation level. By utilizing the strong crosstalk from idle pairs, however, it is possible to boost the rate beyond this saturation level.

1.3 MRC Precoding Scheme for Rate-Boosting

1.3.1 Group-MRC precoder

Consider a scenario with K active users out of N vectored lines. A simplified example with $N = 8$ and $K = 2$ is sketched in Fig. 1.1.

Let $\mathbf{H}_{\mathrm{sub}} \in \mathbb{C}^{K \times N}$ denote the channel paths ending in the active customer-premises equipment (CPE). The signal $\mathbf{r} \in \mathbb{C}^{K \times 1}$ received by the active users is given by $\mathbf{r} = \mathbf{H}_{\mathrm{sub}}\mathbf{s} + \mathbf{n}$, where $\mathbf{s} \in \mathbb{C}^{N \times 1}$ is the transmit signal and $\mathbf{n} \in \mathbb{C}^{K \times 1}$ denotes noise. We are looking for a "good" precoder $\mathbf{P}_{\mathrm{sub}} \in \mathbb{C}^{N \times K}$ yielding $\mathbf{s} = \mathbf{P}_{\mathrm{sub}}\mathbf{x}$, where $\mathbf{x} \in \mathbb{C}^{K \times 1}$ are the symbols to be transmitted, such that the active CPEs get a higher receive signal-to-noise ratio (SNR) compared to vectoring using only the active lines. In order to cancel the destructive crosstalk among the active users, we also want $\mathbf{H}_{\mathrm{sub}}\mathbf{P}_{\mathrm{sub}} = \mathbf{D}$, where $\mathbf{D} \in \mathbb{R}^{K \times K}$ is a diagonal matrix.

We apply the concept of MRC to the precoded signals with the goal of rate-boosting via crosstalk. If all N twisted pairs are available to support CPE no. k (*i.e.,* $K = 1$), the effective channel is the k-th row of $\mathbf{H}$, denoted as $\mathbf{h}_k^{\mathrm{T}} = \left[[\mathbf{H}]_{k,1}, \ldots, [\mathbf{H}]_{k,N} \right]$. Also notice that each element of $\mathbf{h}_k^{\mathrm{T}}$ represents channel attenuation, where $\left\| \mathbf{h}_k^{\mathrm{T}} \right\|_1^2$ is larger than $\left\| \mathbf{h}_k^{\mathrm{T}} \right\|_2^2$. Thus, to maximize the receive SNR and therefore boost the bit-rate, assign the precoder to be a column vector as

$$\mathbf{p}_k = \frac{1}{\mu} \left[\frac{[\mathbf{H}]_{k,1}^*}{\left| [\mathbf{H}]_{k,1} \right|} \ \cdots \ \frac{[\mathbf{H}]_{k,N}^*}{\left| [\mathbf{H}]_{k,N} \right|} \right]^{\mathrm{T}},$$

where μ is the normalization factor defined similarly as in Eq. (1.1). The precoded signals from different transmitters are added up coherently, yielding a

received signal at the active CPE given by

$$r_k = \mathbf{h}_k^{\mathrm{T}} \mathbf{p}_k x_k + n = 1/\mu \sum_{i=1}^{N} \left| [\mathbf{H}]_{k,i} \right| x_k + n. \tag{1.2}$$

In the general case of $K > 1$, group-MRC can be performed. The i-th column of $\mathbf{H}_{\mathrm{sub}}$ represents the channel paths originating from transmitter i. For each transmitter, there should be only one targeted receiver. Therefore, a grouping metric is needed to determine the group of "supporting" line(s) assigned to each active user. Assume for the i-th column of $\mathbf{H}_{\mathrm{sub}}$, $[\mathbf{H}_{\mathrm{sub}}]_{l_i i}$ is chosen to be the supporting path from transmitter i. Accordingly, assign an $N \times K$ MRC precoder matrix $\mathbf{P}_{\mathrm{MRC}}$ whose entries are composed by

$$[\mathbf{P}_{\mathrm{MRC}}]_{i,j} = \begin{cases} \dfrac{[\mathbf{H}_{\mathrm{sub}}]_{j,i}^*}{\left| [\mathbf{H}_{\mathrm{sub}}]_{j,i} \right|} & \text{if } j = l_i, \\ 0 & \text{otherwise.} \end{cases} \tag{1.3}$$

Also include the second precoder matrix

$$\mathbf{P}_{\mathrm{D}} = \left(\mathbf{H}_{\mathrm{sub}} \mathbf{P}_{\mathrm{MRC}} \right)^{-1} \left(\mathbf{H}_{\mathrm{sub}} \mathbf{P}_{\mathrm{MRC}} \right)_{\Sigma}$$

to cancel the destructive crosstalk among the active users. Together with the power scaling factor μ, the overall precoder can be written as

$$\mathbf{P}_{\mathrm{sub}} = 1/\mu \, \mathbf{P}_{\mathrm{MRC}} \mathbf{P}_{\mathrm{D}}$$

where $\mu = \max_{i \in \mathcal{N}} \left\| [\mathbf{P}_{\mathrm{MRC}} \mathbf{P}_{\mathrm{D}}]_{\mathrm{row}\, i} \right\|_2$.

1.3.2 Data-rate performance

With the MRC of the precoded signal, we can realize an equivalent channel

$$\boldsymbol{\rho}_{\mathrm{MRC}} = \mathrm{diag} \left(\mathbf{H}_{\mathrm{sub}} \mathbf{P}_{\mathrm{sub}} \right), \quad \boldsymbol{\rho}_{\mathrm{MRC}} \in \mathbb{R}^{K \times 1}$$

to the active users. To quantify the rate-boosting contribution from the resulting channel, we calculate the increased spectrum efficiency compared to a reference linear precoding system, whose precoded equivalent channel is denoted by $\boldsymbol{\gamma}$. The reference can be the single line performance, normal linear-precoding performance or any other control group. Given a certain $\boldsymbol{\gamma}$ and transmit power P_{tx}, we can calculate the spectrum efficiency gain on line k as

$$g\left([\boldsymbol{\gamma}]_k, P_{\mathrm{tx}} \right) = \log_2 \left(1 + \frac{P_{\mathrm{tx}} \left| [\boldsymbol{\rho}_{\mathrm{MRC}}]_k \right|^2}{\sigma^2 \Gamma} \right) - \log_2 \left(1 + \frac{P_{\mathrm{tx}} \left| [\boldsymbol{\gamma}]_k \right|^2}{\sigma^2 \Gamma} \right)$$

$$= \log_2 \left(1 + \frac{\Delta_k \cdot P_{\mathrm{tx}}}{\sigma^2 \Gamma + P_{\mathrm{tx}} \left| [\boldsymbol{\gamma}]_k \right|^2} \right), \tag{1.4}$$
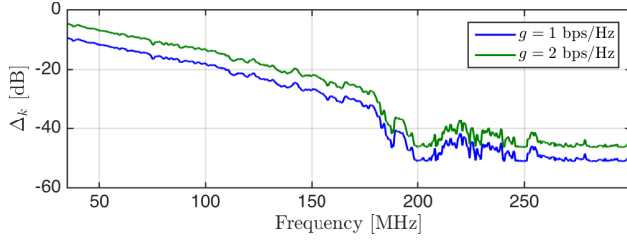
(a) Theoretical requirement on Δ_k (Eq. (1.5))
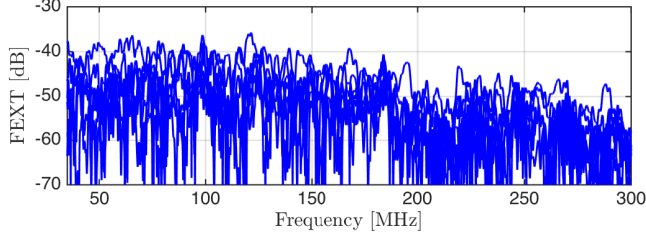
(b) FEXT coupling ending in CPE-2

Fig. 1.3: Comparison between the theoretical requirement on Δ_k to gain a desired g from the normal linear precoder performance and actual FEXT coupling level available to support the gain.

where σ^2 is the background noise power and Γ is the reserved SNR gap. Here we define a parameter $\Delta_k = \left|[\boldsymbol{\rho}_{\text{MRC}}]_k\right|^2 - \left|[\boldsymbol{\gamma}]_k\right|^2$, which denotes the increased channel gain obtained by constructive FEXT on line k. Equivalently, we can expect that the required boosting in channel gain for a certain spectrum efficiency gain should be

$$\Delta_k \text{ [dB]} = \log_{10}(2^g - 1) + c_k, \tag{1.5}$$

where $c_k = \log_{10}\left(\left(\sigma^2\Gamma + P_{\text{tx}}\left|[\boldsymbol{\gamma}]_k\right|^2\right)\Big/P_{\text{tx}}\right)$ is a constant on a certain subcarrier of line k.

Taking line 2 of our measurements as an example, assume $P_{\text{tx}} = -76\,\text{dBm/Hz}$, $\sigma^2 = -140\,\text{dBm/Hz}$ and $\Gamma = 9.8\,\text{dB}$. In Fig. 1.3a, we show the theoretical requirement on Δ_k to increase the spectrum efficiency from the normal linear precoder performance by $g = 1\,\text{bps/Hz}$ and $g = 2\,\text{bps/Hz}$ at different frequencies. For other values of g, the curve shifts in vertical direction with a term of $\log_{10}(2^g - 1)$.

Fig. 1.3a reveals that MRC of constructive FEXT to boost data-rate requires much higher Δ_k at lower frequencies than at higher frequencies. In Fig. 1.3b,

it is shown that the available FEXT coupling at lower frequencies, however, is not that much stronger than the FEXT level of higher frequencies, which significantly limits the potential gain we can extract from the lower part of the frequency range. For frequencies above $150\,\mathrm{MHz}$, it seems more likely to achieve the additional power requirement Δ_k. Therefore, we would rather focus on and explore the right-hand side of the frequency axis and utilize the strong crosstalk to achieve rate-boosting. Hereinafter, we refer to the frequency ranges above and below $150\,\mathrm{MHz}$ as high-frequency range and low-frequency range, respectively.

To show the rate-boosting result with a practical channel setup, we consider a grouping criterion based on the magnitude of crosstalk couplings, *i.e.,*

$$l_i = \arg\max_l \left| [\mathbf{H}_{\mathrm{sub}}]_{l,i} \right|^2, \tag{1.6}$$

and construct $\mathbf{P}_{\mathrm{MRC}}$ as in Eq. (1.3). In our experimental setup, the copper pairs are short and have equal lengths. The corresponding FEXT coupling coefficients are therefore similar in magnitude level. This implies that the maximum power of Eq. (1.6) for different i will not always concentrate on the same l. It enables an "even-share" grouping scheme where the number of supporting lines for each active user is on average the same over the studied frequencies. Based on the measurements described in Section 1.2, Fig. 1.4 presents the average spectrum efficiency of the group-MRC method for both low-frequency and high-frequency range. Considering a bit cap $\bar{b} = 12\,\mathrm{bits}$, the average spectrum efficiency κ for each line is calculated as

$$\kappa = \frac{\sum_{i=1}^{N_{\mathrm{tone}}} \min\left\{ \bar{b}, \log_2\left(1 + SNR/\Gamma\right) \right\}}{N_{\mathrm{tone}}}, \tag{1.7}$$

where N_{tone} is the number of sub-carriers involved and SNR is the receive signal-to-noise power ratio.

According to Fig. 1.4a, the gain in spectrum efficiency is barely noticeable in the low-frequency range since the crosstalk paths are not strong enough to contribute, which is consistent with the conclusion in Fig. 1.3. In the high-frequency range (see Fig. 1.4b), the group-MRC shows more than $2\,\mathrm{bps/Hz}$ spectrum efficiency gain on average compared to its linear-precoding counterpart.

When comparing the performance of the group-MRC precoder to the normal linear precoder on each sub-carrier, however, we notice that the MRC scheme is not always a good solution for rate-boosting. In Fig. 1.5, there are negative gains at some sub-carriers, where the MRC precoder delivers a lower data-rate to active users than the normal linear precoder. This disadvantage of the
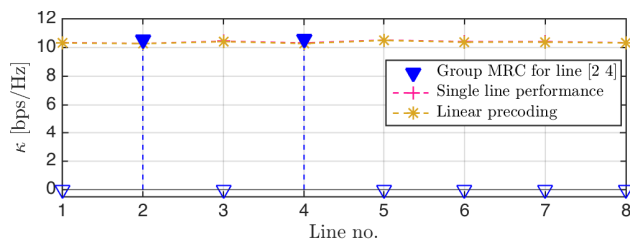
(a) 35 MHz–150 MHz
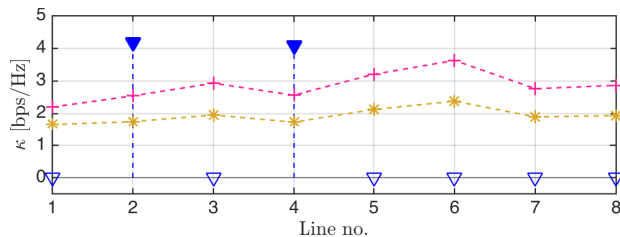
(b) 150 MHz–300 MHz

Fig. 1.4: Spectrum efficiency comparison for group-MRC precoding with the grouping scheme defined in Eq. (1.6) for different frequency ranges.

MRC precoder becomes more notable when the number of available idle lines decreases, or equivalently, K increases (comparing Fig. 1.5a with Fig. 1.5b). The reduced effective channel gain results partly from the normalization factor μ. As μ equals to the maximum norm-2 of the precoder's row-vectors, simply multiplying with $1/\mu$ may cause a large penalty in the resulting channel gain of the MRC precoder. Furthermore, the rate-boosting performance of the MRC precoder depends largely on the chosen grouping metric. As shown in Fig. 1.5, the metric chosen in Eq. (1.6) does not give a "fair" boosting to active users at most sub-carriers.

1.4 Optimized Precoding Scheme for Rate Boosting

As discussed above, the MRC precoder does not guarantee that we can always achieve the optimal utilization of available idle pairs. Therefore, further investigation on the rate-boosting possibility in a general case is desired. We
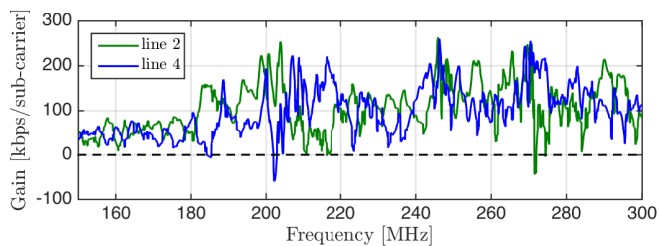
(a) Active users $K = 2$ ($N = 8$)
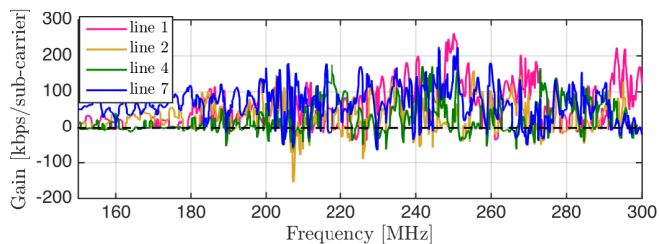
(b) Active users $K = 4$ ($N = 8$)

Fig. 1.5: Bit-rate gain of the group-MRC precoder over $150\,\mathrm{MHz}$–$300\,\mathrm{MHz}$, compared to the normal linear precoder.

formulate this as an optimization problem, where the objective is to find a linear precoder $\mathbf{P}_{\mathrm{opt}}$ giving an equivalent channel

$$\boldsymbol{\Theta} = \mathbf{H}_{\mathrm{sub}}\mathbf{P}_{\mathrm{opt}}, \tag{1.8}$$

subject to the following constraints:

Channel gain   By optimally utilizing the available constructive FEXT, the equivalent channel with a linear precoder results in $\boldsymbol{\rho}_{\mathrm{opt}} = \mathrm{diag}\left(\mathbf{H}_{\mathrm{sub}}\mathbf{P}_{\mathrm{opt}}\right)$, and can deliver a data-rate as high as possible to active users given a certain channel environment.

Residual crosstalk   It is not necessary to have the off-diagonal entries of the effective channel $\boldsymbol{\Theta}$ to be strictly 0, which is the main objective of the traditional linear precoder. Instead, residual crosstalk can be allowed as long as its maximum power is lower than a small number ϵ^2. In order not to decrease the receive SNR, we confine ϵ^2 to be lower than the background noise level.

Transmit power   To fulfil the transmit power constraint, the precoder should have its row vector power confined by $\left\|[\mathbf{P}_{\mathrm{opt}}]_{l,1\ldots K}\right\|_2 \leq 1$, for $l = 1,\ldots,N$.

The objective together with the three constraints result in a feasibility problem. Let $\otimes$ stand for the Kronecker product, and $\mathrm{vec}(\cdot)$ operate on a matrix to stack the columns of the matrix to be a long column vector. We can rewrite the equivalent channel in Eq. (1.8) as $\mathbf{Ap} = \boldsymbol{\theta}$, where $\mathbf{A} = \mathbf{I}_K \otimes \mathbf{H}_{\mathrm{sub}} \in \mathbb{C}^{K^2 \times KN}$, $\mathbf{p} = \mathrm{vec}(\mathbf{P}_{\mathrm{opt}}) \in \mathbb{C}^{KN \times 1}$, and $\boldsymbol{\theta} = \mathrm{vec}(\boldsymbol{\Theta}) \in \mathbb{C}^{K^2 \times 1}$. The related feasibility problem with convex constraints [17] can be written as

$$
\begin{aligned}
\mathbf{p}_{\mathrm{opt}} = \quad &\text{find} \quad &&\mathbf{p} \\
&\text{subject to} \quad &&\mathbf{E}_{\mathrm{d}} \mathbf{A p} = \boldsymbol{\rho}_{\mathrm{opt}} \\
& &&\max \left| \mathbf{E}_{\mathrm{d}}^c \mathbf{A p}\right| \leq \epsilon \\
& &&\left\| \mathbf{E}_{\mathrm{r},l} \mathbf{p} \right\|_2 \leq 1 \ \ \text{for } l = 1,\ldots,N.
\end{aligned}
\tag{1.9}
$$

Here we define three versions of the matrix $\mathbf{E}$ such that $\mathbf{E}\,\mathrm{vec}(\mathbf{X})$ results in a vector composed by specific entries of the original matrix $\mathbf{X}$. $\mathbf{E}_{\mathrm{d}} \in \mathbb{R}^{K \times K^2}$ is defined to extract the diagonal entries such as $\mathbf{E}_{\mathrm{d}}\left(\mathbf{A p}\right) = \mathrm{diag}\left(\mathbf{H}_{\mathrm{sub}}\mathbf{P}_{\mathrm{opt}}\right)$, *i.e.,*

$$
[\mathbf{E}_{\mathrm{d}}]_{i,j} = \left\{ \begin{array}{ll} 1 & \text{if } j = (i-1)K + i, \\ 0 & \text{otherwise.} \end{array} \right.
$$

$\mathbf{E}_{\mathrm{d}}^c \in \mathbb{R}^{K(K-1) \times K^2}$ is defined to extract the off-diagonal entries in a similar manner, *i.e.,*

$$
[\mathbf{E}_{\mathrm{d}}^c]_{i,j} = \left\{ \begin{array}{ll} 1 & \text{if } j = i + \lfloor (i-1)/K \rfloor + 1, \\ 0 & \text{otherwise.} \end{array} \right.
$$

Finally, $\mathbf{E}_{\mathrm{r},l} \in \mathbb{R}^{K \times KN}$ extracts the l-th row of the matrix as $\mathbf{E}_{\mathrm{r},l}\mathbf{p} = [\mathbf{P}_{\mathrm{opt}}]_{l,1\ldots K}$, *i.e.,*

$$
[\mathbf{E}_{\mathrm{r},l}]_{i,j} = \left\{ \begin{array}{ll} 1 & \text{if } j = (i-1)N + l, \\ 0 & \text{otherwise.} \end{array} \right.
$$

The last two constraints in Eq. (1.9) generate a fixed region around the optimal solution. The main source that influences the feasibility of the optimization problem lies in the first function, which is affine. If we are too aggressive in achieving gain and set too high values for the desired $\boldsymbol{\rho}_{\mathrm{opt}}$, the optimization problem in Eq. (1.9) will become unfeasible. Therefore, to approach the highest possible $\boldsymbol{\rho}_{\mathrm{opt}}$ and still fulfil the other two constraints, we propose a feasibility-based iterative method as described in Table 1.1.

As our final goal is to provide the active users with a boosted data-rate, we set the main iteration-driving parameter to be g, as defined in Eq. (1.4), which represents a spectrum efficiency gain on a certain sub-carrier compared to a reference performance. The gains for all K active users compose a vector

Table 1.1: Proposed iteration for optimizing a rate-boosting precoder

---

On sub-carrier t:
Initialize
- Set gain step size as $\triangle_{\mathrm{g}}$;
- Set basic gain for each line $\mathbf{g} = \mathbf{g}_0$;
- Set parameters $\beta_1 = -\sigma^2\Gamma/P_{\mathrm{tx}}$, $\boldsymbol{\beta}_2 = \boldsymbol{\gamma} - \beta_1$;
- $\boldsymbol{\rho}_{\mathrm{opt}}^2 = 2^{\mathbf{g}} \odot \boldsymbol{\beta}_2 + \beta_1$;
- Set feasible $= 1$.

---

    while feasible $= 1$ **do**
- Solve optimization problem in Eq. (1.9);
  if Failed **then**
  – feasible $= 0$;
  end if
- **if** feasible $= 1$ **then**
  – Reshape $\mathbf{p}_{\mathrm{opt}}$ to $\mathbf{P}_{\mathrm{opt}}$;
  – Update $\mathbf{g} = \mathbf{g} + \triangle_{\mathrm{g}}$;
  – Update $\boldsymbol{\rho}_{\mathrm{opt}}^2 = 2^{\mathbf{g}} \odot \boldsymbol{\beta}_2 + \beta_1$;
  end if
    end while

$\mathbf{g}$. Again, let $\boldsymbol{\gamma}$ denote the equivalent channel of the reference performance. Define a scalar parameter $\beta_1 = -\sigma^2\Gamma/P_{\mathrm{tx}}$, which is constant over the whole frequency range, and a vector parameter $\boldsymbol{\beta}_2 = |\boldsymbol{\gamma}|^2 - \beta_1$, which keeps constant on a certain sub-carrier. Together with these parameters, we can calculate the desired $\boldsymbol{\rho}_{\mathrm{opt}}$ using the expected $\mathbf{g}$ as

$$\boldsymbol{\rho}_{\mathrm{opt}} = \left(2^{\mathbf{g}} \odot \boldsymbol{\beta}_2 + \beta_1\right)^{1/2},$$

where $\odot$ denotes the Hadamard product and the power is taken elementwisely. Starting with a conservative gain setting $\mathbf{g}_0$ and increasing the gain gradually with a step size $\triangle_{\mathrm{g}}$, we will reach a $\boldsymbol{\rho}_{\mathrm{opt}}$ after j iterations that makes the whole setup unfeasible. The optimized precoder vector $\mathbf{p}_{\mathrm{opt}}$ obtained as the result of iteration $j-1$ gives the maximum possible $\boldsymbol{\rho}_{\mathrm{opt}}$. The starting points in $\mathbf{g}_0$ are determined by the original and expected data-rate for the active users. For example, the spectrum efficiency on line 2 and 4 are originally 2 bps/Hz and 4 bps/Hz at a certain sub-carrier, and aim for a boosting result of 3 bps/Hz and 5 bps/Hz, respectively. A possible choice for initialization can be $\mathbf{g}_0 = [2,4]^{\mathrm{T}}$, and setting the same $\triangle_{\mathrm{g}}$ for both lines.

In the following simulations, we choose the normal linear precoding performance as the baseline. Fig. 1.6 compares the rate-boosting results between
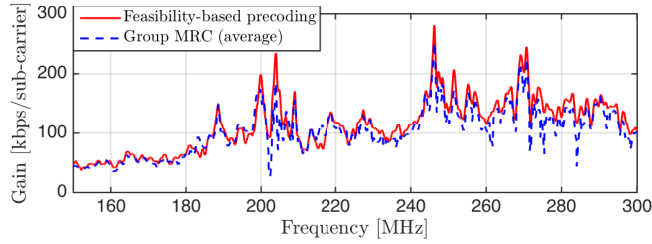
(a) Active users $K = 2$ ($N = 8$)
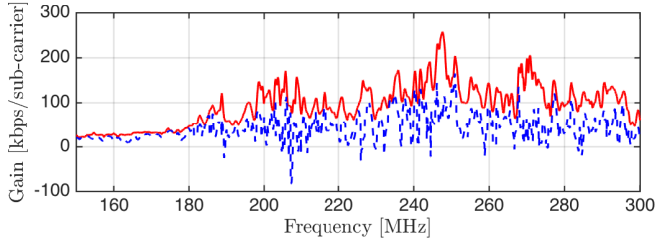
(b) Active users $K = 4$ ($N = 8$)

Fig. 1.6: Data-rate gain at studied frequencies with different number of active users.

the group-MRC method applying the grouping metric in Eq. (1.6) and the feasibility-based optimization method summarized in Table 1.1. We focus on the frequency range between 150 MHz and 300 MHz, where strong crosstalk dominates. For each sub-carrier, the increased bit-rate compared to the throughput of normal linear precoding is calculated. For the feasibility-based optimization method, the curves for active users are identical since we choose the even-gain strategy in the iterative process. For the group-MRC method, the average increase over the targeted lines is presented.

In Fig. 1.6, we observe that the optimized precoder has a curve that is generally higher than the group-MRC curve, which means that the simple metric given by Eq. (1.6) does not fully explore the rate-boosting ability from the constructive FEXT paths. The advantage of the optimized precoder is more obvious when the number of available idle lines for each active user decreases. Most importantly, the optimized precoder will never yield a negative gain as the MRC method does. The superior performance of the optimized precoder is rooted mainly in the following three aspects. First, the normalization factor μ limits the possible power gain of the MRC method. Second, the vectoring precoder $\mathbf{P}_D$ that is included in the group-MRC precoder sets a strict requirement
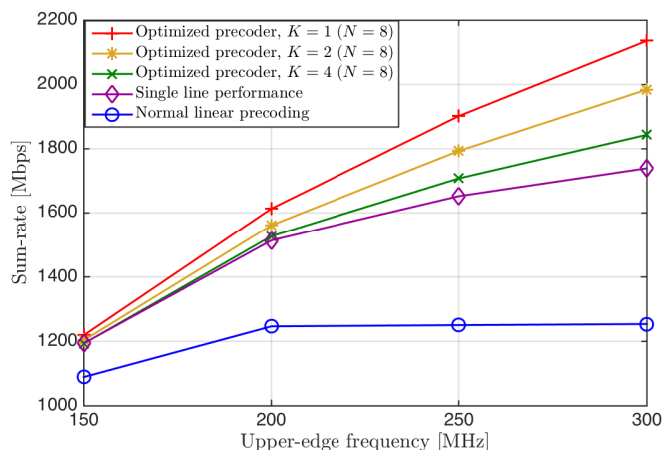
Fig. 1.7: Accumulated average sum-rate per user versus available bandwidth (35 MHz to upper-edge frequency).

in canceling crosstalk. The purpose of $\mathbf{P}_{\text{D}}$ is to diagonalize the channel matrix and generate zero-valued off-diagonal entries for $\mathbf{H}_{\text{sub}}\mathbf{P}_{\text{sub}}$. In fact, as also implemented in the optimized precoder, we only need to limit the power of those entries to be lower than the background noise level so that the related precoder design constraint gets relaxed. Third, the grouping-metric depends highly on frequency and on channel conditions. It is hard to group the idle lines in an optimal way to perform rate-boosting, since the FEXT varies strongly both over frequency and over lines. The optimized precoder, on the other hand, provides a target-oriented solution without limitation from any specific grouping scheme.

In Fig. 1.7, we trace back to the problem raised in Section 1.2, specifically in Fig. 1.2b. Again, the average sum-rate over active users is calculated. For the case of $K = 1$, where 7 idle lines are available to support rate-boosting, the basic MRC precoding in Eq. (1.2) is performed. For the cases of $K = 2$ and $K = 4$, the optimized precoding scheme is applied. It is clear that by utilizing strong crosstalk from idle lines in the vicinity, the linear precoder can break through the saturation level at high frequencies and provide the active users with significant data-rate gain. In the simulation starting from 35 MHz and ending in 300 MHz, we can achieve 589.61 Mbps sum-rate gain per active user compared to the normal linear precoder when 4 idle lines are available for $K = 4$ active users; we gain 729.41 Mbps per user when 6 idle lines are available for $K = 2$ active users; and we gain 882.79 Mbps per user when 7 idle lines are

available for $K = 1$ active user.

1.5   Conclusion

In the next generation wireline systems, the achievable data-rate with linear precoding saturates gradually after a certain frequency (*e.g.,* 150 MHz for our measured channel). To break through this saturation level, we propose rate-boosting for active end-users, utilizing strong crosstalk at high frequencies from idle twisted pairs within the same vectored group. Group-MRC precoding exhibits a substantial data-rate improvement depending on the number of supporting lines. In order to further enhance the performance, we present an optimization-based solution. Compared to standard linear precoding, more than 500 Mbps data-rate gain per active user can be achieved when exploiting bands up to 300 MHz.

References

[1] P. Ödling, T. Magesacher, S. Höst, P. O. Börjesson, M. Berg, and E. Areizaga, "The Fourth Generation Broadband Concept," in *IEEE Communications Magazine*, vol. 47, no. 1, pp. 62-69, January 2009.

[2] ITU, "Fast Access to Subscriber Terminals - Physical Layer Specification," Recommendation Draft ITU-T G.9701, 2014. [Online]. Available: https://www.itu.int/rec/T-REC-G.9701/en

[3] M. Timmers, M. Guenach, C. Nuzman, and J. Maes, "G.fast: Evolving the Copper Access Network," in *IEEE Communications Magazine*, vol. 51, no. 8, pp. 74-79, August 2013.

[4] W. Coomans, R. Moraes, K. Hooghe, A. Duque, J. Galaro, M. Timmers, A. van Wijngaarden, M. Guenach, and J. Maes, "XG-FAST: Towards 10 Gb/s Copper Access," in *Proc. 2014 GLOBECOM Workshops (GC Wkshps)*, pp. 630-635, December 2014.

[5] Celtic-Plus, "Multi-Gigabit Access via Copper," http://goo.gl/cBuoLA (date visited: March 23, 2015), March 2015.

[6] 4GBB, "The Initiator of G.fast - A Paradigm Shift in Access Technology," www.4gbb.eu (date visited: Mar. 23, 2015).

[7] R. Cendrillon, G. Ginis, E. Van den Bogaert, and M. Moonen, "A Near-Optimal Linear Crosstalk Canceler for Upstream VDSL," in *IEEE Transactions on Signal Processing*, vol. 54, no. 18, pp. 3136-3146, 2006.

[8] R. Cendrillon, G. Ginis, E. Van den Bogaert, and M. Moonen, "A Near-Optimal Linear Crosstalk Precoder for Downstream VDSL," in *IEEE Transactions on Communications*, vol. 55, no. 5, pp. 860-863, May 2007.

[9] Lantiq, "G.fast: G.fast Performance over KPN Cable," ITU-T SG15 Contribution 338, July 2013. [Online]. Available: http://goo.gl/qnA9DN

[10] Alcatel, "G.fast: Comparison of Linear and Non-linear Pre-coding," ITU-T SG15 Contribution 2013-01-Q4-046, January 2013.

[11] F. Müller, C. Lu, P.-E. Eriksson, S. Höst, and A. Klautau, "Optimizing Power Normalization for G.fast Linear Precoder by Linear Programming," in *Proc. 2014 IEEE International Conference on Communications (ICC)*, pp. 4160-4165, June 2014.

[12] ITU, "Very high speed digital subscriber line transceivers 2 (VDSL2)," Recommendation ITU-T G.993.2, December 2011. [Online]. Available: https://www.itu.int/rec/T-REC-G.993.2-201112-I/en

[13] D. Wei, A. Fazlollahi, G. Long, and E. Wang, "G.fast for FTTdp: Enabling Gigabit Copper Access," in *Proc. 2014 GLOBECOM Workshops (GC Wkshps)*, pp. 668-673, December 2014.

[14] G. Ginis and J. Cioffi, "Vectored Transmission for Digital Subscriber Line Systems," in *IEEE Journal on Selected Areas in Communications*, vol, 20, no. 5, pp. 1085-1104, June 2002.

[15] ITU, "Self-FEXT cancellation (vectoring) for use with VDSL2 transceivers," Recommendation ITU-T G.993.5, April 2010. [Online]. Available: https://www.itu.int/rec/T-REC-G.993.5/en

[16] Ericsson AB, *Access Network Pair Cable, TEL 312*, 2010. [Online]. Available: http://goo.gl/4RdCXc

[17] S. Boyd and L. Vandenberghe, *Convex Optimization*. Cambridge University Press, 2014.

Paper II

2 Rate-Boosting via Beamforming for Multi-Pair Copper Channels

Abstract

New broadband wireline systems like G.fast aim at delivering multi-gigabit-per-second rates over legacy copper pairs exploiting the full very high frequency (VHF) band and beyond. Since now the crosstalk couplings turn out to be as strong as the direct paths, the MIMO channel becomes ill-conditioned which degrades the effectiveness of vectoring at high frequencies rendering the high end of the system bandwidth practically useless. This paper proposes to signal more around the wires than in the wires by using the strong far-end crosstalk (FEXT) as data channels via beamforming at high frequencies. There unused spectrum on adjacent twisted pairs constitutes a pool of available resources. Both beamforming and crosstalk cancellation are merged to fully harness the diverse characteristics of the channel and boost the data-rates delivered to a set of target users. Regarding the beamforming structure, maximum ratio transmission (MRT), equal gain transmission (EGT) and a special variant of EGT are investigated, each of which has its advantageous conditions. The newly proposed coherent transmission is harmonized to complement vectoring using both zero-forcing precoder (ZFP) and Tomlinson-Harashima precoder (THP), whereas the rate-boosting gain is more obvious in the ZFP-based systems.

2.1 Introduction

In order to meet the exponentially increasing data demand over the hybrid fiber-copper access network, more bandwidth over the copper segment is vital to sustain the intense activities of the digital economy. However, increasing the bandwidth beyond current G.fast [1–3], *i.e.,* > 106 MHz, faces technological barriers due to the increased far-end crosstalk (FEXT) which dominates the direct paths of the physical twisted pairs. This channel behavior restricts the effective use of vectoring [4] since the MIMO channel becomes non-diagonal dominant and ill-conditioned. The spatial multiplexing gain of vectoring deteriorates rapidly with frequency as a result rendering the upper band practically useless.

Exploiting the trade-off between the spatial and frequency domains of the wireline systems promises great theoretical potential in pushing the system bandwidth beyond current limits. In [5], we presented a method for boosting the downstream rates of wireline broadband users by additionally transmitting on otherwise unused twisted copper pairs. The extra-launched signals form constructive interference through the selected strong crosstalk paths at high frequencies while the destructive interference is mitigated via the classical crosstalk cancellation techniques. The intended application is a G.fast-like broadband scenario over dendritic topologies in which network-side transceivers are collocated, *e.g.,* in a cabinet or pole-mounted, but the customer-premises equipment (CPE) transceivers are not. This arrangement is illustrated in Fig. 2.1. It is particularly applicable for a proposed extension of the *fourth-generation broadband* system [6], or similar, where crosstalk is comparably strong as the direct couplings.

One of the adopted channels in this paper is given in Fig. 2.2 which shows the measured attenuation of direct paths and FEXT paths of a 50 m BT cable consisting of 20 pairs of 0.5 mm twisted copper wires. For frequencies below 100 MHz, the direct path is prominently stronger than the FEXT and the channel matrix is diagonal-dominant. Correspondingly, for higher frequencies, the FEXT couplings become comparable to or sometimes even stronger than the direct paths, where the channel matrix is mathematically similar to that of a MIMO radio system. For these frequencies, wireline rate-boosting then bears resemblance to the MIMO techniques seen in LTE and 5G mobile communication.

The strong FEXT and severe attenuation prevent us from increasing datarate by further increasing bandwidth. The gain from using higher power budget is also negligible due to the regulated power spectrum density (PSD) mask. To address this limitation, we propose to take advantage of the unused spectrum of the adjacent pairs and the FEXT from them to achieve an enhanced "direct"
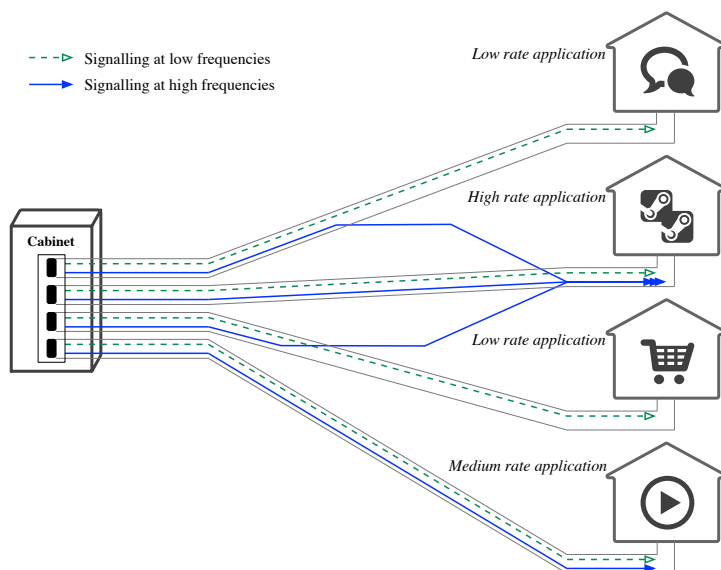
Fig. 2.1: An illustrative arrangement of the rate-boosting scenario that takes advantage of the unused spectrum on the active adjacent pairs.

channel. Other techniques inspired by the high frequency multi-pair channel behavior may involve spatial modulation [7] and space-time coding [8, 9].

While [5] showed a great potential of wireline rate-boosting, it did not address several aspects of practicality and thus indicated optimistic performance figures. This work extends the original paper as follows:

- Exploiting unused spectrum on active adjacent pairs, whose dedicated services are still delivered (see Fig. 2.1), instead of relying on idle pairs only.

- Investigating three beamforming variants regarding the number of target users with respect the available pairs, as well as the channel features at different frequencies.

- Considering both zero-forcing precoder (ZFP) [10, 11] and Tomlinson-Harashima precoder (THP) [12] in the system level design together with two sets of cable measurements to provide fair performances.

- Counting in the transmit power increase invoked by both beamforming and crosstalk-cancellation parts of the precoder, meanwhile implement-
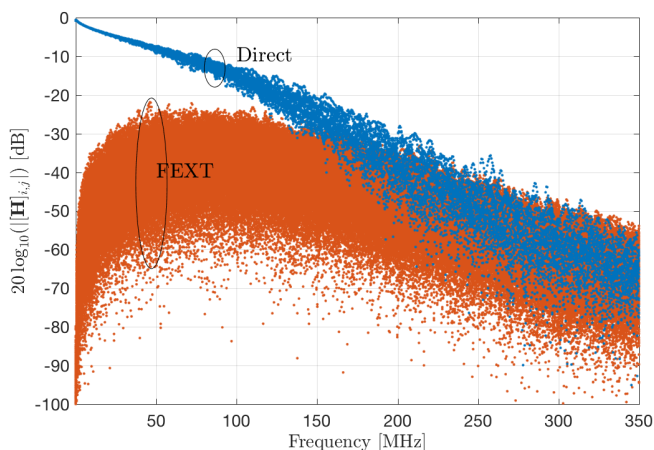
Fig. 2.2: Wideband channel coupling of a measured 20 pair cable bundle.

ing optimized transmit power allocation constrained by the aggregate transmit power limit, the regulated PSD mask in [13], and the bit-cap.

Simulation results show that the additional beamforming functionality can effectively increase the bit-loading capability of the target users at high frequencies. It works better for the ZFP-based systems than the THP-based ones. Specifically regarding the beamforming structures, the investigated maximum ratio transmission (MRT), equal gain transmission (EGT) and a special variant of EGT present different applicabilities considering various number of target users, channel properties and interference-cancellation techniques.

Throughout this paper, $\mathbb{C}$ and $\mathbb{R}$ denote the complex and real number fields, respectively. The bold capital letter $\mathbf{A}$ denotes a matrix and lower case $\mathbf{a}$ denotes a column vector. The element on the i-th row and j-th column of $\mathbf{A}$ is denoted as $[\mathbf{A}]_{i,j}$. The transpose and Hermitian transpose operators are denoted by $(\cdot)^{\mathrm{T}}$ and $(\cdot)^{\mathrm{H}}$, respectively. The operator $\mathrm{diag}(\mathbf{a})$ denotes a diagonal matrix with $\mathbf{a}$ on its main diagonal, and $\mathrm{diag}(\mathbf{A})$ denotes a column vector containing the diagonal entries of $\mathbf{A}$. The operator $\|\cdot\|$ denotes the Euclidean norm.

2.2   Transmitting Schemes in the Cabinet

In the digital subscriber line (DSL) context, vectoring in the downstream direction invokes precoding for mitigating FEXT between adjacent pairs. The multiuser-MIMO channel is then decoupled into parallel independent sub-channels, which simplifies equalization at the distributed receivers.

Consider a vectored group associated with N twisted pairs (therefore N transmit ports) among which cooperative processing is available at the operator side. For the discrete multi-tone modulation (DMT) system, let M denote the number of tones within the operating band. On tone $m \in [1, \ldots, M]$, let $\mathbf{H}^{[m]} \in \mathbb{C}^{K \times N}$ denote the channel matrix, where K denotes the corresponding active receivers at the distributive user side. Particularly for the rate-boosting scenario illustrated in Fig. 2.1, we assume that $K = N$ at low frequencies where all users connected to the N pairs are actively receiving data, while $K < N$ at high frequencies where more transmit ports are available than the receiving ones.

Since most of the following formulations are repetitive on each tone, we hereinafter omit the superscript $[m]$ for brevity unless it is necessary to stress the tone index. For a vectored transmission, the receive signal $\mathbf{y} \in \mathbb{C}^{K \times 1}$ on one tone is formulated as

$$\mathbf{y} = \mathbf{H} \underbrace{\mathbf{P}\sqrt{\mathbf{G}}\mathbf{x}}_{\text{transmitter}} + \mathbf{n}$$
$$= \mathbf{D}\sqrt{\mathbf{G}}\mathbf{x} + \mathbf{n}, \tag{2.1}$$

where the various quantities are as follows:

- $\mathbf{x} \in \mathbb{C}^{K \times 1}$ denotes data symbols destined for the K CPEs;

- $\mathbf{n} \in \mathbb{C}^{K \times 1}$ denotes the background noise in the cable;

- $\mathbf{P} \in \mathbb{C}^{N \times K}$ is the overall precoder so that $\mathbf{D} = \mathbf{H}\mathbf{P}$ is obtained as a diagonal matrix;

- $\sqrt{\mathbf{G}} = \text{diag}\big([\sqrt{g_1}, .., \sqrt{g_k}, .., \sqrt{g_K}]\big)$ is a diagonal matrix where $\sqrt{g_k}$ is the overall gain-scaling coefficient for symbols destined to user k on that tone.

For the convenience of analysis, we decompose the precoder $\mathbf{P}$ into a beamforming part and a crosstalk-cancellation part as $\mathbf{P} = \mathbf{P}_{\text{BF}}\mathbf{P}_{\text{C}}$, where $\mathbf{P}_{\text{BF}} \in \mathbb{C}^{N \times K}$ contains the beamforming coefficients and $\mathbf{P}_{\text{C}} \in \mathbb{C}^{K \times K}$ implements crosstalk cancellation regarding the effective channel $\mathbf{H}_{\text{eff}} = \mathbf{H}\mathbf{P}_{\text{BF}}$. For the tones where $K = N$, $\mathbf{P}_{\text{BF}} = \mathbf{I}$ which is an identity matrix, and therefore $\mathbf{H}_{\text{eff}} = \mathbf{H}$.

In DSL, both ZFP and THP are considered for $\mathbf{P}_\mathrm{C}$, which are linear and non-linear, respectively. Generally, the THP outperforms ZFP at high frequencies, but also has higher complexity, is more sensitive to the accuracy of channel estimation [14,15], and contains modulo operation which makes it incompatible with legacy CPEs [16, 17]. This paper works on both cancellation techniques to provide fair performances. Different $\mathbf{P}_\mathrm{C}$ formulations impact the assignment of $\mathbf{G}$, which is constrained by three factors:

a) the upper bound of the total transmit power of the n-th transmit modem, denoted as $\bar{P}_n$ for $n \in [1, ..., N]$;

b) the regulated PSD mask $P_\mathrm{msk}^{[m]}$ for $m \in [1, \dots, M]$;

c) the loaded bit-cap $\bar{b}$, due to the size limitation of modulation alphabet.

Since now the K power-scaling parameters g_k affect the transmit power from N ports on each tone, a modified power allocation strategy is proposed. The following subsections detail the power allocation for transmit symbols regarding ZFP and THP, respectively.

2.2.1 Linear Vectoring

The ZFP conducts crosstalk cancellation by inversing the effective channel as

$$\mathbf{P}_\mathrm{C,\,ZF} = \mathbf{H}_\mathrm{eff}^{-1}\mathrm{diag}\big(\mathrm{diag}(\mathbf{H}_\mathrm{eff})\big).$$

It yields a crosstalk-free effective channel as $\mathbf{D}_\mathrm{ZF} = \mathrm{diag}\big(\mathrm{diag}(\mathbf{H}_\mathrm{eff})\big)$. The overall precoder $\mathbf{P}_\mathrm{ZF} = \mathbf{P}_\mathrm{BF}\mathbf{P}_\mathrm{C,\,ZF}$ conducts a linear transformation on the input scaled transmit symbol $\sqrt{\mathbf{G}}\mathbf{x}$, yielding the transmit power from the N ports on a certain tone as

$$\mathbf{v} = \mathbf{S}\mathbf{g}, \tag{2.2}$$

where $\mathbf{S}$ and $\mathbf{g}$ denote the element-wise power of $\mathbf{P}_\mathrm{ZF}$ and $\mathrm{diag}(\sqrt{\mathbf{G}})$, respectively as

$$\mathbf{S} = \begin{bmatrix} |[\mathbf{P}_\mathrm{ZF}]_{1,1}|^2 & \cdots & |[\mathbf{P}_\mathrm{ZF}]_{1,K}|^2 \\ \vdots & \ddots & \vdots \\ |[\mathbf{P}_\mathrm{ZF}]_{N,1}|^2 & \cdots & |[\mathbf{P}_\mathrm{ZF}]_{N,K}|^2 \end{bmatrix}$$

$$\mathbf{g} = \begin{bmatrix} g_1 & \cdots & g_k & \cdots & g_K \end{bmatrix}^\mathrm{T}, \tag{2.3}$$

given that $\mathbf{x}$ is power-normalized.

The goal is to assign $\mathbf{G}$, or equivalently $\mathbf{g}$, efficiently within the power budget on each tone that maximizes the sum-rate

$$R = \sum_{k=1}^{K}\Delta_f \sum_{m=1}^{M} \log_2(1 + \mathrm{SNR}_k^{[m]}), \tag{2.4}$$

where Δ_f denotes the frequency spacing between two consecutive tones. Referring to Eq. (2.1), the receive signal-to-noise ratio (SNR) at the k-th CPE on each tone is formulated by

$$\text{SNR}_k = \gamma_k g_k, \tag{2.5}$$

in which γ_k denotes the channel-to-noise power ratio (CNR) of the equivalent direct path as

$$\gamma_k = \frac{\left|[\mathbf{D}]_{k,k}\right|^2}{\sigma^2 \Gamma}, \quad k \in [1, \ldots, K] \tag{2.6}$$

for σ^2 denoting the background noise power on a single tone, and Γ denoting the SNR gap. The optimization problem regarding optimal variable $\mathbf{g}^{[m]}$ for $m \in [1, \ldots, M]$ is then formulated as

$$
\begin{aligned}
&\underset{\mathbf{g}^{[m]}, \ \forall m}{\text{maximize}} && \sum_{k=1}^{K} \sum_{m=1}^{M} \log_2 \left(1 + \gamma_k^{[m]} g_k^{[m]}\right) \\
&\text{subject to} && \sum_{m=1}^{M} [\mathbf{S}_{\text{row } n}^{[m]}] \mathbf{g}^{[m]} \leq \bar{P}_n, \ \forall n \\
& && [\mathbf{S}_{\text{row } n}^{[m]}] \mathbf{g}^{[m]} \leq P_{\text{msk}}^{[m]}, \ \forall k, m \\
& && 0 \leq g_k^{[m]} \leq \frac{2^{\bar{b}} - 1}{\gamma_k^{[m]}}, \ \forall k, m
\end{aligned}
\tag{2.7}
$$

As also analyzed in [18], the optimization complexity of Eq. (2.7) is prohibitively high due to, among others, the large amount of dual variables (on the order of NM) as well as the coupling between the optimal variables of $\mathbf{g}^{[m]}$ by $\mathbf{S}^{[m]}$. Therefore, we implement a modified version of the low-complexity power allocation algorithm proposed in [18] regarding the linear precoder.

The algorithm in [18] first initializes all $\mathbf{g}^{[m]}$ using $P_{\text{msk}}^{[m]}$, and then adjusts $\mathbf{g}^{[m]}$ on each tone via the *column-norm* method [19] to ensure that the resulted transmit power $\mathbf{v}^{[m]}$ in Eq. (2.2) stays below $P_{\text{msk}}^{[m]}$ while at least one port transmits at the mask level. If any port k has its total transmit power larger than $\bar{P}_k$, the maximum values of $g_k^{[m]}, \forall m$ are reduced until the total power limit is met.

This updating strategy, however, is not completely applicable in our case when $K < N$, since there is no one-on-one relation between $\bar{P}_n$ and $g_k^{[m]}, \forall m$. Therefore, we propose a bit-loading based updating strategy that is applicable for all cases of $K \leq N$. It is based on the fact that the total transmit power of port n can be lowered by reducing $g_k^{[m]}$ (by the amount of $[\mathbf{S}^{[m]}]_{n,k} g_k^{[m]}$) at the cost of reducing bit-loading of user k on tone m.

After initialization same as [18], if any transmit port violates the total transmit power limit, we first remove the excess allocated power which do not

change the bit-loading results. Since the bit-loading is applied as

$$b_k^{[m]} = \left\lfloor \log_2(1 + \gamma_k^{[m]} g_k^{[m]}) \right\rfloor, \quad \forall k, m, \tag{2.8}$$

where operator $\lfloor \cdot \rfloor$ yields the maximum integer smaller than its argument, $g_k^{[m]}$ can be updated as

$$\hat{g}_k^{[m]} = \frac{2^{b_k^{[m]}} - 1}{\gamma_k^{[m]}}, \quad \forall k, m.$$

After the first update, if any transmit port n still has its total transmit power larger than $\bar{P}_n$, we calculate the power reduction that can be obtained by losing 1 bit from each user on each tone (*i.e.,* $\tilde{b}_k^{[m]} = b_k^{[m]} - 1, \forall k, m$) as

$$\beta_{n,k}^{[m]} = [\mathbf{S}^{[m]}]_{n,k} \left(\hat{g}_k^{[m]} - \frac{2^{\tilde{b}_k^{[m]}} - 1}{\gamma_k^{[m]}} \right)$$

$$= [\mathbf{S}^{[m]}]_{n,k} \frac{2^{\tilde{b}_k^{[m]}}}{\gamma_k^{[m]}}, \quad \forall k, m. \tag{2.9}$$

Since our objective is to maximize sum-rate as in Eq. (2.4), we do not differentiate from which user the bits are traded for the transmit power reduction. Let α denote a predefined number of bit loss in each updating iteration. The (k, m) pairs corresponding to the α number of maximum $\beta_{n,k}^{[m]}$ values index the group of $g_k^{[m]}$ that needs to be reduced to $(2^{b_k^{[m]}-1} - 1)/\gamma_k^{[m]}$. In each iteration, this g_k reduction is conducted regarding each port n that does not comply with the total power constraint after the previous iteration. The whole power allocation process is summarized in Table 2.1.

2.2.2 Non-linear Vectoring

The THP is shown to be a good practical non-linear precoding structure [20]. The crosstalk cancellation is based on the QR-decomposition of $\mathbf{H}_{\text{eff}}^{\text{H}}$, *i.e.,* $\mathbf{H}_{\text{eff}} = \mathbf{H}\mathbf{P}_{\text{BF}} = \mathbf{R}^{\text{H}}\mathbf{Q}^{\text{H}}$, where $\mathbf{R}^{\text{H}}$ is a lower triangular matrix and $\mathbf{Q}$ is a unitary matrix. The signal transmission can be formulated as

$$\mathbf{y} = \mathbf{H} \underbrace{\mathbf{P}_{\text{BF}} \mathbf{Q} \left\{ \mathbf{R}^{-\text{H}} \mathbf{D}_{\text{TH}} \sqrt{\mathbf{G}} \mathbf{x} \right\}_{\text{modulo}}}_{\text{transmitter}} + \mathbf{n}$$

where $\mathbf{D}_{\text{TH}} = \text{diag}\big(\text{diag}(\mathbf{R}^{\text{H}})\big)$ is the effective crosstalk-free channel. As detailed in [12], the non-linear part of THP applies modulo operations to avoid excess

Table 2.1: Power Allocation for Linear Precoder

Main output: $\hat{g}_k^{[m]}$, $\forall m \in [1, ..., M], k \in [1, ..., K]$

Initialize
- $g_k^{[m]} = P_{\mathrm{msk}}^{[m]}$, $\forall k, m$;
- $i_0 = 0$;

- Normalize $g_k^{[m]}$ as $g_k^{[m]} / \sum_{i=1}^N [\mathbf{S}^{[m]}]_{i,k}$, $\forall k, m$;

- Update transmit PSD: $\mathbf{v}^{[m]} = \mathbf{S}^{[m]} \mathbf{g}^{[m]}$, $\forall m$;

- Assign $\hat{g}_k^{[m]} = g_k^{[m]} P_{\mathrm{msk}}^{[m]} / \max \mathbf{c}^{[m]}$, $\forall k, m$;

- Calculate $P_n = \sum_{m=1}^M [\mathbf{S}_{\mathrm{row}\,n}^{[m]}] \hat{\mathbf{g}}^{[m]}$, $\forall n \in [1, ..., N]$;

while $\exists (P_n > \bar{P}_n)$ **do**

    - $i_0 = i_0 + 1$;

    - $\mathcal{N} = \{n | P_n > \bar{P}_n\}$;

    if $i_0 = 1$ **then**

        - $b_k^{[m]} = \lfloor \log_2(1 + \gamma_k^{[m]} \hat{g}_k^{[m]}) \rfloor$, $\forall k, m$;

        - $\tilde{b}_k^{[m]} = b_k^{[m]}$;

    else

        - $\tilde{b}_k^{[m]} = b_k^{[m]} - 1$;

    end if

    - Assign set $\mathcal{I} = \{(k, m) | \tilde{b}_k^{[m]} > 0\}$;

    for $n \in \mathcal{N}$ **do**

        - Calculate $\beta_{n,k}^{[m]}$ in Eq. (2.9), $\forall (k, m) \in \mathcal{I}$;

        - Find the largest α number of $\beta_{n,k}^{[m]}$ values, and assign the corresponding (k, m) pair in set $\mathcal{J}_n$;

        - Update $\hat{g}_k^{[m]} = (\tilde{b}_k^{[m]} - 1)/\gamma_k^{[m]}$, $\forall (k, m) \in \mathcal{J}_n$;

    end for

    - Calculate $P_n = \sum_{m=1}^M [\mathbf{S}_{\mathrm{row}\,n}^{[m]}] \hat{\mathbf{g}}^{[m]}$, $\forall n \in \mathcal{N}$;

end while

Table 2.2: THP power increase factor for QAM constellations

b (bits)	1, 2	3, 4	5, 6	7, 8	9, 10	11, 12	13, 14	15
$\varphi\{b\}$	1.3333	1.0667	1.0159	1.0039	1.0010	1.0002	1.0001	1.0000

transmit power increase due to the pre-cancelling. Correspondingly, the same modulo operation is implemented at the CPE receivers after equalization and prior to detection.

Although the constellation-based modulo arithmetic bounds the value of precoded signal, studies show that power increase still exists, which does not directly rely on the precoder but varies according to the bit-loading results, or equivalently the applied constellation sizes. In [21], the power increase factors are calculated for all relevant QAM constellations. Transformed into a linear parameter $\varphi\{b\}$, Table 2.2 lists all the relevant numbers we use in simulations. Specifically, the diamond lattice shape is considered for odd constellations. Since the power increase factor $\varphi\{b\}$ is a function of the bit-loading results, it is not counted in the initial assignment for g_k.

The allocated power for each line on each tone is again coupled by the linear part of the precoder $\mathbf{P}_{\mathrm{BF}}\mathbf{Q}$, and jointly impacts the actual transmit power from each of the N ports. To manage this problem, we firstly consider to assign the power at the output of the non-linear part of the precoder as $\tilde{\mathbf{g}} = [\tilde{g}_1, ..., \tilde{g}_K]^{\mathrm{T}}$. For THP, the power factor $\mathbf{S}$ of the linear precoder part as in Eq. (2.3) becomes

$$\mathbf{S} = \begin{bmatrix} |[\mathbf{P}_{\mathrm{BF}}\mathbf{Q}]_{1,1}|^2 & \cdots & |[\mathbf{P}_{\mathrm{BF}}\mathbf{Q}]_{1,K}|^2 \\ \vdots & \ddots & \vdots \\ |[\mathbf{P}_{\mathrm{BF}}\mathbf{Q}]_{N,1}|^2 & \cdots & |[\mathbf{P}_{\mathrm{BF}}\mathbf{Q}]_{N,K}|^2 \end{bmatrix}.$$

Similar power allocation strategy as in Table 2.1 can be implemented for $\tilde{\mathbf{g}}$. The only difference is that the bit-loading based power adjustment as in Eq. (2.9) needs to count in the power increase factor in Table 2.2 as well, *i.e.,*

$$\beta_{n,k}^{[m]} = [\mathbf{S}^{[m]}]_{n,k} \left(\hat{\tilde{g}}_k^{[m]} - \frac{(2^{\tilde{b}_k^{[m]}} - 1)\varphi\{\tilde{b}_k^{[m]}\}}{\gamma_k^{[m]}} \right), \ \forall k, m.$$

After the desired $\hat{\tilde{g}}_k$ values that yield bounded transmit PSD and bounded total transmit power at all the N ports are obtained on each tone, the normalized value considering the power increase factor $\varphi\{b\}$ can be calculated in an iterative manner. Firstly, the bit-loading is calculated as $b_k = \lfloor \log_2(1 + \gamma_k \hat{\tilde{g}}_k) \rfloor$. Then, the allocated power is updated as $\hat{g}_k = \hat{\tilde{g}}_k / \varphi\{b_k\}$, which gives a bit-loading of $b'_k = \lfloor \log_2(1 + \gamma_k \hat{g}_k) \rfloor$. If $b_k = b'_k$, $\hat{g}_k$ is the actual allocated power;

otherwise, update $\hat{\hat{g}}_k$ to $\hat{\hat{g}}_k/\varphi\{b_k\}$ and repeat the calculation until the bit-loading result converges.

2.3   Beamforming Variants

As exemplified in Fig. 2.1, it is likely that not all users in a vectored group use up all the available bandwidth. For example, user j has achieved its target rate by exploiting frequencies below f_0, leaving the spectrum above f_0 idle. Then pair j becomes an *auxiliary pair*, whose transmit resource can be used to support other users over its unused spectrum.

Since there exist more transmit resources (N) than unique data streams (K), we carry out beamforming over the involved pairs for those frequencies to boost the target users' throughput. There both direct and FEXT paths towards the target users are co-phased and summed to create a pattern of constructive interference.

As sketched in Fig. 2.3, the beamforming part of the precoder affects the receive SNR (as in Eq. (2.5)) at the target user in two ways. Each column of $\mathbf{P}_{\mathrm{BF}}$ is a set of beamforming coefficients that create the effective direct channel towards each target user, while the row-coefficients of $\mathbf{P}_{\mathrm{BF}}$, jointly with the allocated gain-scaling parameters $\mathbf{g}$, lead to the transmit power increase (or decrease) at each of the N ports.

Regarding different properties in the resulted coherent channel gain and the induced transmit power changes, we investigate three beamforming structures: MRT, EGT, and single-selective-destination EGT (sEGT), respectively. For simplicity but without loss of generality, the analysis in this section mainly focuses on the linear vectoring system as described in Section 2.2.1. Simulation results of both linear and non-linear vectoring systems will be shown in the next section.

2.3.1   Maximum Ratio Transmission (MRT)

When MRT is implemented, the beamforming part of the precoder is formulated as $\mathbf{P}_{\mathrm{BF,\,MRT}} = \mathbf{H}^{\mathrm{H}}$ on a certain tone. Accordingly, the overall precoder considering linear zero-forcing crosstalk cancellation is formulated as

$$\mathbf{P}_{\mathrm{ZF,\,MRT}} = \mathbf{H}^{\mathrm{H}}(\mathbf{H}\mathbf{H}^{\mathrm{H}})^{-1}\mathbf{D}_{\mathrm{ZF,\,MRT}} = \mathbf{H}^{\dagger}\mathbf{D}_{\mathrm{ZF,\,MRT}},$$

where $\mathbf{H}^{\dagger}$ denotes the pseudo-inverse of $\mathbf{H}$ and $\mathbf{D}_{\mathrm{ZF,\,MRT}} = \mathrm{diag}\big(\mathrm{diag}(\mathbf{H}\mathbf{H}^{\mathrm{H}})\big)$ denotes the effective direct channel for the K target users after conducting the
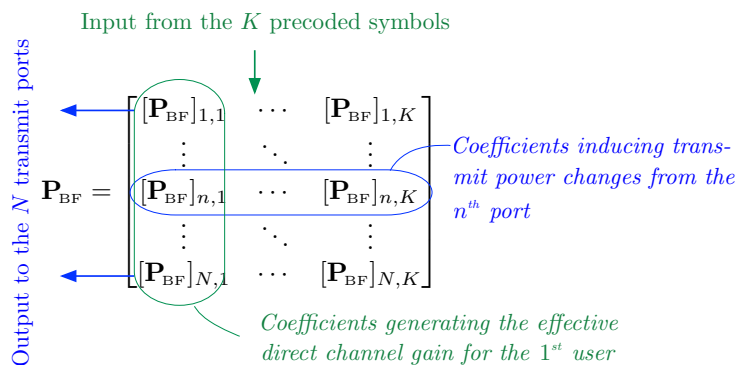
Fig. 2.3: Illustration of the beamforming precoder's impact.

MRT beamforming. Note that each of the direct channel is in form of

$$[\mathbf{D}_{\text{ZF, MRT}}]_{k,k} = \sum_{n=1}^{N} |[\mathbf{H}]_{k,n}|^2.$$

Since the channel couplings $[\mathbf{H}]_{k,n}$ indicate attenuation, the square-sum of them may yield an effective direct channel which is more attenuated than the original direct channel. It means that the coherent combining of the multiple paths does not improve the CNR for target users.

On the other hand, the power of row-norm of $\mathbf{P}_{\text{BF, MRT}}$ is in form of $\sum_{k=1}^{K} |[\mathbf{H}]_{k,n}|^2$. Similarly, it is a term greatly smaller than 1. It means that the overall precoder may not increase but decrease the power of the gain-scaled transmit symbol. In this case, we can assign a scaling value g_k higher than the PSD mask, which in turn improves the receive SNR in Eq. (2.5).

2.3.2 Equal Gain Transmission (EGT)

To enhance the effective direct channel, the EGT structure is explored. In this case, the beamforming part of the precoder is constructed as

$$[\mathbf{P}_{\text{BF, EGT}}]_{n,k} = \frac{[\mathbf{H}]_{k,n}^*}{|[\mathbf{H}]_{k,n}|}, \quad \text{for} \quad \begin{array}{l} n \in [1, ..., N] \\ k \in [1, ..., K] \end{array},$$

which gives an effective direct channel as

$$[\mathbf{D}_{\text{ZF, EGT}}]_{k,k} = \sum_{n=1}^{N} |[\mathbf{H}]_{k,n}|.$$

Comparing to the regular precoder without beamforming, the direct channel is therefore enhanced by the additional $(N-1)$ FEXT magnitude terms.

However, the power of row-norm of $\mathbf{P}_{\text{BF, EGT}}$ is equal to K, which is the number of target users. Given the per-tone transmit power budget $P_{\text{msk}}^{[m]}$ on each tone, the value that can be assigned to g_k is reduced to roughly $1/K$ of that without $\mathbf{P}_{\text{BF, EGT}}$ (considering that the variation of $\mathbf{P}_{\text{C}}$ is smaller than the impact from $\mathbf{P}_{\text{BF, EGT}}$).

Both MRT and EGT have advantage and disadvantage regarding the resulted effective direct channels (which are related to the CNR value γ_k) and the induced transmit power changes (which upper-bound the assignment of g_k) as illustrated in Fig. 2.4. The difference between the gaps in Fig. 2.4a and 2.4b suggests which beamforming structure has a better performance. It is highly dependent on the number of target users K with respect to the group size N as well as the channel properties over the frequency range where beamforming is implemented. Generally, it is more beneficial to apply EGT for small targeted K; otherwise, MRT is preferred. A detailed comparison regarding our measured cables will be shown in the simulation section.

2.3.3 Single-Selective-Destination EGT (sEGT)

To alleviate the power increase caused by $\mathbf{P}_{\text{BF, EGT}}$, we also investigate a special EGT variant that each row of the beamforming precoder only contains a single non-zero element. It is equivalent to select one path sourcing from each transmit port on each tone to be the constructive path towards a target user while the other paths from the same port is viewed as the carriers of destructive interference. It is therefore referred to as sEGT.

To distinguish the "constructive" from the "destructive" paths in $\mathbf{H}$, we introduce a binary steering parameter $\iota_{k,n}$ on each tone. Only when $\iota_{k,n} = 1$, path $[\mathbf{H}]_{k,n}$ is regarded as constructive for the k-th target user on that tone while the destructive paths associated with $\iota_{k,n} = 0$ will be cancelled by $\mathbf{P}_{\text{C}}$. Then the beamforming part of the precoder is constructed by

$$[\mathbf{P}_{\text{BF, sEGT}}]_{n,k} = \iota_{k,n} \frac{[\mathbf{H}]_{k,n}^*}{\left|[\mathbf{H}]_{k,n}\right|}, \ \text{for} \ \begin{array}{l} n \in [1, ..., N] \\ k \in [1, ..., K] \end{array} . \tag{2.10}$$

The special structure of $\mathbf{P}_{\text{BF, sEGT}}$ suggests the associated steering parameter bounded by $\sum_{k=1}^{K} \iota_{k,j} \leq 1$. As a result, the effective direct channel becomes

$$[\mathbf{D}_{\text{ZF, sEGT}}]_{k,k} = \sum_{n=1}^{N} \iota_{k,n} |[\mathbf{H}]_{k,n}|.$$

(a) CNR

(b) g_k in dB scale
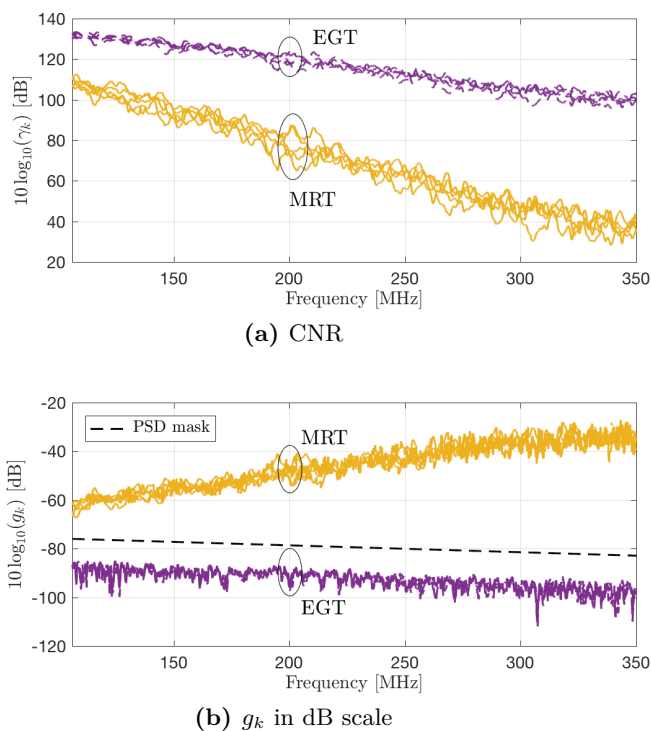
Fig. 2.4: An example of $K = 5$ to show the impact on the effective CNR γ_k and gain-scaling parameter g_k when implementing MRT and EGT, respectively.

Comparing to the normal EGT, the proposed structure of sEGT does not introduce extra power increase since the row-norm of $\mathbf{P}_{\mathrm{BF, \,sEGT}}$ is always 1. It means that the assigned values to g_k could be raised. As a trade-off, the effective direct channel gain is lowered since the number of coherently combined channel paths is reduced from N to N/K on an average for each user. As long as we keep the dominant path, which is noticeably higher than the other paths, for each user, the loss in the resulted effective CNR could be lower than the gain in the scaling value. In this case, systems with sEGT can outperform that with EGT.

To show the benefit of sEGT, the binary steering parameters $\iota_{k,n}, \forall k, n$ are assigned for each tone as follows:

Firstly, the original direct path is always assigned to the dedicated user. For example, if the fourth line in the group is connected to the first target

user, then $\iota_{1,4} = 1$ while $\iota_{i,4} = 0$ for $i \neq 1$. It is guaranteed that $\mathbf{P}_{\text{BF, sEGT}}$ has at least one non-zero element in each column and the resulted $\mathbf{H}_{\text{eff}}$ is always full rank and well-conditioned for inverse. By doing so, we also envision that the sEGT structure will on an average outperforms the EGT counterpart in a linear vectoring system on the frequencies where the direct couplings are still noticeably stronger than the FEXT couplings, for example, below around 160 MHz for the measured cable in Fig. 2.2.

Secondly, the transmit resources of the auxiliary pairs are assigned to utilize the most energy-effective FEXT towards a certain target user. Since $\mathbf{P}_{\text{BF, sEGT}}$ (therefore $\mathbf{H}_{\text{eff}}$ and $\mathbf{P}_{\text{C}}$) is not determined before obtaining the $\iota_{k,n}$, a joint optimization problem like Eq. (2.7) which considers the transmit power changes due to $\mathbf{P}_{\text{C}}$ is not available. Thus, we consider a separated formulation to determine $\iota_{k,j}$ for each auxiliary pair first. The problem is transformed into selecting the "best" FEXT path from a certain port that maximizes the delivered sum-rate over the involved frequencies, no matter which target user it dedicates to on each tone. The details on the formulation and selection procedure are listed in Appendix 2.6.

2.4   Simulations and Comparison

In this section, we analyze and compare the attainable performances of the target users by involving the three beamforming structures above the critical frequency f_0. Below the critical frequency f_0, each pair supplies only the connected users and then exploits the remaining power and spectrum above f_0 to support the target users. As a comparison, results of conducting a regular vectoring above f_0 are also presented as the benchmark.

Table 2.3 lists the applied simulation parameters. Two sets of cable measurements are used in this section. One is an equal length 50-meter BT cable (see Fig. 2.2), the other is an equal length 100-meter EAB cable as plotted in [5]. The strength difference between the direct and FEXT couplings is more obviously observed in the EAB cable. The critical frequency f_0 for each cable is set around the frequency point where the bit-loading of the regular ZFP (without beamforming) starts dropping from the bit-cap, thereby to show the potential of boosting. Above f_0, the additional beamforming functionality can help boost the bit-loading capability. Full knowledge of the channel state information (CSI) is assumed. The same background noise level of -150 dBm/Hz is assumed over the entire band for simplicity. The bit-loading cap is relaxed from 12 bits as in the G.fast standard [1] to 15 bits. When presenting the sum-rate results, we assume that 100% of the time-division duplex (TDD) time is allocated to the downstream. To calculate the average quantities for each K

Table 2.3: Simulation Parameters

	BT cable	EAB cable
Cable length	50 m	100 m
Critical frequency	$f_0 = 106\,\text{MHz}$	$f_0 = 50\,\text{MHz}$
Number of pairs	$N = 20$	$N = 8$
Frequency range	$\sim 350\,\text{MHz}$	$\sim 300\,\text{MHz}$
Tone spacing	$\Delta_f = 51.75\,\text{kHz}$	
AWGN PSD	$\sigma^2 = -150\,\text{dBm/Hz}$	
Bit-loading cap	$\bar{b} = 15\,\text{bits}$	
Total power limit	$\bar{P}_n = 4\,\text{dBm/pair}$	
SNR gap	$\Gamma = 10.8\,\text{dB}$	

value, at least 100 randomly picked combinations of target users are simulated if $\binom{N}{K} > 100$; otherwise, all combinations are simulated.

Fig. 2.5 compares the average bit-loading capability for different K values, when MRT and EGT are implemented, respectively, in the ZFP-based systems. The resulted effective CNR for a certain target user does not change with K as long as the beamforming structure is determined. However, the transmit power portion consumed by the precoder part increases with the value of K, thereby reduces the upper bound of each scaling value g_k on each tone. It is observed that the overall bit-loading capability is lowered with the increased K, no matter which beamforming structure is applied. Specifically, the power increase induced by $\mathbf{P}_{\text{BF, EGT}}$ raises much faster with an increasing K than that of the MRT structure. In Fig. 2.5a with $K = 2$, the average performance of EGT is better. When targeting a bigger K value (*e.g.,* $K = 10$ in Fig. 2.5b), the advantage of the EGT in generating higher coherent gain in the effective direct channel is overwhelmed by its disadvantage of the increased power portion consumed by the precoder, and therefore rendering a poorer average bit-loading than the MRT.

The way we construct $\mathbf{P}_{\text{BF, sEGT}}$ in Section 2.3.3 guarantees that the original direct channel of each target user is added into its effective direct channel after beamforming. As a result, the special variant sEGT shows better performance comparing to the regular form of EGT for the frequencies whose channel have a distinct strength difference between the direct and FEXT paths, as exemplified in Fig. 2.6. The gain of applying sEGT is more obvious in Fig. 2.6b for the 100-meter EAB cable. In Fig. 2.6a, only a limited gain from the sEGT is observed at the mid-range frequencies (below around 160 MHz), which matches the channel

(a) $K = 2$

(b) $K = 10$

Fig. 2.5: Comparison of the average bit-loading capability between MRT and EGT for different number of target users K regarding a linear vectoring system over the 106-350 MHz bandwidth of the BT cable.

properties shown in Fig. 2.2. Although the gain from applying sEGT at its advantageous frequencies is even higher for large K comparing to the regular EGT, it is then more efficient to apply MRT directly in those cases. In short, it is beneficial to implement sEGT when 1) there are a small plurality of target users in the vectored group; and 2) over the frequencies when the direct path is still noticeably stronger than the FEXT (does not necessarily need to have the channel matrix row-wise diagonally dominant (RWDD) [11]). For the best performance regarding small K, a hybrid EGT can be implemented which uses sEGT at the mid-range frequencies and the regular EGT at the higher band.

Analysis of the beamforming structure regarding THP is not as straightforward as the system with ZFP, since the effective direct channel is determined by the QR-decomposition of $\mathbf{H}_{\text{eff}}$. The ordering of target users, which influences
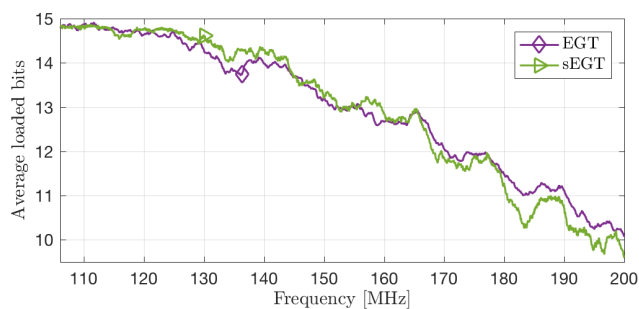
(a) BT cable, $K = 3$
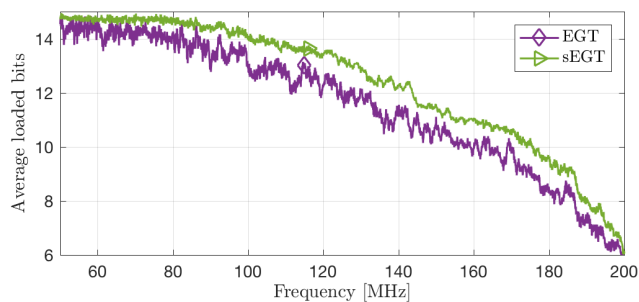
(b) EAB cable, $K = 2$

Fig. 2.6: Comparison of the average bit-loading capability between EGT and sEGT over the frequencies regarding a linear vectoring system.

the per-user performances, is not included in this work. We simply assign the priority order according to the line number of the user in the group. Therefore, the rate difference can be big among the target users. Again, Fig. 2.7 shows the average bit-loading performance for different K values of the same cable when the three beamforming structure is implemented, respectively. The advantage of applying MRT for large K is not obvious in this case. Even for $K = 15$ (see Fig. 2.7b), the MRT and EGT present quite similar performances. Therefore, EGT would be the preferred beamforming structure for systems using THP for crosstalk cancellation. Similar to the linear precoding scenario, a hybrid of sEGT and the regular EGT at different frequencies can be applied for the best performance.

Finally, regarding the two adopted cables, Figs. 2.8 and 2.9 show the average sum-rate of each target user obtained above f_0 when the number of target users

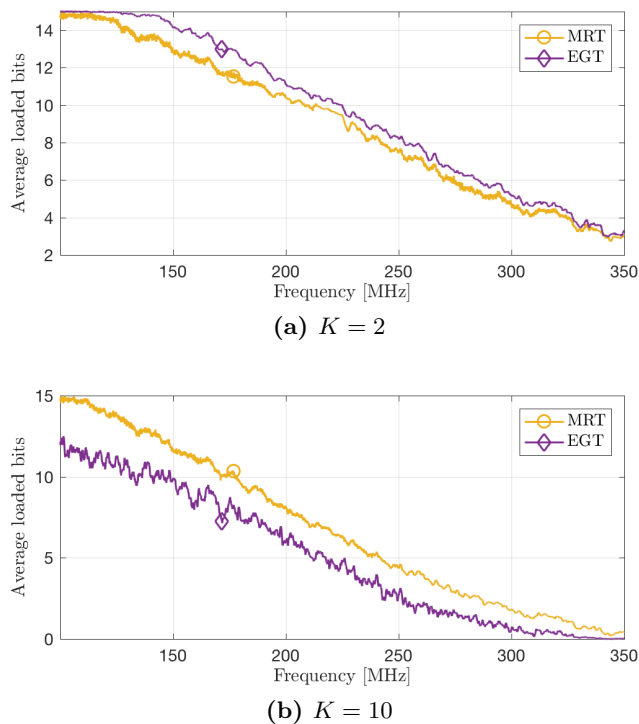**(a)** $K = 2$

(b) $K = 15$
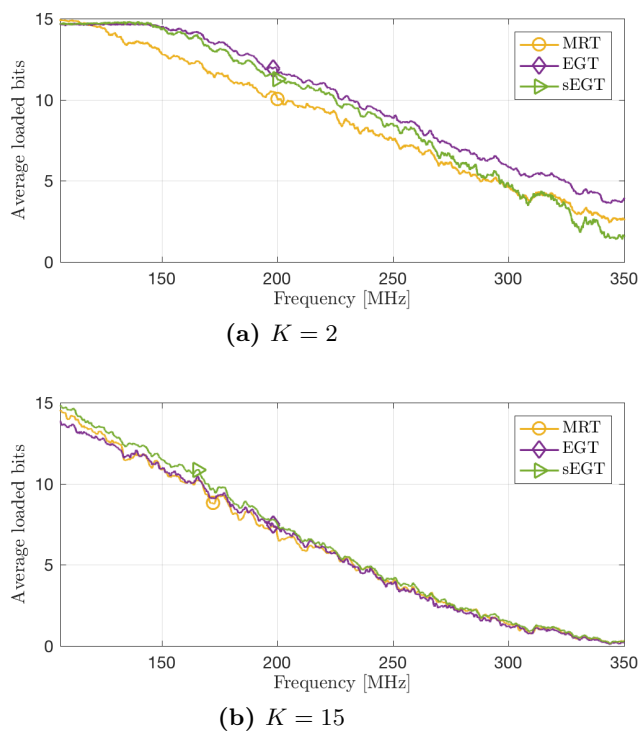
Fig. 2.7: Comparison of the average bit-loading capability between MRT, EGT and sEGT for different number of target users K regarding a non-linear vectoring system over the 106-350 MHz bandwidth of the BT cable.

K in the group varies. The results of the EGT group implement the special sEGT at the mid-range frequencies and implement the regular EGT at the higher frequencies to show the potential of this beamforming structure. For simulations with ZFP (see Figs. 2.8a and 2.9a), the EGT structure is preferred for small K values, while the MRT structure shows obvious advantage when K is larger than a quarter of the number of available pairs N. For simulations with THP (see Figs. 2.8b and 2.9b), the average performance of EGT is better for all K values. Especially when K becomes close to the value of N, applying MRT may yield even lower sum-rate than carrying out the regular THP which does not utilize the auxiliary pairs. In those cases, the loss of conducting MRT in the equivalent direct channel (as the diagonal elements of the triangular matrix out of the QR-decomposition) is higher than the gain in the assigned

(a) ZFP-based system

(b) THP-based system
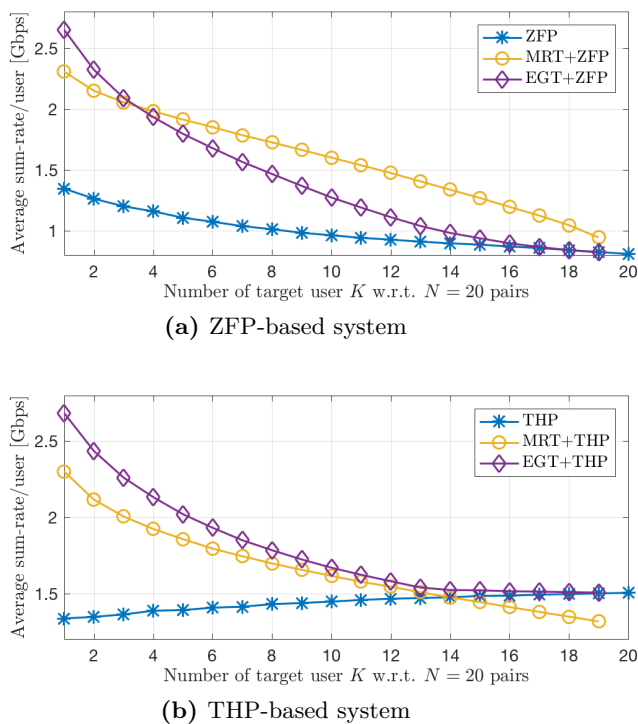
Fig. 2.8: Average sum-rate obtained from the frequencies above $f_0 = 106\,\text{MHz}$ for each of the K target users, considering the 20-pair BT cable. For the case $K = 20$, no resource for beamforming is available.

g_k values.

Additionally, it is observed that systems applying THP may only obtain meaningful rate-boosting from beamforming when K is smaller than half of N. It is more effective to implement beamforming in the ZFP-based systems.

2.5   Conclusions

The previously proposed concept of rate-boosting via beamforming is now complemented by 1) the more practical scenario exploiting unused spectrum on active adjacent pairs; 2) the implementation of both ZFP and THP; 3) three practical beamforming variants; and 4) the transmit power allocation applicable for both precoders with and without beamforming. The new results are
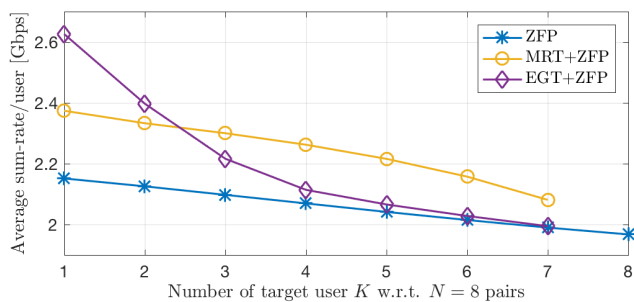
(a) ZFP-based system
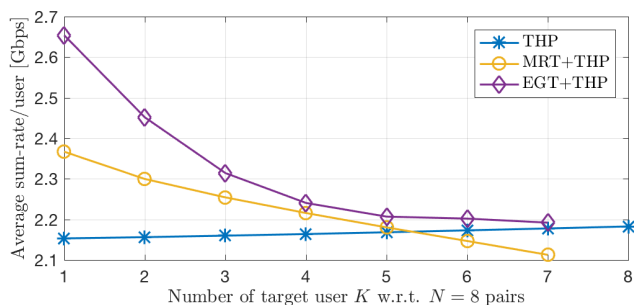
(b) THP-based system

Fig. 2.9: Average sum-rate obtained from the frequencies above $f_0 = 50\,\mathrm{MHz}$ for each of the K target users, considering the 8-pair EAB cable. For the case $K = 8$, no resource for beamforming is available.

thereby more realistic. Particularly based on the adopted cable measurements, the system's bandwidth is divided into two parts: the lower band is dedicated to each pair and its directly connected users applying the regular vectoring, whilst the higher band is used as a shared pool of resources for the target users using beamforming-contained vectoring. The three beamforming variants are suitable for different conditions. For the ZFP-based system, EGT is preferred for small K while MRT is better for large K with respect to the group size N. For the THP-based system, EGT has an overall better performance. Particularly for EGT, an special variant named sEGT is proposed, which can improve the performance of regular EGT at frequencies where the direct channel is still noticeably stronger than the FEXT paths.

2.6   Appendix

This section conducts the assignment of the binary steering parameter for the construction of $\mathbf{P}_{\text{BF, sEGT}}$ in Eq. (2.10). We use the problem formulation which considers each auxiliary pair independently. In the following formulation, each of the corresponding transmit port considers itself as the only active port in the system, connecting to the K receivers via the FEXT paths. On each tone, it chooses one of the K users' symbol to send over. The objective is to maximize the delivered sum-rate over the involved tones from this port within the power budget, no matter which user it dedicates to on each tone.

Let j denote the index of a transmit port connecting to an auxiliary pair. Specifically, path $[\mathbf{H}]_{k,j}$ contributes to the sum-rate of target user k as $\log_2\left(1+\iota_{k,j}c_{k,j}\bar{\gamma}_{k,j}\right)$, or equivalently $\iota_{k,j}\log_2\left(1+c_{k,j}\bar{\gamma}_{k,j}\right)$, where $\bar{\gamma}_{k,j} = |[\mathbf{H}]_{k,j}|^2/(\sigma^2\Gamma)$ denotes the CNR and $c_{k,j}$ is the assigned transmit power corresponding to the selection. Let $\tilde{m} \in [M_0, ..., M]$ denote the tones above the critical frequency f_0, where beamforming starts being involved. Accordingly, we formulate the assignment of $\boldsymbol{\iota}_j = \{\iota_{k,j}^{[\tilde{m}]}|\forall k, \tilde{m}\}$ as a power-allocation-based optimization problem, which becomes similar to the adaptive subcarrier allocation regime of [22]. In our case, the optimization problem for pair j is a mixed integer programming (MIP) problem as

$$
\begin{aligned}
\underset{\mathbf{c}_j, \boldsymbol{\iota}_j}{\text{maximize}} \quad & \sum_{\tilde{m}=M_0}^{M} \sum_{k=1}^{K} \iota_{k,j}^{[\tilde{m}]} \log_2\left(1 + c_{k,j}^{[\tilde{m}]}\bar{\gamma}_{k,j}^{[\tilde{m}]}\right) \\
\text{subject to} \quad & \sum_{k=1}^{K} \iota_{k,j}^{[\tilde{m}]} \leq 1, \forall \tilde{m}. \\
& \sum_{\tilde{m}=M_0}^{M} \sum_{k=1}^{K} c_{k,j}^{[\tilde{m}]} \leq \bar{P}_j' \\
& 0 \leq c_{k,j}^{[\tilde{m}]} \leq \bar{P}_{\text{ub}}^{[\tilde{m}]}, \ \forall \tilde{m}, k. \\
& \iota_{k,j}^{[\tilde{m}]} \in \{0, 1\}, \ \forall \tilde{m}, k.
\end{aligned} \tag{2.11}
$$

where $\bar{P}_j'$ is the remaining total power of port j after filling the spectrum below f_0, and the PSD upper-bound here is defined as

$$
P_{\text{ub}}^{[\tilde{m}]} = \min\left\{ P_{\text{msk}}^{[\tilde{m}]}, \ \max_k\left\{ \frac{2^{\bar{b}} - 1}{\bar{\gamma}_{k,j}^{[\tilde{m}]}} \right\} \right\}, \ \forall \tilde{m}. \tag{2.12}
$$

In the objective function of Eq. (2.11), $R(c_{k,j}) = \log_2\left(1 + c_{k,j}\bar{\gamma}_{k,j}\right)$ is a concave function in $c_{k,j}$. However, $\iota_{k,j}R(c_{k,j})$ is not concave in $(c_{k,j}, \iota_{k,j})$. Let us hence introduce a new parameter $u_{k,j} = c_{k,j}\iota_{k,j}$. The equivalent term of

$\iota_{k,j} R(u_{k,j}/\iota_{k,j})$ becomes a perspective function [23], and therefore is concave in $(u_{k,j}, \iota_{k,j})$. Now we compose the associated Lagrangian function with the aid of $u_{k,j}$ as as

$$L(\mathbf{u}, \boldsymbol{\iota}; \boldsymbol{\mu}, \lambda) = \sum_{\tilde{m}=M_0}^{M} \sum_{k=1}^{K} \iota_{k,j}^{[\tilde{m}]} \log_2 \left(1 + \frac{u_{k,j}^{[\tilde{m}]} \bar{\gamma}_{k,j}^{[\tilde{m}]}}{\iota_{k,j}^{[\tilde{m}]}} \right)$$
$$- \sum_{\tilde{m}=M_0}^{M} \mu^{[\tilde{m}]} \left(\sum_{k=1}^{K} \iota_{k,j}^{[\tilde{m}]} - 1 \right)$$
$$- \lambda \left(\sum_{\tilde{m}=M_0}^{M} \sum_{k=1}^{K} u_{k,j}^{[\tilde{m}]} - \bar{P}_j' \right),$$

where $\mu^{[\tilde{m}]}$ and λ are the Karush-Kuhn-Tucker (KKT) multipliers. The associated dual problem becomes

$$W(\boldsymbol{\mu}, \lambda) = \underset{\mathbf{u}, \boldsymbol{\iota}}{\text{maximize}} \quad L(\mathbf{u}, \boldsymbol{\iota}; \boldsymbol{\mu}, \lambda)$$
$$\text{subject to} \quad \mu^{[\tilde{m}]}, \lambda \geq 0, \ \forall \tilde{m}$$
$$0 \leq u_{k,j}^{[\tilde{m}]} \leq P_{\text{ub}}^{[\tilde{m}]} \iota_{k,j}^{[\tilde{m}]}, \ \forall \tilde{m}, k$$
$$\iota_{k,j}^{[\tilde{m}]} \in \{0, 1\}, \ \forall \tilde{m}, k.$$

The gradient of $L(\mathbf{u}, \boldsymbol{\iota}; \boldsymbol{\mu}, \lambda)$ at each dimension $\hat{u}_{k,j}^{[\tilde{m}]}$ of the optimal variable $\hat{\mathbf{u}}$ satisfies

$$\frac{\partial L}{\partial \hat{u}_{k,j}^{[\tilde{m}]}} = \frac{1}{\ln 2} \left(\frac{1}{\bar{\gamma}_{k,j}^{[\tilde{m}]}} + \frac{\hat{u}_{k,j}^{[\tilde{m}]}}{\iota_{k,j}^{[\tilde{m}]}} \right)^{-1} - \lambda,$$

which varies according to the projection of the objective function onto the feasible region of $u_{k,j}^{[\tilde{m}]}$, $i.e.,$

$$\frac{\partial L}{\partial \hat{u}_{k,j}^{[\tilde{m}]}} \begin{cases} < 0 & \text{if } \hat{u}_{k,j}^{[\tilde{m}]} = 0, \\ = 0 & \text{if } \hat{u}_{k,j}^{[\tilde{m}]} \in \left(0, P_{\text{ub}}^{[\tilde{m}]} \hat{\iota}_{k,j}^{[\tilde{m}]} \right), \\ > 0 & \text{if } \hat{u}_{k,j}^{[\tilde{m}]} = P_{\text{ub}}^{[\tilde{m}]} \hat{\iota}_{k,j}^{[\tilde{m}]}. \end{cases}$$

This is equivalent to

$$\hat{u}_{k,j}^{[\tilde{m}]} = \begin{cases} 0 & \text{if } \lambda > \frac{\bar{\gamma}_{k,j}^{[\tilde{m}]}}{\ln 2}, \\ P_{\text{ub}}^{[\tilde{m}]} \hat{\iota}_{k,j}^{[\tilde{m}]} & \text{if } \lambda < \frac{1}{(\ln 2)\left(1/\bar{\gamma}_{k,j}^{[\tilde{m}]} + P_{\text{ub}}^{[\tilde{m}]} \right)}, \\ \left(\frac{1}{\lambda \ln 2} - \frac{1}{\bar{\gamma}_{k,j}^{[\tilde{m}]}} \right) \hat{\iota}_{k,j}^{[\tilde{m}]} & \text{otherwise.} \end{cases} \qquad (2.13)$$

Similarly, the gradient associated with the optimal variable $\hat{\boldsymbol{\iota}}$ at $\hat{\iota}_{k,j}^{[\tilde{m}]}$ is formulated as

$$\frac{\partial L}{\hat{\iota}_{k,j}^{[\tilde{m}]}} = \log_2\left(1 + \frac{\hat{u}_{k,j}^{[\tilde{m}]}\bar{\gamma}_{k,j}^{[\tilde{m}]}}{\hat{\iota}_{k,j}^{[\tilde{m}]}}\right) - \frac{\frac{\hat{u}_{k,j}^{[\tilde{m}]}\bar{\gamma}_{k,j}^{[\tilde{m}]}}{\hat{\iota}_{k,j}^{[\tilde{m}]}}}{(\ln 2)\left(1 + \frac{\hat{u}_{k,j}^{[\tilde{m}]}\bar{\gamma}_{k,j}^{[\tilde{m}]}}{\hat{\iota}_{k,j}^{[\tilde{m}]}}\right)} - \mu^{[\tilde{m}]}$$

$$= O(k, \tilde{m}) - \mu^{[\tilde{m}]}, \tag{2.14}$$

where $O(k, \tilde{m})$ is a function of $\hat{u}_{k,j}^{[\tilde{m}]}$. From Eq. (2.13) we have:

$$O(k, \tilde{m}) = \log_2\left(1 + \frac{\hat{u}_{k,j}^{[\tilde{m}]}\bar{\gamma}_{k,j}^{[\tilde{m}]}}{\hat{\iota}_{k,j}^{[\tilde{m}]}}\right) - \frac{\frac{\hat{u}_{k,j}^{[\tilde{m}]}\bar{\gamma}_{k,j}^{[\tilde{m}]}}{\hat{\iota}_{k,j}^{[\tilde{m}]}}}{(\ln 2)\left(1 + \frac{\hat{u}_{k,j}^{[\tilde{m}]}\bar{\gamma}_{k,j}^{[\tilde{m}]}}{\hat{\iota}_{k,j}^{[\tilde{m}]}}\right)}$$

$$= \begin{cases} 0 & \text{if } \lambda > \frac{\bar{\gamma}_{k,j}^{[\tilde{m}]}}{\ln 2}, \\ o_1(k, \tilde{m}) & \text{if } \lambda < \frac{1}{(\ln 2)\left(1/\bar{\gamma}_{k,j}^{[\tilde{m}]} + P_{\text{ub}}^{[\tilde{m}]}\right)}, \\ o_2(k, \tilde{m}) & \text{otherwise} \end{cases} \tag{2.15}$$

with

$$o_1(k, \tilde{m}) = \log_2\left(1 + P_{\text{ub}}^{[\tilde{m}]}\bar{\gamma}_{k,j}^{[\tilde{m}]}\right) - \frac{P_{\text{ub}}^{[\tilde{m}]}\bar{\gamma}_{k,j}^{[\tilde{m}]}}{(\ln 2)\left(1 + P_{\text{ub}}^{[\tilde{m}]}\bar{\gamma}_{k,j}^{[\tilde{m}]}\right)},$$

$$o_2(k, \tilde{m}) = \log_2\left(\frac{\bar{\gamma}_{k,j}^{[\tilde{m}]}}{\lambda \ln 2}\right) - \frac{1}{\ln 2} - \frac{\lambda}{\bar{\gamma}_{k,j}^{[\tilde{m}]}}.$$

Again concerning the feasible region of $\iota_{k,j}^{[\tilde{m}]}$, the gradient in Eq. (2.14) obeys:

$$\frac{\partial L}{\hat{\iota}_{k,j}^{[\tilde{m}]}} \begin{cases} < 0 & \text{if } \hat{\iota}_{k,j}^{[\tilde{m}]} = 0, \\ > 0 & \text{if } \hat{\iota}_{k,j}^{[\tilde{m}]} = 1, \end{cases}$$

which can be interpreted with the form of Eq. (2.14) as

$$\hat{\iota}_{k,j}^{[\tilde{m}]} = \begin{cases} 0 & \text{if } \mu^{[\tilde{m}]} > O(k, \tilde{m}), \\ 1 & \text{if } \mu^{[\tilde{m}]} < O(k, \tilde{m}). \end{cases} \tag{2.16}$$

Note that $\mu^{[\tilde{m}]}$ is a constant for each tone, *i.e.*, independent of k, and the frequency orthogonality requirement indicates that there is at most one $\hat{\iota}_{k,j}^{[\tilde{m}]} =$

1, $\forall \tilde{m}$. Eq. (2.16) implies that $\mu^{[\tilde{m}]}$ will only be smaller than the largest $O(k, \tilde{m})$ if we have $\sum_{k=1}^{K} \hat{\iota}_{k,j}^{[\tilde{m}]} = 1$ for a certain $\tilde{m}$. Therefore, only the target user k that yields the largest $\hat{O}(k, \tilde{m})$ in Eq. (2.15) is entitled to use the auxiliary pair j at tone $\tilde{m}$, *i.e.,* we have

$$\hat{\iota}_{k,j}^{[\tilde{m}]} = \begin{cases} 1 & \text{if } k = \arg \max_{k' \in [1,...,K]} O(k', \tilde{m}), \\ 0 & \text{otherwise,} \end{cases} \qquad \forall \tilde{m}. \qquad (2.17)$$

Observe that in the pivotal Eqs. (2.13) and (2.15), λ is the critical parameter leading to the optimal variables $\hat{u}_{k,j}^{[\tilde{m}]}$ and $\hat{\iota}_{k,j}^{[\tilde{m}]}$. We start solving the dual problem by initializing the KKT multiplier λ assisted by the water level concept as

$$\lambda = \frac{(M - M_0 + 1)K}{(\ln 2)\left(\bar{P}_j' + \sum_{\tilde{m}=M_0}^{M} \sum_{k=1}^{K} \left(1/\bar{\gamma}_{k,j}^{[\tilde{m}]}\right) \right)}, \qquad (2.18)$$

which is a scaled inverse of the water level. We then update λ iteratively using a step size of Δ_λ for gradually approaching the aggregate transmit power limit. Details about the updating strategy are is summarized in Table 2.4. Specifically, $\epsilon = 1.15$ and $tol = 0.005$ are used in our simulations.

References

[1] ITU, "Fast Access to Subscriber Terminals (G.fast) - Physical Layer Specification," Recommendation Draft ITU-T G.9701, 2014. [Online]. Available: https://www.itu.int/rec/T-REC-G.9701/en

[2] M. Timmers, M. Guenach, C. Nuzman, and J. Maes, "G.fast: Evolving the Copper Access Network," in *IEEE Communications Magazine*, vol. 51, no. 8, pp. 74-79, August 2013.

[3] V. Oksman, R. Strobel, X. Wang, D. Wei, R. Verbin, R. Goodson, and M. Sorbara, "The ITU-T's New G.fast Standard Brings DSL into the Gigabit Era," in *IEEE Communications Magazine*, vol. 54, no. 3, pp. 118-126, March 2016.

[4] G. Ginis and J. Cioffi, "Vectored Transmission for Digital Subscriber Line Systems," in *IEEE Journal on Selected Areas in Communications*, vol, 20, no. 5, pp. 1085-1104, June 2002.

Table 2.4: Proposed iteration for optimizing the steering coefficients

---

Regarding transmit port j
Main output: $\hat{\imath}_{k,j}^{[\tilde{m}]}$, $\forall \tilde{m}, k$

Initialize
- $P_{\text{ub}}^{[\tilde{m}]}$ as in Eq. (2.12);
- $i_0 = 1$ and $\tau_{\text{prev}} = 1$;
- $U = \infty$;

---

while $(U > \bar{P}_j')\ |\ \left((\bar{P}_j' - U)/\bar{P}_j' > tol\right)$ **do**

    if $U > \bar{P}_j'$ **then**

        - $\lambda = \lambda + \Delta_\lambda$ and $\tau_{\text{current}} = 1$;

    else

        - $\lambda = \lambda - \Delta_\lambda$ and $\tau_{\text{current}} = 0$;

    end if

    if $\tau_{\text{current}} \neq \tau_{\text{prev}}$ **then**

        - $i_0 = i_0 + 1$ and $\tau_{\text{prev}} = \tau_{\text{current}}$;

    end if

    - $\Delta_\lambda = \lambda \cdot \epsilon^{-i_0}$;

    - Calculate $O(k, \tilde{m})$, $\forall \tilde{m}, k$ as in Eq. (2.15);

    - Calculate $\hat{\imath}_{k,j}^{[\tilde{m}]}$, $\forall \tilde{m}, k$ as in Eq. (2.17);

    - Calculate $\hat{u}_{k,j}^{[\tilde{m}]}$, $\forall \tilde{m}, k$ as in Eq. (2.13);

    - $U = \sum_{\tilde{m}=M_0}^{M} \sum_{k=1}^{K} \hat{u}_{k,j}^{[\tilde{m}]}$;

end while

---

[5] Y. Huang, T. Magesacher, E. Medeiros, C. Lu, P.-E. Eriksson and P. Ödling, "Rate-Boosting Using Strong Crosstalk in Next Generation Wireline Systems," in *Proc. 2015 IEEE Global Communications Conference (GLOBECOM)*, San Diego, CA, 2015, pp. 1-6.

[6] P. Ödling, T. Magesacher, S. Höst, P. O. Börjesson, M. Berg, and E. Areizaga, "The Fourth Generation Broadband Concept," in *IEEE Communications Magazine*, vol. 47, no. 1, pp. 62-69, January 2009.

[7] M. Di Renzo, H. Haas, A. Ghrayeb, S. Sugiura, and L. Hanzo, "Spatial Modulation for Generalized MIMO: Challenges, Opportunities, and Implementation," in *Proceedings of the IEEE*, vol. 102, no. 1, pp. 56-103, Jan. 2014.

[8] S. M. Alamouti, "A Simple Transmit Diversity Technique for Wireless Communications," in *IEEE Journal on Selected Areas in Communications*, vol. 16, no. 8, pp. 1451-1458, Oct 1998.

[9] V. Tarokh, A. Naguib, N. Seshadri, and A. R. Calderbank, "Space-Time Codes for High Data Rate Wireless Communication: Performance Criteria in the Presence of Channel Estimation Errors, Mobility, and Multiple Paths," in *IEEE Transactions on Communications*, vol. 47, no. 2, pp. 199-207, Feb 1999.

[10] R. Cendrillon, M. Moonen, J. Verlinden, T. Bostoen, and G. Ginis, "Improved Linear Crosstalk Precompensation for DSL," in *Proc. 2004 IEEE International Conference on Acoustics, Speech, and Signal Processing (ICASSP)*, 2004, pp. iv-1053-6 vol.4.

[11] R. Cendrillon, G. Ginis, E. Van den Bogaert, and M. Moonen, "A Near-Optimal Linear Crosstalk Precoder for Downstream VDSL," in *IEEE Transactions on Communications*, vol. 55, no. 5, pp. 860-863, May 2007.

[12] G. Ginis and J. M. Cioffi, "A Multi-user Precoding Scheme Achieving Crosstalk Cancellation with Application to DSL Systems," in *Proc. Conference Record of the Thirty-Fourth Asilomar Conference on Signals, Systems and Computers*, vol.2, November 2000, pp. 1627-1631.

[13] ITU, "Fast Access to Subscriber Terminals (G.fast) – Power Spectral Density Specification," Recommendation Draft ITU-T G.9700, 2014. [Online]. Available: http://www.itu.int/rec/T-REC-G.9700-201404-I

[14] J. Maes, C. Nuzman, and P. Tsiaflakis, "Sensitivity of Nonlinear Precoding to Imperfect Channel State information in G.fast," in *Proc. 2016 24th European Signal Processing Conference (EUSIPCO)*, Budapest, 2016, pp. 290-294.

[15] Alcatel-Lucent, "G.fast: Perspectives on Nonlinear Precoding," Contribution ITU-T SG15/Q4 2016-06-Q4-041, June 2016.

[16] Intel, "G.fast: Use of Linear Precoding on Frequencies above 106 MHz," Contribution ITU-T SG15/Q4 2016-05-11-Q4-023, May 2016.

[17] Intel, "G.fast: Rate-Reach Comparison for Linear and Non-Linear Precoding up to 212 MHz," Contribution ITU-T SG15/Q4 2016-06-Q4-072R1, June 2016.

[18] M. Guenach, C. Nuzman, P. Tsiaflakis and J. Maes, "Power Optimization in Vectored and Non-vectored G.fast Transmission," in *Proc. 2014 IEEE Global Communications Conference*, Austin, TX, 2014, pp. 2229-2233.

[19] J. Maes and C. Nuzman, "Energy Efficient Discontinuous Operation in Vectored G.fast," in *Proc. 2014 IEEE International Conference on Communications (ICC)*, Sydney, NSW, 2014, pp. 3854-3858.

[20] ASSIA, "Signal Processing for the G.fast 212 MHz Profile," Berlin, Contribution ITU-T 2016-04-Q4-24, April 2016.

[21] Ikanos, "G.fast: Constellations for Use with Non-linear Pre-coding," Contribution ITU-T 2013-01-Q4-028, January 2013.

[22] C. Y. Wong, R. S. Cheng, K. B. Lataief, and R. D. Murch, "Multiuser OFDM with Adaptive Subcarrier, Bit, and Power Allocation," in *IEEE Journal on Selected Areas in Communications*, vol. 17, no. 10, pp. 1747-1758, Oct 1999.

[23] S. Boyd and L. Vandenberghe, *Convex Optimization*. Cambridge University Press, 2014.

Paper III

3   Mitigating Disorderly Leaving Events in G.fast

Abstract

Vectoring is a vital component of wideband wireline communication systems. A disorderly leaving event (DLE) disturbs the vectoring operation since the precoder, which was designed for the channel before the change, is no longer up to date. Measurements indicate that the impact of a DLE can be serious for frequencies beyond 30 MHz, which corresponds to the band used by emerging wideband communication systems over short multi-pair copper cables such as G.fast. As an alternative to the state-of-the-art update procedure, this paper presents an approach to mitigating the DLE problem. By interpreting DLE with the FEXT-reflected-NEXT (FRN) model, we propose a scheme that enables the showtime lines to return to disturbance-free transmission once the loss of signal on a certain line is detected while updating the precoder as a background process. Furthermore, the estimation complexity for a K-user vectoring group is reduced from $\mathcal{O}(K^2)$ to $\mathcal{O}(K)$.

3.1   Introduction

The widespread deployment of cloud-based services and video-on-demand of-
ferings continues to drive data rate and quality of service requirements for
last-mile connections. In response to this trend, the wireline access industry
advances towards a fiber to the last distribution point paradigm [1]. In this sce-
nario, the recently consented G.fast standard [2] exploits shorter copper pairs
and high bandwidth to provide up to around 1 Gbits/s aggregate net data rate.

Modern wideband wireline communication systems (such as G.fast) em-
ploy techniques referred to as vectoring [3] in order to cooperatively mitigate
crosstalk. As vectoring relies on accurate channel information, changes of the
terminating impedance in the multi-port wireline channel may cause severe
performance degradation in terms of signal-to-noise ratio (SNR) as exempli-
fied in Fig. 3.1. A change of impedance alters the perceived channel coupling
conditions, and leads to residual crosstalk caused by an outdated precoder (or
equalizer).

A particular event resulting in sudden termination change occurs when a
modem *within* an active vectored group is turned off abruptly or is disconnected
due to line disruption. This occurrence is called a disorderly leaving event
(DLE), and was first reported during the development of vectored VDSL2 [3].
A fast channel tracking method was proposed in [4] to deal with DLEs in
VDSL2. Unfortunately, it cannot be applied to G.fast since it is based on the
assumption that only one column of the channel matrix changes.

In [5], a procedure is described that allows G.fast transceivers to leave a
vectored group without negatively impacting the performance of other lines in
the same bundle. The main idea is to allow coordination between transceivers at
both ends, and acquire information necessary to update the precoder/equalizer
before the line leaves and its termination impedance changes. While solving
the problem of orderly leaving events, [5] does not address situations where
there is no previous intent announced by the leaving transceiver(s).

This paper has two main contributions: First, we extend the model pre-
sented in [6, 7] to address DLEs, and identify the source of DLE disturbance
that we can control. Second, we develop a novel precoder update procedure
that does not disturb other lines while performing channel estimation as a
background process.

The paper is organized as follows. In Section 3.2 a system model is pre-
sented to explain DLE. Taking advantage of this model, we formulate the DLE
disturbance in Section 3.3 and propose in Section 3.4 a parameter-based chan-
nel estimation procedure that minimizes the impact of DLEs for the remaining
active users. Section 3.5 demonstrates the effectiveness of the proposed method
with channel measurements and simulations. Section 3.6 concludes the work.
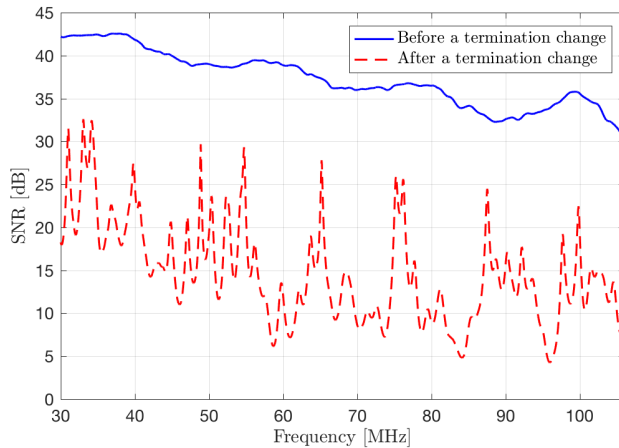
Fig. 3.1: SNR on one victim line before and after a termination change. The SNR drop represents the impact of a disrupted vectoring.

Notation: Bold capital letters (*e.g.,* **A**) and bold lower-case letters (*e.g.,* **a**) denote matrices and column vectors, respectively. $a_{i,j}$ is an element on the i-th row and j-th column of **A** and a_i is the i-th element of **a**. $\mathbf{I}_{n\backslash i}$ is an n-dimensional identity matrix excluding the i-th row. $\mathcal{M}_i\{\mathbf{A}\}$ denotes an operator deleting both the i-th row and column from **A**. Operator "$\backslash$" excludes certain element(s) on the right-hand side from the set on the left-hand side.

3.2   FEXT-Reflected-NEXT (FRN) Model for DLE

Consider a wideband discrete multi-tone modulation (DMT) system with a group of K twisted pairs (or equivalently, users). The twisted pairs connect the transceivers at the distribution point (DP) with the customer-premises equipment (CPE).

In [6,7], a FEXT-reflected-NEXT (FRN) model is proposed to characterize the changed coupling condition due to an alien-line impedance mismatch at the CPE. A DLE is similar—except now the impedance change happens within the vectored group as illustrated in Fig. 3.2. Without loss of generality, we illustrate the DLE coupling model in downstream on a certain sub-carrier. Since G.fast employs time-division duplex (TDD), the model for downstream
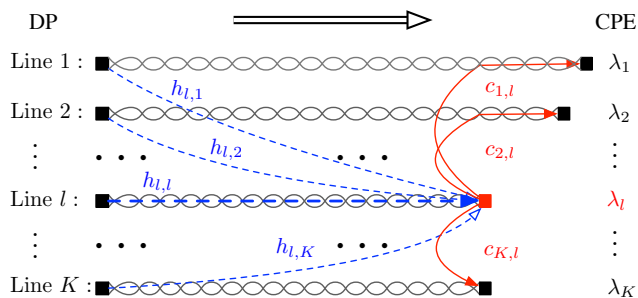
Fig. 3.2: Downstream FRN model. *Dash lines*: Channel paths from DP to the mismatched termination l. *Solid lines*: near-end coupling paths from the mismatched termination l to the remaining CPEs.

applies, *mutatis mutandis*, to upstream.

Let $\mathbf{H} \in \mathbb{C}^{K \times K}$ denote the frequency-domain channel matrix on a certain sub-carrier for the perfectly-terminated case, where diagonal and off-diagonal elements are direct-channel coefficients and far-end crosstalk (FEXT) coefficients, respectively. For the sake of simple notation, but without loss of generality, the sub-carrier index is omitted. Let $\mathbf{\Lambda} = \mathrm{diag}\left([\lambda_1, \lambda_2, \ldots, \lambda_K]\right) \in \mathbb{C}^{K \times K}$ denote a diagonal matrix with termination reflection coefficients and let $\mathbf{C} \in \mathbb{C}^{K \times K}$ denote the near-end crosstalk (NEXT) coupling matrix at the CPE-side. For scenarios with unequal pair-lengths, $\mathbf{C}$ denotes attenuated NEXT (as illustrated in Fig. 3.2 for the l-th column of $\mathbf{C}$). The diagonal entries of $\mathbf{C}$, corresponding to the CPE-side echo coefficients, are assumed to be 0. The channel matrix $\mathbf{H}'$ for the general case is

$$\mathbf{H}' = \mathbf{H} + \mathbf{\Delta},$$

where $\mathbf{\Delta} = \mathbf{C}\mathbf{\Lambda}\mathbf{H}$ quantifies the deviation from the all-terminated case according to the FRN model. When the terminations at the CPE are perfectly matched (*i.e.,* $\lambda_i = 0$ for $i = 1, \ldots, K$), then $\mathbf{\Delta} = \mathbf{0}$ and thus $\mathbf{H}' = \mathbf{H}$.

Vectoring enables cooperative signal processing within the group. A properly designed precoder in downstream and equalizer in upstream at the DP significantly reduces FEXT. In this work, we focus on linear precoding and thus on the frequency range up to 106 MHz (cf. [2]). Specifically in downstream, let $\mathbf{G} = \mathrm{diag}\left([g_1, g_2, \ldots, g_K]\right) \in \mathbb{R}^{K \times K}$ denote a diagonal matrix with the gain adjusters for each line on the main diagonal. Assume that the cyclic prefix of DMT is not shorter than the impulse responses of the coupling paths. Furthermore, assume that the inverse fast Fourier transform (IFFT) for the

group users is well synchronized. After including linear precoder $\mathbf{P}_o$, transmitting $\mathbf{x} \in \mathbb{C}^{K \times 1}$ at the DP side yields the receive signal $\mathbf{y} \in \mathbb{C}^{K \times 1}$ given by

$$\mathbf{y} = \mathbf{H}'\mathbf{P}_o\mathbf{Gx} + \mathbf{n},$$

where $\mathbf{n} \in \mathbb{C}^{K \times 1}$ denotes the background noise. An ideal precoder designed for $\mathbf{H}$ at DP neutralizes the crosstalk effectively such that for the input symbols $\mathbf{x}$

$$\mathbf{HP}_o\mathbf{Gx} = \mathbf{\Sigma x}, \tag{3.1}$$

where $\mathbf{\Sigma} \in \mathbb{C}^{K \times K}$ is diagonal.

In practice, most often only one diagonal element of $\mathbf{\Lambda}$ will deviate significantly from 0 as a result of a DLE (*i.e.,* mismatch of a single line only). Assume line l exhibits a DLE, which is quantified by a reflection coefficient $|\lambda_l| \gg 0$. Consequently, $\mathbf{\Delta} \neq \mathbf{0}$ and all FEXT coupling coefficients change. The new FEXT arriving at termination $k, (k \neq l)$ is determined by

$$(\mathbf{h}'_k)^{\mathrm{T}} = \mathbf{h}_k^{\mathrm{T}} + c_{k,l}\lambda_l\mathbf{h}_l^{\mathrm{T}},$$

where $\mathbf{h}_l^{\mathrm{T}}$ indicates the l-th row of $\mathbf{H}$, and $(\mathbf{h}'_k)^{\mathrm{T}}$ is the k-th row of $\mathbf{H}'$. The outdated precoding with $\mathbf{P}_o$ fulfilling Eq. (3.1) yields the disturbed receive signal

$$\mathbf{y}' = \underbrace{\mathbf{HP}_o\mathbf{Gx} + \mathbf{n}}_{\mathbf{y}_d} + \underbrace{\mathbf{C\Lambda HP}_o\mathbf{Gx}}_{\mathbf{\xi}}, \tag{3.2}$$

where $\mathbf{y}_d$ is the desired receive signal obtained in the perfectly-terminated case and $\mathbf{\xi}$ is the residual crosstalk due to the DLE. Equivalently, the effective channel changes from $\mathbf{H}$ to $\mathbf{H}' = \mathbf{H} + \mathbf{\Delta}$.

The FRN model described in [6, 7] suggests that FEXT arrives at and is reflected by the alien mismatched termination only. Compared to the alien-line case, in a DLE the leaving line is always active. As the direct path $h_{l,l}$ has a lower channel attenuation than the FEXT paths $h_{l,k}$, $k \in \{1, \ldots, K\}\backslash l$, the residual-crosstalk issue in a DLE could be even worse.

We demonstrate the impact of a DLE on the channel coupling conditions by means of crosstalk-paths and direct-path measurements from a 30-pair, 100 m, 0.5 mm cable [8]. 10 pairs from a single binder were chosen at random. The measurement points follow a 51.75 kHz sub-carrier spacing, and we consider 2 048 sub-carriers in total corresponding to the frequency range up to 106 MHz. The all-terminated case and a DLE-case where line $l = 10$ is left unterminated yield two 10×10 matrices $\mathbf{H}$ and $\mathbf{H}'$ respectively. The 10-th row of $\mathbf{H}'$ is left the same as that of $\mathbf{H}$. The corresponding channel-matrix deviation is thus given by $\mathbf{\Delta} = \mathbf{H}' - \mathbf{H}$. We quantify the impact of this DLE on vectoring in
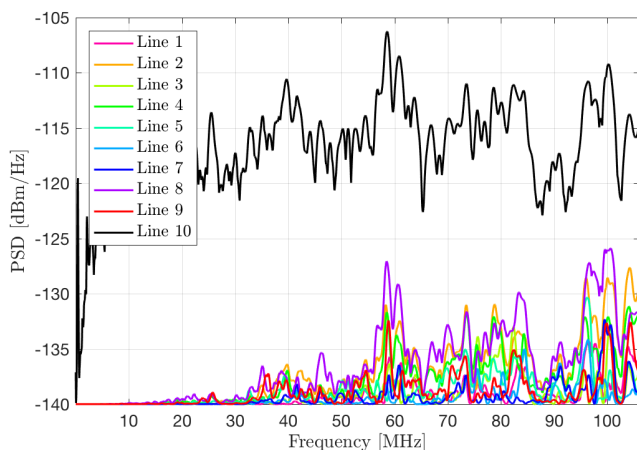
Fig. 3.3: Comparison of the strongest crosstalk caused by each column of $\boldsymbol{\Delta}$, when having a vectored group size of $K = 10$ and line $l = 10$ is leaving.

terms of the worst residual crosstalk $\mathcal{P}_k^{\mathrm{rx}}$ over all lines

$$\mathcal{P}_k^{\mathrm{rx}} = \mathcal{P}^{\mathrm{tx}} + 20 \log_{10}(\max_i |\delta_{i,k}|), \tag{3.3}$$

when line k is excited by a signal with transmit power spectrum density (PSD) $\mathcal{P}^{\mathrm{tx}}$. In essence, Eq. (3.3) evaluates the maximum power of the k-th column of $\boldsymbol{\Delta}$.

Fig. 3.3 shows the crosstalk power for $\mathcal{P}^{\mathrm{tx}} = -76\,\mathrm{dBm/Hz}$ with respect to the background noise of $-140\,\mathrm{dBm/Hz}$. Clearly, the channel changes in the column $l = 10$ (black curve) are dominant, which is consistent with the assumption in [4]. However, channel changes in the other columns become disturbing for frequencies beyond 30 MHz. Except for the l-th row, every other entry of $\boldsymbol{\Delta}$ contributes to the new channel $\mathbf{H}'$. Equivalently, almost every element of $\mathbf{H}$ changes due to a DLE.

3.3   Residual Crosstalk Analysis

In downstream direction, changed channel coupling conditions result in an outdated precoder. Specifically, the linear precoder as in [9] defines

$$\mathbf{P}_o = \mathbf{H}^{-1}\mathbf{H}_\Sigma, \tag{3.4}$$

where the diagonal matrix $\mathbf{H}_\Sigma$ contains direct channel coefficients of the all-terminated channel $\mathbf{H}$.

Consider the DLE case where line l leaves while all other lines are perfectly terminated. Thus, $\mathbf{\Lambda} = \mathrm{diag}\,([0,\ldots,0,\lambda_l,0,\ldots,0])$ and the resulting reflection-followed-by-NEXT paths $\mathbf{C\Lambda}$ are given by

$$\mathbf{C\Lambda} = \begin{bmatrix} \mathbf{0} & \ldots & \mathbf{0} & \mathbf{v}_l & \mathbf{0} & \ldots & \mathbf{0} \end{bmatrix}, \tag{3.5}$$

where the reflecting crosstalk coefficients are defined in a vector as

$$\mathbf{v}_l = \lambda_l \left[c_{1,l},\ldots,c_{i,l},\ldots,c_{K,l}\right]^{\mathrm{T}}. \tag{3.6}$$

According to Eq. (3.2), the residual crosstalk when using the outdated precoder $\mathbf{P}_o$ is given by

$$\begin{aligned}\boldsymbol{\xi} &= \mathbf{C\Lambda H P}_o\mathbf{Gx} \\ &= \mathbf{C\Lambda H}_\Sigma\mathbf{Gx}.\end{aligned} \tag{3.7}$$

Using Eq. (3.5), the expression (3.7) for the residual crosstalk simplifies to

$$\begin{aligned}\boldsymbol{\xi} &= \mathbf{v}_l h_{l,l} g_l x_l \\ &= \mathbf{v}_l \sigma_l x_l,\end{aligned} \tag{3.8}$$

where x_l is the l-th element of $\mathbf{x}$, and $\sigma_l = h_{l,l} g_l$ is the effective gain for path l.

Eq. (3.8) reveals that retaining the outdated precoder $\mathbf{P}_o$ can eliminate the possible FEXT-reflected-NEXT components since the precoder keeps doing its job of mitigating/eliminating FEXT arriving at the reflective surface of termination l. The only source of the residual crosstalk $\boldsymbol{\xi}$ is the transmitted signal x_l on the leaving line via the l-th direct channel $h_{l,l}$ (see the bold dash line in Fig. 3.2), which is then reflected and couples to other CPEs via $\mathbf{v}_l$.

A traditional reaction to DLE, however, is to stop transmission on the leaving line as soon as possible, and quickly update the linear precoder at the DP to $\overline{\mathbf{P}}$ fulfilling

$$\mathcal{M}_l\left\{\mathbf{H}\right\}\overline{\mathbf{P}}\mathcal{M}_l\left\{\mathbf{G}\right\} = \mathcal{M}_l\left\{\mathbf{\Sigma}\right\}, \tag{3.9}$$

to diagonalize the dimension-reduced original channel $\mathcal{M}_l\left\{\mathbf{H}\right\}$. The FRN model implies that stopping transmission on the leaving line only avoids FEXT from line l (*i.e.,* the l-th column of $\mathbf{H}$), but does not avoid FEXT to line l (*i.e.,* the l-th row of $\mathbf{H}$). Instant update of the precoder to $\overline{\mathbf{P}}$ does not cancel FEXT through paths $h_{l,k}$ for $k \in \{1,\ldots,K\}\backslash l$, which are then reflected at mismatched port and couple as NEXT to the victim lines resulting in residual crosstalk. Moreover, immediate line shutoff is sensitive to DLE false alarm or detection failure [4], which leads to unnecessary retraining of the transceivers.
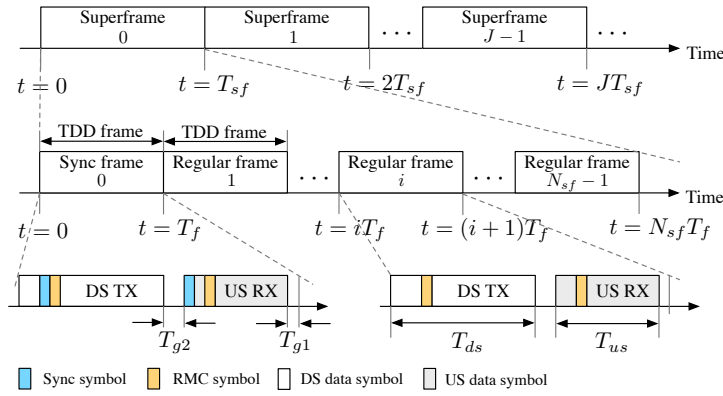
Fig. 3.4: G.fast TDD structure at the DP-side. Time gaps are reserved between paired down- and up-stream as T_{g2} and between upstream and next downstream as T_{g1}. The sum of the T_{g1} and T_{g2} equals to one DMT symbol duration.

In the upstream direction, the FRN model suggests that the leaving line l "emits" an unwanted upstream signal as a result of "incoming" NEXT being reflected by the mismatched port at the CPE side. The resulting upstream FEXT through coupling into $k \in \{1, \ldots, K\} \backslash l$ is taken care of by the interference canceler, whose coefficients are still correct for coupling paths from line l at the CPE to lines $k \in \{1, \ldots, K\} \backslash l$ at the DP. The resulting upstream FEXT coefficients from lines $k \in \{1, \ldots, K\} \backslash l$ into line l change and cause residual FEXT at the interference canceler output on line l, which is no problem since transmission on line l is interrupted anyway.

3.4 Proposed Residual-Crosstalk-Free Channel Estimation

A reference time-line for G.fast TDD frames is shown in Fig. 3.4. A typical TDD frame is $T_f = 750\,\mu s$ long and consists of $N_f = 36$ DMT symbols. A superframe for this setting consists of $N_{sf} = 8$ TDD frames. The first frame of each superframe is a sync-frame, which contains one synchronization symbol located at a predefined symbol position in both directions. The sync-frame is then followed by 7 regular frames without synchronization symbols.

Assume that a DLE happens at time instant t_l at the CPE. In case t_l falls into a downstream transmission interval of the i-th TDD frame ($t_l \in \big[(i-1)T_f, (i-1)T_f + T_{ds}\big]$), the DP will detect this event during the next upstream
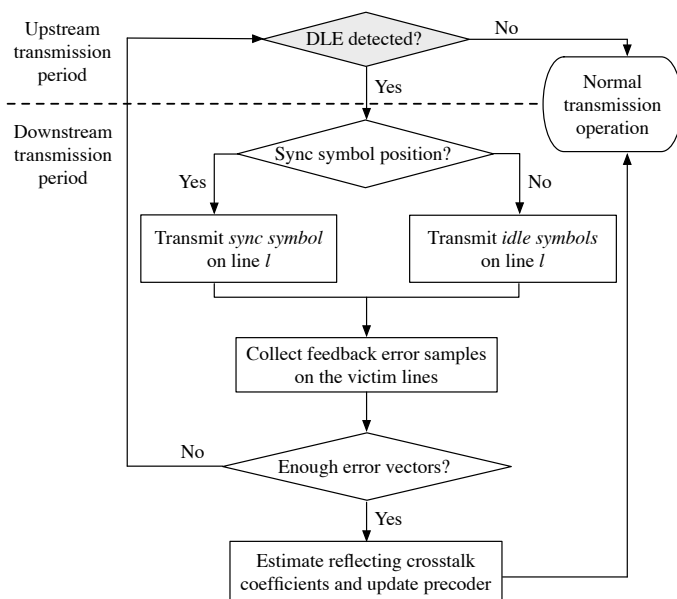
Fig. 3.5: Flowchart of proposed operation at the DP-side

transmission period $\left(t \in \left[(i-1)T_f + T_{ds} + T_{g2}, iT_f - T_{g1}\right]\right)$. The DP initiates upstream channel tracking and in the next downstream transmission period and onwards $(t \geq iT_f)$, it transmits *idle symbols* [2] at non-synchronization symbol positions on the leaving line l. The main idea is to mute the data symbols on line l but keep transmitting the anti-crosstalk signals to cancel out FEXT arriving at the mismatched termination of line l at the CPE. According to the FRN model (cf. Fig. 3.2), there is thus no energy to cause reflections and subsequent NEXT into the other lines. A more detailed illustration for this special operation will be given below. If the DLE occurs during an upstream transmission interval, the channel tracking for upstream and "muting line l" for downstream launch directly.

Generally, instead of turning off the leaving line immediately after detecting a loss of signal (*los*), channel estimation and precoder update in downstream direction is accomplished by alternating two kinds of special symbols: idle symbols and synchronization symbols (as illustrated in Fig. 3.5).

Silent mode By modifying the l-th gain adjuster to be $g_l = 0$ at non-synchronization symbol positions, idle symbols are transmitted on the leav-

ing line. The residual crosstalk $\boldsymbol{\xi}$ in Eq. (3.8) on the victim lines becomes $\boldsymbol{\xi} = \mathbf{v}_l h_{l,l} x_l \cdot 0 = 0$. It enables "silent" estimation and updating in the sense that active users remain undisturbed. Thus, we call this kind of transmission mode *silent mode*. The DLE noisy period is at most $T_{ds} + T_{g2}$ before *los* on line l is detected.

Synchronization mode Synchronization symbols are transmitted every 6 ms (*i.e.,* one superframe duration) on each line in G.fast. Assume J superframes are required before the estimation is completed. Let t_j be the time instant to transmit the j-th downstream synchronization symbol. In this specific time slot, the l-th gain adjuster is set back to g_l, which is used for transmission before DLE. According to Eq. (3.1), Eq. (3.2) and Eq. (3.8), transmitting synchronization symbol $\mathbf{s}(t_j) = [s_1(t_j), \ldots, s_l(t_j), \ldots, s_K(t_j)]^{\mathrm{T}}$ yields

$$\begin{aligned}
\mathbf{q}(t_j) &= \boldsymbol{\Sigma}\mathbf{s}(t_j) + \mathbf{v}_l \sigma_l s_l(t_j) + \mathbf{n} \\
&= \boldsymbol{\Sigma}\left(\mathbf{s}(t_j) + \mathbf{e}(t_j)\right),
\end{aligned}$$

where $\mathbf{e}(t_j) = \boldsymbol{\Sigma}^{-1}\left(\mathbf{v}_l \sigma_l s_l(t_j) + \mathbf{n}\right)$. The synchronization error samples $\mathbf{I}_{K\backslash l}\mathbf{e}(t_j)$ on the victim lines are then fed back to the DP [2].

After sending the synchronization symbol at the scheduled time instant, the transmission on line l goes back to idle symbols for all non-synchronization symbol positions. Keep on alternatively sending idle symbols and synchronization symbols on the leaving line until DP collects J error symbols on the victim lines as

$$\begin{aligned}
\mathbf{E} &= \mathbf{I}_{K\backslash l}\left[\mathbf{e}(t_1), \mathbf{e}(t_2), \ldots, \mathbf{e}(t_J)\right] \\
&= \mathbf{I}_{K\backslash l}\boldsymbol{\Sigma}^{-1}\mathbf{v}_l \sigma_l \mathbf{s}_l^{\mathrm{T}} + \mathbf{N},
\end{aligned}$$

where $\mathbf{s}_l = [s_l(t_1), \ldots, s_l(t_J)]^{\mathrm{T}}$ is the synchronization sequence transmitted on the leaving line l at t_j $(j = 1, \ldots, J)$, and $\mathbf{N} \in \mathbb{C}^{(K-1)\times J}$ is the equalized additive noise on victim lines for J synchronization time instants. The contributing reflecting crosstalk coefficients in Eq. (3.6) can be estimated by

$$\widehat{\mathbf{v}}_l = \frac{\mathcal{M}_l\left\{\boldsymbol{\Sigma}\right\}\mathbf{E}\mathbf{s}_l^*\left(\mathbf{s}_l^{\mathrm{T}}\mathbf{s}_l^*\right)^{-1}}{\sigma_l}, \quad \widehat{\mathbf{v}}_l \in \mathbb{C}^{(K-1)\times 1}, \tag{3.10}$$

where $\mathbf{s}_l^*$ is the conjugate of $\mathbf{s}_l$. Although the full channel matrix of $\mathcal{M}_l\left\{\mathbf{H}\right\}$ is changed due to a single DLE, the estimation effort of the proposed method reduces from $(K-1)^2$ parameters to $K-1$ by modelling the changed coupling condition with reflecting crosstalk coefficients in $\mathbf{v}_l$.

During the whole process, the DP-side is still able to track the received signal power on line l. In case of, for example, a false alarm of DLE, no channel
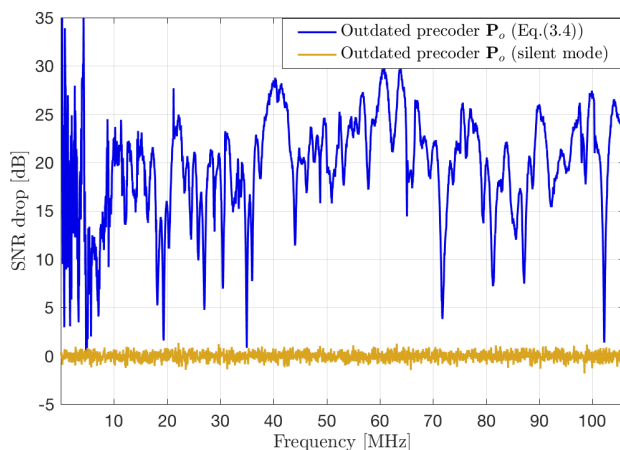
Fig. 3.6: SNR drop on victim line 1 after DLE, given full line transmission with the outdated precoder $\mathbf{P}_o$.

retraining is required and it is fast to get back to the normal transmission by a simple setting on g_l.

With $\mathbf{v}_l$ estimated, the precoder can be updated for the new channel matrix $\mathcal{M}_l\{\mathbf{H}'\}$ according to the FRN model, *i.e.,*

$$\widehat{\mathbf{P}} = \left(\mathcal{M}_l\{\mathbf{H}\} + \widehat{\mathbf{v}}_l \boldsymbol{\mathcal{E}}_l^{\mathrm{T}} \mathbf{H} \mathbf{I}_{K \setminus l}^{\mathrm{T}} \right)^{-1} \mathcal{M}_l\{\mathbf{H}'_\Sigma\}, \qquad (3.11)$$

where $\boldsymbol{\mathcal{E}}_l$ is an elementary column vector with only 1 on the l-th position and 0s elsewhere.

3.5   Simulation Results

In order to evaluate the proposed scheme, we consider a vectoring system with $K = 3$ users operating on the 100 m-cable [8] introduced in Section 3.2. A DLE occurs on line $l = 3$. We use G.fast system parameters [2] and focus on the frequency-range up to 106 MHz. The special silent mode we propose in Section 3.4 is appraised in terms of SNR drop, introduced in Fig.3.1. We also compare our operation with the traditional method both in frequency and in time based on the PSD of the resulting residual crosstalk.

Fig. 3.6 shows that the SNR drop caused by a DLE on the victim lines can be mitigated by setting the gain scaling factor of line l to zero, which would
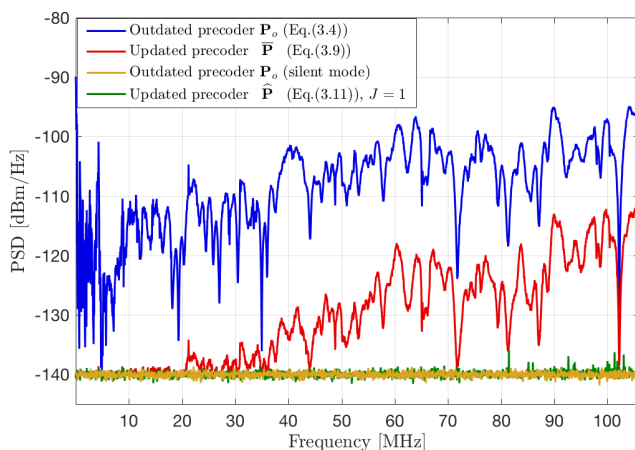
Fig. 3.7: Residual crosstalk in frequency after DLE on victim line 1.

essentially solve the DLE problem. However, keeping the analog front-end running to send pure anti-crosstalk signals consumes power. If the line has already left, it is thus desirable to invoke the second mode in order to update the precoder for the new dimension-reduced channel $\mathcal{M}_l\{\mathbf{H}'\}$.

Fig. 3.7 presents the residual crosstalk PSD on one of the victim lines in the vectored group. By stopping transmission on the leaving line and updating the precoder to $\overline{\mathbf{P}}$ based on the dimension-reduced original channel $\mathcal{M}_l\{\mathbf{H}\}$ (*i.e.,* the traditional operation as defined by Eq. (3.9)), there is an improvement in SNR (comparing the second curve to the top one). However, the residual crosstalk power level is still far above the background noise level, especially for high frequencies where the crosstalk channel has a power level closer to that of the direct channel. Thus, further channel tracking is needed.

In contrast, both modes in our proposed operation suppress the residual crosstalk down to the background noise level throughout the studied frequency range. The victim lines are able to retrieve the residual-crosstalk-free transmission via the silent mode (yellow curve). With $J = 1$ synchronization symbol, the estimated precoder $\widehat{\mathbf{P}}$ can effectively take care of the new channel matrix $\mathcal{M}_l\{\mathbf{H}'\}$ (green curve).

Assume no persistent detection of *los* requirement as in [3] is considered for now, and no signal processing time is counted in. Fig. 3.8 and Fig. 3.9 compare the residual crosstalk on a certain sub-carrier when the DLE happens at two extreme time slots (time instants indicated by the black line): Fig. 3.8 shows the
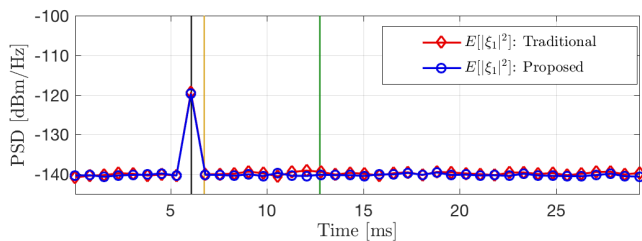
(a) Average residual crosstalk on a sub-carrier at 20 MHz
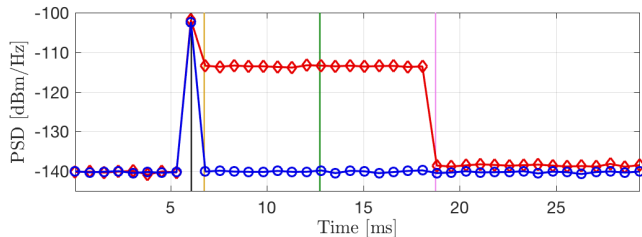
(b) Average residual crosstalk on a sub-carrier at 100 MHz

Fig. 3.8: Average residual crosstalk $E[|\xi_1|^2]$ in time on victim line 1 in downstream at the worst situation: DLE happens one symbol after the synchronization symbol during downstream transmission interval.

longest time distance to the next synchronization symbol, and Fig. 3.9 presents the shortest time distance. The average residual crosstalk power on victim line k is calculated over one frame on one sub-carrier as

$$E[|\xi_k|^2] = \frac{1}{N_{ds}} \sum_{j=1}^{N_{ds}} |\xi_k(j)|^2,$$

where N_{ds} is the number of DMT symbols assigned to downstream transmission in one frame.

As indicated with different vertical time lines in Fig. 3.8 and Fig. 3.9, both the traditional and our proposed method deal with the DLE disturbance in two steps. Once *los* is detected, the first step is taken in the next frame (time instant marked by the yellow line). For the traditional method, the channel dimension is reduced and the precoder is updated to $\overline{\mathbf{P}}$. For our proposed method, the silent mode is activated by transmitting idle symbols on the leaving line. Both methods work well on low-frequency sub-carriers (*e.g.,* 20 MHz in Fig. 3.8a and Fig. 3.9a). However, on higher-frequency sub-carriers (*e.g.,* 100 MHz), $\overline{\mathbf{P}}$
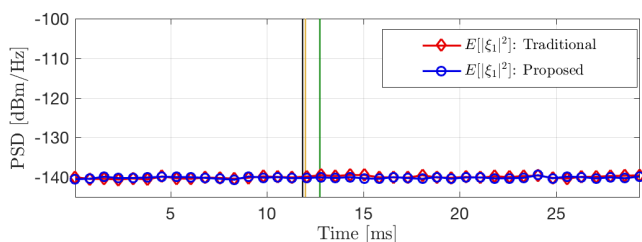
(a) Average residual crosstalk on a sub-carrier at 20 MHz
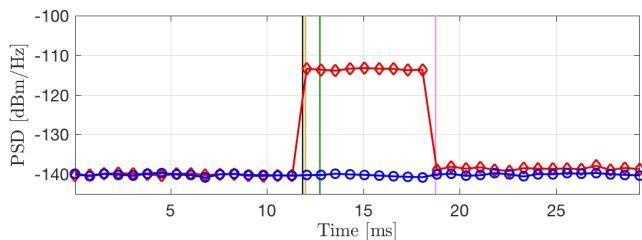
(b) Average residual crosstalk on a sub-carrier at 100 MHz

Fig. 3.9: Average residual crosstalk $E[|\xi_1|^2]$ in time on victim line 1 in downstream at the best situation: DLE happens one frame before the synchronization frame during upstream transmission interval.

is not adequate for crosstalk cancellation, as shown by the error plateau in Fig. 3.8b and Fig. 3.9b. Residual crosstalk severely disturbs the active users before enough error samples can be collected (time instant marked by the pink line) to proceed with a second step, aiming at a precoder update based on the acquired estimates. A traditional way is to perform an elementwise estimation of the dimension-reduced new channel $\mathcal{M}_l\{\mathbf{H}'\}$ using synchronization symbols and pilot sequences. When Hadamard sequences are applied, $2^{\lceil \log_2(K-1) \rceil}$ synchronization symbols are required to estimate $(K-1)^2$ channel matrix elements. For example, a single DLE in a vectored group of $K = 100$ would keep on disturbing the active users for at least $128 \times 6 = 768$ ms, and require an estimation of $99^2 = 9\,801$ entries for each sub-carrier.

The proposed operation, instead, keeps residual crosstalk close to the background noise level during and after the process of estimation and update (time instant marked by the green line), and makes the dimension-reducing operation unnoticeable. Once the DP is aware of the *los*, there is no more crosstalk disturbing the victim lines. Given persistently detected *los* on line l and accomplished estimation of the new channel matrix, it is safe then to completely

remove line l from the vectored group.

It is worth noting that keeping the precoder the same as before the DLE during channel estimation has three advantages. First, other active users in showtime are not disturbed, thanks to the silent mode. Second, it enables FRN-based modelling, which significantly reduces the estimation effort. A traditional method requires orthogonal synchronization sequences to estimate $(K-1)^2$ channel coefficients, while our parameter-based method can exploit the synchronization symbols on line l as a unique reference for estimating the $K-1$ reflecting coefficients only. Third, our estimation does not rely on the orthogonality property. The traditional method shows a slightly higher residual crosstalk-PSD level on severely impacted sub-carriers (cf. Fig. 3.8b and Fig. 3.9b), since the required orthogonality is degraded by background noise.

3.6   Conclusion

A sudden termination change due to a DLE alters the original channel matrix of a vectored group, which can have serious consequences for the vectoring operation. Based on the FRN model, we identify the sources and paths for residual crosstalk after the DLE and introduce a model that is parameterized by reflecting crosstalk coefficients. A procedure for channel estimation and precoder update in the downstream direction is proposed. Temporarily retaining the outdated precoder after a DLE narrows potential residual crosstalk paths down to only the direct channel of the leaving line. Compared to the state-of-the-art method, the period during which active users are disturbed can be significantly shortened to the time it takes to detect the loss of signal and the estimation complexity for a K-user system is reduced from $\mathcal{O}(K^2)$ to $\mathcal{O}(K)$.

3.7   Appendix

This appendix is based on: Y. Huang, T. Magesacher, E. Medeiros, C. Lu, and P.-E. Eriksson, "Method and Arrangement in a DSL Vectoring System," *Patent application*, US15509210, filed 30 September 2014, US20170250731A1, publication date 31 August 2017.

3.7.1   Technical Field

The invention relates to a method and an arrangement in a digital subscriber line (DSL) system, in particular to the handling of disorderly leaving event (DLE) in a DSL vectoring system.

3.7.2 Background

Vectoring technology cancels the far-end crosstalk (FEXT) between DSL lines, and therefore maximizes DSL system performance. Vectoring technology enables offering 100 Mbps per user with DSL lines *e.g.,* between the end of a fiber network and the customer-premises equipment (CPE).

The telecommunication standardization sector of the international telecommunication union (ITU-T) has been standardizing a vectoring standard G.993.5 [3], and the first recommendation of G.993.5 was approved on April 22, 2010. The cancellation of the FEXT is done at the DSL access multiplexer (DSLAM) side. The downstream FEXT is pre-cancelled by a precoder in the DSLAM, while the upstream FEXT is cancelled by an upstream crosstalk canceller in the DSLAM. The recommendation provides a way to estimate the FEXT channel in both downstream and upstream and utilize the estimated channel to cancel the crosstalk.

A DLE, which may alternatively be denoted *e.g.,* disorderly shutdown event (DSE), on a DSL line occurs *e.g.,* when a user unplugs the telephone cable or turns off the CPE abruptly. The disorderly shutdown of a DSL line may change the crosstalk channel characteristics, *i.e.,* the crosstalk coupling to other lines, due to the impedance change at the CPE end which is disorderly shut down.

However, when using vectoring, the precoder in the DSLAM remains unchanged after a DLE and continues to be optimized for the original channel characteristics, *i.e.,* the channel characteristics before the DLE. This could result in a significant signal-to-noise ratio (SNR) drop for other lines, since the precoder is outdated and thus cannot completely cancel the crosstalk from the line which is disorderly shut down. A DLE on one line can make other lines retrain. In VDSL2, retraining a line may take 30 seconds, which is a considerable interruption, *e.g.,* in IP-TV services. Even though the retrain time is significantly shorter in G.fast, it is still several seconds, which would still cause undesirable service interruption.

A method for handling DLEs is presented in [4], which is the work of two of the inventors of the present disclosure, and which is incorporated herein by reference. According to this method, a partial channel estimate is derived after the DLE, and is combined with a channel estimate derived before the DLE. That is, a part of the original channel estimate, in form of a channel coefficient matrix, is replaced with a new estimate, *e.g.,* a column of the channel coefficient matrix. This method works very well for frequencies where the crosstalk between lines is within certain limits. However, when using higher frequencies for communication, such as in G.fast [2], the crosstalk between lines is larger, and thus all parts of the channel coefficient matrix are affected to a larger extent, even though the change in some parts may still be dominant.

Measurements indicate that the impact of DLE is serious for frequencies around 30 MHz and beyond, which is of interest for G.fast.

Thus, there is a need for a fast method for estimating a channel, a channel tracking method, which works well also for higher frequencies.

3.7.3 Summary

An object of the invention is to provide a fast channel tracking mechanism for handling DLEs in DSL systems.

According to a first aspect, a method is provided for handling DLEs causing sudden termination change (STC), in a DSL system. The method comprises, when a DLE occurs on a line l in a vectored group of DSL lines, and the transmission on line l is, at least partly, continued: obtaining at least one error sample from CPEs connected to other lines in the vectored group of DSL lines, and calculating an estimate of the channel coefficients, $\mathbf{H}'$, changed due to the DLE. The estimate is calculated based on the at least one error sample, and thus a channel estimate is provided. The method further comprises modifying a downstream precoder, based on the channel estimate, such that retraining of the other lines in the vectored group due to the DLE is avoided, and errors are also minimized. The estimate of the channel coefficients is calculated based on the model $\mathbf{H}' = \mathbf{H} + \mathbf{C\Lambda H}$.

According to a second aspect, a vectoring control entity (VCE) is provided for handling DLEs causing STC, in a DSL system. The VCE is configured to: when a DLE occurs on a line l in a vectored group of DSL lines, and the transmission on line l is, at least partly, continued: obtain at least one error sample from CPEs connected to other lines in the vectored group of DSL lines, and further to calculate an estimate of the channel coefficients, $\mathbf{H}'$, changed due to the DLE, based on the at least one error sample, thus providing a channel estimate. The VCE is further configured to modify a downstream precoder, based on the channel estimate, such that retraining of the other lines in the vectored group due to the DLE is avoided and errors are also minimized. The VCE is further configured to calculate the estimate of the channel coefficients based on the model $\mathbf{H}' = \mathbf{H} + \mathbf{C\Lambda H}$.

3.7.4 Brief Description of the Drawings

The foregoing and other objects, features, and advantages of the technology disclosed herein will be apparent from the following more particular description of embodiments as illustrated in the accompanying drawings. The drawings are not necessarily to scale, emphasis instead being placed upon illustrating the principles of the technology disclosed herein.

Fig. 3.2 shows a downstream FEXT-reflected-NEXT (FRN) model for orderly leaving event (OLE)/DLE, where $\mathbf{H}(i,j)$ denotes the entry on the i-th row and j-th column of $\mathbf{H}$. Same notation is used for $\mathbf{C}$.

Fig. 3.4 illustrates G.fast time-division duplex (TDD) structure at VCE/ distribution point (DP)/central office (CO).

Fig. 3.10–3.11 illustrate procedures performed by a VCE/DP/CO, according to exemplifying embodiments.

Fig. 3.12–3.13 show a VCE/DP/CO according to exemplifying embodiments.
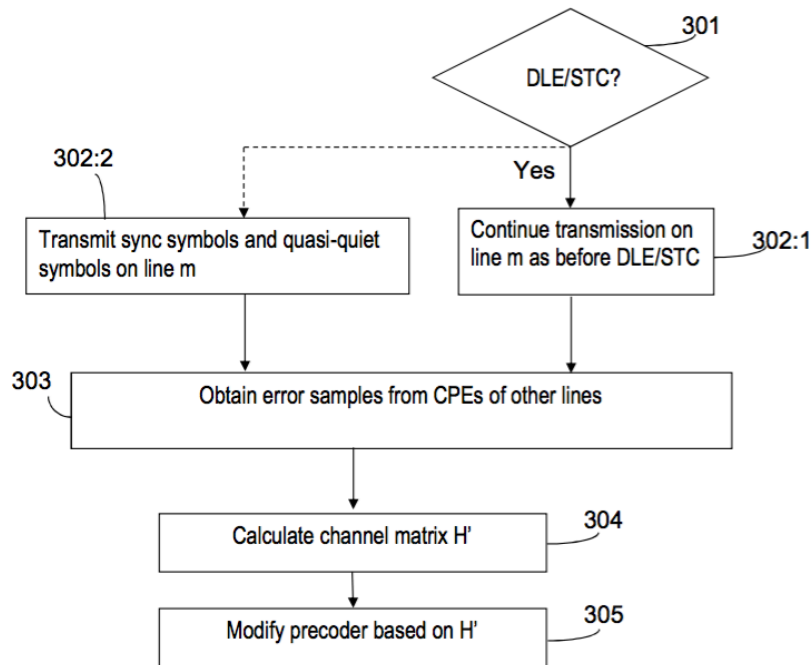
Fig. 3.10
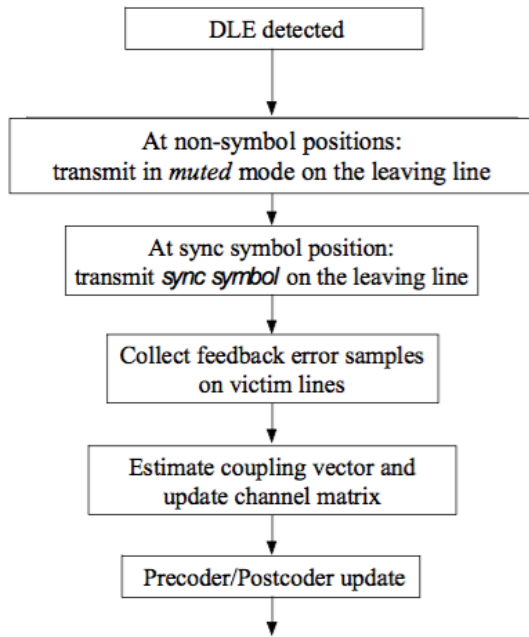
Fig. 3.11
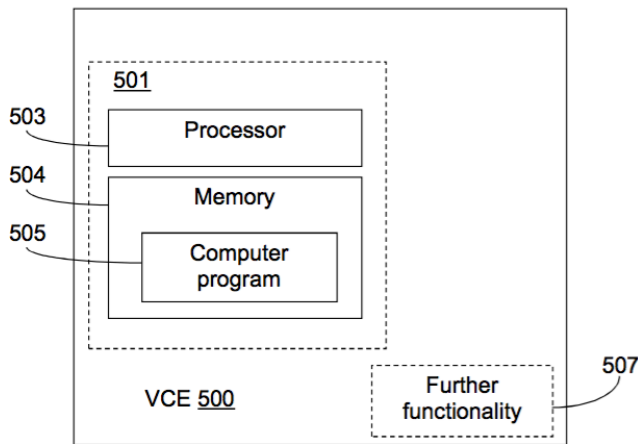
Fig. 3.12
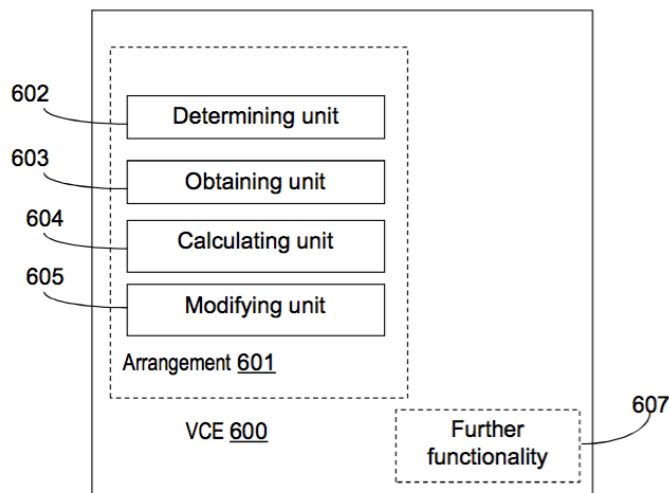
Fig. 3.13

3.7.5 Detailed Description

Briefly described, a solution is provided for enabling a fast update of the precoder for after a sudden impedance change on a line termination. A fast channel estimation method is provided to fast track the channel change and quickly update the precoder accordingly. The fast channel estimation, or tracking, method utilizes a new model for estimating the channel, and is applicable for all frequencies used for DSLL communication, also for higher frequencies around 30 MHz and beyond.

The solution described herein relates in particular to emerging wideband communication systems over multi-pair copper cables, such as the recently drafted standard ITU-T G.fast [2]. In general, it is distinguished between sudden impedance changes, caused by lines <u>inside</u> a vectoring group, hereinafter referred to as disorderly leaving lines, and <u>outside</u> a vectoring group, hereinafter referred to as alien-line termination changes. This invention focuses on the former, *i.e.,* disorderly leaving lines, especially when occurring on the CPE side.

Tracking the channel according to the standardized state-of-the-art way, *i.e.,* relying solely on sync symbols and updating the entire channel matrix using the mechanisms described in the standard, causes FEXT for other users for a considerable amount of time, until the update is completed.

Modems that are suddenly, *i.e.,* without prior warning or preemptive ac-

tions, turned off, change their operating mode, or are disconnected due to line disruption, cause sudden changes of the termination impedance, which they present to a multi-port wireline channel. In the prior art, such events are often referred to as DLEs or DSEs, as stated previously. These terms will also be used herein for denoting such events. Another term which may be used herein to denote such events is STCs. Any change in the termination impedance on one or more of the channel's line(s) manifests itself as a change of a channel coefficient matrix. In general, a DLE alters all the coefficients of a channel matrix, and the changes increase with increasing frequencies. As previously mentioned, measurements indicate that the impact of DLE is serious for frequencies around 30 MHz and beyond.

Advanced wideband wireline communication systems employ signal coordination in order to mitigate crosstalk among lines. Corresponding techniques, referred to as vectoring, rely on accurate channel information. Sudden channel changes disturb the vectoring operation since a precoder, which was designed for the channel before the change, is no longer up to date. The mismatch may result in residual crosstalk causing an SNR drop that is beyond a reserved SNR margin and makes active end users suffer from packet errors and losses.

An exemplifying procedure according to an embodiment of the herein disclosed solution will be described below as comprising three parts, where at least b) is optionally performed in order to reduce interference to other lines in a vectored group.

a) A DLE at the CPE side is detected by a power detector. Particularly if a CPE is unplugged in a DLE, the received power in upstream will go down to zero. In this case, a loss of signal will be detected. In a TDD system like G.fast, if a DLE happens at the CPE side during an upstream slot, it may be detected in the same slot and counter measures (described in b) below) can be taken in the following downstream slot. If an STC happens during a downstream slot, it may be detected in the next upstream slot and counter measures can be taken in the following downstream slot. In a frequency-division duplex (FDD) system like VDSL2, the detection process starts as it happens.

b) As soon as a DLE has been detected, the downstream data signal intended to the disorderly leaving line i may be replaced by zeroes. That is, during data symbol slots, zeroes are transmitted. The precoder then generates a low-power "anti-crosstalk" signal that cancels the FEXT at the CPE port. In this case, on the disorderly leaving line, the direct signal intended to its own CPE is gone. On each victim line, the precompensated signal associated with the direct signal of the disorderly leaving line is also gone, while the precompensated signals associated with the direct signal of all

other victim lines are kept unchanged. Based on the FRN-model, which will be described below, there is no signal entering the port, thus there is no signal to be reflected and subsequently coupled via NEXT to the other ports—the other lines remain undisturbed during DS transmission. An alternative to sending zeroes is sending the DS data signal intended to the disorderly leaving line in a sufficiently low power.

c) During synch-symbol slots, regular synch symbols, and not zeroes as in the data symbol slots, are transmitted, and a specific channel estimation scheme is employed. The scheme, which will be described below is based on the FRN model and reduces the complexity from estimating $(K - 1) \times K$ channel coefficients, *i.e.,* all changed coefficients, needed by the state-of-the-art approach to only $K - 1$ reflection coupling coefficients, in order to track all changed coefficients.

In step b), it has been realized by the inventors that it is advantageous to set the gain scaling factor of the leaving line to zero during the data symbols and other non-sync symbols after the detection of a DLE, or loss of signal on the line, while keeping the precoder coefficients unchanged, especially the coefficients on the columns associated with the victim lines. On the disorderly leaving line, only the direct signal intended to its own CPE is muted, while the precompensated signal from other lines to the disorderly leaving line is kept. On other lines, we keep transmitting both direct signals and the precompensated signals among these victim lines. Therefore, this operation does not stop the transmission on the leaving line completely. If the line is completely stopped, no signal would be present on the leaving line and the precompensated signal component from other lines to the leaving line would also disappear. Basically, the signals associated with the data symbols intended to the leaving line CPE are disappeared on all lines. It should be noted that data symbols here may include all non-sync symbols, if other symbols are also needed to be protected. In this document, we show mathematically and also experimentally via simulations that when using the suggested solution, there will be no residual crosstalk due to the mismatch of the outdated precoder and the changed channel. Note that in this step, the precoder is kept unchanged. At a DLE, the crosstalk channel changes are due to the reflected signals from the disconnected port of the leaving line to other lines. By keeping the original precoder, at least of the coefficients associated with the victim lines, no crosstalk signals from the victim lines will arrive at the disconnected port and thereby no crosstalk will be reflected. And the signal of the disorderly leaving line is also muted. No crosstalk is caused by the leaving line either. Therefore, no residual crosstalk will be present in the system.

Although the method of muting the direct signal of the leaving line de-

scribed above takes away the residual crosstalk at the CPE end, it may cause unnecessary erasures, *i.e.,* errors, on the leaving line in the case of a false detection of a DLE. If step b) above is not performed, and regular transmission is continued and step c) is performed directly, the fast tracking algorithm is very robust with false detections. However, step b) is easy to implement and also relax the time requirement for the fast tracking implementation. With step b), step c) can gain more time for the algorithm execution while not causing errors and therefore reduce the hardware complexity for fast tracking. As previously stated, the muting method is advantageous but optional. An alternative to the muting method/step b) is to continue the transmission on the leaving line as before the DLE. As explained above, the solution described herein would still be applicable. Note that during the transmission of sync symbols, the gain scaling factor of the leaving line is not set to zero. So, when applying an exemplifying embodiment comprising the muting method, the gain scaling factor may alternate between zero, or close to zero, and the original value during data symbols and sync symbols, respectively. In other words, during transmission of sync symbols, the gain scaling factor is equal to, or at least in parity with, the gain scaling factor used for transmission before the DLE; and during transmission in data symbol positions after the DLE, the gain scaling factor is set to zero, or at least close to zero. In principle, during sync symbols, gain scaling can be set to any non-zero number. When the non-zero number is known by the VCE/CO, the channel estimation can be resolved. However, using original value is of interest of practical implementation.

In order to update the precoder to match the channel after the DLE, it is necessary to track the channel change. The precoding coefficients of the other lines, *i.e.,* lines other than the leaving line, should be updated such that residual crosstalk is cancelled by the (updated) precoder when the transmission on the leaving line has been completely stopped. In this invention, the crosstalk channel change is modelled as the reflected crosstalk from the leaving line. Based on this model, a fast channel estimation method is proposed to estimate only the modelled reflected crosstalk coefficients, which are modelled as a vector with the elements of the number of other lines. The estimated elements of the vector are much fewer than that of a matrix. Thus, the channel change can be estimated with only one error sample report corresponding to one sync symbol, which is <u>much</u> faster than for a prior art conventional channel estimation scheme. For example, for 10 lines, a normal conventional channel estimation scheme needs the error samples of 16 sync symbols. Thus, the invented method is potentially much faster.

Method in a Vectoring Control Entity (VCE)

Below, examples of embodiments of a method performed by a VCE will be described with reference to Fig. 3.10–3.11. The method is suitable for handling DLE causing STC in a DSL system. The VCE is a function block which is operable to provide vectoring for a group of lines in a DSL system. Physically, the VCE may be; be comprised in CO or DP. The VCE may be comprised in a DSLAM, connectable to wirelines in the DSL system. Usually, for a small system with a small number of lines, VCE is integrated in to a DSLAM. Alternatively, the VCE may be comprised in a node outside a DSLAM, which is often the case when the system is large and the VCE needs to coordinate multiple DSLAMs.

A method performed by a VCE is illustrated in Fig. 3.10. The network node determines (301) whether a DLE has occurred on a line in a vectored group of DSL lines. When a DLE occurs on a line l, at least one error sample is obtained (303) from CPEs connected to other lines in the vectored group of DSL lines. The transmission on line l, which may also be denoted *e.g.,* the leaving line, is at least partly continued after the DLE, which will be further described below. Further, an estimate is calculated (304), of the channel coefficients, $\mathbf{H}'$, changed due to the DLE. The estimate is calculated based on the obtained at least one error sample, thus providing a channel estimate. The method further comprises modifying (305) a downstream precoder, based on the channel estimate. The estimate of the channel coefficients is calculated based on the model $\mathbf{H}' = \mathbf{H} + \mathbf{C}\mathbf{\Lambda}\mathbf{H}$, where $\mathbf{C}$ is a near-end crosstalk (NEXT) coupling matrix for the CPE end of the vectored group; $\mathbf{\Lambda}$ is a diagonal matrix with the reflection coefficients, after the DLE, of the CPE end of the cables associated with the vectored group; $\mathbf{H}$ is a matrix with the channel coefficients before the DLE; and $\mathbf{H}'$ is a matrix with the estimated channel coefficients after the DLE.

By performing the actions described above, retraining of the other lines in the vectored group due to the DLE on line l may be avoided, and errors are also minimized, which is very advantageous.

The error samples may be obtained by transmitting an error feedback request to the CPEs connected to the other lines in the vectored group. By "other lines" is here meant "other than line l". That is, the error samples may be received from the CPEs in response to such error feedback requests. Such requests may be transmitted to the CPEs over a robust management channel. In VDSL2, it is called robust embedded operations channel (ROC). In G.fast, it is called the robust management channel (RMC). Such requests can also be transmitted to the CPEs over the embedded operations channel (eoc) without robustness enhancement.

Regarding the continued transmission on line l after the DLE, there are

a few alternatives, of which two different are illustrated in Fig. 3.10. In one embodiment, the transmission is continued (302:1) on line l after the DLE just as it was before the DLE. That is, the transmission on line l is not changed in response to the detection of a DLE on line l. In another embodiment, the transmission on line l may be changed (302:2) in response to the DLE, in order to mitigate the interference subjected to the other lines during the channel tracking procedure. For example, in an embodiment comprising the alternative (302:2), the transmission of sync signals in sync symbol positions could be continued but the transmission of the direct signal in line l in data symbol positions on line l could be muted, *e.g.,* by setting a gain value to zero, which will be further described below. Other alternatives for the continued transmission are also possible, and considered to be encompassed by the present disclosure.

It should be noted that at a DLE, which is the case that is discussed herein (as opposed to OLE), there are two problems that arises related to the channel matrix. First, the channel matrix is fully changed, at least in certain frequency ranges, as a consequence of the DLE; and second, the channel matrix dimension is reduced, since a line is leaving. It should further be noted that it is fully possible that more than one line is subjected to a DLE. In the examples herein, in order to facilitate understanding, it is, however, assumed that only one line at a time exhibits an STC of a DLE.

As stated above, according to the invention, the change in the channel matrix is modelled as $\boldsymbol{\Delta} = \mathbf{C}\boldsymbol{\Lambda}\mathbf{H}$. If assuming three lines, the channel matrix will be of the dimension 3×3, and could be denoted $\mathbf{H}_3$. The channel, or channel matrix, could then be described, after DLE, as $\mathbf{H}_{3,\mathrm{DLE}} = \mathbf{H}_3 + \boldsymbol{\Delta}_3$, where $\boldsymbol{\Delta}_3$ is the change

$$\boldsymbol{\Delta}_3 = \mathbf{C}\boldsymbol{\Lambda}\mathbf{H}_3 + \begin{bmatrix} 0 & c_{12} & c_{13} \\ c_{21} & 0 & c_{23} \\ c_{31} & c_{32} & 0 \end{bmatrix} \begin{bmatrix} 0 & 0 & 0 \\ 0 & 0 & 0 \\ 0 & 0 & \lambda_3 \end{bmatrix} \mathbf{H}_3.$$

$\mathbf{C}$ being a NEXT coupling matrix for the CPE end of the vectored group, as previously mentioned. The coefficients in this matrix are changed after the DLE, and are thus unknown when initiating the fast channel tracking described herein. $\boldsymbol{\Lambda}$ is a diagonal matrix with the reflection coefficients, after the STC, of the CPE end of the cables associated with the vectored group, as previously mentioned. It is assumed here that all CPEs, except for the one subjected to a DLE, are perfectly matched to the lines. In this example with three lines, let line 3 be the leaving line. This means that there will be no reflection for lines 1 and 2, since the CPE impedance, alt. termination, is perfectly matched. Thus the reflection coefficients, on the diagonal of $\boldsymbol{\Lambda}$, are zero for lines 1 and 2. However, for line 3, the DLE entails that the termination is no longer matched,

and thus the reflection coefficient will not be zero, *i.e.,* $\lambda_3 \neq 0$. For example, if $\lambda_3 = 1$, the signal arrived at the disconnected port will be fully reflected back. Performing the matrix multiplication will give:

$$\boldsymbol{\Delta}_3 = \mathbf{C\Lambda H}_3 = \begin{bmatrix} 0 & 0 & c_{13}\lambda_3 \\ 0 & 0 & c_{23}\lambda_3 \\ 0 & 0 & 0 \end{bmatrix} \mathbf{H}_3 = \begin{bmatrix} c_{13}\lambda_3 h_{31} & c_{13}\lambda_3 h_{32} & c_{13}\lambda_3 h_{33} \\ c_{23}\lambda_3 h_{31} & c_{23}\lambda_3 h_{32} & c_{23}\lambda_3 h_{33} \\ 0 & 0 & 0 \end{bmatrix}$$

$$= \begin{bmatrix} c_{13} \\ c_{23} \\ 0 \end{bmatrix} \begin{bmatrix} h_{31} & h_{23} & h_{33} \end{bmatrix}.$$

Above, it is seen that 6 channel coefficients have been changed in the channel matrix. In a normal tracking method, all these 6 coefficients need to be estimated. In our fast tracking method, a combined reflection coupling coefficient from port j to port i is defined $c_{ij}\lambda_j$, following the model above, to estimate the channel change $\boldsymbol{\Delta}_3$. Thus, in this example, only two reflection coupling coefficients need to be estimated, *i.e.,* $c_{13}\lambda_3$ and $c_{23}\lambda_3$, since the original channel vector $[h_{31}, h_{32}, h_{33}]$ can be known, either stored in the memory or derived from the original precoder. These two reflection coupling coefficients can be derived from error samples obtained on lines 1 and 2 after the STC. Could alternatively be expressed as after the DLE. Since there are only two unknowns to solve in the equation system above, only one error sample from line 1 and line 2, respectively, will be needed to solve the equations. Then, the precoder can be updated accordingly to adapt to the channel change. Thus, the herein described fast tracking method is potentially much faster than a normal tracking scheme.

When the fast channel tracking is performed, the transmission on line 3 will eventually be stopped. The channel matrix will then have a reduced dimension, *i.e.,* 2×2 in this example. Denoting the 2×2 channel matrix after DLE $\mathbf{H}_{2,\text{DLE}}$:

$$\mathbf{H}_{2,\text{DLE}} = \mathbf{H}_2 + \boldsymbol{\Delta}_2 = \mathbf{H}_2 + \begin{bmatrix} c_{13}\lambda_3 h_{31} & c_{13}\lambda_3 h_{32} \\ c_{23}\lambda_3 h_{31} & c_{23}\lambda_3 h_{32} \end{bmatrix}$$

$$= \mathbf{H}_2 + \begin{bmatrix} c_{13}\lambda_3 \\ c_{23}\lambda_3 \end{bmatrix} \begin{bmatrix} h_{31} & h_{32} \end{bmatrix},$$

where $\mathbf{H}_2$ is part of the original matrix $\mathbf{H}_3$, *i.e.,* the channel matrix for the three lines before the DLE. Here, there are two cases depending on if step b) is implemented or not.

If step b) is not implemented, the precoder may first be updated by fast tracking to adapt to the change while the leaving line, *i.e.,* line 3, keeps transmitting until it is believed left already. During this time, the fast tracking

algorithm may be applied to estimate the channel and calculate the precoder accordingly for the reduced 2-line system, *i.e.,* only line 1 and line 2. Then the leaving line stops its transmission totally while the precoder is updated with the calculated precoder coefficients simultaneously.

The transmission in data symbol positions on other lines than line l, before the DLE, comprises FEXT precompensation signals, including the precompensated signal from line l, and a direct signal of its own. After the DLE, the FEXT precompensation signal from line l may be stopped on the other lines, while the other signals are continued after the DLE, such that the reflection of crosstalk from the precompensated signal from line l on other lines become zero. In other words, the respective signals which precompensate crosstalk from line l on the other lines before the DLE, may be stopped after the DLE, when there is no crosstalk from line l if the direct signal of line l is stopped when step b is performed. As an alternative to stopping the respective precompensated signal from line l on the other lines, this signal could be reduced in power after the DLE, as compared to the power of the signal before the DLE. Herein, a "precompensated signal from line l" is a signal which precompensates for crosstalk from line l. This signal may be generated by the precoder based on the direct signal on line l.

Below, an exemplifying procedure according to an embodiment of the herein disclosed solution will be described in more detail.

Consider a vectoring system with K lines, or users. For simplicity, analysis is performed on a certain sub-carrier and at a certain time instant. Signal transceiving in frequency domain in downstream direction can be described independently as $\mathbf{y} = \mathbf{Hx} + \mathbf{n}$, where the transmit and receive signals are $\mathbf{x} \in \mathbb{C}^{K \times 1}$ and $\mathbf{y} \in \mathbb{C}^{K \times 1}$ respectively; the channel matrix seen by the vectored group is $\mathbf{H} \in \mathbb{C}^{K \times K}$, and additive background noise on the copper pairs is $\mathbf{n} \in \mathbb{C}^{K \times 1}$. The direct channel of each line locates on the diagonal of $\mathbf{H}$, whereas the FEXT composes its off-diagonal entries.

Vectoring enables the cooperative signal processing within the vectored group by configuring an appropriate precoder for the downstream and a crosstalk canceller, in upstream at the DP/CO to cancel FEXT. Specifically in downstream, let $\mathbf{G} \in \mathbb{R}^{K \times K}$ denote a diagonal matrix with the gain adjuster, *i.e.,* gain scaling factor as stated before, for each line on the main diagonal, namely $\mathbf{G} = \mathrm{diag}\left([g_1, g_2, \ldots, g_K]\right)$. After including precoding, $\mathbf{P}_o$, the transmitting of $\mathbf{x}$ at DP/CO yields $\mathbf{y} = \mathbf{HP}_o\mathbf{Gx} + \mathbf{n}$. An ideal precoder neutralizes crosstalk effectively such that for the input symbol $\mathbf{x}$

$$\boldsymbol{\Sigma}\mathbf{x} = \mathbf{HP}_o\mathbf{Gx} \tag{3.12}$$

where $\boldsymbol{\Sigma}$ is a $K \times K$ diagonal matrix.

A DLE at the CPE side exhibits STC and changes the whole channel coupling environment. Equivalently, every entry of the matrix $\mathbf{H}$ changes. Before further processed, the outdated precoder $\mathbf{P}_o$ fails at anti-crosstalk and makes all receiving ends suffer from residual crosstalk.

By modelling the changed coupling condition with near-ends coupling coefficients, the estimation effort reduces from $(K-1) \times K$ parameters to $K-1$. Fast estimation and adaption may further be supported by controlling the transmitted signal on the leaving line.

Specifically, let $\mathbf{\Lambda} \in \mathbb{C}^{K \times K}$ denote a diagonal matrix with the reflection coefficients of the CPEs, or rather of the CPE end of the cables in the vectored group, on the main diagonal, *i.e.,* $\mathbf{\Lambda} = \operatorname{diag}([\lambda_1, \lambda_2, \ldots, \lambda_K])$. The near-end coupling matrix $\mathbf{C} \in \mathbb{C}^{K \times K}$ describes the NEXT or attenuated NEXT at the CPE end, depending on the relative cable length, which is also illustrated in Fig. 3.2 for the l-th column of $\mathbf{C}$. When the terminations at the CPEs are perfectly matched, there will be no reflection, which gives the reflection coefficients $\lambda_i = 0$ for $i = 1, \ldots, K$ ideally. Then, the CPE-near-end coupling matrix $\mathbf{C}$ has no contribution on the whole coupling environment.

After a DLE, when the termination of one line in a vectored group has changed and is mismatched, one diagonal element of $\mathbf{\Lambda}$ will deviate significantly from 0. Assume line no. l exhibits an STC, which is quantified by that the reflection coefficient $\lambda_l \neq 0$. In this case, $\boldsymbol{\xi} = \mathbf{\Lambda}\mathbf{y} = \mathbf{\Lambda}\mathbf{H}\mathbf{P}_o\mathbf{G}\mathbf{x}$ is reflected by mismatched CPE termination. The reflected signal $\boldsymbol{\xi}$ couples back to the CPEs via $\mathbf{C}$, and adds

$$\boldsymbol{\delta} = \mathbf{C}\mathbf{\Lambda}\mathbf{H}\mathbf{P}_o\mathbf{G}\mathbf{x} \tag{3.13}$$

to the expected receive signal $\mathbf{y}$. So the received signal after DLE becomes

$$\begin{aligned}
\mathbf{y}' &= \mathbf{y} + \boldsymbol{\delta} \\
&= \mathbf{H}\mathbf{P}_o\mathbf{G}\mathbf{x} + \mathbf{C}\mathbf{\Lambda}\mathbf{H}\mathbf{P}_o\mathbf{G}\mathbf{x} + \mathbf{n} \\
&= (\mathbf{I} + \mathbf{C}\mathbf{\Lambda})\,\mathbf{H}\mathbf{P}_o\mathbf{G}\mathbf{x} + \mathbf{n} \\
&= (\mathbf{H} + \mathbf{\Delta})\,\mathbf{P}_o\mathbf{G}\mathbf{x} + \mathbf{n}.
\end{aligned} \tag{3.14}$$

Equivalently, the channel changes from $\mathbf{H}$ to $\mathbf{H}' = \mathbf{H} + \mathbf{\Delta}$, where $\mathbf{\Delta} = \mathbf{C}\mathbf{\Lambda}\mathbf{H}$.

A near-optimal linear precoder has been proposed in the prior art as $\mathbf{P}_o = \mu\mathbf{H}^{-1}\mathbf{H}_\Sigma$, where $\mathbf{H}_\Sigma = \operatorname{diag}(\operatorname{diag}(\mathbf{H}))$ is the diagonal matrix of $\mathbf{H}$ and the scaling factor $\mu = \max_i \left\| \left[\mathbf{H}^{-1}\mathbf{H}_\Sigma\right]_{\text{row } i} \right\|$. For example, assume $K = 3$ and

$l = 2$. The mismatched error in Eq. (2) is actually

$$\boldsymbol{\delta} = \mu\mathbf{C}\boldsymbol{\Lambda}\mathbf{H}\mathbf{H}^{-1}\mathbf{H}_\Sigma\mathbf{G}\mathbf{x}$$

$$= \mu \begin{bmatrix} 0 & c_{12} & c_{13} \\ c_{21} & 0 & c_{23} \\ c_{31} & c_{32} & 0 \end{bmatrix} \begin{bmatrix} 0 & 0 & 0 \\ 0 & \lambda_2 & 0 \\ 0 & 0 & 0 \end{bmatrix} \mathbf{H}_\Sigma\mathbf{G}\mathbf{x}$$

$$= \mu \begin{bmatrix} 0 & \lambda_2 c_{12} & 0 \\ 0 & 0 & 0 \\ 0 & \lambda_2 c_{32} & 0 \end{bmatrix} \begin{bmatrix} h_{11}g_1 & 0 & 0 \\ 0 & h_{22}g_2 & 0 \\ 0 & 0 & h_{33}g_3 \end{bmatrix} \begin{bmatrix} x_1 \\ x_2 \\ x_3 \end{bmatrix}$$

$$= \mu \begin{bmatrix} 0 & \lambda_2 c_{12} & 0 \\ 0 & 0 & 0 \\ 0 & \lambda_2 c_{32} & 0 \end{bmatrix} \begin{bmatrix} h_{11}g_1 x_1 \\ h_{22}g_2 x_2 \\ h_{33}g_3 x_3 \end{bmatrix}$$

$$= \mu\lambda_2 \begin{bmatrix} c_{12} \\ 0 \\ c_{32} \end{bmatrix} h_{22}g_2 x_2.$$

The above implies that, in the general case, the mismatched error can be written as:

$$\boldsymbol{\delta} = \mathbf{v}_l \mu h_{ll} g_l x_l, \tag{3.15}$$

where $\mathbf{v}_l = \lambda_l[c_{1l}, \ldots, c_{Kl}]$.

The equation above reveals, and the inventors have realized, that the activating source of mismatched error $\boldsymbol{\delta}$ only comes from the transmit signal x_l on the leaving line via the l-th direct channel h_{ll} (see solid line in line l in Fig. 3.2), which is then reflected and couples to CPE receivers via $\mathbf{v}_l$, the reflection coupling vector of line l.

With the mismatched errors' source and paths targeted, we propose an operation as follows to accomplish changed channel estimation and precoder update while minimizing the disturbance to active end users.

A reference time-line for G.fast TDD frames is shown in Fig. 3.4. A typical TDD frame duration is $T_f = 750\,\mu$s, corresponding to $N_f = 36$ symbol periods (T_s). Time gaps are reserved between paired downstream and upstream as T_{g2}, and between upstream and next downstream as T_{g1}. The number of TDD frames in one superframe, binding to $N_f = 36$, is $N_{sf} = 8$. The first frame of each superframe is specified as sync frame, which contains one sync symbol locating on predefined symbol position in both directions. The sync frame is then followed by 7 regular frames.

Consider a DLE at time instant t_l at a CPE connected to line l during the first superframe in Fig. 3.4, i.e., $t_l \in [0, T_{sf}]$. If the DLE occurs during a downstream transmission interval of the i-th TDD frame ($t_l \in [(i-1)T_f, (i-1)T_f + T_{ds}]$),the VCE/DP/CO will be notified about the event

during next upstream transmission period ($t \in [(i-1)T_f + T_{ds} + T_{g2}, iT_f - T_{g1}]$). In the next downstream transmission period and onwards ($t > iT_f$), the VCE/DP/CO may transmit the *muted signal* on data symbol positions by controlling the gain adjuster g_l on the leaving line. The detailed illustration for this special operation will be given below. If a DLE occurs during an upstream transmission interval, the "muting" for downstream may launch directly, if step b) is implemented.

According to current standard, the transmission on the leaving line is turned off immediately when a DLE is detected. However, according to the solution disclosed herein, the precoder is kept "outdated" as $\mathbf{P}_o$ until estimation is completed if step b) is implemented. That is, the precoder, which is optimized for the channel as it was before the DLE, is kept also after the DLE, even though it then is outdated. The downstream operation for new channel estimation, or "fast tracking", may be accomplished by sending two kinds of special symbols: muted symbol and sync symbol. An exemplifying embodiment is illustrated in Fig. 3.11.

Specifically, by modifying the *l*-th gain adjuster to be $\hat{g}_l = \epsilon$ ($\epsilon \to 0$) at the data symbol positions, symbols are transmitted in what herein is denoted *muting mode, i.e.,* muted symbols are transmitted at non-sync symbol positions on the leaving line. The mismatched error $\boldsymbol{\delta}$ in Eq. (4) adding on the victim lines becomes negligible as $\boldsymbol{\delta} = \mathbf{v}_l \mu h_{ll} \epsilon x_l \to 0$ for $\epsilon \to 0$. This enables the whole process to be "silent" to active end users. Muted symbols can also be obtained by change the symbol constellation points to zeros or close to zeros in the quadrature amplitude modulation (QAM) symbol encoder/mapper.

NOTE: in the G.fast standard, idle symbols are defined as:

10.2.1.7 Idle symbol encoding

For all sub-carriers of an idle symbol the symbol encoder shall generate a constellation point $X_i = 0$, $Y_i = 0$.

If precoding in enabled, transmission of an idle symbol may result in non-zero power at the U interface due to adding of FEXT pre-compensation signals from $\varepsilon(k, n)$ reference point (see Figure 10-1).

If precoding is disabled, transmission of idle symbol results in zero power at the U interface. Therefore, in upstream direction transmission of idle symbol results in a quiet symbol period.

The idle symbols are equivalent to the muted symbols here if set the gain scaling factor to zero or set the symbol constellation points to zero. Here, the expression muted symbols is considered to also cover the alternative option of continuing to transmit the symbols, but at a very low power.

Sync symbols are transmitted every $6\,$ms, *i.e.,* one superframe duration, on each line in G.fast (cf. Fig. 3.4). Assume that J superframes are required before the update is completed. Let t_j^{sc} be the time instant to transmit the j-th downstream sync symbol. On this specific time slot, the l-th gain adjuster is set back to g_l, which may be stored *e.g.,* in the bits-and-gains table assigned during initialization. A Sync vector $\mathbf{s}(t_j^{\text{sc}}) = \left[s_1(t_j^{\text{sc}}), \ldots, s_l(t_j^{\text{sc}}), \ldots, s_K(t_j^{\text{sc}})\right]^{\text{T}}$ is transmitted from DP/CO to CPEs. Accordingly, the received sync vector at CPE end presents as

$$
\begin{aligned}
\mathbf{q}(t_j^{\text{sc}}) &= \mu\mathbf{H}_\Sigma\mathbf{G}\mathbf{s}(t_j^{\text{sc}}) + \mathbf{v}_l\mu h_{ll}g_l s_l(t_j^{\text{sc}}) + \mathbf{n} \\
&= \mu\mathbf{H}_\Sigma\mathbf{G}\left(\mathbf{s}(t_j^{\text{sc}}) + \mathbf{e}(t_j^{\text{sc}})\right),
\end{aligned} \tag{3.16}
$$

assigning $\mathbf{e}(t_j^{\text{sc}}) = \mathbf{G}^{-1}\mathbf{H}_\Sigma^{-1}\left(\mathbf{v}_l\mu h_{ll}g_l s_l(t_j^{\text{sc}}) + \mathbf{n}\right)/\mu$. The error samples of sync symbols $\mathbf{e}(t_j^{\text{sc}})$ on victim lines are then fed back to DP/CO.

After sending the sync symbol on scheduled time instants, the transmission on line l goes back to quasi-quiet symbols for all data symbol positions. The transmitter may keep on alternatively sending quasi-quiet symbols and sync symbols on the disorderly leaving line until DP/CO have collected a reasonable number of $\mathbf{e}(t_j^{\text{sc}})$ to do an elegant coupling vector estimation. Stack the error vectors collected without the l-th elements as:

$$
\begin{aligned}
\mathbf{E} &= \mathbf{I}_{K\backslash l}^{[\text{r}]}\left[\mathbf{e}(t_1^{\text{sc}}), \ldots, \mathbf{e}(t_J^{\text{sc}})\right] \\
&= \mathbf{I}_{K\backslash l}^{[\text{r}]}\mathbf{G}^{-1}\mathbf{H}_\Sigma^{-1}\mathbf{v}_l\mu h_{ll}g_l\mathbf{s}_l^{\text{T}} + \mathbf{N},
\end{aligned} \tag{3.17}
$$

where $\mathbf{I}_{K\backslash l}^{[\text{r}]}$ is an K-dimension identity matrix excluding the l-th row, $\mathbf{s}_l = \left[s_l(t_1^{\text{sc}}), \ldots, s_l(t_J^{\text{sc}})\right]^{\text{T}}$, and $\mathbf{N} \in \mathbb{C}^{(K-1)\times J}$ is the equalized additive noise on victim lines for J sync time instants. By "victim lines" is meant the other lines in a vectored group except the disorderly leaving line. The estimation of $\mathbf{v}_l$ can be done by

$$
\widehat{\mathbf{v}}_l = \frac{\mathcal{M}_l\left\{\mathbf{H}_\Sigma\mathbf{G}\right\}\mathbf{E}(\mathbf{s}_l^{\text{H}}\mathbf{s}_l)^{-1}\mathbf{s}_l^{\text{H}}}{\mu h_{ll}}, \quad \widehat{\mathbf{v}}_l \in \mathbb{C}^{(K-1)\times 1}, \tag{3.18}
$$

where $\mathcal{M}_l\left\{\cdot\right\}$ is a dimension reducing function by excluding the i-th column and row.

When the coupling vector $\mathbf{v}_l$ is estimated and the whole channel matrix change is derived accordingly, the DP/CO may update the precoder based on the channel matrix change and may shut down the transmission on the leaving line completely.

It should be noted that the same scheme as presented above works and may be applied also for the non-linear Tomlinson-Harashima precoder, which will be used in G.fast phase 2 supporting up to 212 MHz in frequency.

The fast channel estimation described herein is different from the one described in [4]. With a deeper understanding regarding the mechanism what exactly causes the channel change, the new method explicitly estimates the reflected crosstalk coefficients which cause the channel changes and then calculate the channel change. This is especially important in high frequencies for G.fast use, where the whole channel matrix changes due to a DLE. The previous method described in [4] actually is an approximate of the new method described herein. In low frequencies, the changes in other columns are much smaller than the column associated with the leaving line. Thus, for certain frequencies, *e.g.,* VDSL2 frequency range, the method in [4] works sufficiently well by estimating the dominant column changed and neglecting other columns. However, the changes in other columns get closer in magnitude to the column associated with the leaving line in higher frequency, where the crosstalk level gets closer to the direct channel. In other words, the dominance of the leaving column decreases over frequencies. Therefore, the performance of the pervious method described in [4] degrades over frequencies. The new method significantly improves the previous method in higher frequencies, and is a complete solution, which covers both low and high frequencies.

Hardware Implementations

The techniques and processes described above can be implemented in a network node which is operable to provide vectoring for a group of lines in a DSL system. As previously mentioned, the node may be denoted VCE, and may be comprised in a CO or a DP. Fig. 3.12 is a schematic illustration of an exemplifying embodiment of a VCE (500) in which a method embodying any of the presently described techniques can be implemented. A computer program for controlling the VCE (500) to carry out a method embodying the present invention is stored in a program storage (504), which comprises one or several memory devices. Data used during the performance of a method embodying the present invention may also be stored in the program storage (504), or a separate data storage, which also may comprise one or more memory devices. During performance of a method embodying the present invention, instructions (505), such as program steps may be fetched from the program storage (504) and be executed by processing means (503), such as a central processing unit (CPU), or other processor. Output information resulting from performance of a method embodying the present invention can be stored back in a data storage, or, be sent to an input/output (I/O) interface, which includes a network interface for sending and receiving data to and from other network nodes and which may also include a radio transceiver for communicating with one or more terminals. The VCE (500) is associated with the same technical features,

objects and advantages as the previously described method embodiments. The VCE is described in brief in order to avoid unnecessary repetition.

The part of the network node (500) which is most affected by the adaptation to the herein described solution is illustrated as an arrangement (501), surrounded by a dashed line. The further functionality (506) illustrated in Fig. 3.12 may be assumed to carry out regular VCE and/or node functions.

Thus, when a DLE occurs on a line l in a vectored group of DSL lines, and the transmission on line l is, at least partly, continued, the execution of the instructions (505) by the processing means (503) causes the VCE (500) to obtain at least one error sample from CPEs connected to other lines in the vectored group of DSL lines, and to calculate an estimate of the channel coefficients, $\mathbf{H}'$, changed due to the DLE, based on the at least one error sample. The execution of the instructions further causes the VCE to modify a downstream precoder, based on the channel estimate. The estimate of the channel coefficients is calculated based on the model $\mathbf{H}' = \mathbf{H} + \mathbf{C\Lambda H}$, as previously described in detail.

The execution of the instructions may further cause the VCE to configured to continue the transmission of sync symbols on line l after the DLE. As previously described, the transmission in data symbol positions on line l before the DLE comprises a FEXT precompensation signal and a direct signal. The execution of the instructions may cause the VCE to continue the transmission of the FEXT precompensation signal after the DLE, and further to transmit the direct signal on line l with reduced power after the DLE, as compared to before the DLE.

The execution of the instructions may further cause the VCE to obtain at least one error sample from the CPE of at least one other line in the vectored group, and further to send at least one error feedback request over the eoc in both VDSL2 and G.fast or over a ROC in VDSL2, or over a RMC in G.fast, in order to collect one or more error samples.

An alternative implementation of the network node (500) is shown in Fig. 3.13. The VCE (600) or arrangement (601) comprises an obtaining unit (602), configured to obtain at least one error sample from CPEs connected to other lines in the vectored group of DSL lines. The VCE (600) further comprises a calculating unit (604), configured to calculate an estimate of the channel coefficients, $\mathbf{H}'$, changed due to the DLE, based on the at least one error sample, thus providing a channel estimate. The VCE (600) further comprises a modifying unit (605), configured to modify a downstream precoder, based on the channel estimate. The arrangement (601) could further comprise a determining or detecting unit (602), configured to detect the occurrence of a DLE on a line in the vectored group. Alternatively, this detection could be regarded as a part of the standard functionality (607).

The VCE described above could comprise further units or modules configured for the different method embodiments described herein.

The units or modules in the arrangements in the respective different network node embodiments and wireless device embodiments described above could be implemented *e.g.,* by one or more of: a processor or a microprocessor and adequate software and memory for storing thereof, a programmable logic device (PLD) or other electronic component(s) or processing circuitry configured to perform the actions described above, and illustrated *e.g.,* in Fig. 3.12. That is, the units or modules in the arrangements in the different nodes described above could be implemented by a combination of analog and digital circuits, and/or one or more processors configured with software and/or firmware, *e.g.,* stored in a memory. One or more of these processors, as well as the other digital hardware, may be included in a single application-specific integrated circuitry (ASIC) or several processors and various digital hardware may be distributed among several separate components, whether individually packaged or assembled into a system-on-a-chip (SoC). The VCE could be implemented as a computer program, *e.g.,* a software module, which is run on a node which is operable to communicate with and/or control at least parts of the DLE system. Such a node may be located locally, near the DSL lines, or remote, such as in a distributed system, *e.g.,* a cloud solution.

When using the word "comprise" or "comprising" it shall be interpreted as non-limiting, *i.e.,* meaning "consist at least of".

It should also be noted that in some alternate implementations, the functions/acts noted in the blocks may occur out of the order noted in the flowcharts. For example, two blocks shown in succession may in fact be executed substantially concurrently or the blocks may sometimes be executed in the reverse order, depending upon the functionality/acts involved. Moreover, the functionality of a given block of the flowcharts and/or block diagrams may be separated into multiple blocks and/or the functionality of two or more blocks of the flowcharts and/or block diagrams may be at least partially integrated. Finally, other blocks may be added/inserted between the blocks that are illustrated, and/or blocks/operations may be omitted without departing from the scope of inventive concepts. Moreover, although some of the diagrams include arrows on communication paths to show a primary direction of communication, it is to be understood that communication may occur in the opposite direction to the depicted arrows.

Modifications and other embodiments of the disclosed invention will come to mind to one skilled in the art having the benefit of the teachings presented in the foregoing descriptions and the associated drawings. Therefore, it is to be understood that the invention is not to be limited to the specific embodiments disclosed and that modifications and other embodiments are intended to be

included within the scope of this disclosure. Although specific terms may be employed herein, they are used in a generic and descriptive sense only and not for purposes of limitation.

It is to be understood that the choice of interacting units, as well as the naming of the units within this disclosure are only for exemplifying purpose, and nodes suitable to execute any of the methods described above may be configured in a plurality of alternative ways in order to be able to execute the suggested procedure actions.

It should also be noted that the units described in this disclosure are to be regarded as logical entities and not with necessity as separate physical entities.

While the embodiments have been described in terms of several embodiments, it is contemplated that alternatives, modifications, permutations and equivalents thereof will become apparent upon reading of the specifications and study of the drawings. It is therefore intended that the following appended claims include such alternatives, modifications, permutations and equivalents as fall within the scope of the embodiments.

3.7.6   Claims

1. A method performed by a VCE for handling DLE causing STC in a DSL system, the method comprising:

   when a DLE occurs on a line l in a vectored group of DSL lines, and the transmission on line l is, at least partly, continued:

   - obtaining (104) at least one error sample from CPEs connected to other lines in the vectored group of DSL lines,
   - calculating (108) an estimate of the channel coefficients, $\mathbf{H}'$, changed due to the DLE, based on the at least one error sample, thus providing a channel estimate, and
   - modifying (110) a downstream precoder, based on the channel estimate, such that retraining of the other lines in the vectored group due to the DLE is avoided,

   wherein the estimate of the channel coefficients is calculated based on the model $\mathbf{H}' = \mathbf{H} + \mathbf{C\Lambda H}$, where

   $\mathbf{C}$ is a NEXT coupling matrix for the CPE end of the vectored group;

   $\mathbf{\Lambda}$ is a diagonal matrix with the reflection coefficients, after the DLE, of the CPE end of the cables associated with the vectored group;

   $\mathbf{H}$ is a matrix with the channel coefficients before the DLE; and

   $\mathbf{H}'$ is a matrix with the estimated channel coefficients after the DLE.

2. The method according to claim 1, wherein the transmission of sync symbols on line l is continued after the DLE.

3. The method according to claim 1 or 2, wherein the transmission in data symbol positions on line l before the DLE comprises a FEXT precompensation signal from other lines and a direct signal of line l, and wherein the FEXT precompensation signal is continued after the DLE, such that the reflection of crosstalk from the other lines remains cancelled at the CPE end of line l.

4. The method according to claim 3 wherein the direct signal transmitted on line l is reduced in power after the DLE, as compared to before the DLE.

5. Method according to any of the preceding claims, further comprising applying one or more of the following for data symbol positions on line l after the DLE:

   - setting a gain scaling factor to zero, or close to zero;
   - setting symbol constellation points to zero, or close to zero, in a symbol encoder.

6. The method according to any of the preceding claims, wherein the transmission in data symbol positions on other lines than line l before the DLE comprises FEXT precompensation signals, including the precompensated signal from line l, and a direct signal of its own, and wherein the FEXT precompensation signal from line l is stopped on the other lines, while the other signals are continued after the DLE.

7. The method according to claim 6 wherein the FEXT precompensation signal from line l on other lines is reduced in power after the DLE, as compared to before the DLE.

8. The method according to any of the preceding claims, wherein the obtaining of error samples comprises sending at least one error feedback request over either the eoc in both VDSL2 and G.fast or a ROC in VDSL2, or a RMC in G.fast.

9. VCE for handling DLE causing STC in a DLE system, the VCE being configured to:

   when a DLE occurs on a line l in a vectored group of DSL lines, and the transmission on line l is, at least partly, continued:

- obtain at least one error sample from CPEs connected to other lines in the vectored group of DSL lines,

- calculate an estimate of the channel coefficients, $\mathbf{H}'$, changed due to the DLE, based on the at least one error sample, thus providing a channel estimate, and

- modify a downstream precoder, based on the channel estimate, such that retraining of the other lines in the vectored group due to the DLE is avoided,

wherein the VCE is further configured to calculate the estimate of the channel coefficients based on the model $\mathbf{H}' = \mathbf{H} + \mathbf{C}\mathbf{\Lambda}\mathbf{H}$, where $\mathbf{C}$ is a NEXT coupling matrix for the CPE end of the vectored group;

$\mathbf{\Lambda}$ is a diagonal matrix with the reflection coefficients, after the DLE, of the CPE end of the cables associated with the vectored group;

$\mathbf{H}$ is a matrix with the channel coefficients before the DLE; and

$\mathbf{H}'$ is a matrix with the estimated channel coefficients after the DLE.

10. The VCE, according to claim 9, being configured to continue the transmission of sync symbols on line l after the DLE.

11. The VCE, according to claim 9 or 10, wherein the transmission in data symbol positions on line l before the DLE comprises a FEXT precompensation signal from other lines and a direct signal of line l, and the VCE is configured to continue the transmission of the FEXT precompensation signal after the DLE, such that the reflection of crosstalk from the other lines remains cancelled at the CPE end of line l.

12. The VCE, according to claim 11, being configured to transmit the direct signal on line l with reduced power after the DLE, as compared to before the DLE.

13. The VCE, according to any of claims 9-12, being configured to apply one or more of the following for data symbol positions on line l after the DLE:

    - setting a gain scaling factor to zero, or close to zero;

    - setting symbol constellation points to zero, or close to zero, in a symbol encoder.

14. The VCE, according to any of claims 9-13 wherein the transmission in data symbol positions on other lines than line l before the DLE comprises FEXT precompensation signals, including the precompensated signal from line l, and a direct signal of its own, and wherein the VCE is

configured to stop the FEXT precompensation signal from line l on the other lines, while other signals are continued after the DLE.

15. The VCE, according to claim 14, being configured to reduce the FEXT precompensation signal from line l on other lines in power after the DLE, as compared to before the DLE.

16. The VCE, according to any of claims 9-15, wherein the obtaining of error samples comprises sending at least one error feedback request over either the eoc in both VDSL2 and G.fast or a ROC in VDSL2, or a RMC in G.fast.

17. DSLAM comprising a VCE according to any of claims 9-16.

References

[1] P. Ödling, T. Magesacher, S. Höst, P. O. Börjesson, M. Berg, and E. Areizaga, "The Fourth Generation Broadband Concept," in *IEEE Communications Magazine*, vol. 47, no. 1, pp. 62-69, January 2009.

[2] ITU, "Fast Access to Subscriber Terminals - Physical Layer Specification," Recommendation Draft ITU-T G.9701, 2014. [Online]. Available: https://www.itu.int/rec/T-REC-G.9701/en

[3] ITU, "Self-FEXT cancellation (vectoring) for use with VDSL2 transceivers," Recommendation ITU-T G.993.5, April 2010. [Online]. Available: https://www.itu.int/rec/T-REC-G.993.5/en

[4] C. Lu and P.-E. Eriksson, "A Fast Channel Estimation Method for Disorderly Leaving Events in Vectored DSL Systems," in *Proc. 2011 IEEE International Conference on Communications (ICC)*, pp. 1-6, June 2011.

[5] Alcatel-Lucent, "Influence of an Impedance Change on a Leaving Line onto the Direct and Crosstalk Channels of the Active Lines," ITU-T SG15 Contribution 2013-10-Q4-058, October 2013.

[6] Futurewei Technologies, "G.fast: SNR Drop and FEXT Channel Variations due to Change of Alien Termination," ITU-T SG15 contribution 2013-10-q4-046, March 2013.

[7] E. Medeiros, T. Magesacher, P. Ödling, D. Wei, X. Wang, Q. Li, P.-E. Eriksson, C. Lu, J. Boschma, and B. van den Heuvel, "Modeling Alien-Line Impedance Mismatch in Wideband Vectored Wireline Systems," in

IEEE Communications Letters, vol. 18, no. 9, pp. 1527-1530, September 2014.

[8] Ericsson AB, *Access Network Pair Cable, TEL 312*, 2010. [Online]. Available: http://goo.gl/4RdCXc

[9] R. Cendrillon, G. Ginis, E. Van den Bogaert, and M. Moonen, "A Near-Optimal Linear Crosstalk Precoder for Downstream VDSL," in *IEEE Transactions on Communications*, vol. 55, no. 5, pp. 860-863, May 2007.

Paper IV

4 Fast Mitigation of Sudden Termination Changes in Wireline Systems

Abstract

Vectoring enables cooperative crosstalk mitigation in wideband wireline systems. A sudden termination change within a vectored group alters the entire perceived channel matrix and thus disturbs the vectoring operation since the precoder, which is tuned to the channel before the change, is no longer up to date. We analyze the resulting residual crosstalk and its impact on performance degradation during showtime for both linear and non-linear precoding systems. To cover, a new channel matrix must be estimated to update the precoder accordingly. We use a model-based approach to track a vector instead of estimating the full matrix. Based on this vector, simplified precoder updating methods for both precoding systems are presented accounting for a sudden line deactivation or (re)activation in a vectored group. As an alternative to the state-of-the-art methods, the proposed procedures significantly reduce the complexity of both channel estimation and precoder updating and minimize the disturbed period for active users.

4.1   Introduction

The wireline access industry advances towards a fiber-to-the-last-distribution-point paradigm [1] to meet increasing capacity demands. The hybrid fiber-DSL architecture [2–4] exploits shorter copper pairs and wider bandwidth to provide multi-gigabit aggregate bit-rate. However, with the increased frequency range, new challenges appear. The transmission channel in the band above around 3 MHz becomes sensitive to reflections and dependent on the quality of connections. A sudden change of the termination impedance alters the channel conditions not only on the line of the change, but on all lines reached by crosstalk.

Vectoring [5,6] enables high-speed communication in wideband wireline systems by mitigating crosstalk between lines. With vectoring implemented, the transceivers of a copper pair group co-located at the distribution point (DP) can work cooperatively to cancel out crosstalk. This kind of cooperation relies on accurate channel information. Previous studies (cf., for example, [7] and references therein) indicate that a sudden termination change (STC) due to a disconnected customer-premises equipment (CPE) leads to serious signal-to-noise ratio (SNR) drops for frequencies around 30 MHz and beyond, which are the frequencies used in the emerging G.fast [2] and similar fixed broadband technologies. The SNR-drop results in a reduced bit-loading (exemplified in Fig. 4.1) for active users in the vectored group. For stability and performance reasons, it is desirable to retrieve the original performance as quickly as possible.

Unwanted impedance mismatch due to an STC can be avoided or mitigated by proper hardware design. For example, [8] designs an adaptive device that adapts its output impedance automatically to the effective load in order to maintain maximum transfer efficiency. It would solve the partial impedance matching problem, such as a switched-off CPE or a changed termination impedance due to temperature variation. In [9], an impedance adapter is designed including an additional adjustment module in network jacks for automatically inserting a compensatory terminating impedance when the CPE is not connected. However, hardware methods rely largely on the implementation at the customer premises which makes them costly to deploy and prone to user tampering. Thus, we investigate network-side signal-processing approaches.

In [10] a procedure is described that allows coordination between transceivers at both DP and CPE ends and acquires information necessary to update the precoder/equalizer before a line leaves and its terminating impedance changes. While solving the problem of orderly leaving events, [10] does not address situations where there is no previous intent announced by the leaving transceiver(s), termed disorderly leaving event (DLE). A DLE is a typical scenario leading
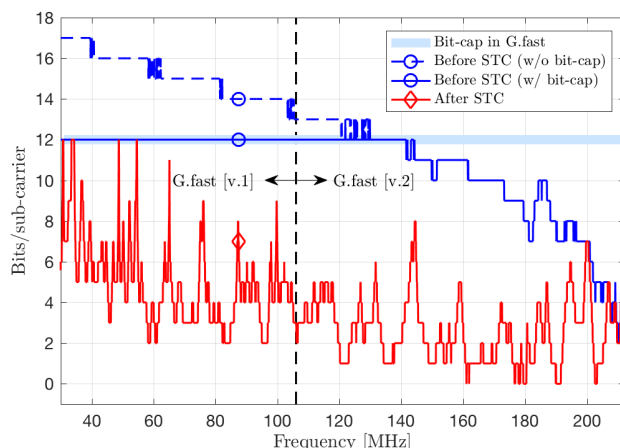
Fig. 4.1: Bit-loading results on a victim line exemplify the STC influence in a linear precoding system. The results are based on cable channel measurements from 30 MHz to 212 MHz assuming a transmit PSD of -76 dBm/Hz and a background noise PSD of -150 dBm/Hz over the copper cable. There is a big drop in loaded bits due to an STC no matter if bit-cap is applied or not.

to an STC due to a disconnected line or a power loss. In [11], a channel-tracking scheme is proposed for linear precoding systems [12] to make DLEs unnoticeable to active users. Due to the diminished direct channel dominance with increasing frequency, non-linear precoding [13, 14] is also proposed as a candidate for the frequency range above 106 MHz. In this paper, we address both linear and non-linear precoding systems. The main contributions of this paper are:

- The interference mitigation scheme proposed in [11] is combined with non-linear precoding (THP) to cover the frequency range of emerging wireline systems.

- All simulations and measurements are extended to 212 MHz allowing a comparison of the proposed schemes used in combination with linear versus non-linear precoding employing the system parameters of G.fast.

- The scheme is extended from the DLE case to the general STC case (including, most notably, the (re)activation of a line).

- Low-complexity precoder-update methods are proposed for both linear

and nonlinear precoding exploiting the rank-1 property of the channel-deviation matrix.

- A precoder-update scheme for the (re)activation case is proposed that significantly reduces the disturbed period for the active users compared to the traditional method.

The paper is organized as follows. In Section 4.2 a system model is presented to interpret STC, which enables the formulation and analysis of STC disturbance in Section 4.3. In Section 4.4, we propose a low-complexity method to quickly mitigate STC interference when a line is deactivated in a vectored group for both linear and non-linear precoding schemes. Section 4.5 derives the precoder updating procedure when a line joins a vectored group. Section 4.6 concludes the work.

Notation: Bold capital letters (*e.g.,* $\mathbf{A}$) and bold lower-case letters (*e.g.,* $\mathbf{a}$) denote matrices and column vectors, respectively. $a_{i,j}$ is the element in i-th row and j-th column of $\mathbf{A}$ and a_i is the i-th element of $\mathbf{a}$. $\mathbf{A}_{\mathcal{I},\mathcal{J}}$ denotes the submatrix of $\mathbf{A}$ constructed by the rows and columns in the index sets $\mathcal{I}$ and $\mathcal{J}$, respectively. For compactness, $\mathbf{A}_{n \setminus i} \in \mathbb{C}^{(n-1) \times (n-1)}$ denotes the (i,i) minor of $\mathbf{A}$ that deletes the i-th row and column from $\mathbf{A} \in \mathbb{C}^{n \times n}$ (*i.e.,* $\mathbf{A}_{n \setminus i} = \mathbf{A}_{\{1,\ldots,n\} \setminus i, \{1,\ldots,n\} \setminus i}$) and $\mathbf{A}_{-i}$ denotes the submatrix obtained by deleting the i-th row from $\mathbf{A}$ (*i.e.,* $\mathbf{A}_{-i} = \mathbf{A}_{\{1,\ldots,n\} \setminus i, \{1,\ldots,n\}}$). a^* denotes the conjugate of a. $\mathbf{A}^{\mathrm{T}}$, $\mathbf{A}^{\mathrm{H}}$, and $\mathbf{A}^{\dagger}$ denote transpose, Hermitian transpose, and pseudo inverse of $\mathbf{A}$, respectively. $\boldsymbol{\epsilon}_i$ is an elementary column vector with a 1 on the i-th position and 0s elsewhere. $\mathbf{I}$ denotes the identity matrix.

4.2   Wireline System Model

4.2.1   Vectoring Operation

Consider a wideband discrete multi-tone modulation (DMT) system with a group of K twisted pairs connecting the DP to CPEs. Let $\mathbf{H} \in \mathbb{C}^{K \times K}$ denote the frequency-domain channel matrix experienced in downstream direction by transceivers when all CPEs are properly connected (equivalently, all terminations are perfectly matched). For the sake of simple notation but without loss of generality, the sub-carrier index is omitted. Diagonal and off-diagonal elements of $\mathbf{H}$ denote direct-channel coefficients and far-end crosstalk (FEXT) coupling coefficients, respectively.

Vectoring enables cooperative signal processing to cancel out crosstalk within the group, by using a properly designed precoder for downstream and an equalizer for upstream at the DP. Specifically in downstream, let

$\mathbf{G} = \text{diag}\left([g_1, g_2, \ldots, g_K]\right) \in \mathbb{R}^{K \times K}$ denote a diagonal matrix, where each element g_i denotes the per-line gain multiplier, including gain adjuster, frequency-domain spectrum shaping coefficient, power-normalization factor, etc. (see [2]) and let $\bar{\mathbf{x}}(t) = \mathbf{G}\mathbf{x}(t)$ denote the signal after gain scaling. Assume that the cyclic prefix of DMT is not shorter than the impulse responses of the coupling paths, and the IFFT of group users is synchronized. Transmitting a precoded signal $P\{\bar{\mathbf{x}}(t)\} \in \mathbb{C}^{K \times 1}$ at time instant t yields a receive signal $\mathbf{y}(t) \in \mathbb{C}^{K \times 1}$ at the CPE side given by

$$\mathbf{y}(t) = \mathbf{H}P\{\bar{\mathbf{x}}(t)\} + \mathbf{n}(t),$$

where $P\{\cdot\}$ denotes a precoder designed for $\mathbf{H}$, and $\mathbf{n}(t) \in \mathbb{C}^{K \times 1}$ denotes the background noise on twisted pairs. Since most derivations in this work consider only a single time instant, we hereinafter omit the time index for brevity unless it is necessary to stress a time dependency.

A properly designed precoder limits the transmit power under the regulated power spectrum density (PSD) mask and mitigates crosstalk such that

$$\mathbf{H}P\{\bar{\mathbf{x}}\} = \boldsymbol{\Sigma}\mathbf{x}, \tag{4.1}$$

where $\boldsymbol{\Sigma} \in \mathbb{C}^{K \times K}$ is a diagonal matrix. The equalized receive signal is then written as

$$\mathbf{z} = \mathbf{E}\mathbf{H}P\{\bar{\mathbf{x}}\} + \mathbf{E}\mathbf{n},$$

where $\mathbf{E} = \boldsymbol{\Sigma}^{-1}$ is a diagonal matrix containing equalizing coefficients at the CPEside.
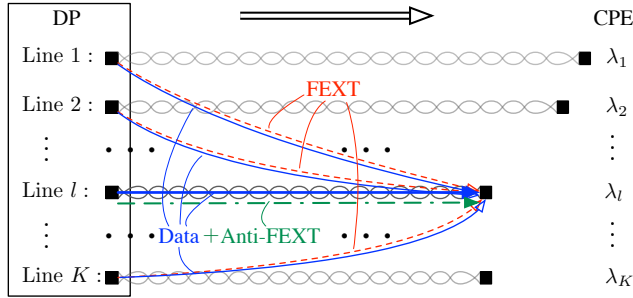
Fig. 4.2: Downstream vectoring operation for a linear precoding system exemplified on line l. The FEXT (red dashed lines) and anti-FEXT (green dashed-dotted line) signals cancel out at the l-th termination at the CPE side. Only the data signal (blue solid lines) is effectively transmitted to the end-user.

Fig. 4.2 illustrates the principle of vectoring based on the notion of "anti-FEXT". For simplicity, we focus on a single line l for linear precoding schemes (*i.e.*, $P\{\bar{\mathbf{x}}\} = \mathbf{P}\bar{\mathbf{x}}$, where $\mathbf{P}$ denotes the linear precoding matrix). The receive signal at the l-th CPE-end can be decomposed as

$$
\begin{aligned}
y_l = \quad & \underbrace{h_{l,l}p_{l,l}\bar{x}_l}_{\text{Data via direct path (bold solid blue in Fig. 4.2)}} \quad + \\
& \underbrace{\mathbf{H}_{l,\{1,...,K\}\backslash l}\mathbf{P}_{\{1,...,K\}\backslash l,l}\bar{x}_l}_{\text{Data via FEXT-paths (thin solid blue in Fig. 4.2)}} \quad + \\
& \underbrace{\mathbf{H}_{l,\{1,...,K\}\backslash l}\mathbf{P}_{\{1,...,K\}\backslash l,\{1,...,K\}\backslash l}\bar{\mathbf{x}}_{\{1,...,K\}\backslash l}}_{\text{FEXT (dashed red in Fig. 4.2)}} + \\
& \underbrace{h_{l,l}\mathbf{P}_{l,\{1,...,K\}\backslash l}\bar{\mathbf{x}}_{\{1,...,K\}\backslash l}}_{\text{Anti-FEXT (dashed-dotted green in Fig. 4.2)}} \quad + \mathbf{n}.
\end{aligned}
\tag{4.2}
$$

The precoder located at the DP knows all FEXT couplings ending in line l and generates an "anti-FEXT" signal (dashed-dotted green line) that cancels out the FEXT (dashed red lines) at the CPE-end so that only the data components arrive. Note that data is not only arriving via line l itself (bold blue line) but also via FEXT paths (thin blue lines) since the other lines are also transmitting their anti-FEXT components to eliminate the FEXT originating from line l. As a result, the vectoring operation transforms the matrix channel into K interference-free channels whose throughput is limited by background noise. The benefit of vectoring, however, is severely degraded by an STC event, as analyzed in the next section.

4.2.2   Reflected-NEXT (RN) Model

In [15, 16], a FEXT-reflected-NEXT (FRN) model is proposed to characterize the changed coupling condition due to an alien-line impedance mismatch at the CPE side. The STC case we study in this work is similar—except now the impedance change happens within the vectored group, as illustrated in Fig. 4.3 before involving any precoding scheme. In this scenario, not only FEXT but also data signals from the direct channel are reflected and coupled via near-end crosstalk (NEXT) paths. Therefore, we term it generally reflected-NEXT (RN) model. Without loss of generality, we illustrate the STC coupling model in downstream on a certain sub-carrier. It applies, *mutatis mutandis*, to upstream.

Let $\boldsymbol{\Lambda} = \text{diag}\left([\lambda_1, \lambda_2, \ldots, \lambda_K]\right) \in \mathbb{C}^{K \times K}$ denote a diagonal matrix containing the reflection coefficients λ_i, $i = 1, \ldots, K$ for each termination at the CPE side. Furthermore, let $\boldsymbol{\Lambda}_\circ$ and $\boldsymbol{\Lambda}'$ denote the reflection coefficient matrices

before and after an STC, respectively. The corresponding perceived channel matrices are $\mathbf{H}\{\boldsymbol{\Lambda}_\circ\}$ and $\mathbf{H}\{\boldsymbol{\Lambda}'\}$, respectively.

For simplicity, assume for a moment that all vectored lines are initially perfectly terminated ($\boldsymbol{\Lambda}_\circ = \mathbf{0}$ and thus $\mathbf{H}\{\boldsymbol{\Lambda}_\circ\} = \mathbf{H}$), which corresponds to the state illustrated in Fig. 4.2. Let $\mathbf{C} \in \mathbb{C}^{K \times K}$ denote the NEXT coupling matrix at the CPEside. The diagonal entries of $\mathbf{C}$, corresponding to the CPE-side echo coefficients, are assumed to be 0. In practice, most often only one diagonal element of $\boldsymbol{\Lambda}$ will deviate significantly from its original value at a given time instant due to an STC (*i.e.,* mismatch of a single line only). Assume line l exhibits a deactivating STC, quantified by a reflection coefficient changing from 0 to $|\lambda_l'| \gg 0$. Consequently, $\boldsymbol{\Lambda}' = \mathrm{diag}\left([0, \ldots, 0, \lambda_l', 0, \ldots, 0]\right)$. The perceived channel matrix after the STC becomes

$$\mathbf{H}\{\boldsymbol{\Lambda}'\} = \mathbf{H}\{\boldsymbol{\Lambda}_\circ\} + \boldsymbol{\Delta},$$

where $\boldsymbol{\Delta} = \mathbf{C}\boldsymbol{\Lambda}'\mathbf{H}$ quantifies the deviation from the all-terminated case according to the RN model. Note that the effective part of $\mathbf{C}\boldsymbol{\Lambda}'$ is contained in one column vector, *i.e.,* $\mathbf{C}\boldsymbol{\Lambda}' = [\mathbf{0} \quad \ldots \quad \mathbf{0} \quad \mathbf{v}_l \quad \mathbf{0} \quad \ldots \quad \mathbf{0}]$, where

$$\mathbf{v}_l = \lambda_l' \left[c_{1,l}, \ldots, c_{i,l}, \ldots, c_{K,l}\right]^\mathrm{T}. \tag{4.3}$$

Thus as in Fig. 4.3, the RN model indicates that the channel deviation matrix is composed of

$$\boldsymbol{\Delta} = \mathbf{C}\boldsymbol{\Lambda}'\mathbf{H} = \mathbf{v}_l\mathbf{H}_{l,\{1,\ldots,K\}}, \tag{4.4}$$

where $\mathbf{H}_{l,\{1,\ldots,K\}}$ is just a row vector. Since $\boldsymbol{\Delta} \neq \mathbf{0}$, the outdated precoding with $P_\circ\{\cdot\}$ designed for $\mathbf{H}\{\boldsymbol{\Lambda}_\circ\} = \mathbf{H}$ yields a perturbed version of $\mathbf{z}$, denoted
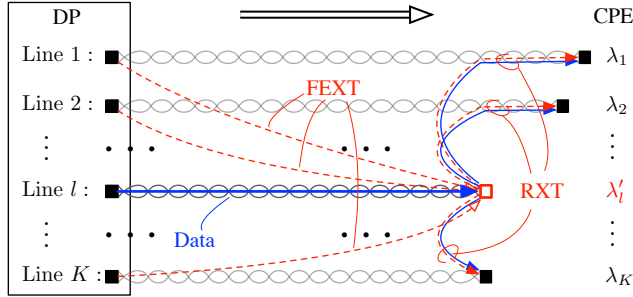
Fig. 4.3: Downstream reflected-NEXT (RN) model. All signals, including data (blue solid lines) and FEXT (red dashed lines), arriving at the mismatched termination l are reflected and coupled via the NEXT paths, generating residual crosstalk (RXT).

by $\mathbf{z}'$, *i.e.,*

$$\mathbf{z}' = \underbrace{\mathbf{EH}P_{\circ}\{\bar{\mathbf{x}}\} + \mathbf{En}}_{\mathbf{z}_d} + \underbrace{\mathbf{EC}\boldsymbol{\Lambda}'\mathbf{H}P_{\circ}\{\bar{\mathbf{x}}\}}_{\boldsymbol{\xi}}, \tag{4.5}$$

where $\mathbf{z}_d$ is the desired receive signal obtained with the precoder tuned to the perceived channel $\mathbf{H}\{\boldsymbol{\Lambda}_{\circ}\}$ before the STC and $\boldsymbol{\xi}$ is the residual crosstalk due to the STC. Our target is to update the precoder to mitigate also the residual crosstalk from reflected-NEXT couplings.

In practice, it is nearly impossible to achieve perfect termination of a multi-pair wireline channel. Thus, already before a deactivating STC occurs, the termination will cause reflected-NEXT components (since $\boldsymbol{\Lambda}_{\circ} \neq \mathbf{0}$) resulting in a perceived channel $\mathbf{H}\{\boldsymbol{\Lambda}_{\circ}\} = \mathbf{H} + \mathbf{C}\boldsymbol{\Lambda}_{\circ}\mathbf{H}$. After an STC changing $\boldsymbol{\Lambda}_{\circ}$ into $\boldsymbol{\Lambda}' = \boldsymbol{\Lambda}_{\circ} + \boldsymbol{\Lambda}_{\delta}$, the outdated precoder tuned to $\mathbf{H}\{\boldsymbol{\Lambda}_{\circ}\}$ yields

$$\mathbf{z}' = \underbrace{\mathbf{EH}\{\boldsymbol{\Lambda}_{\circ}\}P_{\circ}\{\bar{\mathbf{x}}\} + \mathbf{En}}_{\mathbf{z}_d} + \underbrace{\mathbf{EC}\boldsymbol{\Lambda}_{\delta}\mathbf{H}P_{\circ}\{\bar{\mathbf{x}}\}}_{\boldsymbol{\xi}}. \tag{4.6}$$

In the scenario of single line mismatch at a given time instant, the channel deviation is $\boldsymbol{\Delta} = \mathbf{C}\boldsymbol{\Lambda}_{\delta}\mathbf{H} = \mathbf{v}_l^{\delta}\mathbf{H}_{l,\{1,\dots,K\}}$, for $\mathbf{v}_l^{\delta} = (\lambda_l' - \lambda_l)\,[c_{1,l},\dots,c_{i,l},\dots,c_{K,l}]^{\mathrm{T}}$, where λ_l and λ_l' denote the l-th reflection coefficients before and after the STC, respectively. Since there is no difference in formulating Eqs. (4.5) and (4.6), we mainly consider the case where all vectored lines are initially perfectly terminated (*i.e.,* $\boldsymbol{\Lambda}_{\circ} = \mathbf{0}$) in the following discussions to avoid unnecessary confusion.

Apart from the deactivated-line case discussed above, another practically relevant case causing severe performance degradation occurs when a line in vicinity is (re)activated in the vectored group. The only difference from the deactivated-line case is that the outdated precoder $P_{\circ}\{\cdot\}$ is tuned to $\mathbf{H}\{\boldsymbol{\Lambda}_{\circ}\} = \mathbf{H} + \boldsymbol{\Delta}$ and the target channel after STC becomes $\mathbf{H}\{\boldsymbol{\Lambda}'\} = \mathbf{H}$. Therefore, the model component analysis in Section 4.3 focuses on the deactivated-line case only.

The residual crosstalk $\boldsymbol{\xi}$ that is not covered by the outdated precoder $P_{\circ}\{\cdot\}$ is the main reason for performance degradation. To mitigate this interference effectively and minimize the disturbed period for active users, we start by analyzing the residual crosstalk.

4.3   Residual Crosstalk Analysis

The undesirable residual crosstalk $\boldsymbol{\xi}$ in Eq. (4.5) is dependent on the precoded transmit signal $P_{\circ}\{\bar{\mathbf{x}}\}$. For linear and non-linear precoding schemes suggested in [2], we analyze the contributing source(s) of $\boldsymbol{\xi}$ when a line is suddenly deactivated in the vectored group.

4.3.1 Residual Crosstalk in Linear Precoding Systems

The function $P_\circ\{\cdot\}$ in linear precoding systems performs multiplication in frequency domain. The outdated linear precoder (LP) as in [12] defines $\mathbf{P}_\circ^{\mathrm{L}} = (\mathbf{H}\{\mathbf{\Lambda}_\circ\})^{-1} = \mathbf{H}^{-1}$. Note that in this work, the power normalization factor and direct channel gain have already been included in the corresponding multiplier in $\mathbf{G}^{\mathrm{L}}$, where the data signal after gain scaling is $\bar{\mathbf{x}} = \mathbf{G}^{\mathrm{L}}\mathbf{x}$.

Consider again the case when the l-th termination is deactivated while all other lines are perfectly terminated. The residual crosstalk can be simplified as

$$\begin{aligned}\boldsymbol{\xi}^{\mathrm{L}} &= \mathbf{E}\mathbf{C}\mathbf{\Lambda}'\mathbf{H}\mathbf{P}_\circ^{\mathrm{L}}\bar{\mathbf{x}} = \mathbf{E}\mathbf{v}_l\boldsymbol{\epsilon}_l^{\mathrm{T}}\bar{\mathbf{x}} \\ &= \mathbf{E}\mathbf{v}_l\bar{x}_l,\end{aligned} \tag{4.7}$$

where $\mathbf{v}_l$ is defined in Eq. (4.3), $\boldsymbol{\epsilon}_l$ is an elementary vector introduced in Section 4.1 and $\bar{x}_l = g_l^{\mathrm{L}}x_l$ is the gain-scaled data symbol transmitted on line l.

According to Eq. (4.7), we conclude that the only activating source of the residual crosstalk, given the outdated LP, is the data signal sent to the l-th CPE. In addition, the strength of the residual crosstalk is mainly determined by the effective direct channel gain g_l^{L} of the deactivating line and the NEXT coupling magnitude included in $\mathbf{v}_l$.

4.3.2 Residual Crosstalk in Non-Linear Precoding Systems

When exploring a wider frequency range (*e.g.,* beyond 100 MHz), the diagonal dominance of the channel matrix declines which reduces the merit of applying LP. Non-linear precoding is suggested as an alternative [2, 17]. Specifically, a Tomlinson-Harashima precoder (THP) is implemented [13] modifying the transmit signal non-linearly to achieve crosstalk-free transmission without invoking transmit power increase.

Performing QR-decomposition on the Hermitian-transpose of the original channel matrix $\mathbf{H}\{\mathbf{\Lambda}_\circ\} = \mathbf{H}$ yields $\mathbf{H}^{\mathrm{H}} = \mathbf{Q}\mathbf{R}$ (or $\mathbf{H} = \mathbf{R}^{\mathrm{H}}\mathbf{Q}^{\mathrm{H}}$), where $\mathbf{Q}$ is a unitary matrix and $\mathbf{R}^{\mathrm{H}}$ is a lower-triangular matrix. To achieve crosstalk-free transmission, dirty paper coding (DPC) [18] can be used to precode the transmit signal as $\mathbf{Q}(\mathbf{R}^{\mathrm{H}})^{-1}\mathbf{G}^{\mathrm{NL}}\mathbf{x}$ such that $\mathbf{G}^{\mathrm{NL}}\mathbf{x}$ is received at the CPE side. However, there is an inherent power increase issue in DPC. In practice, THP is used instead, which can be written as

$$P_\circ^{\mathrm{NL}}\{\bar{\mathbf{x}}\} = \mathbf{Q}\bar{\bar{\mathbf{x}}}, \tag{4.8}$$

where $\bar{\bar{\mathbf{x}}}$ denotes the recursive computation of the inverse $\left(\mathbf{R}^{\mathrm{H}}\right)^{-1}$ in combination with a modulo operation on the gain-scaled transmit signal $\bar{\mathbf{x}} = \mathbf{G}^{\mathrm{NL}}\mathbf{x}$:

$$\bar{\bar{x}}_m = \Gamma\left\{\frac{1}{r_{m,m}}\bar{x}_m - \langle m > 1\rangle \sum_{i=1}^{m-1} \frac{r_{i,m}^*}{r_{m,m}} \bar{\bar{x}}_i\right\}, \text{ for } m = 1,\ldots,K. \qquad (4.9)$$

The operator $\langle\cdot\rangle$ produces 1 if the statement inside is true and 0 otherwise. The non-linear modulo operation on each M-QAM symbol x is defined [13] as

$$\Gamma\{x\} \triangleq x - \sqrt{M}d\left\lfloor \frac{x}{\sqrt{M}d} + \frac{1}{2} + j\frac{1}{2}\right\rfloor,$$

where d is the minimum constellation spacing.

To make the THP feasible, the modulo arithmetic $\Gamma\{\cdot\}$ is employed at both transmitter and receiver. Based on $\Gamma\{x\pm y\} = \Gamma\{\Gamma\{x\}\pm\Gamma\{y\}\}$, the disturbed receive signal in Eq. (4.5) becomes

$$\boldsymbol{\Gamma}\{\mathbf{z}'\} = \boldsymbol{\Gamma}\Big\{\boldsymbol{\Gamma}\{\mathbf{z}_d\} + \underbrace{\boldsymbol{\Gamma}\{\mathbf{EC}\boldsymbol{\Lambda}'\mathbf{H}P_{\mathrm{o}}^{\mathrm{NL}}\{\bar{\mathbf{x}}\}\}}_{\boldsymbol{\xi}^{\mathrm{NL}}}\Big\},$$

where $\boldsymbol{\Gamma}\{\cdot\}$ denotes modulo operation on each entry of the input vector. The residual crosstalk part can be expanded using Eq. (4.8) as

$$\boldsymbol{\xi}^{\mathrm{NL}} = \boldsymbol{\Gamma}\Big\{\mathbf{EC}\boldsymbol{\Lambda}'\mathbf{H}P_{\mathrm{o}}^{\mathrm{NL}}\{\bar{\mathbf{x}}\}\Big\}$$
$$= \boldsymbol{\Gamma}\Big\{\mathbf{Ev}_l\big(\mathbf{R}_{\{1,\ldots,K\},l}\big)^{\mathrm{H}}\bar{\bar{\mathbf{x}}}\Big\}. \qquad (4.10)$$

Further expanding Eq. (4.10) with Eq. (4.9), we have

$$\boldsymbol{\xi}^{\mathrm{NL}} = \boldsymbol{\Gamma}\left\{\mathbf{Ev}_l \sum_{i=1}^{l} r_{i,l}^* \bar{\bar{x}}_i\right\}$$
$$= \boldsymbol{\Gamma}\left\{\mathbf{Ev}_l r_{l,l}\left(\sum_{i=1}^{l-1}\frac{r_{i,l}^*}{r_{l,l}}\bar{\bar{x}}_i + \Gamma\left\{\frac{1}{r_{l,l}}\bar{x}_l - \sum_{i=1}^{l-1}\frac{r_{i,l}^*}{r_{l,l}}\bar{\bar{x}}_i\right\}\right)\right\}$$
$$= \boldsymbol{\Gamma}\{\mathbf{Ev}_l \bar{x}_l\}, \qquad (4.11)$$

since $\Gamma\{ax\} = \Gamma\{a\Gamma\{x\}\}$ where a is a constant. Similarly to the situation in Section 4.3.1, the residual crosstalk in non-linear precoding systems is driven by the transmitted data signal for the deactivated termination and its strength depends on the l-th effective channel gain and the NEXT couplings. In addition, it is also influenced by the non-linear modulo operation $\boldsymbol{\Gamma}\{\cdot\}$.

4.3.3   STC Impact on Linear and Non-Linear Precoders

In order to quantify the impact of a deactivating STC, we focus on a single
sub-carrier and apply both LP and THP for predefined channel conditions.
The results presented in this subsection are averaged over a large ensemble of
coupling values drawn from distributions whose parameters are aligned with
cable measurements. The motivation for explicitly using theoretical channel
realizations in this subsection is to separate different impact factors and iso-
late the effect of discussed coupling magnitudes from possible performance
variations due to non-ideal measurements. Also, artificial channel data allows
the observation of trends over wider magnitude ranges compared to snapshot
channel-measurements.

   Since the average NEXT magnitude does not change much for a certain
cable setup, we consider the influence of magnitude difference between direct
and FEXT couplings, which determines the effective channel gains for LP and
THP respectively. Random 3×3 channel matrices are generated where each
entry has a preset magnitude value $A_{i,j}$ and a uniformly distributed phase,
i.e., $h_{i,j} \sim A_{i,j}\exp(\mathrm{i}2\pi\phi_{i,j})$ where $\phi_{i,j} \sim \mathcal{U}(0,1]$. The average receive SNR on
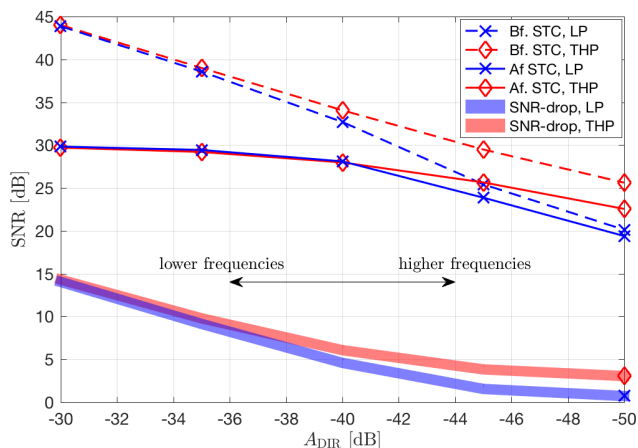
Fig. 4.4: Impact of STC on one victim line given different diagonal dominance of
the channel, pre-setting a FEXT coupling of $A_{\mathrm{FEXT}} = -50\,\mathrm{dB}$, a NEXT coupling of
$A_{\mathrm{NEXT}} = -30\,\mathrm{dB}$, and a vectoring group size of $K = 3$. The reflection coefficient of the
disrupted termination changes from 0 to 1 when STC happens. The left-hand side
of the abscissa with higher A_{DIR} values corresponds to the lower frequency range and
the right-hand side with lower A_{DIR} values corresponds to the higher frequency range.

victim lines is computed for a transmit PSD of $-76\,\text{dBm/Hz}$, a background noise of $-150\,\text{dBm/Hz}$, and the reflection coefficient of disrupted termination changing from $\lambda_l = 0$ to $\lambda'_l = 1$.

In Fig. 4.4, the diagonal dominance of channel matrices degrades along the abscissa as the FEXT magnitude is fixed. The right extremity of the axis is the situation that might happen at very high frequencies where the direct and FEXT couplings are at the same magnitude level. We observe that the SNR-drop is more obvious for diagonal dominant channels (*i.e.,* $A_{\text{DIR}} \gg A_{\text{FEXT}}$) than for channels with direct and FEXT coefficients of similar magnitude (*i.e.,* $A_{\text{DIR}} \approx A_{\text{FEXT}}$). The reason is that the higher values of direct channel gain g_l indicate both higher original SNR values before STC and higher residual crosstalk (see Eqs. (4.7) and (4.11)) after STC. Along with the diminishing A_{DIR} values both SNR results before and after STC, as well as the relative SNR-drop, decrease.

As one of the major advantages, THP generally yields higher effective channel gains compared to the LP when the coupling magnitude of FEXT becomes comparable to that of the direct paths. Since the g_l^{NL} also contributes in generating residual crosstalk, this advantage in turn makes the non-linear precoding system more vulnerable to the STC problem than the linear precoding system, showing a larger SNR-drop in Fig. 4.4 for the same channel condition.

In Fig. 4.5, group-size impact is discussed. In both Fig. 4.5a and Fig. 4.5b and for both precoders, SNR values after the deactivating STC do not change much with respect to different group sizes. When diagonal dominance is high (see Fig. 4.5a) the performance of THP does not depend on group size, both before and after STC. The SNR value of LP decreases for larger group size, whereas the relative SNR-drop also gets smaller. When the direct and FEXT coupling magnitudes become comparable (see Fig. 4.5b), the effective direct coupling for LP is quite low. As also shown in Fig. 4.4, the STC impact in this case becomes negligible. But for THP which is designed for this channel condition, the relative SNR-drop gets slightly bigger for larger group size.

4.3.4   Silent-Mode for Residual Crosstalk Cancellation

To mitigate the aforementioned residual crosstalk effectively and retrieve the original performance efficiently, we first summarize Eqs. (4.7) and (4.11) as

$$\boldsymbol{\xi} = \begin{cases} \mathbf{Ev}_l g_l^\top x_l & \text{for linear precoding,} \\ \boldsymbol{\Gamma}\{\mathbf{Ev}_l g_l^{\text{NL}} x_l\} & \text{for non-linear precoding.} \end{cases} \tag{4.12}$$

It is observed in Eq. (4.12) that the only activating source of the residual crosstalk $\boldsymbol{\xi}$ in both precoding schemes is the data signal x_l on the deactivated line with a gain multiplier g_l.
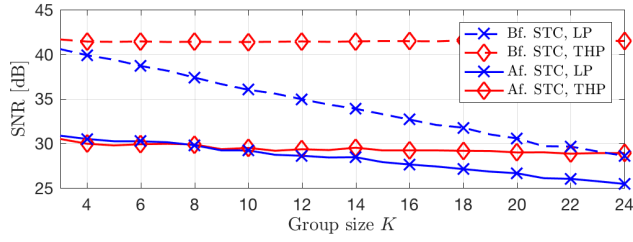
(a) $A_{\text{DIR}} - A_{\text{FEXT}} = 20\,\text{dB}$ (diagonal dominant)
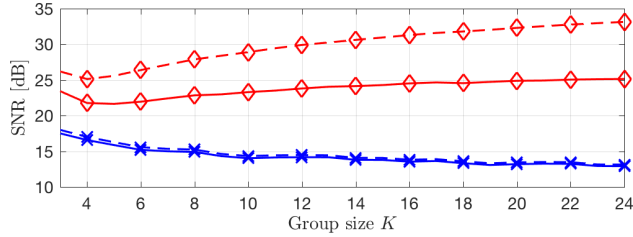
(b) $A_{\text{DIR}} = A_{\text{FEXT}}$

Fig. 4.5: Impact of STC on one victim line given different vectoring group size, presetting a FEXT coupling of $A_{\text{FEXT}} = -50\,\text{dB}$, and a NEXT coupling of $A_{\text{NEXT}} = -30\,\text{dB}$. The reflection coefficient of the disrupted termination changes from 0 to 1 when STC happens. Two sets of simulations are presented when diagonal dominance is and is not valid for channel matrices.

For a fast mitigation of the residual crosstalk in Eq. (4.12), [11] proposes that the DP transmits *idle symbols* [2] on the leaving line l by modifying only the l-th multiplier to be $g_l = 0$, which yields $\boldsymbol{\xi} = 0$ for both precoding schemes. As sketched in Fig. 4.6, the main idea is to transmit only the anti-FEXT signal (equivalently, the idle symbols) on line l after an STC. The pure anti-FEXT cancels out FEXT and thus there is no energy arriving at the mismatched termination to cause any reflections and subsequent NEXT into other lines. No precoder update is needed at this stage. It enables an "STC-silent" scenario in the sense that active users remain undisturbed, which is termed *silent mode* transmission. As a result, the STC-interfering period to active users is shortened to the time it takes the DP to detect the loss of signal on line l.

Fig. 4.7 shows that the rate degradation introduced in Fig. 4.1 can be fixed by simply zeroing the l-th multiplier, which essentially solves the disrupted-vectoring problem caused by a deactivating STC. However, keeping the analog front-end running to send pure anti-crosstalk signals consumes power. If the
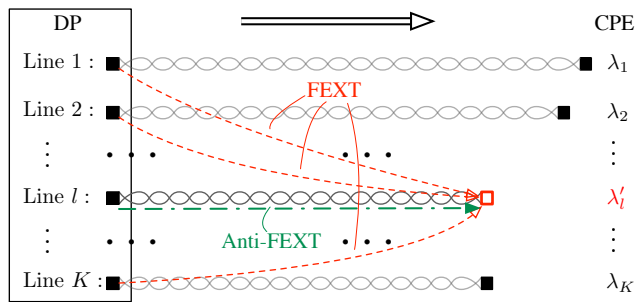
Fig. 4.6: Silent-mode for residual crosstalk cancellation. Transmit idle symbols which contain pure anti-FEXT signal on the disruptive line l. No signal will be reflected at the mismatched termination. Residual crosstalk is avoided.

deactivated termination leaves for long, it is thus desirable to invoke a further
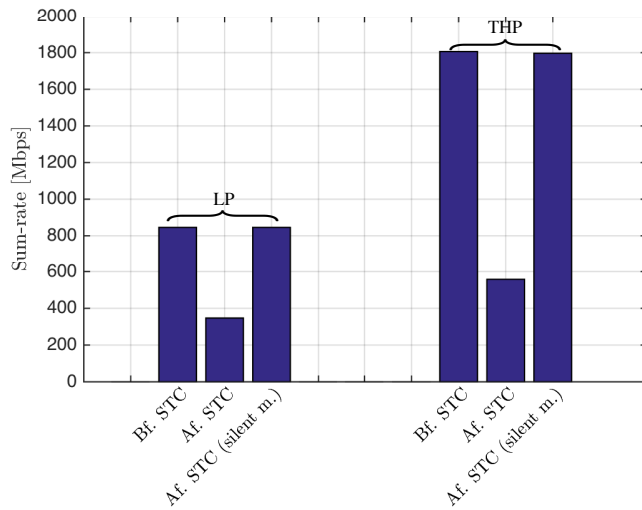
Fig. 4.7: Sum-rate comparison on one victim line, given a full line transmission with the outdated precoder $P_{\mathrm{o}}\{\cdot\}$. Cable measurements are used for a group size of $K = 3$. The results are calculated over $30\,\mathrm{MHz}$–$106\,\mathrm{MHz}$ for linear precoding, and over $30\,\mathrm{MHz}$–$212\,\mathrm{MHz}$ for non-linear precoding. A bit cap of 12 bits is assumed. The sum-rate drop caused by a deactivating STC can be quickly recovered by the proposed silent mode transmission in both precoding systems.

process in order to track the dimension reduced new channel, and update the precoder accordingly.

4.4   Precoder Update When Deactivating The Disruptive Line

4.4.1   Parameterized Channel Estimation

Both cable measurements and the RN model indicate that the whole channel matrix except for the l-th row is changed after an STC. However as interpreted in Eq. (4.4), the non-sparse deviation matrix $\boldsymbol{\Delta} = \mathbf{v}_l \mathbf{H}_{l,\{1,\dots,K\}}$ is composed by two vectors, where $\mathbf{H}_{l,\{1,\dots,K\}}$ is already known as part of the original channel $\mathbf{H}\{\boldsymbol{\Lambda}_\circ\}$. To estimate the new channel matrix $\mathbf{H}\{\boldsymbol{\Lambda}'\}_{K\setminus l}$ after shutting down the disruptive line, we only need to estimate the vector $\mathbf{v}_l$ without the l-th element.

In [11], a parameterized channel estimation for linear precoding is proposed in order to deactivate a disruptive line. To make the whole process unnoticeable to active users, idle symbols and synchronization symbols are alternately transmitted on the leaving line until the estimated reflecting crosstalk coefficients in vector $\widehat{\mathbf{v}}_l \in \mathbb{C}^{(K-1)\times 1}$ are obtained. Transmitting idle symbols guarantees that the data symbols on showtime lines are not disturbed. Synchronization symbols are utilized as pilots for the estimation of vector $\mathbf{v}_l$ based on the resulting residual crosstalk.

When the lines are initially not perfectly terminated, *i.e.,* $\boldsymbol{\Lambda}_\circ \neq \mathbf{0}$, Eq. (4.6) indicates that the residual crosstalk is given by

$$\boldsymbol{\xi}_{\mathrm{imperfect}} = \mathbf{E}\mathbf{C}\boldsymbol{\Lambda}_\delta \mathbf{H} P_\circ\{\bar{\mathbf{x}}\}.$$

In this case, the LP which is tuned to $\mathbf{H}\{\boldsymbol{\Lambda}_\circ\}$ can be formulated by

$$\begin{aligned}
\mathbf{P}_\circ^{\mathrm{L}} &= (\mathbf{H} + \mathbf{C}\boldsymbol{\Lambda}_\circ\mathbf{H})^{-1} \\
&= \mathbf{H}^{-1} - \mathbf{H}^{-1}\mathbf{C}\left(\boldsymbol{\Lambda}_\circ^{-1} + \mathbf{C}\right)^{-1},
\end{aligned}$$

if all diagonal entries of $\boldsymbol{\Lambda}_\circ$ are non-zero. The residual crosstalk for the imperfect case becomes

$$\begin{aligned}
\boldsymbol{\xi}_{\mathrm{imperfect}} &= \mathbf{E}\mathbf{C}\boldsymbol{\Lambda}_\delta \mathbf{H}\mathbf{P}_\circ^{\mathrm{L}}\bar{\mathbf{x}} \\
&= \mathbf{E}\mathbf{C}\boldsymbol{\Lambda}_\delta \left(\mathbf{I} - \mathbf{C}\left(\boldsymbol{\Lambda}_\circ^{-1} + \mathbf{C}\right)^{-1}\right)\bar{\mathbf{x}} \\
&= \mathbf{v}_l^\delta \Big(\bar{x}_l - \underbrace{\left[\mathbf{C}\left(\boldsymbol{\Lambda}_\circ^{-1} + \mathbf{C}\right)^{-1}\right]_{l,\{1,\dots,K\}}\bar{\mathbf{x}}}_{\mathrm{scalar}}\Big). \qquad (4.13)
\end{aligned}$$

As a comparison, the scalar term in Eq. (4.13) for the perfect-termination case (as in [11] and in the following simulations) is perceived to be zero when estimating $\mathbf{v}_l$ based on $\boldsymbol{\xi}$. To quantify possible estimation errors due to this scalar term, we define the relative measure τ as

$$\tau \triangleq \frac{\|\widehat{\mathbf{v}}_l^\delta - \mathbf{v}_l^\delta\|^2}{\|\mathbf{v}_l^\delta\|^2} = \left| \frac{\left[\mathbf{C} \left(\boldsymbol{\Lambda}_\circ^{-1} + \mathbf{C} \right)^{-1} \right]_{l,\{1,\dots,K\}} \bar{\mathbf{x}}}{\bar{x}_l} \right|^2 .$$

It is observed that the main estimation error source when applying the method in [11] to an imperfect case is the initial reflection coefficients in $\boldsymbol{\Lambda}_\circ$, and it does not rely on $\boldsymbol{\Lambda}'$ after the STC.

The simulated relative estimation error τ with measured channel data is shown in Fig. 4.8, assuming that all CPEs in the vectored group start with the same reflection coefficient magnitude $|\lambda_o|$, and the phase being uniformly distributed. Channel measurements at three frequency points are selected to exemplify the influence from the scalar term throughout the studied frequency range. Generally, the relative estimation error increases for larger initial values of $|\lambda_o|$ due to the ignorance of the scalar term in Eq. (4.13). In many countries, return loss, which is defined as the ratio between the incident signal power and the reflected signal power, is strictly constrained, which in turn limits the reflection coefficient magnitude when a termination is connected.
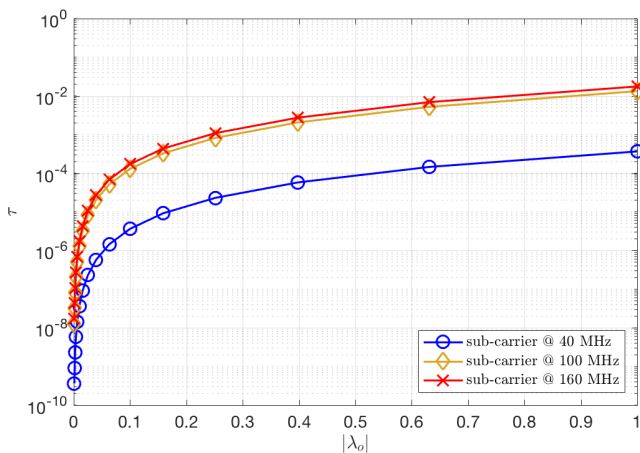
Fig. 4.8: Relative estimation error on $\mathbf{v}_l$ given imperfect initial terminations. Channel measurements are used for a group size $K = 3$. Assume a transmit PSD of $-76\,\mathrm{dBm/Hz}$ and a background noise PSD of $-150\,\mathrm{dBm/Hz}$ over the copper cable.

Although the process in [11] is derived based on LP, simulation shows that it is feasible for THP as well. The detailed simulation results will be illustrated in a dedicated subsection.

A traditional way to counteract the STC, however, is to shut down line l as soon as possible. As clarified in [11], this is not adequate to cancel out all residual crosstalk. To retrieve the original performance, an additional elementwise estimation for $\mathbf{H}\{\boldsymbol{\Lambda}'\}_{K\setminus l}$ is required using synchronization symbols and pilot sequences. If Hadamard sequences are used, it requires at least $2^{\lceil \log_2(K-1)\rceil}$ synchronization symbols to estimate $(K-1)^2$ channel elements for each subcarrier. Since the orthogonality of Hadamard sequences can be degraded by background noise, a multiple of $2^{\lceil \log_2(K-1)\rceil}$ synchronization symbols may be needed to achieve the desired estimation performance.

In Fig. 4.9, computational complexities of the traditional and proposed estimation methods on one sub-carrier are compared by counting the number C of involved additions and multiplications. For the traditional method, J mutual orthogonal sequences, corresponding to $J \cdot 2^{\lceil \log_2(K-1)\rceil}$ synchronization symbols, are used for a full channel estimation. The number of required synchronization symbols also determines the length of the disturbed period for active users. As a comparison, J in the proposed estimation method is the
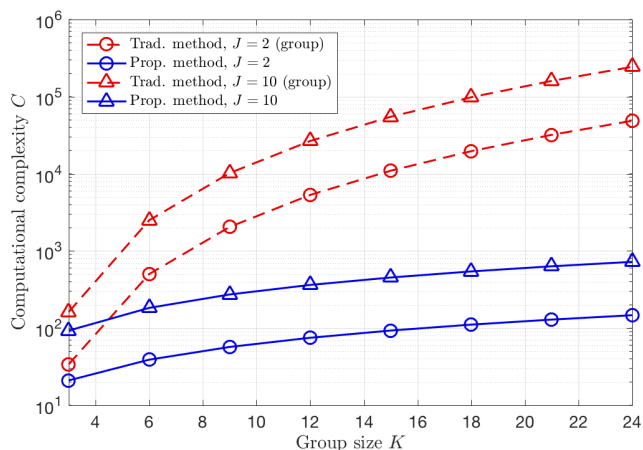
Fig. 4.9: Comparison of computational complexity C measured as number of multiplications and additions required for estimating $\mathbf{H}\{\boldsymbol{\Lambda}'\}_{K\setminus l}$ on one sub-carrier. The computational efficiency of the proposed method is more obvious for a larger group size.

number of involved synchronization symbols since no orthogonality is assumed. It is clear in Fig. 4.9 that the parameterized estimation is much simpler than the traditional way, and its advantage is more evident for larger group size.

A further observation is that in the case of a single line deactivation, the new channel is a rank-1 update of the original channel since

$$\mathbf{H}\{\boldsymbol{\Lambda}'\} = \mathbf{H}\{\boldsymbol{\Lambda}_\circ\} + \mathbf{v}_l \mathbf{H}_{l,\{1,\ldots,K\}}. \tag{4.14}$$

This property facilitates precoder updating in a complexity-efficient way, which is addressed in the following subsections for both precoding schemes.

4.4.2 Linear Precoder (LP) Update

With $\mathbf{v}_l$ estimated, the LP can be updated as the inverse of the new channel matrix $\mathbf{H}\{\boldsymbol{\Lambda}'\}_{K\backslash l}$ according to the RN model, *i.e.*, $\widehat{\mathbf{P}}^{\mathrm{L}}_{\mathrm{basic}} = (\mathbf{H}_{K\backslash l} + \widehat{\mathbf{v}}_l \mathbf{H}_{l,\{1,\ldots,K\}\backslash l})^{-1}$. However, the original $\mathbf{H}$ is not always directly available and full matrix inversion is not the best choice. We perform the precoder updating by utilizing only the outdated precoder $\mathbf{P}^{\mathrm{L}}_\circ$ and the estimated $\widehat{\mathbf{v}}_l$ instead.

Consider that the LP operates for frequencies up to $106\,\mathrm{MHz}$, where the channel matrix is diagonally dominant. Separating $\mathbf{P}^{\mathrm{L}}_\circ = \mathbf{P}_\Sigma + \mathbf{P}_\Delta$, where $\mathbf{P}_\Sigma$ carries the diagonal entries and $\mathbf{P}_\Delta$ carries the off-diagonal entries, the original $\mathbf{H}$ can be approximated by

$$\mathbf{H} \approx \mathbf{P}^{-1}_\Sigma \left(\mathbf{I} - \mathbf{P}_\Delta \mathbf{P}^{-1}_\Sigma \right), \tag{4.15}$$

using the first-order inverse approximation. Its l-th row, excluding $h_{l,l}$, is given by

$$\widehat{\mathbf{H}}_{l,\{1,\ldots,K\}\backslash l} = \frac{-\boldsymbol{\epsilon}^{\mathrm{T}}_l \mathbf{P}^{\mathrm{L}}_\circ \mathbf{P}^{-1}_\Sigma \mathbf{I}^{\mathrm{T}}_{-l}}{p_{l,l}}. \tag{4.16}$$

Let $\mathbf{M}_{\boldsymbol{\sigma}}$ denote a permutation matrix, *i.e.*, $\mathbf{M}_{\boldsymbol{\sigma}} = [\boldsymbol{\epsilon}_{\boldsymbol{\sigma}(1)} \quad \boldsymbol{\epsilon}_{\boldsymbol{\sigma}(2)} \quad \cdots \quad \boldsymbol{\epsilon}_{\boldsymbol{\sigma}(K)}]^{\mathrm{T}}$, where $\boldsymbol{\sigma}$ is a vector indicating the desired order. Compose $\mathbf{M}_{\boldsymbol{\sigma}_1}$ with $\boldsymbol{\sigma}_1 = [\{1,\ldots,K\}\backslash l, l]$ such that the channel matrix can be re-arranged into

$$\mathbf{M}_{\boldsymbol{\sigma}_1} \mathbf{H} \mathbf{M}^{\mathrm{T}}_{\boldsymbol{\sigma}_1} = \left[\begin{array}{cc} \mathbf{H}_{K\backslash l} & \mathbf{H}_{\{1,\ldots,K\}\backslash l,l} \\ \mathbf{H}_{l,\{1,\ldots,K\}\backslash l} & h_{l,l} \end{array} \right],$$

where only $\mathbf{H}_{K\backslash l}$ is of interest while the other submatrices relate to the leaving line and are thus irrelevant to the new precoder. Use this $\mathbf{M}_{\boldsymbol{\sigma}_1}$ to construct a permuted version of precoder as

$$\mathbf{P}_{\boldsymbol{\sigma}} = \mathbf{M}_{\boldsymbol{\sigma}_1} \mathbf{P}^{\mathrm{L}}_\circ \mathbf{M}^{\mathrm{T}}_{\boldsymbol{\sigma}_1} = \begin{bmatrix} \mathbf{P}_{\mathrm{A}} & \mathbf{p}_{\mathrm{B}} \\ \mathbf{p}_{\mathrm{C}} & p_{\mathrm{D}} \end{bmatrix},$$

where $\mathbf{P}_\mathrm{A}$ has the same size as $\mathbf{H}_{K\backslash l}$. A preliminarily updated precoder $\widetilde{\mathbf{P}}$ is then generated by

$$\widetilde{\mathbf{P}} = \mathbf{P}_\mathrm{A} - \frac{\mathbf{p}_\mathrm{B}\mathbf{p}_\mathrm{C}}{p_\mathrm{D}}, \tag{4.17}$$

which is $\left(\mathbf{H}_{K\backslash l}\right)^{-1}$.

According to the rank-1 update property in Eq. (4.14) and using the Sherman-Morrison formula, the LP for $\mathbf{H}\{\mathbf{\Lambda'}\}_{K\backslash l}$ can be updated by using the estimated vector $\widehat{\mathbf{v}}_l$, the derived row vector $\widehat{\mathbf{H}}_{l,\{1,\dots,K\}\backslash l}$ in Eq. (4.16) and the preliminarily updated precoder $\widetilde{\mathbf{P}}$ in Eq. (4.17) as

$$\widehat{\mathbf{P}}^{\mathrm{L}} = \widetilde{\mathbf{P}} \left(\mathbf{I} - \frac{\widehat{\mathbf{v}}_l\widehat{\mathbf{H}}_{l,\{1,\dots,K\}\backslash l}\widetilde{\mathbf{P}}}{1 + \widehat{\mathbf{H}}_{l,\{1,\dots,K\}\backslash l}\widetilde{\mathbf{P}}\widehat{\mathbf{v}}_l} \right), \tag{4.18}$$

without inverting any matrix. Also, the multiplier matrix $\mathbf{G}^{\mathrm{L}}$ can be updated accordingly.

4.4.3 Tomlinson-Harashima Precoder (THP) Update

For a small group number K, updating the THP can be achieved by a new QR-decomposition on the dimension-reduced new channel $\mathbf{H}\{\mathbf{\Lambda'}\}_{K\backslash l} = \mathbf{H}\{\mathbf{\Lambda}_\circ\}_{K\backslash l} + \widehat{\mathbf{v}}_l\mathbf{H}_{l,\{1,\dots,K\}\backslash l}$. For large K, the computational complexity can be reduced by QR-update of the original $\mathbf{Q}$ and $\mathbf{R}$ exploiting the property of the Hessenberg matrix and Givens rotations [19].

Let $\mathcal{J}_1 = \mathbf{J}_{K-1}^{(1)}\cdots\mathbf{J}_l^{(1)}$ denote a sequence of Givens rotations which zeros out the extra sub-diagonal entries of $\mathbf{R}\mathbf{I}_{-l}^{\mathrm{T}}$. $\mathcal{J}_2 = \mathbf{J}_1^{(2)}\cdots\mathbf{J}_{K-1}^{(2)}$ is another Givens rotation sequence such that

$$\mathcal{J}_2\mathcal{J}_1\mathbf{Q}^{\mathrm{H}}\boldsymbol{\epsilon}_l = \alpha_1\boldsymbol{\epsilon}_1,$$

where α_1 is a complex number with $|\alpha_1| = 1$. The preliminary QR-update for the dimension-reduced original channel $\mathbf{H}_{K\backslash l}^{\mathrm{H}}$ can be executed as

$$\begin{aligned} \widetilde{\mathbf{R}} &= \mathbf{I}_{-1}\mathcal{J}_2\mathcal{J}_1\mathbf{R}\mathbf{I}_{-l}^{\mathrm{T}}, \\ \widetilde{\mathbf{Q}} &= \mathbf{I}_{-1}\mathbf{M}_{\boldsymbol{\sigma}_2}\mathbf{Q}\mathcal{J}_1^{\mathrm{H}}\mathcal{J}_2^{\mathrm{H}}\mathbf{I}_{-1}^{\mathrm{T}}, \end{aligned} \tag{4.19}$$

where $\mathbf{M}_{\boldsymbol{\sigma}_2}$ is a permutation matrix with order $\boldsymbol{\sigma}_2 = [l, \{1,\dots,K\}\backslash l]$. Equivalently, we estimate the Hermitian transpose of the dimension-reduced new channel (see Eq. (4.14)) as

$$(\mathbf{H}\{\mathbf{\Lambda'}\})_{K\backslash l}^{\mathrm{H}} = \widetilde{\mathbf{Q}}(\widetilde{\mathbf{R}} + \mathbf{u}\widehat{\mathbf{v}}_l^{\mathrm{H}}),$$

where $\mathbf{u} = \widetilde{\mathbf{Q}}^{\mathrm{H}}\mathbf{Q}_{-l}\mathbf{R}_{\{1,\dots,K\},l}$. Perform the third Givens rotation sequence $\mathcal{J}_3 = \mathbf{J}_1^{(3)}\cdots\mathbf{J}_{K-2}^{(3)}$ for

$$\mathcal{J}_3\mathbf{u} = \alpha_2\boldsymbol{\epsilon}_1,$$

where α_2 is a complex number that $|\alpha_2| = \|\mathbf{u}\|_2$. Follow with the forth Givens rotation sequence $\mathcal{J}_4 = \mathbf{J}_{K-2}^{(4)}\cdots\mathbf{J}_l^{(4)}$ for upper-triangularizing the upper Hessenberg matrix $\mathcal{J}_3(\widetilde{\mathbf{R}} + \mathbf{u}\widehat{\mathbf{v}}_l^{\mathrm{H}})$. The rank-1 update of Eq. (4.19) yields

$$\widehat{\mathbf{R}} = \mathcal{J}_4\mathcal{J}_3(\widetilde{\mathbf{R}} + \mathbf{u}\widehat{\mathbf{v}}_l^{\mathrm{H}}),$$
$$\widehat{\mathbf{Q}} = \widetilde{\mathbf{Q}}\mathcal{J}_3^{\mathrm{H}}\mathcal{J}_4^{\mathrm{H}}.$$

Eventually, the updated THP works as

$$\widehat{P}^{\mathrm{NL}}\big\{\bar{\mathbf{x}}_{K\backslash l}\big\} = \widehat{\mathbf{Q}}\widehat{\bar{\bar{\mathbf{x}}}}, \tag{4.20}$$

where

$$\widehat{\bar{\bar{x}}}_m = \Gamma\left\{\frac{1}{\hat{r}_{m,m}}\bar{x}_m - \langle m > 1\rangle\sum_{i=1}^{m-1}\frac{\hat{r}_{i,m}^*}{\hat{r}_{m,m}}\widehat{\bar{\bar{x}}}_i\right\}, \text{ for } m = 1,\dots,K-1.$$

As stated in [19], a new QR-decomposition from scratch needs a factor $\mathcal{O}(K^3)$ flops, whereas the above update procedure can be executed in $\mathcal{O}(K^2)$ flops.

4.4.4   Simulation Comparison

In order to evaluate the performance of the proposed precoder updating schemes, we measure direct and crosstalk paths from a 30-pair, 100 m, 0.5 mm cable [20]. To separate the influence of effective direct channel gain and the effectiveness of the proposed precoder updating methods, 3 pairs from a single binder are chosen such that there is no big difference between g_l^{L} and g_l^{NL} of the deactivating line (see Fig. 4.10). The measuring points follow a 51.75 kHz subcarrier spacing, and we consider 4 096 sub-carriers in total covering a frequency range up to 212 MHz. The all-terminated case and a deactivating STC-case, where line $l = 3$ is left unterminated, yield two 3×3 matrices $\mathbf{H}\{\boldsymbol{\Lambda}_\circ\}$ and $\mathbf{H}\{\boldsymbol{\Lambda}'\}$ for each sub-carrier, respectively. Note that crosstalk measurements while simultaneously synthesizing an exact open-line terminating impedance for the victim line are impossible and a specially tailored measurement setup could at best approximate the scenario. Since the crosstalk coefficients from other lines into the leaving line are of no importance to the precoder update, we thus copy the l-th row of $\mathbf{H}\{\boldsymbol{\Lambda}'\}$ from $\mathbf{H}\{\boldsymbol{\Lambda}_\circ\}$.

We study the effectiveness of the proposed schemes by exploring the entire frequency range up to 212 MHz for both precoding schemes to allow for a fair
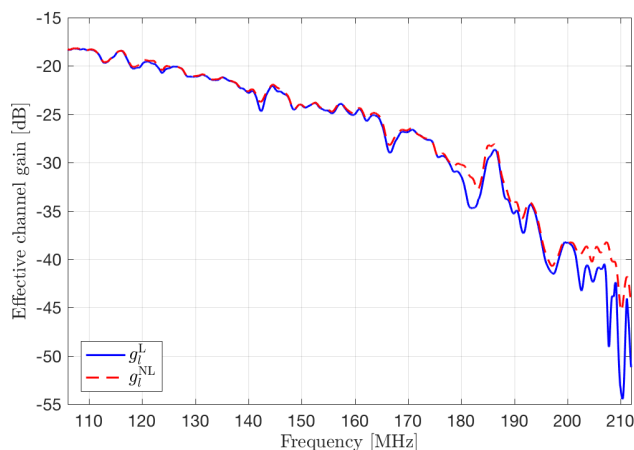
Fig. 4.10: Effective channel gains on the deactivating line when applying LP and THP respectively to the measured channel. There is no big difference in the effective direct channel gains when applying different precoding schemes, which is the reason for similar residual crosstalk patterns in the following simulations.

comparison. The PSD of resulting residual crosstalk is calculated, based on system parameters of G.fast [2].

Fig. 4.11 presents the residual crosstalk PSD on one of the victim lines in the vectored group using LP. Confirming the theoretical results in Section 4.3.3, the deactivating STC generates lower residual crosstalk at higher frequencies (beyond 180 MHz for our measured channel data) due to the reduced effective channel gain g_l^L. Nevertheless, on most of the studied frequency points, an STC produces non-negligible residual crosstalk which must be effectively mitigated.

By stopping transmission on the leaving line and updating the precoder to $\left(\mathbf{H}\{\mathbf{\Lambda}_\circ\}_{K\backslash l}\right)^{-1}$ (*i.e.,* the traditional operation), a reduction in residual crosstalk (from the red diamond-marked curve to the yellow triangle-marked one) is observed. However, the reduced residual crosstalk is still far above background noise level. Thus, further channel tracking is needed.

In contrast, the resulting residual crosstalk of the proposed methods (blue circle-marked and green star-marked curves) are almost unnoticeable, as they stay quite close to the background noise. Using $J = 1$ synchronization symbol to estimate $\widehat{\mathbf{v}}_l$, the updated precoder $\widehat{\mathbf{P}}^\mathrm{L}$ in Eq. (4.18) can effectively cover the new channel $\mathbf{H}\{\mathbf{\Lambda}'\}_{K\backslash l}$. In addition, the blue circle-marked curve in Fig. 4.11 applies the approximation in Eq. (4.15) to update the precoder directly from the outdated $\mathbf{P}_\circ^\mathrm{L}$, whereas the green star-marked curve assumes prior knowledge

Fig. 4.11: Residual crosstalk PSD on the victim line after an STC in linear precoding systems. Parameterized estimation is performed with $J = 1$. The left-hand side of the vertical dashed line denotes the frequency range where LP is recommended. It shows that the traditional method can lower the residual crosstalk but not adequately for high frequencies, while the proposed method with different prior knowledge can effectively bring the residual crosstalk down to the background noise level.

of the original channel $\mathbf{H}\{\mathbf{\Lambda}_o\} = \mathbf{H}$ to be available. The approximation in Eq. (4.15) becomes less accurate when the diagonal dominance is not valid. Consequently, the blue circle-marked curve exhibits a slightly higher residual crosstalk at some frequency points around 120 MHz and beyond. But for the frequency range where LP is recommended (*i.e.,* left-hand side of the vertical dashed line in Fig. 4.11), the method proposed in Section 4.4.2 is fully valid.

Similarly, we can reduce the residual crosstalk in non-linear precoding systems effectively to the background noise level with the proposed QR-update. In Fig. 4.12, the same parameterized estimation of $\widehat{\mathbf{v}}_l$ is performed using only $J = 1$ synchronization symbol, and the precoder updating procedure proposed in Section 4.4.3 is applied.

4.5 Precoder Update When (Re)Activating an Additional Line

Similarly to the leaving-line case, a vectoring interruption occurs when a line is (re)activated in the vectored group. It can be generalized as an STC problem
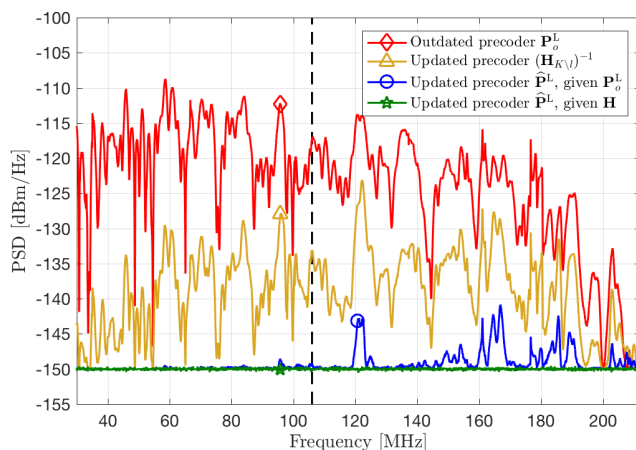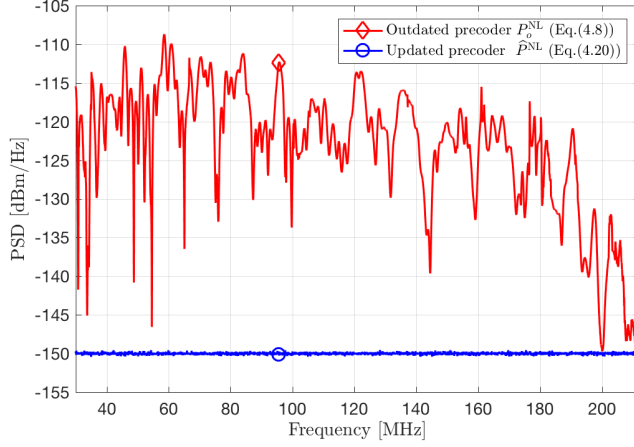
Fig. 4.12: Residual crosstalk PSD on the victim line after an STC in non-linear precoding systems. Parameterized estimation is performed with $J = 1$. It shows that the proposed updating scheme for THP is effective in mitigating the residual crosstalk.

with a reflection coefficient changing from non-zero to zero.

If the joining line is unknown to the DP, it is necessary to estimate all related channel coefficients. Consider that one neighboring line is joining a vectored group of size K. According to the RN model, the original channel before an activating STC is composed by two parts:

$$\overline{\mathbf{H}}\{\mathbf{\Lambda}_\circ\} = \mathbf{H} + \mathbf{v}\mathbf{h}_r^{\mathrm{T}},$$

where $\mathbf{v} \in \mathbb{C}^{K \times 1}$ denotes a column vector of reflected crosstalk coefficients from the joining termination, and $\mathbf{h}_r^{\mathrm{T}} \in \mathbb{C}^{1 \times K}$ denotes the FEXT from vectored lines into the joining line. The effective channel matrix after the STC becomes

$$\overline{\mathbf{H}}\{\mathbf{\Lambda}'\} = \begin{bmatrix} \mathbf{H} & \mathbf{h}_c \\ \mathbf{h}_r^{\mathrm{T}} & h_{K+1} \end{bmatrix}, \tag{4.21}$$

where h_{K+1} is the new direct channel and $\mathbf{h}_c \in \mathbb{C}^{K \times 1}$ denotes FEXT from the joining line into vectored lines.

Consider a simplified traditional channel discovery procedure [2] with two phases, where only direct and FEXT couplings relating to the joining line are estimated. *Phase-1* estimates the FEXT from the joining line into the vectored lines (*i.e.,* $\mathbf{h}_c$), updates precoder coefficients to cancel out this crosstalk, and

then *phase-2* estimates the FEXT into the joining line (*i.e.,* $\mathbf{h}_r^{\mathrm{T}}$). However, there has already been a deviation in *phase-1* due to the ignorance of $-\mathbf{v}\mathbf{h}_r^{\mathrm{T}}$ in $\overline{\mathbf{H}}\{\boldsymbol{\Lambda}'\}$, which changes the coupling conditions among the original vectored lines as well. The effectiveness of the traditional procedure is thus degraded. A full channel retraining may be needed if the basic routine is not adequate.

Thus, we propose a new channel discovery order, which is detailed for linear precoding systems. A similar updating principle can also be applied in non-linear precoding systems.

4.5.1 Error-Based Channel Estimation and Precoder Update

The precoder fulfilling vectoring diagonalizes the original channel as

$$\overline{\boldsymbol{\Sigma}} = (\mathbf{H} + \mathbf{v}\mathbf{h}_r^{\mathrm{T}})\overline{\mathbf{P}}\overline{\mathbf{G}},$$

where $\overline{\mathbf{P}} = \left(\overline{\mathbf{H}}\{\boldsymbol{\Lambda}_\circ\}\right)^{-1}$. Let $\overline{\mathbf{E}} = \left(\overline{\boldsymbol{\Sigma}}\right)^{-1}$ denote a diagonal matrix of equalizing coefficients.

When the line $K + 1$ is connected, its refection coefficient changes from $|\lambda_{K+1}| \gg 0$ to $\lambda'_{K+1} = 0$. The deviation term $\mathbf{v}\mathbf{h}_r^{\mathrm{T}}$ changing from non-zero to zero causes a disturbance to the vectored lines. To minimize this disruption, we propose a reordered channel discovery procedure summarized in Table 4.1.

The transceiver unit for the joining line at the DP side first transmits *quiet symbols* for all symbol positions. The quiet symbol is constructed by setting the constellation point to 0, which results in zero transmit power. Equivalently, the multiplier matrix, precoder and equalizer can be represented by $\overline{\mathbf{G}}_{+0} = \begin{bmatrix} \overline{\mathbf{G}} & \mathbf{0} \\ \mathbf{0}^{\mathrm{T}} & 0 \end{bmatrix}$, $\overline{\mathbf{P}}_{+0} = \begin{bmatrix} \overline{\mathbf{P}} & \mathbf{0} \\ \mathbf{0}^{\mathrm{T}} & 0 \end{bmatrix}$, and $\overline{\mathbf{E}}_{+0} = \begin{bmatrix} \overline{\mathbf{E}} & \mathbf{0} \\ \mathbf{0}^{\mathrm{T}} & 1 \end{bmatrix}$ respectively.

During the synchronization period, the *phase-1* estimation is performed. Since nothing is sent from the $(K + 1)$-th transmitter, the received signal at the joining CPE is the pure FEXT from the vectored lines. Mathematically, transmitting a synchronization symbol $\mathbf{s}_\circ(1) = [s_1(1), \ldots, s_K(1)]^{\mathrm{T}}$ on the vectored lines yields

$$q_{K+1}(1) = \mathbf{h}_r^{\mathrm{T}}\overline{\mathbf{P}}\overline{\mathbf{G}}\mathbf{s}_\circ(1) + n,$$

at the joining CPE at the first synchronization time instant. The errors occurring at other active CPEs are formulated as

$$\mathbf{e}_\circ(1) = -\overline{\mathbf{E}}\left(\mathbf{v}\mathbf{h}_r^{\mathrm{T}}\overline{\mathbf{P}}\overline{\mathbf{G}}\mathbf{s}_\circ(1) + \mathbf{n}\right),$$

which are caused by the "disappeared" deviation term $\mathbf{v}\mathbf{h}_r^{\mathrm{T}}$. Let J_1 denote the number of synchronization time instants needed to accomplish a *phase-1*

estimation. During this period, $\mathbf{S}_{\circ,J_1} = [\mathbf{s}_\circ(1), \ldots, \mathbf{s}_\circ(J_1)]$ are transmitted from the K vectored lines. The received symbols at the joining CPE are represented by $\mathbf{q}_{K+1,J_1} = [q_{K+1}(1), \ldots, q_{K+1}(J_1)]^{\mathrm{T}}$ and the error symbols at the original CPEs are represented by $\boldsymbol{\mathcal{E}}_{\circ,J_1} = [\mathbf{e}_\circ(1), \ldots, \mathbf{e}_\circ(J_1)]$. Two vectors can be estimated based on feedback receive symbols as

$$
\begin{aligned}
\widehat{\mathbf{h}}_r^{\mathrm{T}} &= \mathbf{q}_{K+1,J_1}^{\mathrm{T}} \left(\overline{\mathbf{P}}\,\overline{\mathbf{G}}\mathbf{S}_\circ \right)^\dagger \\
\widehat{\mathbf{v}} &= -\overline{\boldsymbol{\Sigma}}\boldsymbol{\mathcal{E}}_{\circ,J_1} \left(\widehat{\mathbf{h}}_r^{\mathrm{T}} \overline{\mathbf{P}}\,\overline{\mathbf{G}}\mathbf{S}_\circ \right)^\dagger,
\end{aligned}
\tag{4.22}
$$

which cover not only the FEXT couplings into the joining CPE, but the deviation $-\mathbf{v}\mathbf{h}_r^{\mathrm{T}}$.

During the next data transmission period, update the first sub-block of the precoder $\overline{\mathbf{P}}_{+0}$ as

$$
\widetilde{\mathbf{P}} = \overline{\mathbf{P}} \left(\mathbf{I} + \frac{\widehat{\mathbf{v}}\widehat{\mathbf{h}}_r^{\mathrm{T}}\overline{\mathbf{P}}}{1 - \widehat{\mathbf{h}}_r^{\mathrm{T}}\overline{\mathbf{P}}\widehat{\mathbf{v}}} \right),
\tag{4.23}
$$

Table 4.1: Channel discovery procedure for a joining line

(Re)activate line
if Joining request is received for line $K+1$ **then**
$\quad$ ***PHASE-1***:
$\quad$ **repeat**
$\quad\quad$ Transmit quiet symbols for all symbols positions on the joining line.
$\quad$ **until** J_1 received synchronization symbols from all $K+1$ CPEs are collected.
$\quad$ Estimate $\widehat{\mathbf{h}}_r^{\mathrm{T}}$ and $\widehat{\mathbf{v}}$ (Eq. (4.22)).
$\quad$ ***PHASE-2***:
$\quad$ Update the precoder related to the original vectored group to $\widetilde{\mathbf{P}}$ (Eq. (4.23))
$\quad$ **repeat**
$\quad\quad$ On line $K+1$:
$\quad\quad\quad$ • transmit quiet symbols on non-sync-symbol positions;
$\quad\quad\quad$ • transmit synchronization symbols on sync-symbol positions;
$\quad$ **until** J_2 received synchronization symbols from all $K+1$ CPEs are collected.
end if
Estimate $\left[\widehat{\mathbf{h}}_c^{\mathrm{T}},\ \widehat{h}_{K+1}\right]^{\mathrm{T}}$ (Eq. (4.24));
Update the precoder to $\widehat{\overline{\mathbf{P}}}$ (Eq. (4.25)).

to cover the deviation $-\mathbf{v}\mathbf{h}_r^{\mathrm{T}}$. Update the first sub-block of $\overline{\mathbf{G}}_{+0}$ accordingly to be $\widetilde{\mathbf{G}}$. The STC disturbance on the vectored lines is eliminated hereafter.

During *phase-2*, synchronization symbols are transmitted on all the $K+1$ lines. Equivalently, the precoder works as $\overline{\mathbf{P}}_{+1} = \begin{bmatrix} \widetilde{\mathbf{P}} & \mathbf{0} \\ \mathbf{0}^{\mathrm{T}} & 1 \end{bmatrix}$, and the multiplier matrix is $\overline{\mathbf{G}}_{+1} = \begin{bmatrix} \widetilde{\mathbf{G}} & \mathbf{0} \\ \mathbf{0}^{\mathrm{T}} & g_{K+1} \end{bmatrix}$ with the gain multiplier g_{K+1} for the joining line. Similarly after J_2 synchronization time instants, the new direct channel and FEXT couplings from the vectored lines can then be estimated by

$$
\begin{aligned}
\widehat{h}_{K+1} &= \left(\mathbf{q}_{K+1,J_2}^{\mathrm{T}} - \widehat{\mathbf{h}}_r^{\mathrm{T}} \widetilde{\mathbf{P}} \widetilde{\mathbf{G}} \mathbf{S}_{\circ,J_2} \right) (\mathbf{s}_{K+1}^{\mathrm{T}})^{\dagger}/\alpha, \\
\widehat{\mathbf{h}}_c &= \overline{\mathbf{\Sigma}} \boldsymbol{\mathcal{E}}_{\circ,J_2} (\mathbf{s}_{K+1}^{\mathrm{T}})^{\dagger}/\alpha,
\end{aligned}
\tag{4.24}
$$

where $\mathbf{q}_{K+1,J_2}^{\mathrm{T}}$ are the received symbols on the joining line, $\boldsymbol{\mathcal{E}}_{\circ,J_2}$ are the received error symbols on the vectored lines, and $\mathbf{s}_{K+1}^{\mathrm{T}} = [s_{K+1}(1), \ldots, s_{K+1}(J_2)]^{\mathrm{T}}$ is the synchronization sequence sent on the joining line during J_2 synchronization time instants.

At this point, the estimation $\widehat{\widehat{\mathbf{H}}}\{\boldsymbol{\Lambda}'\}$ for the dimension increased new channel in Eq. (4.21) is completed with $\widehat{\mathbf{h}}_c$, $\widehat{\mathbf{h}}_r^{\mathrm{T}}$ and $\widehat{h}_{K+1}$. Note that the Shur complement of $\mathbf{H}$ in matrix $\widehat{\widehat{\mathbf{H}}}\{\boldsymbol{\Lambda}'\}$, *i.e.*,

$$
\gamma = \widehat{h}_{K+1} - \widehat{\mathbf{h}}_r^{\mathrm{T}} \widetilde{\mathbf{P}} \widehat{\mathbf{h}}_c,
$$

is just a scalar. Also, the Shur complement of $\widehat{h}_{K+1}$, *i.e.*, $\mathcal{S}_{\widehat{h}} = \mathbf{H} - \widehat{\mathbf{h}}_c \widehat{\mathbf{h}}_r^{\mathrm{T}} \big/ \widehat{h}_{K+1}$, is again a rank-1 update of matrix $\mathbf{H}$ implying

$$
\mathcal{S}_{\widehat{h}}^{-1} = \widetilde{\mathbf{P}} \left(\mathbf{I} + \widehat{\mathbf{h}}_c \widehat{\mathbf{h}}_r^{\mathrm{T}} \widetilde{\mathbf{P}}/\gamma \right).
$$

No explicit matrix inversion is needed to recalculate the precoder for $\widehat{\widehat{\mathbf{H}}}\{\boldsymbol{\Lambda}'\}$. Based on previous knowledge of $\widetilde{\mathbf{P}}$ in Eq. (4.23) with the estimated couplings, the precoder can be updated by

$$
\widehat{\widehat{\mathbf{P}}} = \left(\widehat{\widehat{\mathbf{H}}}\{\boldsymbol{\Lambda}'\} \right)^{-1} = \begin{bmatrix} \mathcal{S}_{\widehat{h}}^{-1} & -\widetilde{\mathbf{P}}\widehat{\mathbf{h}}_c/\gamma \\ -\widehat{\mathbf{h}}_r^{\mathrm{T}} \mathcal{S}_{\widehat{h}}^{-1} \big/ \widehat{h}_{K+1} & 1/\gamma \end{bmatrix}.
\tag{4.25}
$$

A similar line discovery procedure as outlined in Table 4.1 can be derived for non-linear precoding systems. The basic principle is to swap the estimation order such that the channel deviation $-\mathbf{v}\mathbf{h}_r^{\mathrm{T}}$ is already covered after *phase-1*. We will not repeat formulas for THP updating.

4.5.2 Simulation Comparison

In this subsection, we compare the traditional and proposed line initializing approach in timeline, using the same data setup as in Section 4.4.4.

The *phase-1* estimation of the traditional method does not obtain the actual FEXT from the joining line (see Fig.4.13a) because of the coupling deviation which is now recognized as the influence of an STC. Although in *phase-2* the precoder is active based on the previous couplings among vectored lines and estimated FEXT from the joining line into the vectored lines, we observe in Fig.4.13a that the vectored lines still receive strong crosstalking disturbance once the joining line starts transmitting. The disturbed period may be extended since [2] defines a transmission repetition on the joining line in presence of strong crosstalk. Even if $\mathbf{h}_c$ is re-estimated in *phase-2*, a full channel retraining may still be needed to regain the original sum-rate. In Fig. 4.13a, a gap is observed between the blue diamond-marked line after *phase-2* and the sum-
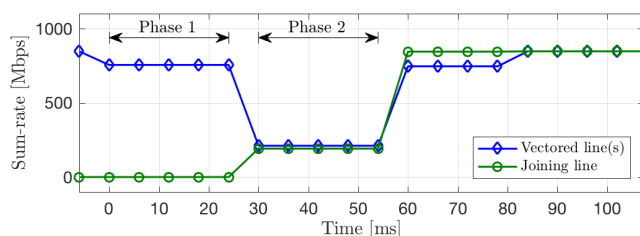
(a) Traditional procedure
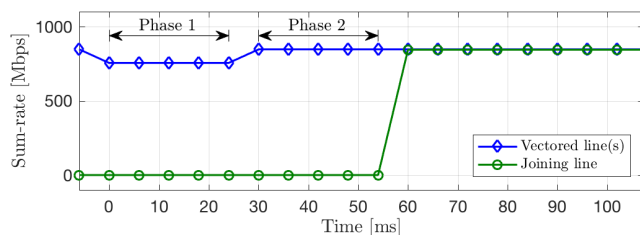
(b) Proposed procedure

Fig. 4.13:   Sum-rate over 30 MHz–106 MHz during the process of new line (re)activation. Activating STC occurs at time 0. Calculations are taken using channel measurements described in Section 4.4.4. It shows that the negative impact on vectoring lines from the joining line can be significantly mitigated by modifying the channel discovery process.

rate level before STC, due to the inadequate crosstalk cancellation. Then, full-channel retraining is performed at around 80 ms to recover the original sum-rate level. During the whole process, the vectored lines suffer from a persistent disturbance which grows with group size.

The proposed procedure, however, suggests to first estimate $\mathbf{h}_r^{\mathrm{T}}$, which is part of the attributes that composes the STC deviation. The errors collected at the original CPEs contribute to both estimating $\mathbf{h}_r^{\mathrm{T}}$ and correcting the perceived couplings among the vectored lines. As shown in Fig.4.13b, the sum-rate degradation for vectored lines is minor within a much shorter period of time compared to the traditional procedure in Fig.4.13a. The vectored lines can recover their original performance once the *phase-1* estimation is completed. Although the starting time for the joining line is delayed a bit, the disturbance to the original active users becomes unnoticeable during the whole line initializing process.

4.6   Conclusion

A sudden termination change (STC) caused when a line is abruptly deactivated or (re)activated in a vectored group alters the perceived channel coupling conditions, which leads to significant service degradation for active users in the neighborhood. Based on the proposed reflected-NEXT (RN) model, we characterize the changed channel with a vector composed by reflecting crosstalk coefficients and identify the residual crosstalk caused by an STC. The proposed precoder updating procedures for both linear and non-linear precoding schemes minimize the residual crosstalk disturbance to active users compared to the state-of-the-art methods. In addition, both channel estimation and precoder updating procedures are simplified, lowering complexity and cost for the modems at the distribution point (DP) side.

References

[1] P. Ödling, T. Magesacher, S. Höst, P. O. Börjesson, M. Berg, and E. Areizaga, "The Fourth Generation Broadband Concept," in *IEEE Communications Magazine*, vol. 47, no. 1, pp. 62-69, January 2009.

[2] ITU, "Fast Access to Subscriber Terminals - Physical Layer Specification," Recommendation Draft ITU-T G.9701, 2014. [Online]. Available: https://www.itu.int/rec/T-REC-G.9701/en

[3] M. Timmers, M. Guenach, C. Nuzman, and J. Maes, "G.fast: Evolving the Copper Access Network," in *IEEE Communications Magazine*, vol. 51, no. 8, pp. 74-79, August 2013.

[4] M. Timmers, R. B. Moraes, K. Hooghe, A. Duque, J. Galaro, M. Timmers, A. J. van Wijngaarden, M. Guenach, J. Maes, "XG-fast: the 5th Generation Broadband," in *IEEE Communications Magazine*, vol. 53, no. 12, pp. 83-88, December 2015.

[5] G. Ginis and J. Cioffi, "Vectored Transmission for Digital Subscriber Line Systems," in *IEEE Journal on Selected Areas in Communications*, vol, 20, no. 5, pp. 1085-1104, June 2002.

[6] ITU, "Self-FEXT cancellation (vectoring) for use with VDSL2 transceivers," Recommendation ITU-T G.993.5, April 2010. [Online]. Available: https://www.itu.int/rec/T-REC-G.993.5/en

[7] E. Medeiros, T. Magesacher, P.-E. Eriksson, C. Lu, and P. Ödling, "How Vectoring in G.fast May Cause Neighborhood Wars," in *Proc. 2014 IEEE International Conference on Communications (ICC)*, pp. 3859-3864, June 2014.

[8] B. Bareis, "Adaptive Transmission Line Impedance Matching Device and Method," April 2004, US Patent 6,724,890. [Online]. Available: https://www.google.com/patents/US6724890

[9] A. Rayher and H. Mariotte, "Impedance Adapter for a High-Bandwidth Transmission Channel of a Copper-Wired Terminal System," July 2009, US Patent 7,558,385. [Online]. Available: https://www.google.com/patents/US7558385

[10] Alcatel-Lucent, "Influence of an Impedance Change on a Leaving Line onto the Direct and Crosstalk Channels of the Active Lines," ITU-T SG15 Contribution 2013-10-Q4-058, October 2013.

[11] Y. Huang, T. Magesacher, E. Medeiros, C. Lu, P.-E. Eriksson, and P. Ödling, "Mitigating Disorderly Leaving Events in G.fast," in *Proc. 2015 IEEE International Conference on Communications (ICC)*, pp. 939-944, June 2015.

[12] R. Cendrillon, G. Ginis, E. Van den Bogaert, and M. Moonen, "A Near-Optimal Linear Crosstalk Precoder for Downstream VDSL," in *IEEE Transactions on Communications*, vol. 55, no. 5, pp. 860-863, May 2007.

[13] G. Ginis and J. Cioffi, "A Multi-User Precoding Scheme Achieving Crosstalk Cancellation with Application to DSL Systems," in *Proc. Conference Record of the Thirty-Fourth Asilomar Conference on Signals, Systems and Computers*, vol.2, pp. 1627-1631, October 2000.

[14] C. Windpassinger, R. Fischer, T. Vencel, and J. Huber, "Precoding in Multiantenna and Multiuser Communications," in *IEEE Transactions on Wireless Communications*, vol. 3, no. 4, pp. 1305-1316, July 2004.

[15] Futurewei Technologies, "G.fast: SNR Drop and FEXT Channel Variations due to Change of Alien Termination," ITU-T SG15 contribution 2013-10-q4-046, March 2013.

[16] E. Medeiros, T. Magesacher, P. Ödling, D. Wei, X. Wang, Q. Li, P.-E. Eriksson, C. Lu, J. Boschma, and B. van den Heuvel, "Modeling Alien-Line Impedance Mismatch in Wideband Vectored Wireline Systems," in *IEEE Communications Letters*, vol. 18, no. 9, pp. 1527-1530, September 2014.

[17] Alcatel, "G.fast: Comparison of Linear and Non-linear Pre-coding," ITU-T SG15 Contribution 2013-01-Q4-046, January 2013.

[18] M. Costa, "Writing on Dirty Paper (Corresp.)," in *IEEE Transactions on Information Theory*, vol. 29, no. 3, pp. 439-441, May 1983.

[19] Gene H. Golub and Charles F. Van Loan, *Matrix Computations (3rd Ed.)*, Baltimore, MD, USA: Johns Hopkins University Press, 1996.

[20] Ericsson AB, *Access Network Pair Cable, TEL 312*, 2010. [Online]. Available: http://goo.gl/4RdCXc

Paper V

5 Crosstalk Mitigation for LTE-over-Copper in Downlink Direction

Abstract

We present an architecture for transparent crosstalk mitigation in LTE-over-copper systems. By taking advantage of reference symbols present in downlink LTE signals we propose two methods for estimating the copper channel. System performance is evaluated using channel measurements and error vector magnitude calculations.

5.1   Introduction

High-capacity residential small cells represent an opportunity for operators to increase coverage and penetration of their mobile broadband services. With this paradigm, operators can deliver higher bitrates where most of the content consumption occurs. Additionally, cell site costs and energy consumption can be significantly reduced.

Residential small cells may become even more attractive with the impending introduction of long term evolution (LTE) over unlicensed spectrum bands. Wireline operators, for example, could complement their product portfolio by reusing the copper plant to offer mobile subscriptions.

Early works such as [1] suggest a centralized radio-over-copper concept as an alternative to uncoordinated femtocell deployment. In [2], transparent remote radio heads (RRHs) and shared baseband processors are used to achieve full coordination between small cells and the macro layer, eliminating the main drawback of femtocells. This system in particular targets the enterprise market and takes advantage of shielded networking cables (category 6 and up) to deal with crosstalk and radio frequency interference (RFI).

In [3], we proposed an architecture for small cell deployment that reutilizes the copper access infrastructure (unshielded category 3 cables), while coexisting with legacy digital subscriber line (DSL) services. The proposed system converts baseband radio signals to an intermediate frequency, adequate to the low-pass copper channel and could be deployed in cabinets collocated, for instance, with VDSL2 modems.

In [4], we analyzed the implications of third generation partnership project (3GPP) compliance to the reach of an LTE-over-copper solution. The analysis indicated that a 3GPP compliant system could be built at a reasonable price point and deployed up to 350 meters away from the cabinet.

While papers [3, 4] have covered band-planning, rate-reach simulations and filter design, they have not dealt with the main impairment present in copper networks: crosstalk. Solutions for mitigating crosstalk among synchronized transmitters have long been adopted in the DSL community, where these techniques are referred to as *vectoring*. In brief, vectoring stands for the joint processing of transmit or receive symbols in DSL systems. Works such as [5, 6] proposed efficient algorithms for achieving near-optimal crosstalk cancellation in vectored systems. The international telecommunication union (ITU) standardized interfaces for VDSL2 vectoring with the G.993.5 recommendation [7]. Vectoring is also part of the newer G.fast standard [8].

Ideally, the crosstalk problem we address here would be solved by implementing vectoring in the baseband unit (BBU) software, see the left part of Fig. 5.1. However, proposing to change the BBU software to adapt to one

particular fronthaul technology cannot be expected to be met with great enthusiasm as it complicates software architecture and maintenance. A solution needs to be implemented further out and kept transparent to the BBU.
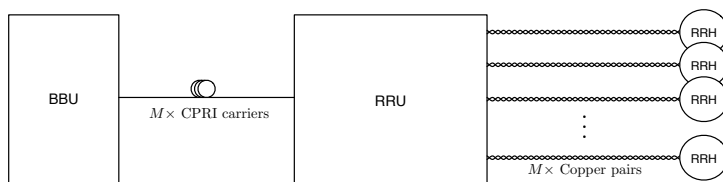
Fig. 5.1: Centralized Baseband Architecture for an LTE-over-copper system.

The contribution of this letter is threefold: First, we present an architecture for channel estimation and precoding that mitigates the effects of crosstalk on downlink LTE-over-copper systems. Second, we propose two methods for estimating the copper channel using the reference signals already present in LTE signals. Last, we validate the concept using channel measurements and error vector magnitude (EVM) calculations.

5.2   Frequency Domain Precoding at RRU

Consider the centralized baseband system represented in Fig. 5.1. A single shared BBU processes LTE signals for M independent LTE small cells. The baseband signal samples are transmitted using an appropriate protocol (*e.g.,* CPRI) to a remote radio unit (RRU). The radio unit is responsible for up and down-conversion to an intermediate frequency f_c suitable for transmission over copper. Each twisted pair is terminated by a RRH, responsible for filtering, conversion to RF frequencies and amplification before sending the LTE signal to an antenna.

Assume that all M independent cells are synchronized, that each cell transmits orthogonal frequency-division multiplexing (OFDM) symbols with N subcarriers and that these cells employ the same duplexing method.

Let $x_i^{(k,l)}$ represent the frequency domain contents of the resource element[1] with OFDM symbol l, subcarrier k and transmitter i. Dropping the symbol index and focusing the analysis on a single resource element, the following description applies. Let $\mathbf{x}^{(k)} = \left[x_1^{(k)}, \ldots, x_i^{(k)}, \ldots, x_M^{(k)}\right]^{\mathrm{T}} \in \mathbb{C}^{M \times 1}$ represent the transmitted symbol vector obtained by stacking the output of M synchronized

---

[1]The smallest time-frequency resource in an LTE grid.

cells at subcarrier k. At the output of the copper channel, the received frequency domain symbol vector $\mathbf{y}^{(k)} \in \mathbb{C}^{M \times 1}$ can be described as

$$\mathbf{y}^{(k)} = \mathbf{H}^{(k)}\mathbf{x}^{(k)} + \mathbf{z}^{(k)}, \tag{5.1}$$

where $\mathbf{H}^{(k)} \in \mathbb{C}^{M \times M}$ is the frequency domain channel matrix for subcarrier k and $\mathbf{z}^{(k)} \in \mathbb{C}^{M \times 1}$ represents an additive noise vector.

The signal received at RRH i and subcarrier k can then be expressed as

$$y_i^{(k)} = H_{i,i}^{(k)} x_i^{(k)} + \sum_{j \neq i} H_{i,j}^{(k)} x_j^{(k)} + z_i^{(k)}. \tag{5.2}$$

where $H_{i,i}^{(k)}$ represents the direct channel gain for pair i and $H_{i,j}^{(k)}, i \neq j$ represents the far-end crosstalk (FEXT) from RRU transmitter j to RRH i.

If the off-diagonal elements of the channel matrix $\mathbf{H}^{(k)}$ are non-negligible, as is typical for unshielded telephony-grade cables, the crosstalk contribution will significantly distort the LTE signal before it is up-converted and transmitted via the RRH radio frequency (RF) front-end, possibly leading to unacceptable EVM increase.

In this letter we propose to modify the design of the remote radio unit in order to eliminate crosstalk via frequency domain precoding. The proposed arrangement, depicted in Fig. 5.2, has the benefit of being transparent to the baseband processor, avoiding the necessity of making the radio access equipment aware of the fronthaul medium.

Let $\mathbf{s}_i = \left[s_i^{(N-L+1)}, \ldots, s_i^{(N)}, s_i^{(1)}, \ldots, s_i^{(N)}\right]^{\mathrm{T}} \in \mathbb{C}^{(L+N) \times 1}$ be a vector constituted by $L + N$ samples of the ith RRU input signal, covering exactly one OFDM symbol, including its cyclic prefix of size L. The vector $\tilde{\mathbf{x}}_i = \left[x_i^{(1)}, \ldots, x_i^{(k)}, \ldots, x_i^{(N)}\right]^{\mathrm{T}} \in \mathbb{C}^{N \times 1}$ containing the transmit symbols for every subcarrier used by transmitter i can be obtained by cyclic prefix removal followed by a discrete Fourier transform (DFT). A matrix representation of such operation is given by

$$\tilde{\mathbf{x}}_i = \mathcal{F}\mathbf{R}\mathbf{s}_i \tag{5.3}$$

where $\mathbf{R}$ is the cyclic prefix removal matrix and $\mathcal{F}$ is a DFT matrix of size N.

Next, the transmit symbols for each user on subcarrier k can be collected in a vector $\mathbf{x}^{(k)} = \left[x_1^{(k)}, \ldots, x_i^{(k)}, \ldots, x_M^{(k)}\right]^{\mathrm{T}}$ and used as input to the precoder. The precoded symbol vector $\bar{\mathbf{x}}_k$ is obtained via the matrix multiplication $\bar{\mathbf{x}}^{(k)} = \mathbf{P}^{(k)}\mathbf{x}^{(k)}$, where the precoding matrix $\mathbf{P}^{(k)} \in \mathbb{C}^{M \times M}$ is chosen appropriately. Good candidate precoder designs are presented in [6], with the diagonalizing precoder shown to be near optimal.

After precoding an inverse DFT is performed on each sequence $\bar{\mathbf{x}}_i = \left[\bar{x}_i^{(1)}, \ldots, \bar{x}_i^{(k)}, \ldots, \bar{x}_i^{(N)}\right]^{\mathrm{T}} \in \mathbb{C}^{N \times 1}$, followed by cyclic prefix insertion. The
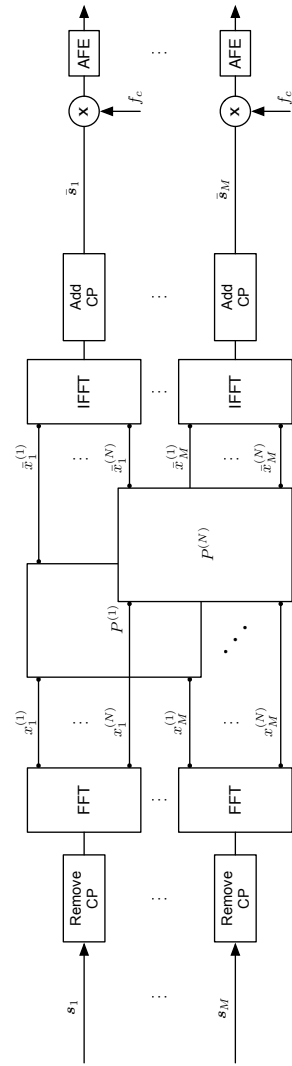
Fig. 5.2: Proposed remote radio unit architecture. The samples for M independent LTE cells are present at the input, have their cyclic prefixes stripped, are brought to frequency domain and precoded, being transformed back to time domain before modulation and transmission over the twisted pairs.

resulting precoded time domain samples $\bar{\mathbf{s}}_i$ go through digital to analog conversion and are shifted to the carrier frequency f_c before copper transmission.

For good precoder performance it is of fundamental importance that good estimates of the channel matrices $\mathbf{H}^{(k)}$ are available. In the next section we describe practical methods for obtaining these estimates.

5.3 Channel Estimation Methods

The LTE physical layer [9] specifies a number of reference signals used in the communication between base stations and UE to achieve different objectives such as cell identification, cell selection and channel estimation.

We propose to utilize LTE's downlink cell-specific reference signals (CRSs) to estimate the copper channel. CRS are well suited for the task at hand since they are distributed along the entire bandwidth of the cell and are independent of cell load and scheduling algorithms.

For each slot in a subframe, CRS are present in the first and fifth symbols. The values of CRS symbols are obtained by QPSK modulating a pseudo-random Gold sequence [9]. By knowing the physical layer cell identity, $N_{\mathrm{ID}}^{\mathrm{cell}}$, the slot number within a radio frame n_s and the symbol number l one can perfectly reconstruct each of the CRS sequences.

A frequency shift derived from the $N_{\mathrm{ID}}^{\mathrm{cell}}$ parameter also controls which subcarriers will be loaded with pilot symbols. This cell-specific frequency shift, defined as $v_{\mathrm{shift}} = N_{\mathrm{ID}}^{\mathrm{cell}} \bmod 6$, was introduced to improve pilot performance in environments with high interference.

The effect of different $N_{\mathrm{ID}}^{\mathrm{cell}}$ assignments on pilot positioning is exemplified in the left diagram of Fig. 5.3. The pilot symbols for three different cells are drawn over the same resource grid. Each cell's pilots are represented by the symbols $\circ, +, \times$ and correspond to the choice of cell identity $N_{\mathrm{ID}}^{\mathrm{cell}} = 0, 1, 2$ respectively. For this sequential cell identity assignment, the pilot symbols clearly do not overlap.

Taking advantage of the cell-specific frequency shift, we propose that instead of using an arbitrary cell identity assignment, the $N_{\mathrm{ID}}^{\mathrm{cell}}$ values should be selected according to the following sequence

$$
\begin{aligned}
&N_{\mathrm{ID}}^{\mathrm{cell}}(1) \in \{0, 1, \ldots, 503\}, \\
&N_{\mathrm{ID}}^{\mathrm{cell}}(i) = \left(N_{\mathrm{ID}}^{\mathrm{cell}}(i-1) + 6\right) \bmod 504, \ i \in \{2, \ldots, M\}.
\end{aligned}
\tag{5.4}
$$

When the $N_{\mathrm{ID}}^{\mathrm{cell}}$ parameters are set according to Eq. (5.4), pilots for each cell are assigned to the same resource elements. This is represented in the right diagram of Fig. 5.3. Based on this pilot alignment we propose two channel estimation
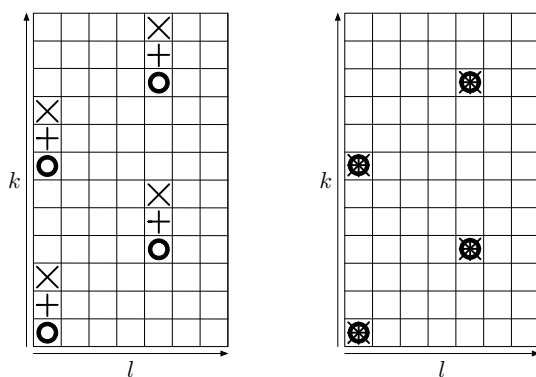
Fig. 5.3: Depiction of a stack of LTE resource grids for three cells. On the left, the first slot of a resource block is represented, and the cells are assigned the cell identities 0, 1 and 2. On the right, with the proposed cell assignment scheme, one notices that the cell reference symbol positions coincide in time and frequency. The cell identities for the second diagram are 0, 6 and 12.

architectures, that differ in the amount of feedback necessary between RRH and RRU.

5.3.1 Feedback-based estimator

For the following discussion, it is assumed that there exists a control channel between the RRU and each RRH. It is also assumed that each RRH is capable of synchronizing to its LTE signal, extract the received CRS symbols and feed them back to the RRU. We also assume that the copper channel is constant over many symbols, changing slowly due, for example, to temperature variations [10]. The formulations presented next are valid for subcarriers in which pilot symbols are transmitted.

Let W, $W \geq M$, represent the number of pilot symbols in an observation window. Let r denote the pilot symbol number within an observation window. Define $\eta \in \mathbb{C}^{WM \times 1}$ and $\mathbf{X} \in \mathbb{C}^{WM \times M^2}$ as

$$
\eta = \begin{bmatrix} \mathbf{z}^{(k,r)} \\ \mathbf{z}^{(k,r-1)} \\ \vdots \\ \mathbf{z}^{(k,r-W+1)} \end{bmatrix}, \quad \mathbf{X} = \begin{bmatrix} \left(\mathbf{x}^{(k,r)}\right)^{\mathrm{T}} \otimes \mathbf{I}_M \\ \left(\mathbf{x}^{(k,r-1)}\right)^{\mathrm{T}} \otimes \mathbf{I}_M \\ \vdots \\ \left(\mathbf{x}^{(k,r-W+1)}\right)^{\mathrm{T}} \otimes \mathbf{I}_M \end{bmatrix},
$$

where $\otimes$ is the Kronecker product and $\mathbf{I}_M$ is the identity matrix of size M.

Let $\mathbf{h} \in \mathbb{C}^{M^2 \times 1}$ be a vector obtained by stacking the columns of $\mathbf{H}^{(k)}$. The last W received symbol vectors can then be described as

$$\gamma = \begin{bmatrix} \mathbf{y}^{(k,r)} \\ \mathbf{y}^{(k,r-1)} \\ \vdots \\ \mathbf{y}^{(k,r-W+1)} \end{bmatrix} = \mathbf{X}\mathbf{h} + \eta. \tag{5.5}$$

Taking advantage of Eq. (5.5), one can obtain an estimate of $\mathbf{h}$ by using a Moore-Penrose pseudo-inverse

$$\hat{\mathbf{h}} = (\mathbf{X}^{\mathrm{H}}\mathbf{X})^{-1}\mathbf{X}^{\mathrm{H}}\gamma. \tag{5.6}$$

Re-stacking the elements of $\hat{\mathbf{h}}$ column-wise leads to the desired channel matrix estimate $\hat{\mathbf{H}}^{(k)}$.

5.3.2   RRH channel estimator

An alternative approach is to estimate a single row of the copper channel matrix $\mathbf{H}^{(k)}$ at each RRH, feeding back the estimation results instead of the received symbols. This estimation procedure relies on the fact that transmit pilot symbol vectors $\mathbf{x}^{(k)}$ can be reconstructed at each receiver as long as they are aware of the $N_{\mathrm{ID}}^{\mathrm{cell}}$ values used in the system.

Let W represent the number of symbols in an observation window such that $W \geq M$. Rewrite (5.2) as

$$y_i^{(k)} = \underline{\mathbf{h}}\mathbf{x}^{(k)} + z_i^{(k)}, \tag{5.7}$$

where $\underline{\mathbf{h}} = \left[H_{i,1}^{(k)}, \ldots, H_{i,i}^{(k)}, \ldots, H_{i,M}^{(k)} \right]$ is the vector corresponding to the ith row of channel matrix $\mathbf{H}^{(k)}$. Next, define $\underline{\mathbf{X}} \in \mathbb{C}^{W \times M}$ and $\underline{\eta} \in \mathbb{C}^{W}$ as

$$\underline{\mathbf{X}} = \begin{bmatrix} \left(\mathbf{x}^{(k,r)}\right)^{\mathrm{T}} \\ \left(\mathbf{x}^{(k,r-1)}\right)^{\mathrm{T}} \\ \vdots \\ \left(\mathbf{x}^{(k,r-W+1)}\right)^{\mathrm{T}} \end{bmatrix}, \quad \underline{\eta} = \begin{bmatrix} z_i^{(k,r)} \\ z_i^{(k,r-1)} \\ \vdots \\ z_i^{(k,r-W+1)} \end{bmatrix}.$$

The last W symbols received by RRH i can be written as

$$\underline{\gamma} = \begin{bmatrix} y_i^{(k,r)} \\ y_i^{(k,r-1)} \\ \vdots \\ y_i^{(k,r-W+1)} \end{bmatrix} = \underline{\mathbf{X}}\underline{\mathbf{h}}^{\mathrm{T}} + \underline{\eta}. \tag{5.8}$$

The Moore-Penrose pseudo-inverse then leads to the estimate

$$\hat{\underline{\mathbf{h}}}^{\mathrm{T}} = (\underline{\mathbf{X}}^{\mathrm{H}}\underline{\mathbf{X}})^{-1}\underline{\mathbf{X}}^{\mathrm{H}}\underline{\gamma}. \tag{5.9}$$

5.4   Crosstalk Mitigation Performance

In order to assess the performance of the proposed RRU architecture and channel estimation methods we have executed time domain simulations. Initially, the Vienna LTE link level simulator [11] was used to generate downlink LTE radio frames. Each cell was configured to use a single antenna port, and its $N_{\mathrm{ID}}^{\mathrm{cell}}$ number was assigned according to Eq. (5.4).

We have measured direct and FEXT transfer functions for six pairs in telephony-grade copper cables [12] with different lengths. The frequency range of interest is from 21 to 24 MHz, in accordance to the system proposed in [3,4].

The simulations were divided in two stages. At first, for each pilot subcarrier, a channel matrix estimate $\hat{\mathbf{H}}$ is obtained using the methods proposed in the previous section. For subcarriers not loaded with pilot symbols, channel estimates were obtained via linear interpolation. Next, each estimated channel matrix $\hat{\mathbf{H}}$ was used to calculate a diagonalizing precoder $\mathbf{P} = (1/u)\,\hat{\mathbf{H}}^{-1}\mathrm{diag}\{\hat{H}_{1,1}, \ldots, \hat{H}_{M,M}\}$, where $\mathrm{diag}\{\hat{H}_{1,1}, \ldots, \hat{H}_{M,M}\}$ represents a diagonal matrix with elements $\hat{H}_{1,1}, \ldots, \hat{H}_{M,M}$ along its main diagonal. The normalization factor u is chosen to guarantee that the precoding operation does not lead to increases in transmit power [6]. These precoders were then used in simulations against the measured channels $\mathbf{H}$.

To quantify performance we calculate EVM as specified in [13]. 3GPP specifies limit EVM values for each of the constellations used for LTE's physical downlink shared channel (PDSCH). The limits are 17.5%, 12.5%, 8% and 3.5% for QPSK, 16-QAM, 64-QAM and 256-QAM respectively.

For each loop length we have varied the additive noise power spectrum density (PSD), calculating EVM before the RF front-end at the RRH. The simulation results for the worst performing cell are gathered in Fig. 5.4.

The performance for a baseline system, deployed over a 100 meters of cable without crosstalk cancellation, is represented in Fig. 5.4 by a dashed blue line with pentagram markers. The resulting EVM would limit the system to using QPSK modulation. For longer cables without crosstalk cancellation, the EVM curves exceed the scale of the plot and 3GPP compliance is infeasible.

As a reference, single user bounds are depicted as dotted lines for all cable lengths. These represent the EVM when the cell in question is the only active transmitter.
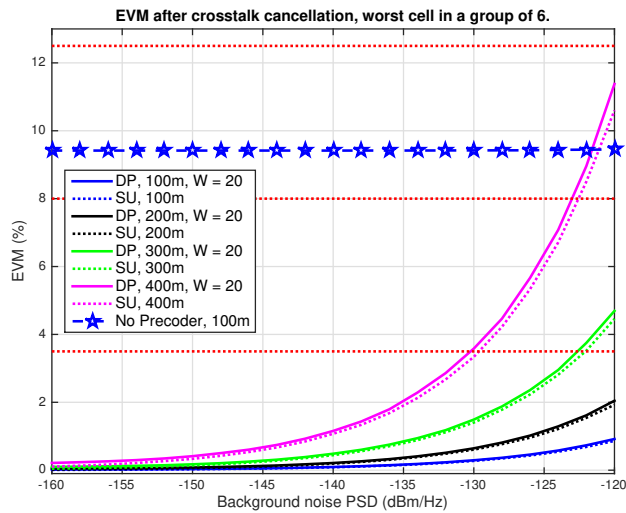
Fig. 5.4: EVM performance for the worst cell in a group of six LTE-over-copper systems, deployed over different cable lengths. DP represents the curves obtained with a diagonalizing precoder, while SU represents single user bounds.

The solid lines represent the performance with diagonalizing precoders and approach the single user bounds for all cable lengths. The channel estimates used to design the precoders were obtained using the feedback-based estimator (Sec. 5.3.1) with $W = 20$, corresponding to the number of pilot symbols observed in one LTE frame. Results for the RRH estimator (Sec. 5.3.2) were equivalent and therefore omitted.

The gap between EVM limits (red dotted lines) and a certain curve indicate the margin left for implementation losses. As an example, consider that one would design an LTE-over-copper system for deployment over 300 meters of copper, subject to a background noise level of -140 dBm/Hz. In order to support 256-QAM implementation losses caused, for example, by imperfections in the RF front-end would be limited to 3.5%.

5.5 Conclusion

We have presented an architecture for crosstalk mitigation in LTE-over-copper systems. It is transparent to baseband processors and can be implemented in a radio unit, where up and down-conversion are performed. Two channel

estimation methods that take advantage of LTE's downlink reference signals were also presented.

5.6   Appendix

This appendix is based on: E. Medeiros, P.-E. Eriksson, Y. Huang, and C. Lu, "Methods and Nodes of a Wireless Communication Network for Mitigating Crosstalk in a Base Station System," *Patent application*, PCT/EP2015/052888, filed 11 February 2015, WO2016128045A1, publication date 18 August 2016.

5.6.1   Technical Field

The present disclosure relates generally to methods, nodes and computer programs of a wireless communication network for mitigating crosstalk in a base station system. More specifically, the disclosure relates to a base station system comprising a baseband unit connected to an intermediate radio unit which in turn is connected to a plurality of radio heads via a plurality of metallic conductors, and the methods, nodes and computer programs are for mitigating crosstalk over the metallic conductors in the base station system.

5.6.2   Background

Mass-deployment of small cells is a candidate solution for solving the ever-increasing bandwidth demands on wireless communication networks. By employing coordination among macro cells and small cells, such as micro, pico and femto cells, operators can provide good coverage and a high quality mobile broadband experience to pieces of user equipments (UEs), which camp on the network.

A recent enabler for solving the increasing bandwidth demands is a system called radio dot system (RDS). The RDS enables operators to utilize local area network (LAN) cables like CAT6/7 for indoor radio deployments. This system improves over older distributed antenna systems by providing streamlined installation procedures, low cost and energy efficiency. The RDS is a distributed base station system wherein the base station functionality is separated in different nodes called a baseband unit (BBU), in which signal treatment in the baseband frequency area is performed, an intermediate radio unit (IRU), which is arranged to receive (in the downlink direction) the baseband signals from the BBU, convert them to an intermediate frequency and distribute the signals to a destined radio head (RH), (also called the radio dot) of a plurality of RHs connected via dedicated cables to the IRU. The IRU then up-converts the received

intermediate frequency signal to a radio frequency for radio transmission from an antenna of the RH towards UEs being in radio connection with the RH. As a further application of the RDS, there is a new initiative extending RDS into residential domain reusing existing telephony twisted-pair cable infrastructure between the IRU and the RHs, which are also used by today's digital subscriber line (DSL). The basic idea is to transfer radio signals in lower frequency at DSL spectrum range, for example below 200 MHz.

However, the twisted-pairs in the same cable bundle are subjected to crosstalk. The crosstalk can reduce the signal-to-noise ratio (SNR) significantly. This will result in reduced bandwidth and reach of the residential RDS. Crosstalk cancellation/mitigation is needed to increase the performance.

5.6.3 Summary

It is an object of the invention to address at least some of the problems and issues outlined above. It is another object to reduce the influence of crosstalk between cables of a distributed base station system in a wireless communication system. It is possible to achieve these objects and others by using a method and an apparatus as defined in the attached independent claims.

According to one aspect, a method is provided for mitigating crosstalk performed by a network node of a wireless communication network operable in a base station system of the wireless communication network. The base station system comprises an IRU, a BBU connected to the IRU, and a plurality of RHs, connected to the IRU via a plurality of metallic conductors. The method comprises receiving from a first of the plurality of RHs, a measure of an error of one or more symbols of a signal received by the first RH from the IRU over a first of the plurality of metallic conductors, the measure of the error being detected by the first RH, the signal being destined to a UE wirelessly connected to the first RH. The method further comprises determining precoding coefficients for a precoder according to the received error measure, and triggering applying the determined precoding coefficients when sending further signals to the first RH over the first of the plurality of metallic conductors, the further signals being destined to UEs wirelessly connected to the first RH.

According to another aspect, a method is provided performed by a first RH operable in a base station system of a wireless communication network, for mitigating crosstalk. The base station system comprises an IRU, a BBU connected to the IRU, and a plurality of RHs including the first RH, the plurality of RHs being connected to the IRU via a plurality of metallic conductors. The method comprises receiving, from the IRU over a first of the plurality of metallic conductors, a signal destined to a UE wirelessly connected to the first RH, the signal comprising one or more symbols. The method further comprises

detecting, from the received one or more symbol, a measure of an error of the one or more symbol and sending, to the IRU, the measure of the one or more symbol error, for further determining of precoding coefficients for a pre-coder of the IRU based on the received measure of symbol error.

According to another aspect, a network node is provided, operable in a wireless communication network and configured to mitigate crosstalk of a base station system. The base station system comprises an IRU, a BBU connected to the IRU, and a plurality of RHs connected to the IRU via a plurality of metallic conductors. The network node comprises a processor and a memory. The memory contains instructions executable by said processor, whereby the network node is operative for receiving from a first of the plurality of RHs, a measure of an error of one or more symbols of a signal received by the first RH from the IRU over a first of the plurality of metallic conductors, the measure of the error being detected by the first RH, the signal being destined to a UE, wirelessly connected to the first RH, determining precoding coefficients for a precoder according to the received error measure, and triggering applying the determined precoding coefficients when sending further signals to the first RH over the first of the plurality of metallic conductors, the further signals being destined to UEs wirelessly connected to the first RH.

According to another aspect, a first RH is provided, operable in a base station system of a wireless communication network and configured to contribute in mitigating crosstalk. The base station system comprises an IRU, a BBU connected to the IRU, and a plurality of RHs including the first RH, the plurality of RHs being connected to the IRU via a plurality of metallic conductors. The first RH comprises a processor and a memory. The memory contains instructions executable by said processor, whereby the first RH is operative for receiving, from the IRU over a first of the plurality of metallic conductors, a signal destined to a UE wirelessly connected to the first RH, the signal comprising one or more symbols, detecting, from the received one or more symbol, a measure of an error of the one or more symbol, and sending, to the IRU, the measure of the one or more symbol error, for further updating of precoding coefficients for a precoder based on the received measure of symbol error.

According to other aspects, computer programs and carriers are also provided, the details of which will be described in the claims and the detailed description.

Further possible features and benefits of this solution will become apparent from the detailed description below.

5.6.4 Brief Description of Drawings

The solution will now be described in more detail by means of exemplary embodiments and with reference to the accompanying drawings, in which:

- Fig. 5.5 is a schematic block diagram of a base station system in which the present invention may be used.

- Fig. 5.6 is a schematic view of an exemplary cellular communication network to which coverage is provided by the base station system.

- Fig. 5.7 is a flow chart illustrating a method performed by a network node, according to possible embodiments.

- Fig. 5.8 is a flow chart illustrating a method performed by an RH, according to possible embodiments.

- Fig. 5.9 is a schematic block diagram of a RH according to a possible embodiment.

- Fig. 5.10 is a schematic block diagram of an IRU according to a possible embodiment.

- Fig. 5.11 is a schematic block diagram of a digital signal processor (DSP) of an RH according to a possible embodiment.

- Figs 5.12a and 5.12b are tables illustrating cell-specific reference signal (CRS) patterns for two antennas.

- Fig. 5.13 is a table illustrating cell-ID assignment for crosstalk channel estimation.

- Figs. 5.14-5.15 are block diagrams illustrating a network node in more detail, according to further possible embodiments.

- Figs. 5.16-5.17 are block diagrams illustrating a radio head in more detail, according to further possible embodiments.

Fig. 5.5

Fig. 5.6

Fig. 5.7

Fig. 5.8

Control channel through which
error sample is fed back to IRU

Fig. 5.9

error sample feedback path
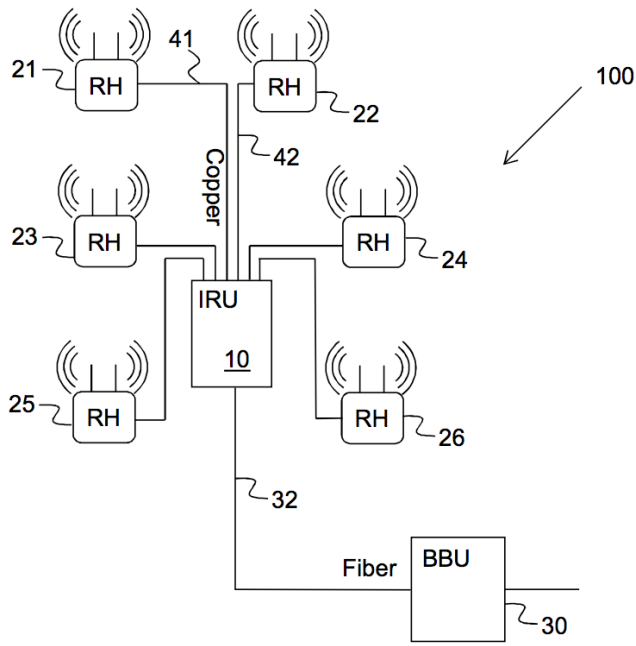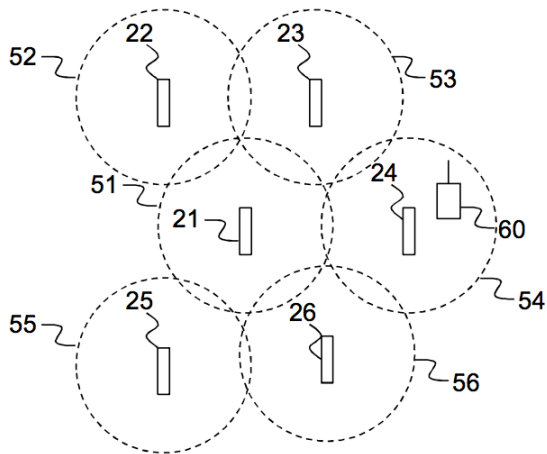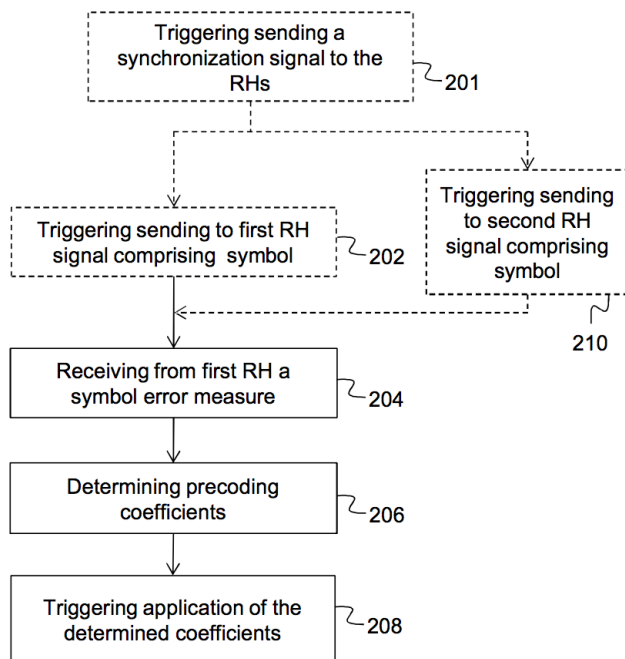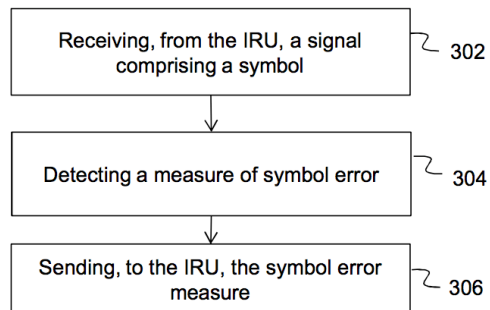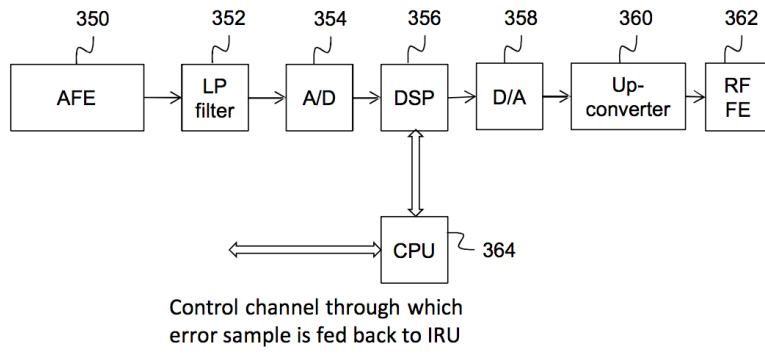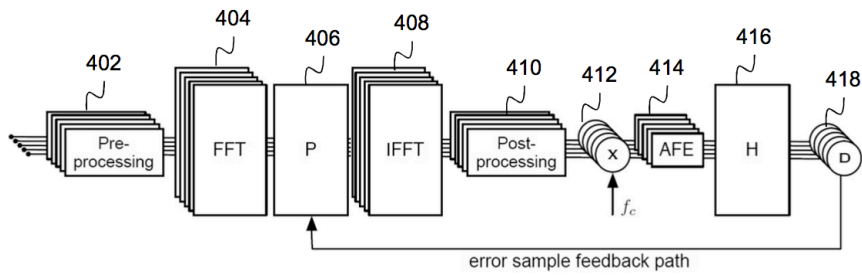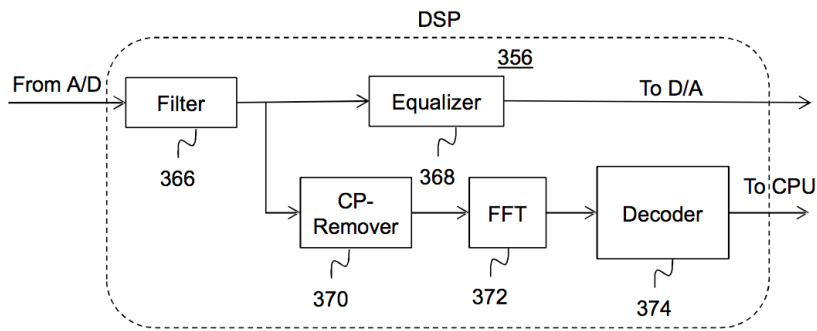
Fig. 5.10

Fig. 5.11

XXXX				R0			XXXX				R0		
R0				XXXX			R0				XXXX		
XXXX				R0			XXXX				R0		
R0				XXXX			R0				XXXX		

(a)

R1				XXXX			R1				XXXX		
XXXX				R1			XXXX				R1		
R1				XXXX			R1				XXXX		
XXXX				R1			XXXX				R1		

(b)

Fig. 5.12

SYMB1	SYMB2	SYMB3	SYMB4	SYMB5	SYMB6	SYMB7
				0,6,12,18		
0,6,12,18						
				0,6,12,18		
0,6,12,18						

Fig. 5.13
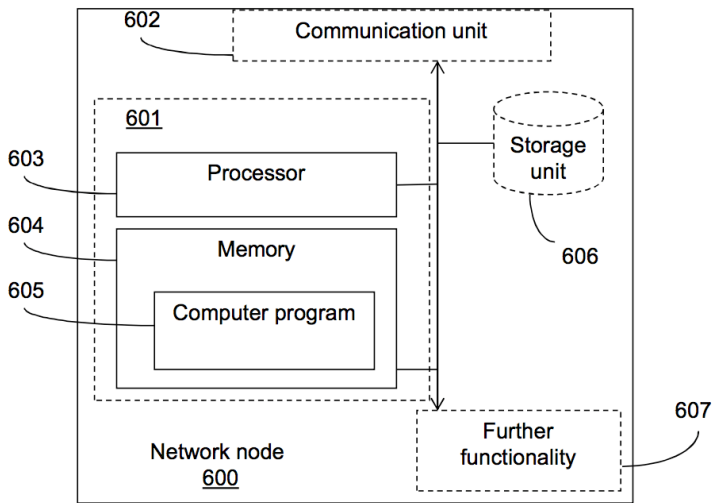
Fig. 5.14
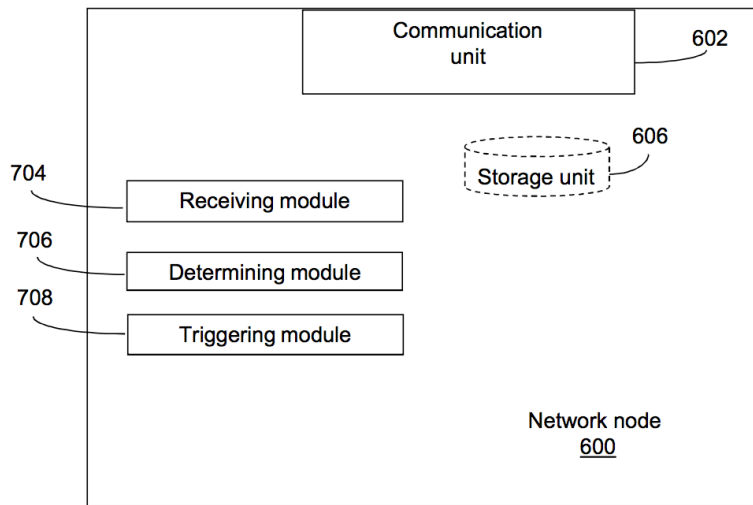
Fig. 5.15
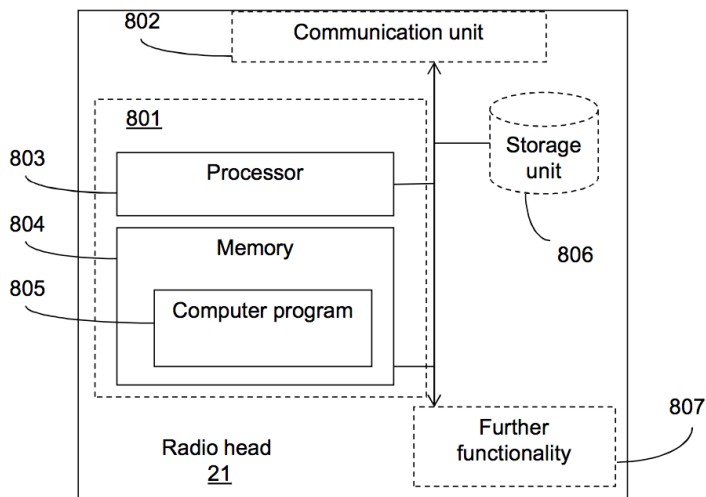
Fig. 5.16
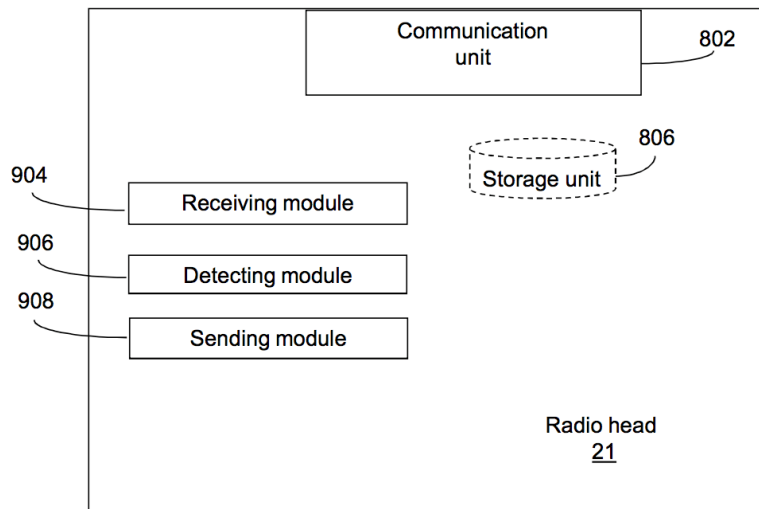
Fig. 5.17

5.6.5 Detailed Description

In a distributed base station system comprising a BBU, an IRU connected to the BBU and a plurality of RHs connected via dedicated cables to the IRU, there is a risk that crosstalk between nearby lying cables connecting different RHs to the IRU may have negative influence on the quality of signals sent over the cables. A decreased signal quality would reduce the cable reach and the usable bandwidth available, which are key performance aspects of such a system. For this reason, a solution is provided to reduce or mitigate the influence of crosstalk between nearby lying cables connecting an IRU with different RHs of such a base station system. An embodiment of the solution comprises detecting at a first RH, a received symbol sent from the IRU and sending back to the IRU an error sample (also called a slicing error) of the received symbol, *i.e.,* how the symbol has been distorted from a "clean" symbol when received at the first RH from the IRU. The error sample is then used to set coefficients of a precoder, so that further symbols are properly precoded before being sent over the cable so that the symbols will be received as clean (or at least cleaner) symbols. This is achieved because the crosstalk is pre-canceled out by the precoder. Observe that the mentioned precoder is an additional precoder than the radio precoder used for multi-antenna processing in the BBU. The radio precoder is designed to take care of the radio signals transmitted at the different antennas.

It cannot handle the crosstalk between nearby lying cables. Therefore, in the claimed system a separate precoder is added to cancel the crosstalk. This separate precoder may reside in the IRU. This approach is transparent to the radio process including the radio precoder. No change is needed in the BBU processing algorithms.

Fig. 5.5 shows an architecture of a base station system (100), also called a radio dot system, according to an embodiment of the invention. The base station system (100) comprises a BBU (30) which is arranged to treat signals in a baseband frequency region. The base station system (100) further comprises an IRU (10) connected to the BBU (30) via *e.g.,* an optical fiber (32). Alternatively, for example when the IRU and the BBU are closely located, the connection between the RU and the BBU may be electrical via *e.g.,* copper cables. The system 100 further comprises a number of RHs (21-26) connected to the IRU (10) via metallic conductors (41, 42). The metallic conductors may be twisted pair cables, *e.g.,* copper cables such as Cat 3/5/6/7 cables. Each RH is connected with a dedicated metallic conductor back to the IRU. In the following we focus on telephone grade cables like Cat 3 cables. Such cables have multi-pairs (*e.g.,* more than four) in a bundle and the pairs are gradually split out to different RHs, for example at different homes. This is a common scenario for a telephony network. In this case, there is always a common cable segment where the pairs for different RHs go through the same bundle and therefore suffer from the mutual crosstalk between them in the cable.

When transporting signals in the downlink direction, the BBU (30) generates and sends a number of baseband signals, *e.g.,* base band LTE signals. Corresponding in-phase and quadrature (IQ) data flows of the baseband signals are sent to the IRU, which IQ data flows are directed to different RHs (21-26) for further distribution to UEs in radio connection with one of the RHs (21-26). The number of downlink baseband signals may be sent as a single digital signal from the BBU to the IRU, over the optical fiber, *e.g.,* encapsulated using a common public radio interface (CPRI) protocol. The IRU (10) then decapsulates the CPRI stream to baseband signals as IQ data flows per antenna carrier and up-converts the downlink baseband signals received from the baseband unit (30) to a low intermediate frequency (IF) that is suitable for transmission on the metallic conductor. The IRU (10) then sends the downlink IF radio signals to the RHs via the respective metallic conductor. By transmitting IF signals instead of high frequency RF signals over the metallic conductors, the cable loss is reduced. The RHs (21-26) are arranged for receiving the analog IF signals from its respective metallic conductor to which the RH is connected and for up-converting the IF signals to the actualradio frequency (RF) to be transmitted over the air from antenna(s) of the respective RH. A radio frequency region may be *e.g.,* 400 MHz to 6 GHz. The RH comprises at least one antenna

element for transmitting the downlink signal to UEs.

In the uplink direction, the RHs (21-26) are each arranged to receive RF radio signals from UEs, *e.g.,* mobile stations, down-convert the RF signals to IF signals to be transported over the metallic conductors towards the RU (10) for further processing. The RU is arranged to down-convert the received IF signal to a baseband frequency for further transmission to the BBU (30). Uplink and downlink IF signals may be transported over the metallic conductors 40 via frequency duplexing for frequency-division duplex (FDD) radios, and/or time duplexing for time-division duplex (TDD) radios. A RDS is a cost-effective radio system, especially for indoor deployment.

Fig. 5.6 shows a schematic view of an example of how the RHs (21-26) of Fig. 5.5 may be positioned to cover a geographical area. Each RH (21-26) covers a geographical area (51-56). A mobile station (60) that is situated in *e.g.,* geographical area (54) will be connected to RH (24) and receive downlink RF signals over the air from RH (24) and transmit uplink RF signals over the air to RH (24). Even though Fig. 5.6 shows circular geographical areas, so called Omni-cells, any other type of geographical area may be covered, such as an angular section, a part of a building floor, etc. The RHs may be arranged in a building, *e.g.,* on different floors of the building.

Fig. 5.7 (and Fig. 5.5) describes a method for mitigating crosstalk, performed by a network node of a wireless communication network operable in a base station system (100) (see Fig. 5.5) of the wireless communication network. The base station system comprises an IRU (10), a BBU (30) connected to the IRU, and a plurality of RHs (21-26) connected to the IRU via a plurality of metallic conductors. The method comprises receiving (204) from a first (21) of the plurality of RHs, a measure of an error of one or more symbols of a signal received by the first RH from the IRU over a first (41) of the plurality of metallic conductors, the measure of the error being detected by the first RH and the signal being destined to a UE (60) wirelessly connected to the first RH (21). The method further comprises determining (206) precoding coefficients for a precoder according to the received error measure, and triggering (208) application of the determined precoding coefficients when sending further signals to the first RH over the first of the plurality of metallic conductors, the further signals being destined to UEs wirelessly connected to the first RH.

The network node may be the IRU. The IRU handles the interface between the baseband signal and the metallic conductor. The IRU may transform the signal from the baseband frequency to the intermediate frequency. The IRU may apply the determined precoding coefficients on the precoder. Alternatively, the network node may be the BBU. The BBU is the node that handles signals in the baseband frequency. Alternatively, the network node may be situated somewhere else in the network, determining precoding coefficients and

triggering to apply the determined precoding coefficients when sending further signals to the first RH. In case the method is performed in the BBU or in some other network node different from the IRU, the BBU (or other network node) triggers the application of the determined precoding coefficients. In case the precoder is situated in the IRU the BBU (or other network node would trigger the IRU to apply the determined precoding coefficients. The term "triggering applying of the determined coefficients" may signify that the fact that new precoding coefficients are determined results in the new coefficients being used by the precoder for future or following sending of signals. The signal destined to a UE is a signal to be sent over a wireless interface in a wireless communication system towards a UE. The signal destined to a UE may be a signal according to the 3GPP long term evolution (LTE) standard. The error represents a difference between a sent symbol and a received symbol. The error may be an error vector. The received measure of the one or more symbol error may either be the actual error (also called slicing error) or a measure of the received one or more symbol. In the former, the actual error is calculated by the IRU as a difference between the sent symbol and the measure of the received one or more symbol. For example, if the sent symbol is $(+1, -j)$ and the received one or more symbol is $(+0.8, -0.6j)$, the actual error would be $(-0.2, +0.4j)$. The plurality of RHs is connected to the IRU via a respective metallic conductor. In other words, there may be a one to one relationship between the number of RHs and the number of metallic conductors. However, the invention is also applicable where an RH is connected to more than one metallic conductor, as long as each conductor is connected to carry a signal from distinct LTE antenna ports. Except for the mentioned precoder, which may be called a conductor precoder, there is normally also a precoder implemented in the BBU. The BBU precoder precodes the radio signal in a baseband format to preform multi-antenna processing, for example MIMO processing, which can increase bit rate and robustness by spatial multiplexing, diversity and/or interference cancellation. The conductor precoder on the other hand precodes the signal to mitigate metallic conductor interface crosstalk, or interference between pairs. The precoders are independent of each other.

By such a method it is possible to reduce cross-talk over neighboring metallic conductors in a base station system. As opposed to crosstalk in VDSL this method deals with crosstalk for signals that are to be sent over an air interface to the end users but before reaching the antenna they are sent over a metallic conductor for further transmission by the antenna over the air interface, and then it has been found that there may be crosstalk over the metallic conductor. VDSL on the other hand is a wireline technology that is adapted for wireline interfaces. If you try to deploy a base station over the same metallic conductors in a VDSL-like scenario, the crosstalk will degrade the performance figures of

the transmitter. It may also cause inband interference on neighboring frequency carriers which is not allowed in 3GPP. In both cases you can only attempt to keep 3GPP compliance if you perform crosstalk cancellation.

With the error samples from one RH, it is possible to cancel out the crosstalk to this conductor from other conductors connected to the same IRU. In this case, for a linear precoder, the corresponding column vector of the precoding matrix will be updated. In order to completely determine the precoder to cancel out the mutual crosstalk between all conductors connected to the same IRU, the information of the whole channel matrix may be needed, which requires error samples from all conductors.

According to an embodiment, the one or more symbol is a data symbol.

According to another embodiment, the one or more symbol is a reference signal symbol, such as CRS symbol. The reference signal symbols are repetitively broadcasted by the RH irrespective of whether there are data to be sent or not. This means that in comparison to using the data symbols the reference signal symbols are always there to measure on. When using data symbols and there is no data to be sent over the metallic conductor, it may be necessary to send dummy symbols to the RH on which the RH can detect the measure of the error.

According to an embodiment, the method further comprises triggering sending (202), to the first of the plurality of RHs, the signal destined to the UE connected to the first of the plurality of RHs. In case the network node is the IRU, a unit such as a processor in the IRU triggers the sending, and the network node also performs the actual sending. In case the network node is another node, such as a BBU, the network node triggers the IRU to send the signal to the first RH.

According to another embodiment, the method further comprises triggering sending (210), to a second of the plurality of RHs, a signal destined to a UE connected to the second of the plurality of RHs. This signal sent to the second RH comprises a reference signal symbol. Further, the signal sent to the first RH and the signal sent to the second RH is sent in the same frequency and time slot. When CRS signal is used, the error samples can be calculated accurately without decoding errors since the CRS is predefined and known. When the CRS signals are sent simultaneously and over the same frequency over two conductors that experience mutual crosstalk, the mutual crosstalk components can be detected by error samples fed back from the RH side. So it is advantageous to align the CRS signals on different pairs to different cells in the frequency grid. To be able to achieve that for LTE signals, the CRS signals over two conductors to two different RHs are sent in the same frequency and time slot, cell-IDs are allocated to the first and the second RH separated by 6. The allocation of cell-IDs may be performed by the same node that per-

forms this function in a regular LTE deployment, which is the e-NodeB, more specifically the BBU of the e-NodeB. This node may be instructed to follow the sequence suggested by the present method.

Fig. 5.8 shows a method performed by a first RH (21) operable in a base station system (100) of a wireless communication network, for mitigating crosstalk. The base station system comprises an IRU (10), a BBU 30 connected to the IRU, and a plurality of RHs (21-26) including the first RH (21), the plurality of RHs being connected to the IRU via a plurality of metallic conductors. The method comprises receiving (302), from the IRU over a first (41) of the plurality of metallic conductors, a signal destined to a UE 60, wirelessly connected to the first RH, the signal comprising one or more symbols. The method further comprises detecting (304), from the received one or more symbol, a measure of an error of the one or more symbol and sending (306), to the IRU, the measure of the one or more symbol error, for further determining of precoding coefficients for a precoder based on the received measure of symbol error.

According to an embodiment, the one or more symbol is a data symbol. According to another embodiment, the one or more symbol is a reference signal symbol, such as CRS symbol.

Fig. 5.9 shows an RH according to an embodiment. The RH (also called dot) receives the IF signal from the metallic conductor to which it is connected via an analog front-end (AFE) (350) connected to the metallic conductor. The received IF signal is low-pass, LP, filtered in an LP filter (352) connected to the AFE, thereafter analog to digital, A/D converted in an A/D (354) connected to the LP filter, after which the signal is digitally processed in a DSP (356). Then the signal is digital to analog converted back to analog signal in a D/A (358) connected to the DSP, and then up-converted by an Up-converter (360) to the required RF signal, which is sent to a RF frontend (362) for transmission over the air interface to UEs.

According to an embodiment, an estimate of the complex metallic conductor channel gains, *i.e.,* the crosstalk channel coefficients, are available at the IRU calculated from feedback of error samples detected by the RH on signals received from the IRU. A possible embodiment to realize this is based on executing additional digital signal processing in the IRU as is described in the following. A frequency-domain crosstalk cancellation scheme can be implemented as shown in Fig. 5.10 in which boxes (402-414) symbolized functions in the IRU, box (416) symbolizes the metallic conductor channel gain and box (418) the RH.

The input to a pre-processing unit (402) of the IRU for crosstalk cancellation is a set of N IQ flows received from the BBU, which IQ flows contain the IQ samples per antenna-carrier. In the figure, the number of stacked blocks for each unit (or function) may equal the number of IQ flows and the stacked

blocks symbolize separate treatment of each IQ flow. In other words, when the IQ flows reaches the pre-processing unit (402), the CPRI stream has already been decapsulated into the individual streams. After receiving the IQ flows, the pre-processing unit (402) first removes the cyclic prefix for each orthogonal frequency-division multiplexing (OFDM) symbol. The remaining samples are then converted from serial to parallel and used as inputs to a fast Fourier transform (FFT) unit (404) that performs an FFT on the symbols. In the FFT unit, the symbols are transferred to frequency domain, in which each subcarrier is modulated by quadrature amplitude modulation (QAM). For every subcarrier, the k-th element (*i.e.,* the k-th subcarrier) of the N FFT outputs is stacked into a vector and used as input to a precoder (406).

Next, a precoding operation is performed in the precoder (406), on the input vectors (*i.e.,* QAM symbols) on each subcarrier. The precoder here pre-cancels the crosstalk between pairs. There are mainly two types of precoding techniques, linear precoding and non-linear precoding techniques, respectively. To have an example here, given the knowledge of the crosstalk channel coefficients $\mathbf{H}$, a linear precoder can be simply inverse of the crosstalk channel coefficients scaled by the direct channel coefficients, $\mathbf{P} = \mathbf{H}^{-1}\mathbf{H}_{\mathrm{d}}$, where $\mathbf{H}_{\mathrm{d}}$ is the diagonal matrix of $\mathbf{H}$. $\mathbf{P}$ is the precoding matrix (or precoding coefficients). In this case, the received signals at the RH side is $\mathbf{y} = \mathbf{HPx} + \mathbf{n}$ where $\mathbf{y}$ is the received signal vector comprising the received signals from different RHs, $\mathbf{x}$ is the transmitted signal vector comprising the transmitted signals to different RHs, $\mathbf{P}$ is the precoding matrix, $\mathbf{H}$ is a channel matrix comprising direct channel coefficients as the diagonal elements and crosstalk channel coefficients as the off-diagonal elements, and $\mathbf{n}$ is the background noise vector on different pairs. Take $\mathbf{P} = \mathbf{H}^{-1}\mathbf{H}_{\mathrm{d}}$, then the received signal vector is $\mathbf{y} = \mathbf{H}_{\mathrm{d}}\mathbf{x} + \mathbf{n}$. As $\mathbf{H}_{\mathrm{d}}$ is a diagonal matrix, no crosstalk components are remained in $\mathbf{y}$. So the crosstalk is pre-cancelled. The method works for both types of the precoding schemes, as the method favors channel estimation.

The precoded symbols are then transformed back to time domain by an inverse fast Fourier transform (IFFT) unit (408). Thereafter, in a post-processing unit (410), the cyclic prefix is added to the precoded OFDM symbols. After adding a cyclic prefix, the OFDM signals are up-converted in an up-converter (412) (also called mixer) to an IF frequency f_c that is suitable for transmission over the metallic conductors. The up-converted samples are then digital-to-analog converted and sent through an analog frontend (414) to be further transmitted on the metallic conductors (416) to be received at the individual RHs (418). The RHs (418) then receives the up-converted analog OFDM signals and calculates error samples of the precoded symbols and sends the error samples back to the precoder (406) of the IRU, as will now be described further.

In the following it is assumed that the IRU and the RHs are synchronized

on clock-level, symbol-level and also subframe-level. The clock synchronization may be done by a dedicated synchronization channel between the IRU and the RHs. The symbol and subframe synchronization may be done by for example an LTE UE receiver functionality implemented in the IRU and in the RHs. Clock synchronization is needed for up/down conversion. Symbol synchronization is for encoding/decoding OFDM symbols. Subframe synchronization is to identify reference signals, which are embedded in specific subframes.

Each RH (418) calculates the slicing error or error samples of a selected type of symbol of the received OFDM signal, *e.g.,* of specific reference symbols or of data symbols, and then sends the error samples back to the IRU. Fig. 5.11 shows an example of a DSP (356) (see Fig. 5.9 also) in an RH, adapted for error sample calculation and feedback. The DSP (356) comprises a filter (366) to filter out unwanted signals and an equalizer (368) to equalize the slope of the line attenuation. The selected symbols are extracted after passing the filter (366). After removing the cyclic prefix in the cyclic prefix remover (370) and transforming the digital signal to the frequency domain in an FFT (372), the error samples are calculated in a decoder (374) and fed to the central processing unit (CPU) (364) (Fig. 5.9). The decoder decodes the received OFDM symbols used for precoder update. The decoder has a frequency-domain equalizer to recover the received symbol back to the original constellation plane, in order to decode the symbol and calculate the error samples. As one implementation example, this equalizer can be trained and updated using CRS signals. The CPU then feeds the error samples back through the control channel from the RH to the IRU. The feedback process may be done upon the requests from the IRU.

The IRU then calculates the precoder coefficients according to the received error samples. Two exemplary methods for calculating precoding coefficients based on CRS symbols and data symbols, respectively, are presented below.

The data symbol based method uses the feedback of error samples detected by the RH from data symbols. Statistical processing methods like minimum mean square error (MMSE)-based, least square (LS)-based and least mean square (LMS)-based methods, etc. Precoder update can be driven by the error samples to minimize the errors and therefore cancel out the crosstalk. In the following example, an LS-based method is described, to estimate the crosstalk channel matrix based on the error samples from the RHs. After the channel is estimated, one can update the precoder following a linear or non-linear precoding approach.

The formulation described below assumes a single subcarrier case, without loss of generality for multi-carrier cases. It is assumed that transmitted and received symbols for all lines are known at the transmitter. This is possible, for example, after the received symbols are fed back via the control channel.

Consider a Distributed Antenna System carrying downlink LTE over twisted pairs, where M independent cells are synchronized. Let $\mathbf{x}_k \in \mathbb{C}^{M \times 1}$ represent the transmitted symbol vector at time slot k. The received symbol vector $\mathbf{y}_k \in \mathbb{C}^{M \times 1}$ can then be described as

$$\mathbf{y}_k = \mathbf{H}\mathbf{x}_k + \mathbf{n}_k, \tag{5.10}$$

where $\mathbf{H} \in \mathbb{C}^{M \times M}$ is the frequency-domain channel matrix and $\mathbf{n}_k \in \mathbb{C}^{M \times 1}$ is the additive noise vector. Let W represent the number of symbols in an observation window. Define

$$\boldsymbol{\gamma} = \begin{bmatrix} y_k \\ y_{k-1} \\ \vdots \\ y_{k-W+1} \end{bmatrix} \in \mathbb{C}^{WM \times 1},$$

$$\boldsymbol{\eta} = \begin{bmatrix} n_k \\ n_{k-1} \\ \vdots \\ n_{k-W+1} \end{bmatrix} \in \mathbb{C}^{WM \times 1},$$

$$\mathbf{X} = \begin{bmatrix} \mathbf{x}_k^{\mathrm{T}} \otimes \mathbf{I}_M \\ \mathbf{x}_{k-1}^{\mathrm{T}} \otimes \mathbf{I}_M \\ \vdots \\ \mathbf{x}_{k-W+1}^{\mathrm{T}} \otimes \mathbf{I}_M \end{bmatrix} \in \mathbb{C}^{WM \times M^2}$$

and let $\mathbf{h} \in \mathbb{C}^{M^2 \times 1}$ be a vector obtained by stacking the columns of $\mathbf{H}$. The last W received symbols can then be described as

$$\boldsymbol{\gamma} = \mathbf{X}\mathbf{h} + \boldsymbol{\eta} \tag{5.11}$$

Following an LS method, taking advantage of Eq. (5.11), one can obtain an LS estimate of $\mathbf{h}$, for example, by using a pseudo-inverse

$$\hat{\mathbf{h}} = (\mathbf{X}^{\mathrm{H}}\mathbf{X})^{-1}\mathbf{X}^{\mathrm{H}}\boldsymbol{\gamma}. \tag{5.12}$$

Therefore, by stacking the elements of $\hat{\mathbf{h}}$ column-wise back, one obtains the desired channel matrix estimate $\hat{\mathbf{H}}$. With the known transmitted symbols and the corresponding error samples, one can obtain $\boldsymbol{\gamma}$ in Eq. (5.11) and further estimate the channel coefficients by Eq. (5.12).

If data symbols are used, the above described exemplary method requires that the data symbols are not corrupted by the crosstalk, such that the symbol

can be correctly decoded and the error samples can be calculated correctly. Therefore it may be needed to control the number of RHs to which signals are sent simultaneously from the IRU. If too many RHs receive signals simultaneously, the crosstalk may be so high resulting in that the signal gets degraded so much that the data symbol may get corrupted. Also, when there is no data in the buffer to transmit, dummy data symbols need to be transmitted to be able to have something to calculate error samples upon. The randomness of the dummy data symbols on each antenna should preferably be statistically independent, for example, based on different pseudo-random sequences.

The reference signal based method uses the feedback of the error samples of the CRS symbols. The advantage of this method is that the CRS is always broadcasted (periodically). In other words, no dummy symbols have to be sent as when using data symbols and there is no data to be sent. The CRS is a two dimensional cell specific sequence in LTE to aid UEs in performing channel estimation and cell identification of a cell and is the basis for the cell selection and hand-over decisions. The CRS spans each resource block and is sent at predefined resource elements. An example of CRS pattern for two different antenna ports of one RH, which has two pairs, each transport the signal of one antenna port, are shown in Fig. 5.12a and 5.12b, respectively. Each square in the pattern represents a resource element. R0 represents a resource element on which a CRS is sent from the first antenna port. R1 represents a resource element on which a CRS is sent from the second antenna. "XXXX" signifies that no reference symbol is sent in the information element for this antenna port. The CRS signals are transmitted in each resource block in every downlink subframe in the frequency domain and are covering the whole cell bandwidth. The CRS for different cells can use the same resource elements and can also be shifted in resource elements.

When to send an LTE CRS depends on its cell-id, which is a numeric identifier that defines (504) unique cells. The cell-ID defines not only the reference signal constellation points by associated M-sequences, but also their allocation within the resource grid (Figs. 5.12a and 5.12b). The period of the CRS sequence is one radio frame, *e.g.,* 10 ms. Cells with consecutive ids have their reference signal frequency allocation shifted by one. If two cells have IDs separated by 6, *i.e.,* 0, 6, 12, ..., their reference signals are allocated in the same positions in the downlink resource grid. In order to see the mutual crosstalk components on the received CRS symbols, the CRS for different cells should use the same frequency/time pattern, so that the error samples per RH comprise all crosstalk components from other RHs connected to the same IRU. To achieve this, this invention proposes to assign the cell-IDs for different cells

whose RHs are connected to the same IRU according to:

$$N_{\mathrm{ID}}^{\mathrm{cell}}(1) \in \{0, 1, \ldots, 503\},$$
$$N_{\mathrm{ID}}^{\mathrm{cell}}(i) = (N_{\mathrm{ID}}^{\mathrm{cell}}(i-1) + 6) \bmod 504, \; i \in \{2, \ldots, M\}.$$

This guarantees that the CRS symbols are transmitted synchronously in time and frequency, as shown in Fig. 5.13. In this example, four cells whose RHs are connected to the same IRU are assigned cell-ID 0, 6, 12 and 18, respectively, which results in that the CRS symbols are transmitted on the same resource element in each resource block for the four cells (12 REs in 7 OFDM symbols), as illustrated by the cell-ID numbers "0, 6, 12, 18" residing in the same resource element square.

In this way, the error samples on the received CRS symbols of each RH comprises the crosstalk components from the other RHs' CRS symbols transmitted on closely lying conductors. Treating the CRS as independent random symbols, the error samples can be used to drive statistical processing methods like the MMSE-based, the LS-based and the LMS-based methods, etc., mentioned before to update the precoder to cancel out the crosstalk. The same methods can be used as in the data symbol based method. Particularly, the LS method described above in detail is presented for crosstalk channel estimation with the known transmitted CRS symbols and the received CRS symbols (*i.e.,* error samples plus the transmitted CRS symbols) from the feedback. Furthermore, CRS may be generated based on a Gold sequence, which is a class of pseudo random sequences having good periodic cross-correlation properties. If the cross-correlation property is utilized by more advanced methods, an even better performance may be achieved.

In this way, the precoding coefficients on every 3-rd subcarrier is explicitly calculated, because the CRS is defined on every 3-rd subcarrier (1, 4, 7,...), as shown in Fig. 5.13 (every row of squares defines a subcarrier). The precoding coefficients on the rest of the subcarriers can be obtained by interpolation techniques. It can even simply use the same precoding coefficients, as the 3 subcarriers are within the coherent bandwidth for the cable channel.

It is noted that the proposed CRS-based method works also for multiple antennas per RH, because of the shifted structure of CRS per antenna port defined in 3GPP, as shown in Fig. 5.12a and 5.12b.

The described solution significantly lowers crosstalk of a base station system where the IRS is connected to its RHs via metallic conductors between which crosstalk may occur. This result in a significant improvement of reach and bandwidth for signals sent from an RH to UEs in connections the RH. Since the crosstalk cancellation is done in the IRU, no modifications are needed on today's BBU. Further, the described solution reuses existing radio signaling, *e.g.,* LTE

signaling, for updating the precoder for downlink crosstalk cancellation, which means that no extra signaling is needed on the metallic conductors.

Fig. 5.14 describes an embodiment of a network node (600) operable in a wireless communication network, configured to mitigating crosstalk of a base station system (100). The dashed lines in the figures are used to illustrate that those boxes are only optional. The base station system comprises an IRU (10), a BBU (30) connected to the IRU, and a plurality of RHs (21-26) connected to the IRU via a plurality of metallic conductors. The network node (600) comprises a processor (603) and a memory (604). The memory contains instructions executable by said processor, whereby the network node (600) is operative for receiving from a first (21) of the plurality of RHs, a measure of an error of one or more symbols of a signal received by the first RH from the IRU over a first of the plurality of metallic conductors, the measure of the error being detected by the first RH, the signal being destined to a user equipment, UE (60) wirelessly connected to the first RH (21). The memory further contains instructions executable by said processor, whereby the network node (600) is operative for determining precoding coefficients for a precoder according to the received error measure, and triggering applying the determined precoding coefficients when sending further signals to the first RH over the first of the plurality of metallic conductors, the further signals being destined to UEs wirelessly connected to the first RH.

According to an embodiment, the one or more symbol is a data symbol. According to another embodiment, the one or more symbol is a reference signal symbol, such as CRS symbol.

According to another embodiment, the memory contains instructions executable by said processor, whereby the network node (600) is operative for triggering sending, to the first of the plurality of RHs, the signal destined to the UE connected to the first of the plurality of RHs.

According to another embodiment, the memory contains instructions executable by said processor, whereby the network node (600) is operative for triggering sending, to a second of the plurality of RHs, a signal destined to a UE connected to the second of the plurality of RHs, the signal sent to the second RH comprising a reference signal symbol, wherein the signal sent to the first RH and the signal sent to the second RH are sent in the same frequency and time slot.

The network node (600) may further comprise a communication unit (602), which may be considered to comprise conventional means for wirelessly communicating from and/or to other nodes in the communication network, such as the BBU (30), the UE (60) and the IRU, depending on where the functionality is installed. The communication unit may comprise one or more communication ports for communicating with other nodes in the network. The network

node may further comprise one or more storage units (606) and further functionality (607) useful for the network node to serve its purpose as network node. The instructions executable by said processor may be arranged as a computer program (605) stored in said memory (604). The processor (603) and the memory (604) may be arranged in an arrangement (601). The arrangement (601) may be a micro processor and adequate software and storage therefore, a programmable logic device (PLD) or other electronic component(s)/processing circuit(s) configured to perform the actions, or methods mentioned above.

The computer program (605) may comprise computer readable code means, which when run in the network node (600) causes the network node to perform the steps described in any of the described embodiments. The computer program may be carried by a computer program product connectable to the processor. The computer program product may be the memory (604). The memory (604) may be realized as for example a random-access memory (RAM), read-only memory (ROM) or an electrical erasable programmable ROM (EEPROM). Further, the computer program may be carried by a separate computer-readable medium, such as a CD, DVD or flash memory, from which the program could be downloaded into the memory (604). Alternatively, the computer program may be stored on a server or any other entity connected to the communication network to which the network node has access via its communication unit (602). The computer program may then be downloaded from the server into the memory (604).

Fig. 5.15 describes another embodiment of a network node (600) of a wireless communication network operable in a base station system (100) of the wireless communication network. The base station system comprises an IRU (10), a BBU (30) connected to the IRU and a plurality of RHs (21-26) connected to the IRU via a plurality of metallic conductors. The network node comprises a receiving module (704) for receiving from a first (21) of the plurality of RHs, a measure of an error of one or more symbols of a signal received by the first RH from the IRU over a first of the plurality of metallic conductors, the measure of the error being detected by the first RH, the signal being destined to a UE (60) wirelessly connected to the first RH (21). The network node further comprises a determining module (706) for determining precoding coefficients for a precoder according to the received error measure, and a triggering module (708) for triggering applying the determined precoding coefficients when sending further signals to the first RH over the first of the plurality of metallic conductors, the further signals being destined to UEs wirelessly connected to the first RH.

Fig. 5.16 describes an embodiment of a first RH (21) operable in a base station system (100) of a wireless communication network, configured to contribute in mitigating crosstalk. The base station system comprises an IRU (10), a BBU (30) connected to the IRU, and a plurality of RHs (21-26) in-

cluding the first RH, the plurality of RHs being connected to the IRU via a plurality of metallic conductors. The first RH comprises a processor (803) and a memory (804). The memory contains instructions executable by said processor, whereby the first RH (21) is operative for receiving, from the IRU over a first (41) of the plurality of metallic conductors, a signal destined to a UE (60) wirelessly connected to the first RH, the signal comprising one or more symbols. The memory further contains instructions executable by said processor, whereby the first RH (21) is operative for detecting, from the received one or more symbol, a measure of an error of the one or more symbol; and sending, to the IRU, the measure of the one or more symbol error, for further updating of precoding coefficients for a precoder based on the received measure of symbol error.

According to an embodiment, the one or more symbol is a data symbol. According to another embodiment, the one or more symbol is a reference signal symbol, such as CRS symbol.

The radio head (21) may further comprise a communication unit (802), which may be considered to comprise conventional means for wirelessly communicating from and/or to the UE (60) and the IRU (10). The communication unit may comprise a wireless transceiver and at least one antenna. The communication unit may comprise one or more communication ports for communicating with the IRU over the metallic conductor. The radio head may further comprise one or more storage units (806) and further functionality (807) useful for the radio head to serve its purpose as radio head. The instructions executable by said processor may be arranged as a computer program 805 stored in said memory (804). The processor (803) and the memory (804) may be arranged in an arrangement (801). The arrangement 801 may be a micro processor and adequate software and storage therefore, a Programmable Logic Device, PLD, or other electronic component(s)/processing circuit(s) configured to perform the actions, or methods mentioned above.

The computer program (805) may comprise computer readable code means, which when run in the radio head (21) causes the radio head to perform the steps described in any of the described embodiments. The computer program may be carried by a computer program product connectable to the processor. The computer program product may be the memory (804). The memory (804) may be realized as for example a RAM, ROM or an EEPROM. Further, the computer program may be carried by a separate computer-readable medium, such as a CD, DVD or flash memory, from which the program could be downloaded into the memory (804). Alternatively, the computer program may be stored on a server or any other entity connected to the communication network to which the radio head (21) has access via its communication unit (802). The computer program may then be downloaded from the server into the memory

(804).

Fig. 5.17 describes another embodiment of a first RH (21) operable in a base station system (100) of a wireless communication network, configured to contribute in mitigating crosstalk. The base station system comprises an IRU (10), a BBU (30) connected to the IRU, and a plurality of RHs (21-26) including the first RH, the plurality of RHs being connected to the IRU via a plurality of metallic conductors. The first RH comprises a receiving module (904) for receiving, from the IRU over a first (41) of the plurality of metallic conductors, a signal destined to a UE (60) wirelessly connected to the first RH, the signal comprising one or more symbols. The first RH further comprises a detecting module (906) for detecting, from the received one or more symbol, a measure of an error of the one or more symbol, and a sending module (908) for sending, to the IRU, the measure of the one or more symbol error, for further updating of precoding coefficients for a precoder based on the received measure of symbol error.

In Figs. 5.16 and 5.17 the term "first radio head" is used for being able to distinguish the first RH out of the plurality of RHs mentioned in the text to the figures. However, any of the plurality RHs could be the first RH.

Although the description above contains a plurality of specificities, these should not be construed as limiting the scope of the concept described herein but as merely providing illustrations of some exemplifying embodiments of the described concept. It will be appreciated that the scope of the presently described concept fully encompasses other embodiments which may become obvious to those skilled in the art, and that the scope of the presently described concept is accordingly not to be limited. Reference to an element in the singular is not intended to mean "one and only one" unless explicitly so stated, but rather "one or more". All structural and functional equivalents to the elements of the above-described embodiments that are known to those of ordinary skill in the art are expressly incorporated herein by reference and are intended to be encompassed hereby. Moreover, it is not necessary for an apparatus or method to address each and every problem sought to be solved by the presently described concept, for it to be encompassed hereby.

5.6.6   Claims

1. A method for mitigating crosstalk performed by a network node of a wireless communication network operable in a base station system (100) of the wireless communication network, the base station system comprising an IRU (10), a BBU (30), connected to the IRU and a plurality of RHs (21-26) connected to the IRU via a plurality of metallic conductors, the method comprising:

- receiving (204) from a first (21) of the plurality of RHs, a measure of an error of one or more symbols of a signal received by the first RH from the IRU over a first of the plurality of metallic conductors, the measure of the error being detected by the first RH, the signal being destined to a UE (60), wirelessly connected to the first RH (21),
- determining (206) precoding coefficients for a precoder according to the received error measure, and
- triggering applying (208) the determined precoding coefficients when sending further signals to the first RH over the first of the plurality of metallic conductors, the further signals being destined to UEs wirelessly connected to the first RH.

2. Method according to claim 1, wherein the one or more symbol is a data symbol.

3. Method according to claim 1, wherein the one or more symbol is a reference signal symbol, such as CRS symbol.

4. Method according to any of claims 1-3, further comprising:

- triggering sending (202), to the first of the plurality of RHs, the signal destined to the UE connected to the first of the plurality of RHs.

5. Method according to claim 3 and 4, further comprising:

- triggering sending (210), to a second of the plurality of RHs, a signal destined to a UE connected to the second of the plurality of RHs, the signal sent to the second RH comprising a reference signal symbol, wherein the signal sent to the first RH and the signal sent to the second RH are sent in the same frequency and time slot.

6. A method performed by a first RH (21) operable in a base station system (100) of a wireless communication network, for mitigating crosstalk, the base station system comprising an IRU (10) a BBU (30) connected to the IRU, and a plurality of RHs (21-26) including the first RH (21), the plurality of RHs being connected to the IRU via a plurality of metallic conductors, the method comprising:

- receiving (302), from the IRU over a first (41) of the plurality of metallic conductors, a signal destined to a user equipment, UE, (60) wirelessly connected to the first RH, the signal comprising one or more symbols;

- detecting (304), from the received one or more symbol, a measure of an error of the one or more symbol;

- sending (306), to the IRU, the measure of the one or more symbol error, for further determining of precoding coefficients for a precoder of the IRU based on the received measure of symbol error.

7. Method according to claim 6, wherein the one or more symbol is a data symbol.

8. Method according to claim 6, wherein the one or more symbol is a reference signal symbol, such as CRS symbol.

9. A network node (600) operable in a wireless communication network, configured to mitigating crosstalk of a base station system (100), the base station system comprising an IRU (10), a BBU (30) connected to the IRU, and a plurality of RHs (21-26) connected to the IRU via a plurality of metallic conductors, the network node (600) comprising a processor (603) and a memory (604), said memory containing instructions executable by said processor, whereby the network node (600) is operative for:

- receiving from a first (21) of the plurality of RHs, a measure of an error of one or more symbols of a signal received by the first RH from the IRU over a first of the plurality of metallic conductors, the measure of the error being detected by the first RH, the signal being destined to a UE (60), wirelessly connected to the first RH (21),

- determining precoding coefficients for a precoder according to the received error measure, and

- triggering applying the determined precoding coefficients when sending further signals to the first RH over the first of the plurality of metallic conductors, the further signals being destined to UEs wirelessly connected to the first RH.

10. Network node according to claim 9, wherein the one or more symbol is a data symbol.

11. Network node according to claim 9, wherein the one or more symbol is a reference signal symbol, such as CRS symbol.

12. Network node according to any of claims 9-11, wherein the memory contains instructions executable by said processor, whereby the network node (600) is operative for:

- triggering sending, to the first of the plurality of RHs, the signal destined to the UE connected to the first of the plurality of RHs.

13. Network node according to claim 11 and 12, wherein the memory contains instructions executable by said processor, whereby the network node (600) is operative for triggering sending, to a second of the plurality of RHs, a signal destined to a UE connected to the second of the plurality of RHs, the signal sent to the second RH comprising a reference signal symbol, wherein the signal sent to the first RH and the signal sent to the second RH are sent in the same frequency and time slot.

14. A first RH (21) operable in a base station system (100) of a wireless communication network, configured to contribute in mitigating crosstalk, the base station system comprising an IRU (10), a BBU (30) connected to the IRU, and a plurality of RHs (21-26) including the first RH, the plurality of RHs being connected to the IRU via a plurality of metallic conductors, the first RH comprising a processor (803) and a memory (804), said memory containing instructions executable by said processor, whereby the first RH (21) is operative for:

   - receiving, from the IRU over a first (41) of the plurality of metallic conductors, a signal destined to a UE (60) wirelessly connected to the first RH, the signal comprising one or more symbols;
   - detecting, from the received one or more symbol, a measure of an error of the one or more symbol; and
   - sending, to the IRU, the measure of the one or more symbol error, for further updating of precoding coefficients for a precoder based on the received measure of symbol error.

15. A computer program (605) comprising computer readable code means to be run in a network node (600) of a wireless communication network, configured to mitigating crosstalk of a base station system (100), the base station system comprising an IRU (10), a BBU (30) connected to the IRU, and a plurality of RHs (21-26) connected to the IRU via a plurality of metallic conductors, which computer readable code means when run in the network node causes the network node (600) to perform the following steps:

   - receiving from a first (21) of the plurality of RHs, a measure of an error of one or more symbols of a signal received by the first RH from the IRU over a first of the plurality of metallic conductors, the measure of the error being detected by the first RH, the signal being destined to a UE (60), wirelessly connected to the first RH (21),

- determining precoding coefficients for a pre-coder of the IRU according to the received error measure, and

- triggering applying the determined precoding coefficients when sending further signals to the first RH over the first of the plurality of metallic conductors, the further signals being destined to UEs wirelessly connected to the first RH.

16. A carrier containing the computer program (605) according to claim 15, wherein the carrier is one of an electronic signal, optical signal, radio signal or computer readable storage medium.

17. A computer program (805) comprising computer readable code means to be run in a first RH (21) operable in a base station system (100) of a wireless communication network, the base station system comprising an IRU (10), a BBU (30) connected to the IRU, and a plurality of RHs (21-26) including the first RH, the plurality of RHs being connected to the IRU via a plurality of metallic conductors, which computer readable code means when run in the first RH causes the first RH (21) to perform the following steps:

- receiving, from the IRU over a first of the plurality of metallic conductors, a signal destined to a UE wirelessly connected to the first RH, the signal comprising one or more symbols;

- detecting, from the received one or more symbol, a measure of an error of the one or more symbol;

- sending, to the IRU, the measure of the one or more symbol error, for further updating of precoding coefficients for a pre-coder of the IRU based on the received measure of symbol error.

18. A carrier containing the computer program (805) according to claim 17, wherein the carrier is one of an electronic signal, optical signal, radio signal or computer readable storage medium.

References

[1] J. Gambini and U. Spagnolini, "Wireless over Cable for Femtocell Systems," in *IEEE Communications Magazine*, vol. 51, no. 5, pp. 178-185, May 2013.

[2] C. Lu, M. Berg, E. Trojer, P.-E. Eriksson, K. Laraqui, O. V. Tidblad, and H. Almeida, "Connecting the dots: small cells shape up for high-performance indoor radio," *Ericsson Review*, vol. 91, pp. 38-45, December 2014.

[3] Y. Huang, E. Medeiros, S. Höst, T. Magesacher, P.-E. Eriksson, C. Lu, P. Ödling, and P. O. Börjesson, "Enabling DSL and Radio on the Same Copper Pair," in *Proc. 2015 IEEE International Conference on Communications (ICC)*, London, U.K., June 2015, pp. 1031-1035.

[4] Y. Huang, E. Medeiros, N. Fonseca, S. Höst, T. Magesacher, P.-E. Eriksson, C. Lu, P. Ödling, and P. O. Börjesson, "LTE over Copper – Potential and Limitations," in *Proc. IEEE 26th Annual International Symposium on Personal, Indoor and Mobile Radio Communications (PIMRC)*, Hong Kong, China, September 2015, pp. 1339-1343.

[5] G. Ginis and J. Cioffi, "Vectored Transmission for Digital Subscriber Line Systems," in *IEEE Journal on Selected Areas in Communications*, vol, 20, no. 5, pp. 1085-1104, June 2002.

[6] R. Cendrillon, G. Ginis, E. Van den Bogaert, and M. Moonen, "A Near-Optimal Linear Crosstalk Precoder for Downstream VDSL," in *IEEE Transactions on Communications*, vol. 55, no. 5, pp. 860-863, May 2007.

[7] ITU, "Self-FEXT cancellation (vectoring) for use with VDSL2 transceivers," Recommendation ITU-T G.993.5, April 2010. [Online]. Available: https://www.itu.int/rec/T-REC-G.993.5/en

[8] ITU, "Fast Access to Subscriber Terminals (G.fast)- Physical Layer Specification," Recommendation Draft ITU-T G.9701, 2014. [Online]. Available: https://www.itu.int/rec/T-REC-G.9701/en

[9] 3GPP, "Evolved Universal Terrestrial Radio Access (E-UTRA); Physical channels and modulation," 3rd Generation Partnership Project (3GPP), TS 36.211 V12.7.0, October 2015.

[10] Alcatel-Lucent Bell, "G.vdsl: On the Tracking Speed Required for Changing Crosstalk Channels," ITU-T SG15 Contribution, May 2007. [Online]. Available: https://www.itu.int/md/T05-SG15-C-0540

[11] S. Schwarz, J. C. Ikuno, M. Šimko, M. Taranetz, Q. Wang, and M. Rupp, "Pushing the Limits of LTE: A Survey on Research Enhancing the Standard," in *IEEE Access*, vol. 1, no. , pp. 51-62, 2013.

[12] Ericsson AB, *Access Network Pair Cable, TEL 312*, 2010. [Online]. Available: http://goo.gl/4RdCXc

[13] 3GPP, "Evolved Universal Terrestrial Radio Access (E-UTRA); Base Station (BS) radio transmission and reception," 3rd Generation Partnership Project (3GPP), TS 36.104 V12.8.0, July 2015.

Paper VI

6 Time-Domain Precoding for LTE-over-Copper Systems

Abstract

Crosstalk cancellation is a crucial issue for traditional digital subscriber line systems. For LTE-over-copper systems, however, the need for crosstalk cancellation varies depending on the analog fronthauling architecture and its parameters. A crosstalk handler that is decoupled as much as possible from the rest of the system architecture is thus preferred. Therefore, we propose a time-domain precoding scheme specifically in downstream direction to separate the precoding unit from the LTE signal flow, and perform crosstalk cancellation in an on-demand manner. Estimation of all direct and crosstalk paths is assisted by LTE cell-specific reference signals. The time-domain precoder transforms the interference channel into a crosstalk-free channel with identical direct paths, which allows for low-complexity inter-symbol interference mitigation. We evaluate the concept in terms of signal-to-noise ratio provided for LTE signals using measured wireline channel data.

6.1   Introduction

Small cells are promoted as an important enabler for high capacity indoor radio. However, fronthauling and backhauling that connect small cells to the core network turn out to be challenging due to the deploying locations and set-up cost per user. Reusing fixed broadband networks in this regard can be an economic solution to achieve the small cell densification.

In [1], a femto-wireless-over-cable architecture is proposed to reuse cable infrastructure for femtocell deployment. It cascades cable and air channels together to implement compound MIMO processing, which requires mobile end-users to be aware of the cable related architecture. In [2], the macro network extension and densification are combined together with specific indoor small-cell solutions fronthauling through LAN cables. Our previous work [3, 4] considers a longer deploying distance—up to 300 meters from the street cabinet to the customer premises with existing telephone wires, in which case the coexistence of LTE analog fronthaul and digital subscriber line (DSL) systems is investigated.

A challenge of using the existing unshielded copper-based infrastructure is the crosstalk from the neighboring pairs due to electromagnetic coupling (as illustrated in Fig. 6.1). To make the infrastructure between remote radio unit (RRU) and remote radio head (RRH) transparent to mobile end-users, crosstalk cancellation should be employed if the interference is noticeable. In the prevailing DSL systems such as VDSL2 [5], vectoring [6] is implemented to mitigate crosstalk. It applies precoding in downstream and joint equalization in upstream, where the channel estimation and crosstalk cancellation techniques are typically implemented in frequency domain.

Compared to the air channel, the copper-pair channel is more stable in time
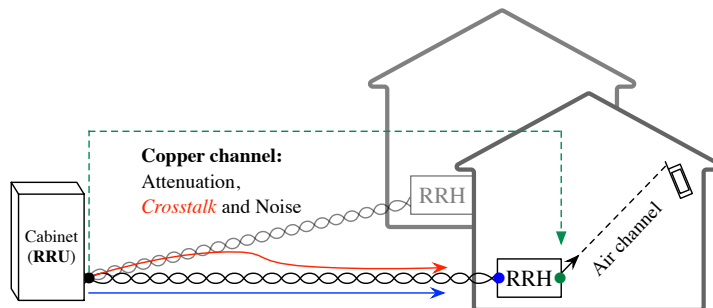
Fig. 6.1: Systematic sketch of LTE-over-copper in the downstream direction.

and has much higher signal-to-noise ratio (SNR). Crosstalk which was harmful to DSL signals may not be detrimental to LTE signals, as the latter are designed to cope with more severe impairments in the air channel. Depending on the cable quality, the frequency band used over copper, and the processing components inside the RRH, the need for crosstalk cancellation in LTE-over-copper (LoC) systems varies. The involved crosstalk cancellation unit should be more flexible in the sense that it can be easily turned off/on without noticeably interrupting the original LTE signal flow. Moreover, the generated LTE signal from the RRU is typically a time-domain signal, and thus implementing crosstalk cancellation also in time domain is an appealing solution.

In [7], a time-domain precoding method is proposed for DSL systems based on fractionally-spaced filtering. It performs SNR-based coupling estimation and parameter-based multi-filter updating. Since it concerns a scenario with several DSL access multiplexers (DSLAMs), the algorithm complexity becomes unnecessarily high for our case.

In this work, we focus on far-end crosstalk (FEXT) pre-cancellation between copper pairs sharing the same cable binder and connecting to the same RRU for LoC systems. The proposed precoding unit operates in parallel to the original LTE signal flow as interpreted in Section 6.2. A channel impulse response (CIR) estimation method for all direct and FEXT paths is proposed in Section 6.3 by taking advantage of LTE cell-specific reference signals (CRSs). Time-domain precoding for crosstalk cancellation and inter-symbol interference (ISI) mitigation is presented and analyzed in Section 6.4.

6.2 Precoding Architecture

At the RRU side, signals are loaded on copper pairs with adequate transmit power for distant copper transmission. We consider a transmit power spectrum density (PSD) of $P_{tx} = -60\,\mathrm{dBm/Hz}$ and a background noise PSD of $N_{bg} = -140\,\mathrm{dBm/Hz}$, which result in an initial transmit $\mathrm{SNR}_{init} = 80\,\mathrm{dB}$. At the antenna connector of the RRH (*i.e.,* the right-hand-side of the RRH in Fig. 6.1), a minimum error vector magnitude (EVM) requirement for LTE signals should be achieved as discussed in [4]. Translating into SNR values, it demands around $\mathrm{SNR}_{target} = 15.14\,\mathrm{dB}$ for QPSK, $\mathrm{SNR}_{target} = 18.06\,\mathrm{dB}$ for 16-QAM, and $\mathrm{SNR}_{target} = 21.98\,\mathrm{dB}$ for 64-QAM. From $80\,\mathrm{dB}$ on one end to around $20\,\mathrm{dB}$ on the other end, a large SNR margin is available for the copper transmission and the implementation of the RRH.

If the SNR degradation due to FEXT over copper pairs stays within this SNR margin, we say this FEXT is tolerable and no extra effort for crosstalk cancellation is needed. Otherwise, a precoder should be involved at the RRU side.

The tolerable FEXT magnitude depends on, among other factors, the cable type, the frequency band where LTE signals are loaded, and the SNR-impacting components within the RRH. While the cable type and applied frequency determine the insertion loss of direct paths (denoted by C_{dir}), the components inside the RRH yield an overall noise figure value (denoted by NF). Consider that K RRHs share the same cable binder. To reach a certain $\mathrm{SNR_{target}}$ for the EVM requirement, the average tolerable FEXT magnitude C_{fext} from each involved pair can be estimated as

$$C_{\mathrm{fext}}/\mathrm{pair} = \frac{1}{K-1} \left(\frac{C_{\mathrm{dir}}}{\mathrm{SNR_{target}} \cdot NF} - \frac{1}{\mathrm{SNR_{init}}} \right), \qquad (6.1)$$

by counting every variable in linear scale. The impact of different variables in Eq. (6.1) on the tolerable FEXT is illustrated in Fig. 6.2. For example for $K = 4$, if the RRH generates $NF = 0\,\mathrm{dB}$ and the direct channel insertion loss C_{dir} is around $-25\,\mathrm{dB}$, no precoding is needed as long as the average FEXT from neighboring pairs is below $-50\,\mathrm{dB}$. The tolerable value per pair reduces for a larger group size (*e.g.,* $K = 8$), which is equivalent to having more interfering sources. A noisier RRH environment with higher NF value also lowers the tolerable FEXT level as the SNR margin left for copper transmission shrinks. Thus, the need for crosstalk cancellation varies.

Since the RRU delivers LTE signals in time domain, we propose a time-domain precoding scheme for LoC systems as illustrated in Fig. 6.3. Pre-compensated signals are generated by the precoder and added directly to LTE signals. Because the precoding unit is parallel to the signal path, it can be easily turned off/on based on demand without unnecessarily interrupting the original LTE signal flow.

6.3 Time-Domain Channel Estimation

When precoding for crosstalk cancellation is necessary, we first need to acquire prior knowledge of CIRs for all direct and FEXT paths. In this work, we propose an error-based CIR estimation assisted by CRSs [8] of the carried LTE signal.

6.3.1 LTE Cell-Specific Reference Signal (CRS) Alignment

The smallest unit of the LTE frame structure is resource element (RE). It represents one OFDM symbol in time on one sub-carrier in frequency (small
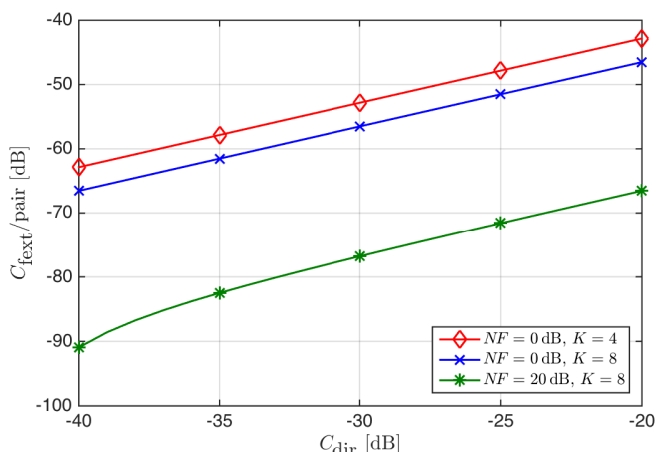
Fig. 6.2: Tolerable FEXT magnitude per copper pair for different system scenarios. $\mathrm{SNR_{target}} = 18.06\,\mathrm{dB}$ for 16-QAM is used as an example. A transmit PSD of $-60\,\mathrm{dBm/Hz}$ and background noise PSD of $-140\,\mathrm{dBm/Hz}$ are assumed for the copper channel.

squares in Fig. 6.4). Along the time axis, 7 OFDM symbols with normal customer premise (CP) compose one slot, 2 slots compose one subframe, and 10 subframes compose one frame. A two-dimensional grid containing 1 slot in time domain and 12 consecutive sub-carriers in frequency domain is termed resource block (RB). A 3 MHz LTE signal, for example, has $N_{\mathrm{rb}} = 15$ RBs corresponding to 180 sub-carriers in every slot.

In each slot there are 2 CRS-containing OFDM symbols, numbered 0 and 4 in Fig. 6.4(a). For symbol-0, there is one reference symbol (black square in Fig. 6.4) on every 6 sub-carriers. On symbol-4, the reference-symbol positions shift by 3 sub-carriers. The following slots use the same CRS mapping scheme, which forms a diamond mapping pattern to capture channel variations in frequency domain. When applied to estimating the copper channel which changes little in time, this kind of mapping pattern approximates to having one pilot on every 3 sub-carriers.

There are 504 different CRS sequences defined for LTE, where each sequence corresponds to one of 504 different physical-layer cell identities. Let $N_{\mathrm{ID}}^{\mathrm{cell}}$ denote a certain cell identity. A cell-specific frequency shift of $[N_{\mathrm{ID}}^{\mathrm{cell}} \bmod 6]$ is applied to determine the reference-symbol positioning on the sub-carriers. Equivalently, there are only 6 possible mapping patterns that jointly cover all 504 different cell identities.
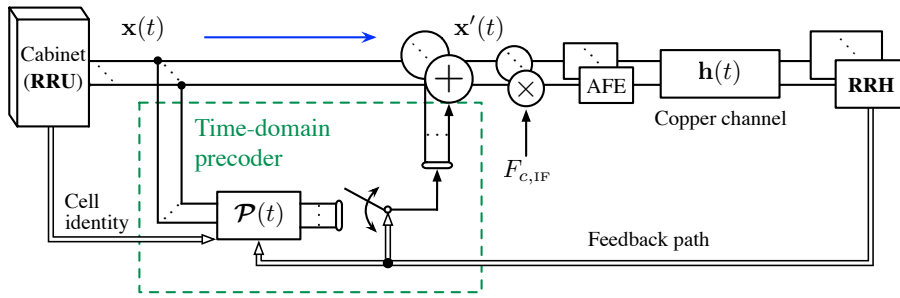
Fig. 6.3: Time-domain precoding architecture for LoC systems. The precoding unit can be easily turned off/on by de-/activating additive time-domain signals without any processing block located in the LTE path.

Accordingly, the baseband unit can control the CRS positioning by assigning a specific cell identity to each RRH/cell. In turn, we are essentially informed of the reference symbols and their mapping pattern contained in the coming LTE signal by knowing its cell identity. For an RRH group sharing the same cable binder, the CRS mappings can be set to be identical (as illustrated in Fig. 6.4(b)) by assigning their cell identities to be an integer multiple of 6 apart. For example, let cell identities be $[2, 8, 14, 26]$ for $K = 4$.

Note that small cells supported by the LoC system have low output power and are deployed in environments with high path-loss (*e.g.,* due to walls). Therefore the above reference signal alignment will not diminish pilot effectiveness due to neighboring cell interference in the air.

6.3.2 Estimation of Copper Channel Impulse Responses (CIRs)

Assume that the precoder knows the cell identities. Consider the case where LTE signals transmitted on a group of K pairs share the same CRS mapping structure. Let $\mathbf{F}_N$ denote an $N \times N$ discrete Fourier transform (DFT) matrix and $\mathbf{F}_L$ is the first L columns of $\mathbf{F}_N$, where N and L denote the DFT size and the CIR length, respectively.

The implication above that $L < N$ is generally valid in our work. To demonstrate this, we use measured frequency-domain channel data to simulate direct and FEXT couplings of a 30-pair, 300-meter, 0.5 mm cable [9] with 15 kHz sub-carrier spacing (same as LTE signals). $K = 4$ pairs are randomly picked from the same binder. The band between 21 MHz and 24 MHz (as suggested in [3]), which can fit a 3 MHz LTE signal, is studied as an example.
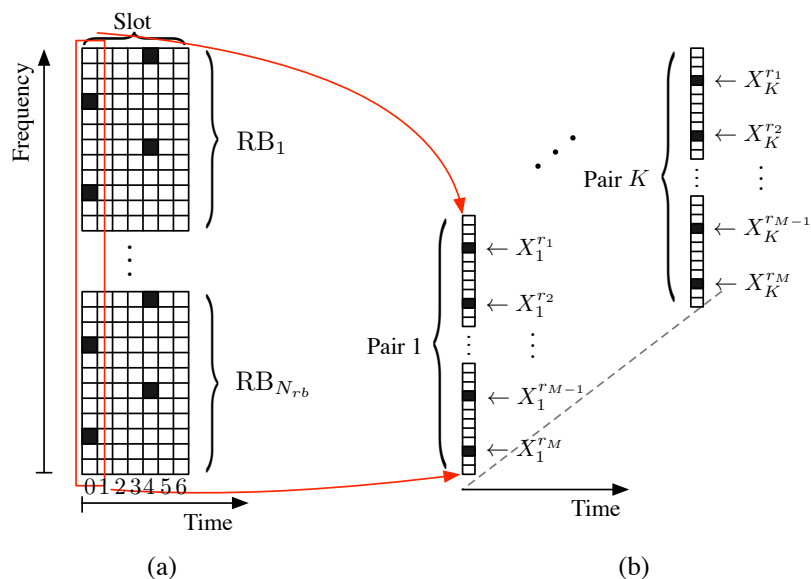
Fig. 6.4: Illustration of CRS-aided channel estimation. Each small square represents one RE. Each black square represents one reference symbol.

Transforming all K^2 measured paths into time domain with $N = 256$, Fig. 6.5 shows that $L = 15$ is the time-domain tap number containing at least 99% CIR power of each path. Thus, we consider a channel spread of $L = 15$ for all K^2 paths in this work.

The channel path from transmitter i to the j-th RRH can be represented by

$$\mathbf{H}_{j,i} = \mathbf{F}_L \mathbf{h}_{j,i},$$

where $\mathbf{H}_{j,i} = \left[H_{j,i}^1, \ldots, H_{j,i}^{r_1}, \ldots, H_{j,i}^{r_M}, \ldots, H_{j,i}^N\right]^{\mathrm{T}}$ (including zero-padding if the number of sub-carriers is smaller than the DFT size N) denotes the frequency-domain channel representation and $\mathbf{h}_{j,i} = [h_{j,i}(0), \ldots, h_{j,i}(L-1)]^{\mathrm{T}}$ denotes the time-domain CIR, respectively. Within one CRS-containing OFDM symbol as exemplified in Fig. 6.4, let $\mathbf{X}_i = [X_i^{r_1}, \ldots, X_i^{r_M}]^{\mathrm{T}}$ denote the reference symbols sent on pair i, where M is the number of reference symbols in one OFDM symbol, and $\mathcal{R} = [r_1, \ldots, r_M]^{\mathrm{T}}$ denotes the set of sub-carrier indices which are loaded with reference symbols. For a group of K RRHs/cells, transmission over copper pairs on a reference-symbol sub-carrier
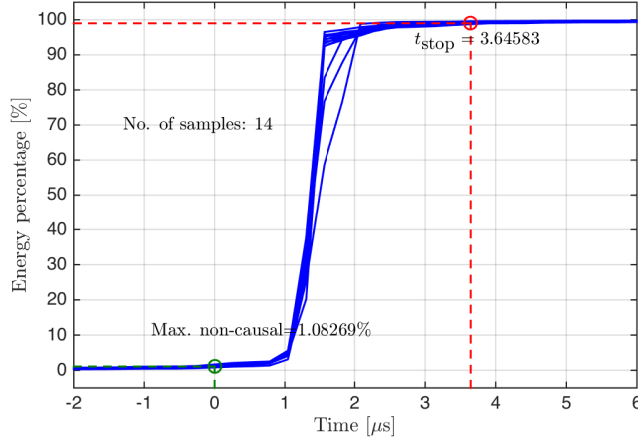
Fig. 6.5: Energy-based time-domain CIR truncation. For the case of $K = 4$, 16 channel paths are plotted. t_{stop} marks the time stamp for the channel spread that contains at least 99% CIR power of each path.

r_i can be modeled as

$$
\underbrace{\begin{bmatrix} Y_1^{r_i} \\ \vdots \\ Y_K^{r_i} \end{bmatrix}}_{\mathbf{Y}^{r_i}} = \begin{bmatrix} H_{1,1}^{r_i} & \cdots & H_{1,K}^{r_i} \\ \vdots & \ddots & \vdots \\ H_{K,1}^{r_i} & \cdots & H_{K,K}^{r_i} \end{bmatrix} \begin{bmatrix} X_1^{r_i} \\ \vdots \\ X_K^{r_i} \end{bmatrix} + \mathbf{N}
$$

$$
= \begin{bmatrix} \mathbf{F}_L^{r_i} \mathbf{h}_{1,1} & \cdots & \mathbf{F}_L^{r_i} \mathbf{h}_{1,K} \\ \vdots & \ddots & \vdots \\ \mathbf{F}_L^{r_i} \mathbf{h}_{K,1} & \cdots & \mathbf{F}_L^{r_i} \mathbf{h}_{K,K} \end{bmatrix} \begin{bmatrix} X_1^{r_i} \\ \vdots \\ X_K^{r_i} \end{bmatrix} + \mathbf{N}
$$

$$
= \underbrace{\begin{bmatrix} \mathbf{I}_K \otimes X_1^{r_i} \mathbf{F}_L^{r_i} & \cdots & \mathbf{I}_K \otimes X_K^{r_i} \mathbf{F}_L^{r_i} \end{bmatrix}}_{\mathbf{A}^{r_i}} \underbrace{\begin{bmatrix} \mathbf{h}_{1,1} \\ \vdots \\ \mathbf{h}_{K,1} \\ \vdots \\ \mathbf{h}_{K,K} \end{bmatrix}}_{\mathbf{h}} + \mathbf{N}, \qquad (6.2)
$$

where $\mathbf{F}_L^{r_i}$ denotes the r_i-th row of $\mathbf{F}_L$, $\mathbf{N}$ denotes the background noise, $\mathbf{I}_K$ denotes a $K \times K$ identity matrix, $\otimes$ denotes Kronecker product, and $\mathbf{Y}^{r_i}$

denotes the receive symbols on subcarrier r_i at the RRH side.

Observe in Eq. (6.2) that the unknown vector $\mathbf{h}$ is frequency independent, which connects the reference-symbol-containing matrix $\mathbf{A}^{r_i}$ to the receive signal $\mathbf{Y}^{r_i}$ on each reference-symbol sub-carrier r_i. Stacking and interleaving all the information collected from the M reference-symbol sub-carriers yield

$$\underbrace{\begin{bmatrix}\mathbf{Y}_1^\mathrm{T} & \cdots & \mathbf{Y}_K^\mathrm{T}\end{bmatrix}^\mathrm{T}}_{\mathbf{y}} = \underbrace{\begin{bmatrix}\mathbf{A}_1 & \cdots & \mathbf{A}_K\end{bmatrix}}_{\mathbf{A}}\mathbf{h} + \mathbf{N}, \tag{6.3}$$

where $\mathbf{Y}_i = [Y_i^{r_1}, \ldots, Y_i^{r_M}]^\mathrm{T}$ and

$$\mathbf{A}_i = \mathbf{I}_K \otimes \begin{bmatrix} X_i^{r_1}\mathbf{F}_L^{r_1} \\ \vdots \\ X_i^{r_M}\mathbf{F}_L^{r_M} \end{bmatrix}.$$

To make the rank of $\mathbf{A}$ in Eq. (6.3) equal the dimension of its column space and also to average out the noise influence, we extend $\mathbf{y}$ and $\mathbf{A}$ in Eq. (6.3) vertically by stacking more $\mathbf{Y}_i$ and $\mathbf{A}_i$ from the following CRS-containing OFDM symbols yielding $\bar{\mathbf{y}}$ and $\bar{\mathbf{A}}$. The K^2 CIRs, which are vertically stacked in one column vector $\mathbf{h}$ can be estimated by

$$\widehat{\mathbf{h}} = \left(\bar{\mathbf{A}}^\mathrm{H}\bar{\mathbf{A}}\right)^{-1}\bar{\mathbf{A}}^\mathrm{H}\bar{\mathbf{y}}. \tag{6.4}$$

Since the CRS related matrix $\bar{\mathbf{A}}$ in Eq. (6.4) can be directly generated from the corresponding cell identities and $\bar{\mathbf{y}}$ is fed back from RRHs, the whole estimation process can be accomplished without interrupting the LTE signal flow.

6.4   Time-Domain Precoding

The proposed time-domain precoder includes two functional parts: crosstalk cancellation and ISI mitigation.

6.4.1   Crosstalk Cancellation

With the estimated $\widehat{\mathbf{h}}$ in Eq. (6.4), we can reconstruct it into the direct-and-FEXT-path format as

$$\mathcal{H} = \begin{bmatrix} \widehat{\mathbf{h}}_{1,1} & \cdots & \widehat{\mathbf{h}}_{1,K} \\ \vdots & \ddots & \vdots \\ \widehat{\mathbf{h}}_{K,1} & \cdots & \widehat{\mathbf{h}}_{K,K} \end{bmatrix},$$

where each entry $\widehat{\mathbf{h}}_{j,i}$ denotes a length-L time-domain impulse response from the i-th transmitter to the j-th RRH. In this case, $\boldsymbol{\mathcal{H}}$ is essentially a three-dimensional matrix.

Similar to the normal two-dimensional matrix case, it is shown in [10] that the following relation exists for $\boldsymbol{\mathcal{H}}$:

$$\boldsymbol{\mathcal{H}} * \mathrm{adj}(\boldsymbol{\mathcal{H}}) = \det(\boldsymbol{\mathcal{H}}) * \boldsymbol{\mathcal{I}}, \tag{6.5}$$

where $*$ denotes the convolutional operator and $\boldsymbol{\mathcal{I}}$ is a diagonal matrix with each diagonal entry being a Dirac delta function $\boldsymbol{\delta}$. Similar to the Leibniz formula for the determinant of a two-dimensional matrix, $\det(\boldsymbol{\mathcal{H}})$ in Eq. (6.5) is defined by

$$\det(\boldsymbol{\mathcal{H}}) = \sum_{\sigma \in S_K} \mathrm{sgn}(\sigma) \prod_{i=1}^{K}{}^{*} \mathbf{h}_{i,\sigma_i},$$

where $\overset{*}{\prod}$ denotes a series of convolution instead of multiplication, σ is one permutation vector out of the permutation group S_K, and $\mathrm{sgn}(\sigma)$ is the signature of σ that calculates the determinant of corresponding permutation matrix. The permutation group S_K contains all possible permutations of $[1, \ldots, K]$. Each entry of the adjoint matrix is defined accordingly as

$$[\mathrm{adj}(\boldsymbol{\mathcal{H}})]_{i,j} = (-1)^{i+j} \det\left(\boldsymbol{\mathcal{H}}_{(j,i)}\right), \tag{6.6}$$

where $\boldsymbol{\mathcal{H}}_{(j,i)}$ denotes the (j, i) minor of $\boldsymbol{\mathcal{H}}$ that deletes j-th row and i-th column from $\boldsymbol{\mathcal{H}}$.

Assign the time-domain diagonalizing precoder to be $\boldsymbol{\mathcal{P}}_{\mathrm{D}} = \mathrm{adj}(\boldsymbol{\mathcal{H}})$. Disregarding the transmit power limitation for now, the receive signal in time domain becomes

$$\begin{aligned}
\boldsymbol{\mathcal{Y}} &= \boldsymbol{\mathcal{H}} * \boldsymbol{\mathcal{P}}_{\mathrm{D}} * \boldsymbol{\mathcal{X}} + \boldsymbol{\mathcal{N}} \\
&= \det(\boldsymbol{\mathcal{H}}) * \boldsymbol{\mathcal{I}} * \boldsymbol{\mathcal{X}} + \boldsymbol{\mathcal{N}},
\end{aligned} \tag{6.7}$$

where $\boldsymbol{\mathcal{X}} = [\mathbf{x}_1, \ldots, \mathbf{x}_K]^{\mathrm{T}}$, and $\mathbf{x}_i$ denotes the time-domain LTE signal transmitted on pair i. The receive signal $\boldsymbol{\mathcal{Y}} = [\mathbf{y}_1, \ldots, \mathbf{y}_K]^{\mathrm{T}}$ and background noise $\boldsymbol{\mathcal{N}}$ are defined similarly.

Note that $\det(\boldsymbol{\mathcal{H}})$ in Eq. (6.7) is *one* CIR with length $KL - (K - 1)$. The term $\det(\boldsymbol{\mathcal{H}}) * \boldsymbol{\mathcal{I}}$ implies that the effective channel after precoding has *identical* CIR on every direct path, while FEXT is zeroed out. The $\boldsymbol{\mathcal{P}}_{\mathrm{D}}$ implemented to generate results in Fig. 6.6 is constructed based on the estimated CIRs using Eq. (6.4) with 10 slots of CRS. It is observed that the effective direct CIRs (see black circle-marked lines in Fig. 6.6) are identical and the FEXT paths (blue square-marked lines) are effectively suppressed to much lower power levels compared to the original FEXT paths (red triangle-marked lines).
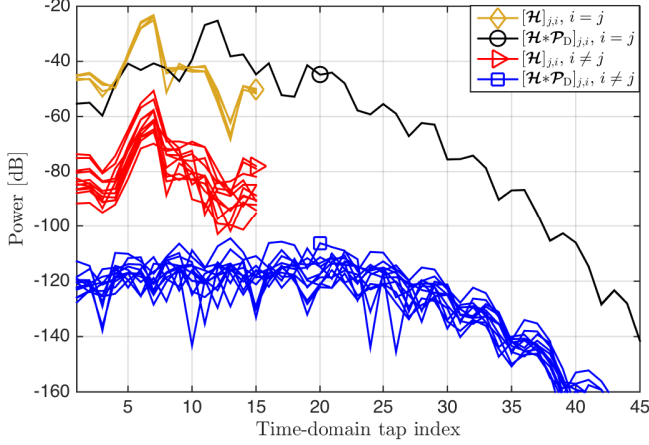
Fig. 6.6: Equivalent CIRs before and after performing the time-domain diagonalizing precoding. A delay of $\Delta = 13$ taps is considered after precoding. Matrix entries with $i = j$ indicate direct paths, while entries with $i \neq j$ indicate FEXT paths.

6.4.2   Inter-Symbol Interference (ISI) Mitigation

One outcome of the precoding scheme in Section 6.4.1 is that the direct channel spread is extended from L to $KL - (K - 1)$ (also shown in Fig. 6.6 when comparing the yellow diamond-marked lines to the black circle-marked lines). The short version of LTE CP duration is $4.6875\,\mu s$, whereas 90% of indoor delay spread is below $500\,ns$ (see Table 5 in [11]). It implies that at least 85% of the LTE CP length can be consumed by the transmission over copper pairs. If the effective copper channel spread after applying $\mathcal{P}_{\mathrm{D}}$ is longer than this CP portion, it is worthwhile introducing further spread-confining filters in the precoder to mitigate ISI.

As the time-domain channel representation is a finite impulse response (FIR), full equalization aiming for a Dirac delta function will require an infinite impulse response (IIR) filter. In practice, we compromise by only confining the direct channel spread to be shorter than the reserved CP length for copper transmission. In [12], an optimal shortening filter is proposed which maximizes the shortening SNR (SSNR). Since all K direct paths are the same after applying $\mathcal{P}_{\mathrm{D}}$, it is sufficient to design a single shortening filter.

Let $\mathbf{w}$ denote the impulse response shortening (IRS) filter with length L_{IRSF}. Let $\mathbf{H}_{\mathrm{conv}}$ denote the convolutional matrix of $\det(\mathcal{H})$ and let $\mathbf{h}_{\mathrm{prec}}$ denote the effective direct CIR after implementing the complete time-domain precoding,

i.e.,

$$\mathbf{h}_{\mathrm{prec}} = \det(\boldsymbol{\mathcal{H}}) * \mathbf{w} = \mathbf{H}_{\mathrm{conv}} \mathbf{w}.$$

With a certain amount of delay Δ considered and a shortened CIR length of L_{target} targeted, the objective part of $\mathbf{h}_{\mathrm{prec}}$ that has effective CIR values is given by

$$\mathbf{h}_{\mathrm{eff}} = \mathbf{Z}_{\mathrm{eff}} \mathbf{h}_{\mathrm{prec}} = \mathbf{H}_{\mathrm{eff}} \mathbf{w},$$

where $\mathbf{H}_{\mathrm{eff}} = \mathbf{Z}_{\mathrm{eff}} \mathbf{H}_{\mathrm{conv}}$ and

$$\mathbf{Z}_{\mathrm{eff}} = \begin{bmatrix} \mathbf{0}_{L_{\mathrm{target}} \times (\Delta - 1)} & \mathbf{I}_{L_{\mathrm{target}}} & \mathbf{0}_{L_{\mathrm{target}} \times (KL - K + L_{\mathrm{IRSF}} - L_{\mathrm{target}} - \Delta + 1)} \end{bmatrix}$$

is a matrix that picks the rows $\mathcal{T} = [\Delta, \ldots, \Delta + L_{\mathrm{target}} - 1]$ from a matrix/vector. Similarly, the rest of $\mathbf{h}_{\mathrm{prec}}$ is denoted by

$$\mathbf{h}_{\mathrm{rest}} = \mathbf{Z}_{\mathrm{rest}} \mathbf{h}_{\mathrm{prec}} = \mathbf{H}_{\mathrm{rest}} \mathbf{w},$$

where $\mathbf{H}_{\mathrm{rest}} = \mathbf{Z}_{\mathrm{rest}} \mathbf{H}_{\mathrm{conv}}$ and $\mathbf{Z}_{\mathrm{rest}}$ picks the rows $[1, \ldots, KL - K + L_{\mathrm{IRSF}}] \backslash \mathcal{T}$ from a matrix/vector. Accordingly, the energy inside and outside the chunk of interest is formulated respectively as

$$\mathbf{h}_{\mathrm{eff}}^{\mathrm{H}} \mathbf{h}_{\mathrm{eff}} = \mathbf{w}^{\mathrm{H}} \mathbf{H}_{\mathrm{eff}}^{\mathrm{H}} \mathbf{H}_{\mathrm{eff}} \mathbf{w} = \mathbf{w}^{\mathrm{H}} \mathbf{B} \mathbf{w},$$
$$\mathbf{h}_{\mathrm{rest}}^{\mathrm{H}} \mathbf{h}_{\mathrm{rest}} = \mathbf{w}^{\mathrm{H}} \mathbf{H}_{\mathrm{rest}}^{\mathrm{H}} \mathbf{H}_{\mathrm{rest}} \mathbf{w} = \mathbf{w}^{\mathrm{H}} \mathbf{C} \mathbf{w},$$

where $\mathbf{B} = \mathbf{H}_{\mathrm{eff}}^{\mathrm{H}} \mathbf{H}_{\mathrm{eff}}$ and $\mathbf{C} = \mathbf{H}_{\mathrm{rest}}^{\mathrm{H}} \mathbf{H}_{\mathrm{rest}}$. Implementing eigen-decomposition as in [12] and summarized in Table 6.1, the optimal IRS filter $\mathbf{w}_{\mathrm{opt}}$ can be obtained in the sense of maximizing the SSNR $= \frac{\mathbf{w}^{\mathrm{H}} \mathbf{B} \mathbf{w}}{\mathbf{w}^{\mathrm{H}} \mathbf{C} \mathbf{w}}$ as

$$\mathbf{w}_{\mathrm{opt}} = \arg \max_{\mathbf{w}} \left[\frac{\mathbf{w}^{\mathrm{H}} \mathbf{B} \mathbf{w}}{\mathbf{w}^{\mathrm{H}} \mathbf{C} \mathbf{w}} \right].$$

The length relation between L_{target} and L_{IRSF} differentiated in Table 6.1 determines the singularity of matrix $\mathbf{B}$.

Fig. 6.7 reveals that there is a trade-off between the time-domain shortening effectiveness and the frequency-domain effective channel gain. A longer shortening filter (*e.g.,* $L_{\mathrm{IRSF}} = 30$, yellow diamond-marked line in Fig. 6.7a) suppresses the channel spread outside L_{target} to a much lower level compared to a shorter filter (*e.g.,* $L_{\mathrm{IRSF}} = 10$, blue star-marked line). The counterparts in frequency domain in Fig. 6.7b show that the effective channel using a shorter filter (*e.g.,* $L_{\mathrm{IRSF}} = 10$) has a higher channel gain over the 3 MHz bandwidth compared to that of a longer filter (*e.g.,* $L_{\mathrm{IRSF}} = 30$). Since the time-domain spread affects the ISI and the frequency-domain effective channel gain affects the receive signal power, using a longer L_{IRSF} does not necessarily result in a higher receive SNR. The effect of this trade-off is illustrated in terms of SNR in the next subsection.

Table 6.1: Maximum SSNR shortening impulse response filter

	$L_{\text{target}} >= L_{\text{IRSF}}$	$L_{\text{target}} < L_{\text{IRSF}}$
Eigen-decomp.	$\mathbf{B} = \mathbf{Q}\boldsymbol{\Sigma}\mathbf{Q}^{\text{H}}$	$\mathbf{B} = \begin{bmatrix} \mathbf{U} & \mathbf{V} \end{bmatrix} \begin{bmatrix} \boldsymbol{\Sigma} & \mathbf{0} \\ \mathbf{0} & \mathbf{0} \end{bmatrix} \begin{bmatrix} \mathbf{U}^{\text{H}} \\ \mathbf{V}^{\text{H}} \end{bmatrix}$
$\mathbf{D}$	$(\sqrt{\mathbf{B}})^{-1}\mathbf{C}(\sqrt{\mathbf{B}}^{\text{H}})^{-1}$	$(\boldsymbol{\Lambda}^{\text{H}} - \boldsymbol{\Lambda}^{\text{H}}\mathbf{O}^{\text{H}})\mathbf{C}(\boldsymbol{\Lambda} - \mathbf{O}\boldsymbol{\Lambda})$ for $\mathbf{O} = \mathbf{V}(\mathbf{V}^{\text{H}}\mathbf{C}\mathbf{V})^{-1}\mathbf{V}^{\text{H}}\mathbf{C}$, and $\boldsymbol{\Lambda} = \mathbf{U}(\sqrt{\boldsymbol{\Sigma}})^{-1}$.
$\mathbf{q}_{\min}$	Eigenvector of the minimum eigenvalue $\lambda_{\min}$ of $\mathbf{D}$.	
$\mathbf{w}_{\text{opt}}$	$(\sqrt{\mathbf{B}})^{-1}\mathbf{q}_{\min}$	$(\mathbf{I} - \mathbf{O})\boldsymbol{\Lambda}\mathbf{q}_{\min}$

In summary, the time-domain precoder is formulated as

$$\boldsymbol{\mathcal{P}} = \mu \cdot \text{adj}(\boldsymbol{\mathcal{H}}) * \mathbf{w}', \qquad (6.8)$$

where $\text{adj}(\boldsymbol{\mathcal{H}})$ diagonalizes the interference channel as defined in Eq. (6.6). $\mathbf{w}' = \mathbf{w}_{\text{opt}}$ is the filter given by Table 6.1 if the direct CIR shortening is needed; otherwise $\mathbf{w}' = \boldsymbol{\delta}$. The power normalization factor μ that constrains the transmit power is defined as

$$\mu = \frac{1}{\max\limits_{i \in [1,...,K]} \sum_{j=1}^{K} \left\| [\text{adj}(\boldsymbol{\mathcal{H}}) * \mathbf{w}']_{i,j} \right\|_2}.$$

6.4.3   Precoding Simulation Results

In Fig. 6.8, the average receive SNR is calculated over a 3 MHz band. The carrier frequency of each band is shifted from 22.5 MHz (referring to a band 21 MHz–24 MHz) to 58.5 MHz (referring to a band 57 MHz–60 MHz) to study the impact of different channel characteristics. A flat transmit PSD of −60 dBm/Hz is applied and a copper channel background noise PSD of −140 dBm/Hz is assumed. The data symbols are 16-QAM modulated as an example.

The single-user performance is calculated as a reference using only the direct-path measurements. No crosstalk and transmit power constraint is considered. It can be viewed as an ideal situation after precoding. For the single-user and the crosstalk-corrupted performances in Fig. 6.8, average and worst
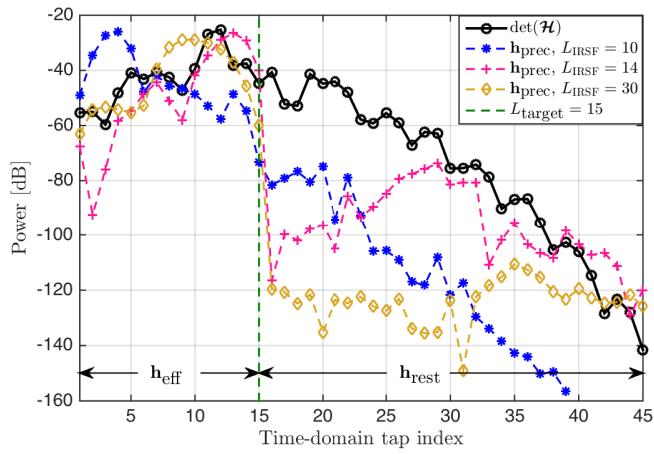
(a) Time-domain channel representation.
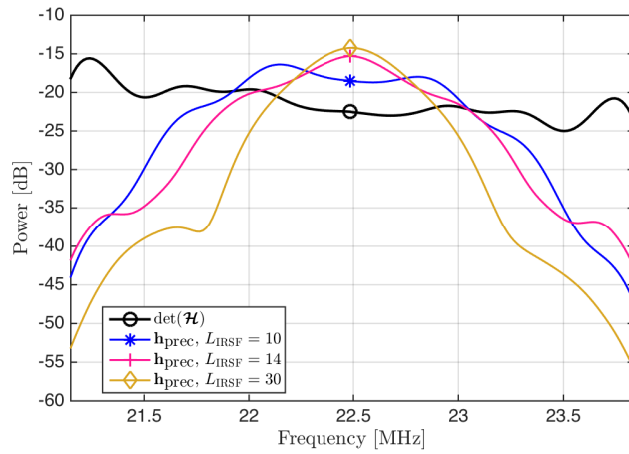
(b) Frequency-domain channel representation.

Fig. 6.7: Direct channel IRS for $L_{\text{target}} = 15$, considering channel measurements between 21 MHz and 24 MHz. A delay of $\Delta = 13$ taps is considered after precoding.
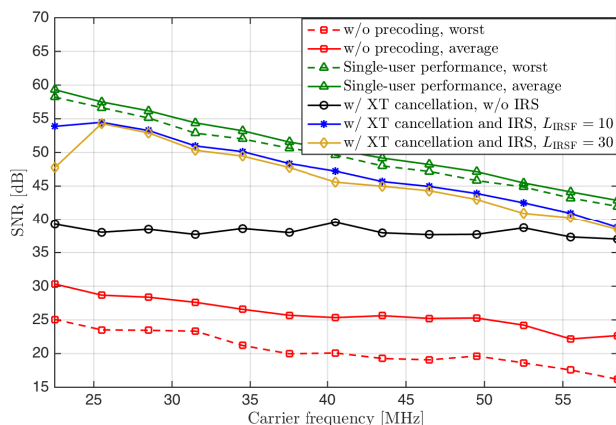
Fig. 6.8: Receive SNR comparison at the copper and RRH connecting point.

situations are presented, respectively. For the other lines that have the time-domain crosstalk cancellation (as in Section 6.4.1) implemented, the receive SNR for one RRH is presented since we show in Fig. 6.6 that the crosstalk is effectively suppressed and the direct paths are identical.

Whether or not the IRS filter should be added is also implementation dependent. If the SNR result without IRS (*e.g.,* the black circle-marked line in Fig. 6.8) is already acceptable, there is no need to add the IRS filter which changes the shape of the frequency-domain equivalent channel as shown in Fig. 6.7b and may increase the complexity of the frequency-domain equalizer. Especially when considering a higher frequency range where the direct coupling magnitude decreases, the SNR difference among the single-user performance, the precoded performances with and without IRS becomes much smaller.

6.5   Conclusion

Time-domain crosstalk cancellation provides more flexibility and is less intrusive than traditional vectoring for LTE-over-copper (LoC) systems. The proposed approach exploits LTE reference signals to estimate the copper channel, cancels crosstalk, and yields effective direct paths that are identical for all pairs. The latter enables low-complexity channel shortening in case the desired receive SNR at the RRH side is not achieved because of the direct channel spread. Simulation results with measured copper channel data confirm that

the precoder performance is close to the single-user bound.

References

[1] J. Gambini and U. Spagnolini, "Wireless over Cable for Femtocell Systems," in *IEEE Communications Magazine*, pp. 716-720, vol. 51, no. 5, pp. 178-185, May 2013.

[2] C. Lu, M. Berg, E. Trojer, P.-E. Eriksson, K. Laraqui. O. V. Tidblad, and H. Almeida, "Connecting the dots: small cells shape up for high-performance indoor radio," *Ericsson Review*, vol. 91, December 2014. [Online]. Available: http://goo.gl/YvdY5N

[3] Y. Huang, E. Medeiros, S. Höst, T. Magesacher, P.-E. Eriksson, C. Lu, P. Ödling, and P. O. Börjesson, "Enabling DSL and Radio on the Same Copper Pair," in *Proc. 2015 IEEE International Conference on Communications (ICC)*, pp. 1031-1035, June 2015.

[4] Y. Huang, E. Medeiros, N. Fonseca, S. Höst, T. Magesacher, P.-E. Eriksson, C. Lu, P. Ödling, and P. O. Börjesson, "LTE over Copper – Potential and Limitations," in *Proc. IEEE 26th Annual International Symposium on Personal, Indoor and Mobile Radio Communications (PIMRC)*, August 2015.

[5] ITU, "Very high speed digital subscriber line transceivers 2 (VDSL2)," Recommendation ITU-T G.993.2, December 2011. [Online]. Available: https://www.itu.int/rec/T-REC-G.993.2-201112-I/en

[6] G. Ginis and J. Cioffi, "Vectored Transmission for Digital Subscriber Line Systems," *IEEE Journal on Selected Areas in Communications*, vol, 20, no. 5, pp. 1085-1104, June 2002.

[7] F. A. Mruck, C. Stierstorfer, J. B. Huber, and R. Tzschoppe, "Time-Domain MIMO Precoding for FEXT Cancellation in DSL Systems," in *Proc. 2013 17th International ITG Workshop on Smart Antennas (WSA)*, pp. 1-7, March 2013.

[8] 3GPP, "LTE; Evolved Universal Terrestrial Radio Access (E-UTRA); Physical channels and modulation," 3rd Generation Partnership Project (3GPP), TS 36.211 V12.6.0, July 2015. [Online]. Available: http://goo.gl/jepG09

[9] Ericsson AB, *Access Network Pair Cable, TEL 312*, 2010. [Online]. Available: http://goo.gl/4RdCXc

[10] E. Auger, B. Rankov, M. Kuhn, and A. Wittneben, "Time Domain Precoding for MIMO-OFDM Systems," in *10th International OFDM-Workshop*, August 2005.

[11] ITU-R, Propagation data and prediction methods for the planning of indoor radiocommunication systems and radio local area networks in the frequency range 300 MHz to 100 GHz, International Telecommunication Union (ITU), Recommendation P.1238-8, July 2015. [Online]. Available: https://goo.gl/UG1HmB

[12] P. Melsa, R. Younce, and C. Rohrs, "Impulse Response Shortening for Discrete Multitone Transceivers," in *IEEE Transactions on Communications*, vol. 44, no. 12, pp. 1662-1672, December 1996.

Paper VII

7 Massive MIMO Functional Split for Fronthaul Load Reduction

Abstract

The evolution towards centralized radio access network (C-RAN) for 5G is driven by the need for improved network performance and reduced total-cost-of-ownership (TCO). In C-RAN, physically separated remote radio units (RRUs) and baseband units (BBUs) are connected via fronthaul (FH) links, which are capacity constrained. When base-station antennas are upgraded to support massive MIMO techniques, an intra PHY split between RRU and BBU becomes favorable to avoid the dramatic rate growth on the FH links. In this paper, we present a new uplink functional split alternative that decomposes the massive MIMO processing, on the basis of zero-forcing (ZF) equalization, into two phases: dimension-reduction phase and interference cancellation phase, which are implemented in RRU and BBU respectively. Compared with the traditional C-RAN architecture having all baseband processing in the BBU, the new scheme largely alleviates the FH load by reducing the number of FH streams to be equal to the number of MIMO user layers. Compared with an existing split that places all MIMO processing in RRU, the new scheme reduces the RRU complexity without compromising the post-processing performances.

7.1 Introduction

In centralized radio access network (C-RAN) deployment, remote radio units (RRUs) are located close to the antennas, performing radio frequency (RF) to baseband conversion, while baseband units (BBUs) are centralized, carrying out baseband (*i.e.,* PHY, MAC and upper layers on the radio protocol stack) processing. This arrangement enhances network capacity and improves user experiences by applying advanced radio coordination features [1], as well as reduces the total-cost-of-ownership (TCO) by pooling the BBU baseband resources. The connection between RRUs and the centralized BBUs is referred to as fronthaul (FH), in comparison with backhaul from BBU towards core network. In the current setup, the digitized time-domain samples of each antenna-carrier are transported over FH links between RRU and BBU, typically applying the common public radio interface (CPRI) protocol [2], as sketched in Fig. 7.1a. Such a CPRI-type of FH is also referred to as PHY-RF split [3].

In the continued 4G evolution and 5G, massive MIMO [4] is a key radio feature to significantly improve spectral efficiency and network capacity by providing high beamforming gain and supporting multi-user MIMO (MU-MIMO) [5]. However, fronthauling the signals of such a large number of antennas (*e.g.,* 64, 128, 256 antennas) becomes a major problem for the current CPRI-based C-RAN implementation. The required FH capacity will increase proportionally to the number of antennas [6], which drives up the cost of transport network dramatically. Merely compressing the time-domain samples of each FH stream, such as [7–9], is not sufficient to compensate for the increased FH load due to the extended antenna size. Therefore, reducing the number of FH streams is the key to reduce the FH network cost and increase the system scalability against the number of antennas.

To address this, new functional split options on radio protocol stack have been discussed [10,11]. Among these possibilities, two lower layer options most relevant to C-RAN are the MAC-PHY and intra-PHY splits [3]. The MAC-PHY split (*e.g.,* in [12]), illustrated in Fig. 7.1b, implements the PHY layer in the RRU and centralize the MAC layer operations in BBUs, while the intra PHY split (*e.g.,* in [13–15]) moves only part of the PHY functions to RRU and leaves the rest to the BBUs, as sketched in Fig. 7.1c. The MAC-PHY split reduces the number of FH streams down to the number of scheduled MIMO user layers, which reduces the FH load down to the user throughput level. This split strategy, however, largely increases the complexity in the new RRU design, especially when the computationally intensive massive MIMO processing is considered. It will also limit the coordination gain to the MAC level only, which incapacitates advanced joint processing features like cooperative MIMO

(a) CPRI fronthaul (PHY-RF split)

(b) MAC-PHY split
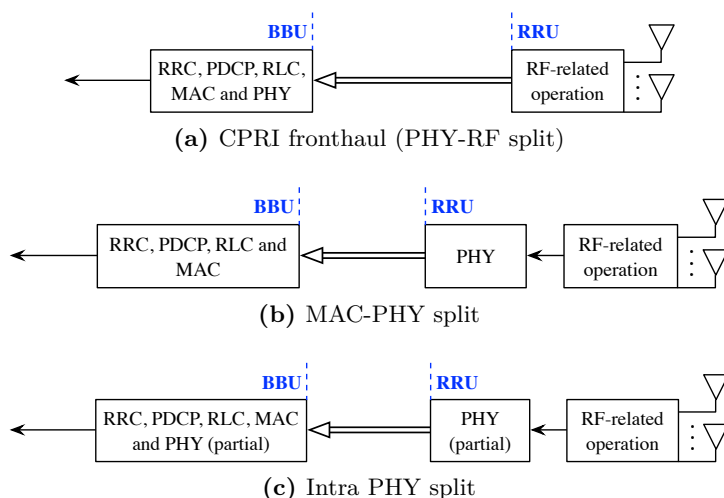
(c) Intra PHY split

Fig. 7.1: System sketch of functional splits regarding the uplink direction.

in PHY for further boosting the networks performance.

In this paper, we focus on the option of intra PHY split and extend the investigation particularly for the zero-forcing (ZF)-based massive MIMO operations in the uplink direction. The problem is formulated to reduce the number of FH streams as much as possible, while keeping the RRU away from high computational processing and still maintaining a system performance similar to today's PHY-RF split. The proposed solution is to decompose the MIMO operations into two phases, which are implemented in RRU and BBU, respectively. The first phase, referred to as *dimension reduction*, is implemented in RRU to reduce the number of spatial streams. The second phase further processes the generated data streams in BBU for interference cancellation. Specifically, three dimension reduction schemes are investigated in this work:

- *Direction-selection (DS)* scheme which selects a subset of the abundant fixed directive beams to be sent over. It is based on the fact that the multipath channel components concentrate on limited directions, and the selection should be able to capture the majority of channel energy. The DS scheme has been studied for hybrid beamforming context in [16−19] regarding "beamspace" [20].

- *Maximum ratio combining (MRC)* scheme which uses MRC to combine all directive signals for each MIMO user layer. Section 7.3.2 will show that the ZF process is mathematically equivalent to an MRC followed by

a smaller ZF operation. Conducting the two operations separately enable us to reduce the FH dimension down to the number of MIMO user layers in RRU, meanwhile achieve the same ZF cancellation performance at the BBU side. Also, the complexity of acquiring the MRC coefficients is much lower than directly calculating pseudo-inverse of a big matrix to obtain the ZF cancellation coefficients.

- *Selective MRC (sMRC)* scheme which is an extension of the MRC scheme by combining only a small subset of the directive signals for each MIMO user layer to further reduce complexity in the combining process.

The performances are studied with simulated multipath channel realizations. Given the assumption of perfect channel state information (CSI) in RRU, the results show that the DS scheme needs to select much more streams to achieve a comparable signal-to-interference-and-noise ratio (SINR) performance as the MRC scheme which only produces one stream for each MIMO user layers. The sMRC scheme has the same property as MRC in dimension reduction, while further reducing the complexity in RRU by slightly compromising the performance. The impact of the channel estimation error (CEE) in RRU is also evaluated, where the performances of all three schemes are degraded. Again, the DS scheme needs to select much more streams. It also shows that the sMRC scheme can even outperform the MRC scheme when the estimation signal-to-noise ratio (SNR) is low. The gain is from the fact that the estimated channel coefficients with large errors contribute negatively to coherent gain, and are therefore beneficial to be excluded. The investigation shows that the MRC-based approaches are good choices for massive MIMO functional split considering its high FH dimension reduction, low complexity in RRUs, and high system performances.

Throughout this paper, $\mathbb{C}$ denotes the complex number field. The bold capital letter $\mathbf{A}$ denotes a matrix and lower case $\mathbf{a}$ denotes a column vector. The element in the i-th row and j-th column of $\mathbf{A}$ is denoted as $[\mathbf{A}]_{i,j}$, and i-th element of $\mathbf{a}$ is denoted as a_i. The transpose and Hermitian transpose operators are denoted by $(\cdot)^{\mathrm{T}}$ and $(\cdot)^{\mathrm{H}}$, respectively. For matrix $\mathbf{A}$ that has linearly independent columns $\mathbf{A}^{\dagger} = (\mathbf{A}^{\mathrm{H}}\mathbf{A})^{-1}\mathbf{A}^{\mathrm{H}}$ denotes the pseudo-inverse. A $k \times k$ identity matrix is denoted by $\mathbf{I}_k$.

7.2 System Model

To study the possibilities of the functional split for massive MIMO processing, we model the uplink transmission as illustrated in Fig. 7.2. Let $\mathbf{x} \in \mathbb{C}^{K \times 1}$ denote the uplink transmit signal for K user layers. Signals are received at an
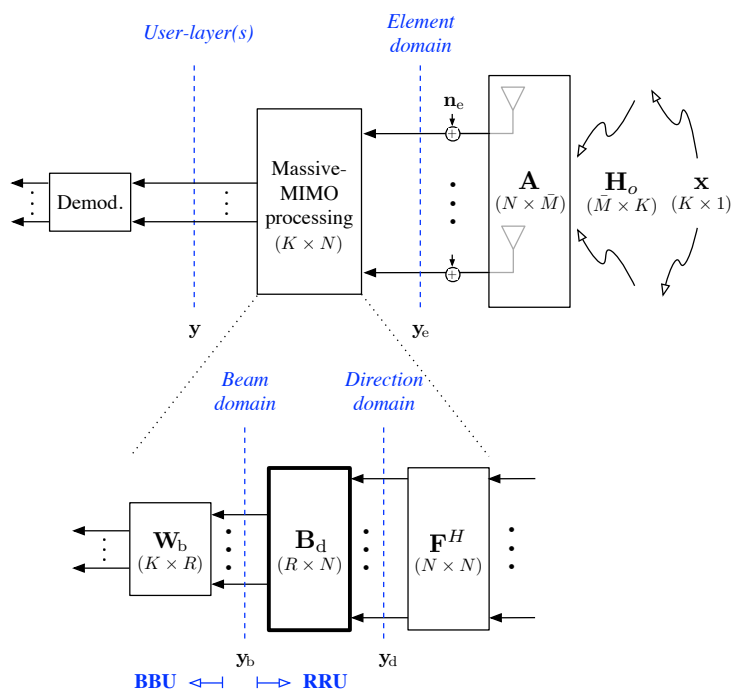
Fig. 7.2: Uplink system diagram and an illustration of functional split for massive MIMO processing.

RRU supporting an array of N antennas. Outputs of the N antennas compose an N-dimensional *element domain* signal $\mathbf{y}_e$. Massive MIMO processing, which is performed either in RRU or in BBU in the existing solutions, transforms $\mathbf{y}_e$ into a K-dimensional signal $\mathbf{y}$ with separated user layers for further processing.

In this paper, we focus on linear transformation like ZF such that the whole MIMO processing can be modeled as one matrix $\mathbf{W}$. The split is formularized by decomposing $\mathbf{W}$ into three components as $\mathbf{W} = \mathbf{W}_b \mathbf{B}_d \mathbf{F}^H$. The first component, modeled as $\mathbf{F}^H$ (*e.g.,* a discrete Fourier transform (DFT)-based matrix forming directive beams), transforms $\mathbf{y}_e$ into *direction domain* to explore the spatial properties of the channel, *e.g.,* for performing direction-domain channel estimation. The dimension reduction block, modeled as $\mathbf{B}_d$, follows to reduce signal dimension from N to R in RRU before sending to FH. This component is our main focus and will be detailed with three options in the next section. The equalization modeled by $\mathbf{W}_b$ is then carried out in BBU for layer separation.

More details regarding the quantities in Fig. 7.2 are given as follows.

7.2.1 Channel Model and Element Domain

The element domain signal $\mathbf{y}_e \in \mathbb{C}^{N \times 1}$ as an output of the antenna array is formulated as

$$\mathbf{y}_e = \mathbf{H}_e \mathbf{x} + \mathbf{n}_e,$$

where $\mathbf{n}_e \in \mathbb{C}^{N \times 1}$ denotes the additive white Gaussian noise (AWGN) in element domain, and $\mathbf{H}_e \in \mathbb{C}^{N \times K}$ denotes the MIMO channel in element domain modeled as

$$\mathbf{H}_e = \mathbf{A}(\bar{\boldsymbol{\theta}}^{\mathrm{T}})\mathbf{H}_o,$$

which is referred to as the correlation channel model featuring the receive antenna correlation in a multi-path environment. Specifically, let M_k denotes the number of multi-paths from user layer k (*i.e.,* regarding x_k). The total number of multi-paths involved in the system is $\bar{M} = \sum_{k=1}^{K} M_k$. The matrix representation of the propagation channel couplings $\mathbf{H}_o \in \mathbb{C}^{\bar{M} \times K}$ is then composed as

$$\mathbf{H}_o = \begin{bmatrix} \mathbf{h}_1 & \cdots & \mathbf{0} \\ \vdots & \ddots & \vdots \\ \mathbf{0} & \cdots & \mathbf{h}_K \end{bmatrix}, \tag{7.1}$$

where $\mathbf{h}_k \in \mathbb{C}^{M_k \times 1}$ denotes a vector of fading coefficients associated with user layer k. Also, let $\boldsymbol{\theta}_k^{\mathrm{T}} \in \mathbb{C}^{1 \times M_k}$ denote angle of arrivals (AoAs) corresponding to the M_k channel paths denoted in $\mathbf{h}_k$. The matrix $\mathbf{A}(\bar{\boldsymbol{\theta}}^{\mathrm{T}}) \in \mathbb{C}^{N \times \bar{M}}$ regarding $\bar{\boldsymbol{\theta}}^{\mathrm{T}} = [\boldsymbol{\theta}_1^{\mathrm{T}}, .., \boldsymbol{\theta}_k^{\mathrm{T}}, .., \boldsymbol{\theta}_K^{\mathrm{T}}]$ models the antenna array which consists of $\bar{M}$ array response vectors, each of which corresponds to one direction of the incoming path.

Use the uniform linear array (ULA) as an example. The array response vector $\mathbf{a}(\theta_l)$ regarding the arriving angle $\theta_l \in [-90°, 90°]$ is defined as

$$\mathbf{a}(\theta_l) = \begin{bmatrix} 1 & e^{-j2\pi \sin(\theta_l)\frac{d}{\lambda} \cdot 1} & \cdots & e^{-j2\pi \sin(\theta_l)\frac{d}{\lambda}(N-1)} \end{bmatrix}^{\mathrm{T}},$$

where d is the antenna spacing and λ denotes the wavelength. The matrix representation is therefore expressed as

$$\mathbf{A}(\bar{\boldsymbol{\theta}}^{\mathrm{T}}) = \begin{bmatrix} \mathbf{a}(\theta_1) & \cdots & \mathbf{a}(\theta_{\bar{M}}) \end{bmatrix}.$$

7.2.2 Direction Domain

The element-domain channel is typically with low SNR and low correlation, which makes it hard for channel estimation and dimension reduction. An additional step could be taken in the massive MIMO processing to transform the

channel into direction domain for better harnessing the spatial correlation. In direction domain, the channel is presented in a group of fixed directions.

Regarding ULA, we implement spatial DFT to tune on N fixed azimuth directions, which are mutually orthogonal [21]. Specifically, the DFT matrix $\mathbf{F}$ has its entry defined as $[\mathbf{F}]_{i,j} = \frac{1}{\sqrt{N}} e^{-\mathrm{j}2\pi k_j n_i / N}$, where k_j is the j-th entry of $k = [-N/2, ..., N/2-1]$ and n_i is the i-th entry of $n = [0, ..., N-1]$. The receive signal in direction domain becomes

$$\mathbf{y}_{\mathrm{d}} = \mathbf{F}^{\mathrm{H}}\mathbf{y}_{\mathrm{e}} = \mathbf{H}_{\mathrm{d}}\mathbf{x} + \mathbf{n}_{\mathrm{d}},$$

where $\mathbf{H}_{\mathrm{d}} = \mathbf{F}^{\mathrm{H}}\mathbf{H}_{\mathrm{e}}$ is the channel representation in direction domain, and $\mathbf{n}_{\mathrm{d}} = \mathbf{F}^{\mathrm{H}}\mathbf{n}_{\mathrm{e}}$. Since $\mathbf{F}$ (or equivalently $\mathbf{F}^{\mathrm{H}}$) is a unitary matrix, $\mathbf{n}_{\mathrm{d}}$ possesses the same statistical property as $\mathbf{n}_{\mathrm{e}}$. When the antennas are spaced half-wavelength apart, *i.e.,* $d/\lambda = 1/2$, the fixed orthogonal directions which the channel is focused on are $\phi_k = \arcsin(2k/N)$ for $k = [-N/2, ..., N/2-1]$.

7.2.3   Beam Domain

The direction-domain signal $\mathbf{y}_{\mathrm{d}}$ is N-dimensional while the number of user layers is K. In massive MIMO systems, it is typically that $N \gg K$. Using N FH streams to transport the data for K user layers is not efficient. In order to lighten the FH burden while maintaining simple RRU operation, we consider to reduce the signal dimension from N to R via a beamformer $\mathbf{B} \in \mathbb{C}^{R \times N}$ in the RRU such that $N > R \geq K$. This paper focuses on performing dimension reduction from direction domain, denoted as $\mathbf{B}_{\mathrm{d}}$, to explore the spatial signatures of the channel. The received signal in *beam domain* becomes

$$\mathbf{y}_{\mathrm{b}} = \mathbf{B}_{\mathrm{d}}\mathbf{y}_{\mathrm{d}} = \mathbf{H}_{\mathrm{b}}\mathbf{x} + \mathbf{n}_{\mathrm{b}}, \tag{7.2}$$

where $\mathbf{H}_{\mathrm{b}} = \mathbf{B}_{\mathrm{d}}\mathbf{H}_{\mathrm{d}}$ for $\mathbf{H}_{\mathrm{b}} \in \mathbb{C}^{R \times K}$ is the beam-domain channel, and $\mathbf{n}_{\mathrm{b}} = \mathbf{B}_{\mathrm{d}}\mathbf{n}_{\mathrm{d}}$ is the beam-domain noise.

7.2.4   Zero-Forcing Equalization

The beam domain signal $\mathbf{y}_{\mathrm{b}}$ with a reduced dimension is then sent through the FH link and received at the BBU side. There we implement ZF equalization, which is formulated as

$$\mathbf{W}_{\mathrm{b}} = (\mathbf{H}_{\mathrm{b}}^{\mathrm{H}}\mathbf{H}_{\mathrm{b}})^{-1}\mathbf{H}_{\mathrm{b}}^{\mathrm{H}},$$

to cancel the mutual interference. The received signal with separated user layers is obtained as

$$\mathbf{y} = \mathbf{x} + \mathbf{W}_{\mathrm{b}}\mathbf{n}_{\mathrm{b}}$$

Given that the transmit signal fulfills $\mathbf{x} \sim \mathcal{CN}(\mathbf{0}, \gamma^2 \mathbf{I}_K)$ and the element-domain noise fulfills $\mathbf{n}_\mathrm{e} \sim \mathcal{CN}(\mathbf{0}, \sigma^2 \mathbf{I}_N)$, it can be derived that $\mathbf{n}_\mathrm{b} \sim \mathcal{CN}(\mathbf{0}, \sigma^2 \boldsymbol{\Sigma})$ for $\boldsymbol{\Sigma} = \mathbf{B}_\mathrm{d} \mathbf{B}_\mathrm{d}^\mathrm{H}$. The post-processing SINR for the k-th user layer is thereby

$$\mathrm{SINR}_k = \frac{\mathrm{E}\big[|x_k|^2\big]}{\mathrm{E}\big[|y_k - x_k|^2\big]} = \frac{\rho^2}{\big[\mathbf{W}_\mathrm{b} \boldsymbol{\Sigma} \mathbf{W}_\mathrm{b}^\mathrm{H}\big]_{k,k}}, \tag{7.3}$$

where $\rho^2 = \gamma^2/\sigma^2$ denotes the input SNR per antenna element.

7.3 Dimension Reduction Schemes

Regarding the implementation of $\mathbf{B}_\mathrm{d}$, three dimension reduction options, referred to as DS, MRC and sMRC schemes, respectively, are presented in this section. The following analysis assumes perfect CSI in all domains.

7.3.1 Direction Selection (DS)

In DS, dimension reduction is performed by selecting a subset of the directions, which can be viewed as a sub-type of beamforming. In this case, the number of selected directions S is equal to the number of generated beams R, which is also the number of required FH streams.

Exploiting the sparse nature of $\mathbf{H}_\mathrm{d}$, the DS was initially introduced in a hybrid beamforming context to limit the processing resources and effort within a subset of the N orthogonal directions. The approaches, also termed as "beam-selection" corresponding to the term "beamspace", in [16–19] as well as the references herein provide a series of criteria to choose the directions of interest to reduce the operational RF chains in massive MIMO. The same methodology can be applied to reduce the FH streams.

Given perfect CSI of $\mathbf{H}_\mathrm{d}$, one way to determine the direction selection is, as in [16,18], to maximize the total post-processing SINR, which is formulated as

$$\mathrm{SINR}_\mathrm{total} = \sum_{k=1}^{K} \mathrm{SINR}_k = \frac{\rho^2}{\mathrm{Tr}\big[(\mathbf{H}_\mathrm{b}^\mathrm{H} \mathbf{H}_\mathrm{b})^{-1}\big]},$$

where $\mathbf{H}_\mathrm{b}$ is composed by S selected rows of $\mathbf{H}_\mathrm{d}$, and SINR_k is defined in Eq. (7.3) considering that $\boldsymbol{\Sigma}_\mathrm{DS} = \mathbf{B}_\mathrm{d,DS} \mathbf{B}_\mathrm{d,DS}^\mathrm{H} = \mathbf{I}_S$ is fulfilled irrespective of the selection results. The equivalent optimization problem becomes

$$\begin{aligned} \underset{\mathbf{B}_\mathrm{d,DS}}{\text{minimize}} \quad & \mathrm{Tr}\big[(\mathbf{H}_\mathrm{b}^\mathrm{H} \mathbf{H}_\mathrm{b})^{-1}\big] \\ \text{subject to} \quad & \mathbf{H}_\mathrm{b} = \mathbf{B}_\mathrm{d,DS} \mathbf{H}_\mathrm{d} \end{aligned} \tag{7.4}$$

where $\mathbf{B}_{\mathrm{d,DS}}$ is composed by S picked rows from matrix $\mathbf{I}_N$. The solution to Eq. (7.4) can be obtained by calculating all SINRs of the $\binom{N}{S}$ selection combinations, and use the one yielding the maximum SINR. But this exhaustive search is typically infeasible due to the tremendous number of possible $\mathbf{B}_{\mathrm{d,DS}}$. In [16], a decremental method is proposed as a suboptimal solution, which iteratively deletes one direction (or one row of $\mathbf{H}_{\mathrm{d}}$) at a time. In each step, it calculates all pseudo-inverses of the channel matrix after temporarily removing one row of the matrix from the previous step. The selected row that gives the maximum $\mathrm{SINR}_{\mathrm{total}}$ result will be removed from $\mathbf{H}_{\mathrm{d}}$.

To provide more insights regarding the performance impact from removing matrix rows, we reformulate this problem as follows. The objective function of Eq. (7.4) can be expanded as shown in Appendix A as

$$\mathrm{Tr}\left[(\mathbf{H}_{\mathrm{b}}^{\mathrm{H}}\mathbf{H}_{\mathrm{b}})^{-1}\right] = \mathrm{Tr}\left[(\mathbf{H}_{\mathrm{d}}^{\mathrm{H}}\mathbf{H}_{\mathrm{d}})^{-1}\right] + \sum_{l=1}^{N-S}\beta_{l-1},$$

for

$$\beta_l = \frac{[(\bar{\mathbf{H}}_l^{\dagger})^{\mathrm{H}}\bar{\mathbf{H}}_l^{\dagger}]_{j_l,j_l}}{1 - [\bar{\mathbf{H}}_l\bar{\mathbf{H}}_l^{\dagger}]_{j_l,j_l}}, \tag{7.5}$$

where $\bar{\mathbf{H}}_l$ denotes the matrix after deleting l selected rows from $\mathbf{H}_{\mathrm{d}}$ (particularly $\bar{\mathbf{H}}_0 = \mathbf{H}_{\mathrm{d}}$) and j_l denotes the row index which is deleted from $\bar{\mathbf{H}}_l$ to yield $\bar{\mathbf{H}}_{l+1}$. The β_l is a measure of the impact on the final result of $\mathrm{Tr}\left[(\mathbf{H}_{\mathrm{b}}^{\mathrm{H}}\mathbf{H}_{\mathrm{b}})^{-1}\right]$ when deleting one more row from $\mathbf{H}_{\mathrm{d}}$ in the l-th iteration. In each step of this approach, the index of the row to be deleted is decided by

$$\hat{j}_l = \arg\min_{j_l \in [1,..,N-l]} \beta_l. \tag{7.6}$$

This formulation theoretically achieves the same results as the decremental method proposed in [16], but with lower complexity. It is further observed that the term $\bar{\mathbf{H}}_l\bar{\mathbf{H}}_l^{\dagger}$ in the denominator of Eq. (7.5) forms a projection matrix, of which the diagonal elements are always valued between 0 and 1. Therefore, β_l is always non-negative. It indicates that $\mathrm{Tr}[(\bar{\mathbf{H}}_{l+1}^{\mathrm{H}}\bar{\mathbf{H}}_{l+1})^{-1}] > \mathrm{Tr}[(\bar{\mathbf{H}}_l^{\mathrm{H}}\bar{\mathbf{H}}_l)^{-1}]$, as well as $\mathrm{SINR}_{\mathrm{total}}(\bar{\mathbf{H}}_{l+1}) < \mathrm{SINR}_{\mathrm{total}}(\bar{\mathbf{H}}_l)$. This means that ignoring any direction of the channel via DS always impairs the total post-processing SINR. When the targeted S is too small comparing to N, the SINR performance may be largely degraded by the selection.

7.3.2   Maximum Ratio Combining (MRC)

It is preferable to have a dimension reduction scheme that does not compromise the performance like the DS scheme. If disregarding the separated BBU and

RRU architecture for now, the ZF equalization can be implemented in direction domain as a pseudo-inverse of $\mathbf{H}_\mathrm{d}$, *i.e.,*

$$\mathbf{y} = \mathbf{W}_\mathrm{d}\mathbf{y}_\mathrm{d} = (\mathbf{H}_\mathrm{d}^\mathrm{H}\mathbf{H}_\mathrm{d})^{-1}\mathbf{H}_\mathrm{d}^\mathrm{H}\mathbf{y}_\mathrm{d}. \tag{7.7}$$

Back to the decomposed architecture in Fig. 7.2, we assign the dimension reduction beamformer to be $\mathbf{B}_{\mathrm{d,MRC}} = \mathbf{H}_\mathrm{d}^\mathrm{H}$. Since now $\mathbf{H}_\mathrm{b} = \mathbf{B}_{\mathrm{d,MRC}}\mathbf{H}_\mathrm{d} = \mathbf{H}_\mathrm{d}^\mathrm{H}\mathbf{H}_\mathrm{d}$ is a square matrix, the beam domain equalizer becomes $\mathbf{W}_\mathrm{b} = \mathbf{H}_\mathrm{b}^{-1}$. Therefore, Eq. (7.7) is equivalent to

$$\mathbf{H}_\mathrm{b}^{-1}\mathbf{B}_{\mathrm{d,MRC}}\mathbf{y}_\mathrm{d} = \mathbf{W}_\mathrm{b}\mathbf{B}_{\mathrm{d,MRC}}\mathbf{y}_\mathrm{d}.$$

In other words, the above process divides the direction-domain equalization $\mathbf{W}_\mathrm{d} = (\mathbf{H}_\mathrm{d}^\mathrm{H}\mathbf{H}_\mathrm{d})^{-1}\mathbf{H}_\mathrm{d}^\mathrm{H}$ into two steps (from right to left since $\mathbf{y}_\mathrm{d}$ is left-multiplied by $\mathbf{W}_\mathrm{d}$ in Eq. (7.7)):

- $\mathbf{B}_{\mathrm{d,MRC}} = \mathbf{H}_\mathrm{d}^\mathrm{H}$ conducts MRC regarding channel $\mathbf{H}_\mathrm{d}$;

- $\mathbf{W}_\mathrm{b} = (\mathbf{H}_\mathrm{d}^\mathrm{H}\mathbf{H}_\mathrm{d})^{-1}$ conducts ZF regarding the equivalent beam-domain channel $\mathbf{H}_\mathrm{b} = \mathbf{B}_{\mathrm{d,MRC}}\mathbf{H}_\mathrm{d} = \mathbf{H}_\mathrm{d}^\mathrm{H}\mathbf{H}_\mathrm{d}$.

Even if the two steps are placed in RRU and BBU respectively, the same performance as via direction-domain equalization is still maintained. Leaving only the MRC part in RRU reduces the computational complexity compared to implementing the whole MIMO processing in RRU. More importantly, the MRC operation carries out dimension reduction by transforming the N-dimension signal $\mathbf{y}_\mathrm{d}$ into a K-dimension signal $\mathbf{y}_\mathrm{b}$, therefore, reducing the FH load to be equal to the number of user layers.

According to Eq. (7.3), the k-th user layer SINR for the split MRC-ZF scheme can be expressed as

$$\mathrm{SINR}_k = \frac{\rho^2}{[(\mathbf{H}_\mathrm{d}^\mathrm{H}\mathbf{H}_\mathrm{d})^{-1}]_{k,k}}. \tag{7.8}$$

Although the scheme is derived from the ZF-based approach, the same split principle is applicable to other cancellation approaches, such as the MMSE-based equalization.

7.3.3   Selective Maximum Ratio Combining (sMRC)

To further reduce the amount of computations in the MRC operation for large channel matrices, one can exploit the "sparsity" of the direction-domain channel, meaning that the major channel power of $\mathbf{H}_\mathrm{d}$ only concentrates on a small

number (greatly smaller than NK) of the components. Especially when propagating at the millimeter-wave frequencies in the air, the highly reflective environment yields a sparse set of single-bound multi-path components [22]. Ignoring the insignificant components in the process of MRC helps reduce the amount of computations in RRU without obviously degrading the performance. More importantly, when CEE is considered (which will be discussed in the next section), the estimated $\tilde{\mathbf{H}}_d$ can easily have its weak components overwhelmed by the CEEs. Zeroing out the beamforming coefficients corresponding to those channel components may even help improve the performance. Here, we refer to this approach as the *sMRC* scheme.

Let $\mathcal{S}_k$ denote a set of direction indices which are selected for user layer k (*i.e.*, regarding the k-th column of $\mathbf{H}_d$). For easy implementation, we assume that the number of selected directions is the same for all user layers, *i.e.*, $S = \|\mathcal{S}_k\|_0$ for $k = 1, ..., K$. Typically, S is much smaller than N but fulfils $S \geq K$ to guarantee the matrix after combining is well-conditioned for matrix inverse. The sMRC beamformer is structured as

$$[\mathbf{B}_{d,sMRC}]_{k,n} = \begin{cases} [\mathbf{H}_d]^*_{n,k} & \text{if } n \in \mathcal{S}_k, \\ 0 & \text{otherwise,} \end{cases} \tag{7.9}$$
$$\text{for } k \in \{1, \ldots, K\}, n \in \{1, \ldots, N\},$$

where $(\cdot)^*$ denotes complex conjugate. Since $\mathbf{B}_{d,sMRC}$ is a sparse matrix, the required computation in RRU is reduced comparing to applying $\mathbf{B}_{d,MRC}$.

Although both select a subset of directions, the fundamental difference between the sMRC and DS schemes is shown in Fig. 7.3. The selection made by the sMRC scheme is user-layer specific. It allows each user layer to keep the most beneficial directions from its own perspective. Channel energy is thereby better captured compared to the DS scheme, which selects a common set of directions for all users.

7.3.4 Performance Comparison with Perfect CSI

To numerically compare the SINRs of the three dimension reduction schemes, we use the Monte Carlo method to simulate spatially correlated MIMO channels. In the simulation setup, a 64-element ULA with half-wavelength element spacing is assumed. Signal for each user layer is received in form of 1 line-of-sight (LoS) and 7 multipath components [22]. The strength of the multipath components is 5 to 10 dB lower than that of the LoS [19] and the power offset is uniformly distributed within this range. The AoAs are uniformly distributed between $-60°$ and $60°$[1], which is consistent with the 3-sector-cell scenario.

---

[1]This setting instead of $[-90°, 90°]$ also precludes performance degradation caused by bad antenna array resolution.
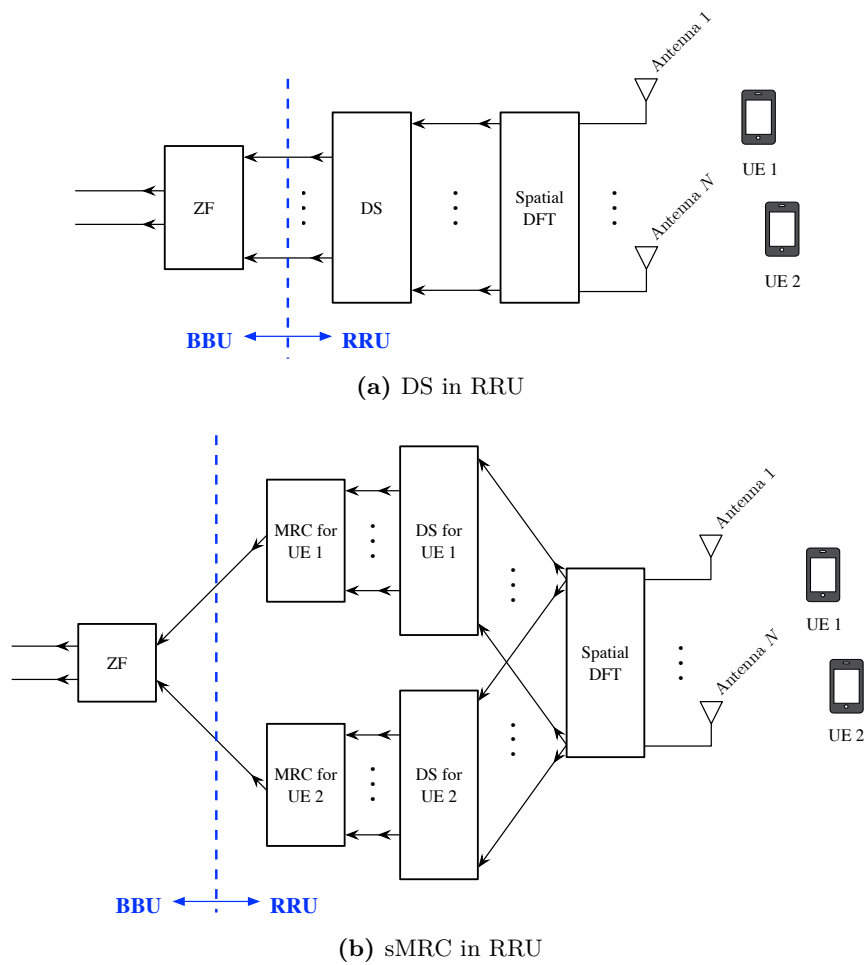
(a) DS in RRU

(b) sMRC in RRU

Fig. 7.3: Block diagrams illustrating the differences between implementing DS and sMRC in RRU regarding 2 user equipments (UEs) with a single user layer each.
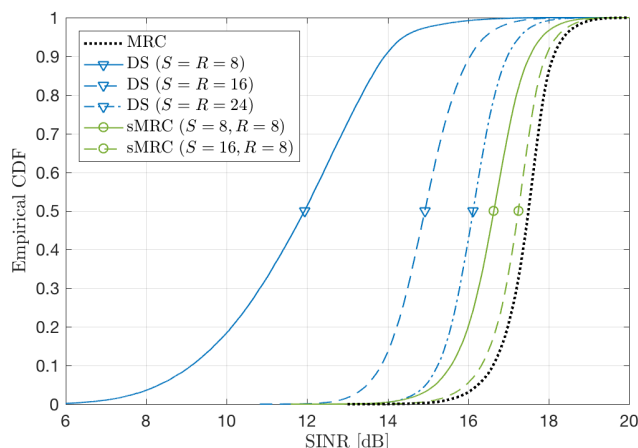
Fig. 7.4: Comparison of the per-user SINR when $N = 64$, $K = 8$, and input SNR $\rho^2 = 0\,\mathrm{dB}$, with perfect CSI. S denotes the number of selected directions and R denotes the number of generated beams/FH-streams.

The fading coefficient vector $\mathbf{h}_k$ for each user layer is normalized. To evaluate statistically, $\mathbf{H}_\mathrm{o}$ as structured in Eq. (7.1) is randomly generated as 5000 real-izations. In all simulations, the ZF-based cancellation is used to cancel out the interferences between user layers after dimension reduction. The input SNR per element is set as $\rho^2 = 0$ dB.

Given perfect CSI, the empirical cumulative distribution functions (CDFs) of the SINR per user layer as in Eq. (7.3) is presented in Fig. 7.4. Firstly, the MRC scheme achieves the best performance, which is equivalent to the full ZF performance. Secondly, the three triangle-marked curves related to the DS scheme given different S values verify that the smaller S value seriously impairs the SINR performance. Since the number of FH streams fulfils $R = S$ which is preferably to be small, either the performance or dimension reduction is compromised when applying DS. Finally, to construct $\mathbf{B}_\mathrm{d,sMRC}$ in Eq. (7.9), we select S strongest directions from the k-th column of $\mathbf{H}_\mathrm{d}$ for $\mathcal{S}_k$. It shows in Fig. 7.4 that having sMRC with $S = 8$ which generates $R = 8$ FH streams outperforms using the DS method which generates $R = 24$ FH streams. The results of the sMRC scheme can be further improved if $S = 16$ is selected, which processes with a quarter of the beamforming coefficients comparing to the MRC scheme. In this case, there is just a minor SINR loss comparing to the full MRC approach.

7.4 Impact of Channel Estimation Errors

In practice, channel estimation error (CEE) can have a significant impact on the MIMO performance. Regarding dimension reduction, the CEEs influence the construction of the dimension reduction beamformer $\mathbf{B}_\mathrm{d}$, which fully depends on the estimated direction-domain channel. This impact further propagates to the BBU side, where the more advanced processing capability can alleviate but not eliminate the performance degradation caused by the CEEs in the RRU. This section particularly investigates the influence of the channel estimation accuracy in RRU on the performance.

The CEE of $\mathbf{H}_\mathrm{d}$ can be modeled as an additive term that is uncorrelated to $\mathbf{H}_\mathrm{d}$ [23], *i.e.,*

$$\tilde{\mathbf{H}}_\mathrm{d} = \mathbf{H}_\mathrm{d} + \boldsymbol{\Delta}, \tag{7.10}$$

where $\tilde{\mathbf{H}}_\mathrm{d}$ is the estimated direction-domain channel and $\boldsymbol{\Delta}$ denotes the CEE with *i.i.d.* entries $[\boldsymbol{\Delta}]_{i,j} \sim \mathcal{CN}(0, \varepsilon^2)$. The corresponding mismatched beamformer is denoted as $\tilde{\mathbf{B}}_\mathrm{d}$.

To investigate its specific influence on the dimension reduction schemes, we studied the following three cases:

case 1: perfect CSI is available both in RRU and in BBU (as in Section 7.3.2), which is labeled with $[0, 0]$, where the first 0 indicates the CEE term in RRU and the second 0 indicates the CEE term in BBU;

case 2: the estimated $\tilde{\mathbf{H}}_\mathrm{d}$ in RRU contains CEE, and BBU uses the same estimation to conduct ZF equalization regarding $\tilde{\mathbf{H}}_\mathrm{b} = \tilde{\mathbf{B}}_\mathrm{d}\tilde{\mathbf{H}}_\mathrm{d}$, labeled with $[\varepsilon^2, \varepsilon^2]$;

case 3: the estimated $\tilde{\mathbf{H}}_\mathrm{d}$ in RRU contains CEE, whereas BBU has the perfect CSI regarding the true beam-domain channel $\mathbf{H}_\mathrm{b} = \tilde{\mathbf{B}}_\mathrm{d}\mathbf{H}_\mathrm{d}$, labeled with $[\varepsilon^2, 0]$.

While case 1 is present as a reference for the SINR upper bound, case 2 shows the impact from the channel estimation errors in RRUs and case 3 illustrates the potential of performance improvement if the BBU can further improve the channel estimation by applying more resources, such as more advanced estimation methods.

7.4.1 MRC Scheme

When CEEs are present in RRU, a mismatched MRC beamformer will be constructed as $\tilde{\mathbf{B}}_\mathrm{d,MRC} = \tilde{\mathbf{H}}_\mathrm{d}^\mathrm{H}$. Accordingly, the actual beam-domain channel becomes $\mathbf{H}_\mathrm{b} = \tilde{\mathbf{H}}_\mathrm{d}^\mathrm{H}\mathbf{H}_\mathrm{d}$.

For case 2, the received signal for individual user layer is formulated as

$$\mathbf{y} = \tilde{\mathbf{H}}_{\mathrm{b}}^{-1}\tilde{\mathbf{B}}_{\mathrm{d,MRC}}\big(\mathbf{H}_{\mathrm{d}}\mathbf{x} + \mathbf{n}_{\mathrm{d}}\big)$$
$$= \big(\tilde{\mathbf{H}}_{\mathrm{d}}^{\mathrm{H}}\tilde{\mathbf{H}}_{\mathrm{d}}\big)^{-1}\tilde{\mathbf{H}}_{\mathrm{d}}^{\mathrm{H}}\big(\mathbf{H}_{\mathrm{d}}\mathbf{x} + \mathbf{n}_{\mathrm{d}}\big)$$

which is equivalent to using $\tilde{\mathbf{H}}_{\mathrm{d}}^{\dagger} = (\tilde{\mathbf{H}}_{\mathrm{d}}^{\mathrm{H}}\tilde{\mathbf{H}}_{\mathrm{d}})^{-1}\tilde{\mathbf{H}}_{\mathrm{d}}^{\mathrm{H}}$ to conduct equalization in direction domain. The mismatched ZF equalizer leads to residual interference. Given a certain channel realization $\mathbf{H}_{\mathrm{d}}$ and the variance of estimation error ε^2, the SINR for the k-th user layer is derived in [24] as

$$\widetilde{\mathrm{SINR}}_{\mathrm{case\,2},k} \approx \frac{\rho^2}{\big(1 + \rho^2 K\varepsilon^2 + \varepsilon^2\,\mathrm{Tr}[\mathbf{\Gamma}]\big)[\mathbf{\Gamma}]_{k,k}}, \tag{7.11}$$

where $\mathbf{\Gamma} = (\mathbf{H}_{\mathrm{d}}^{\mathrm{H}}\mathbf{H}_{\mathrm{d}})^{-1}$. Eq. (7.11) is an approximation where $\tilde{\mathbf{H}}_{\mathrm{d}}^{\dagger}$ is approximated by using the linear terms of its Taylor expansion.

For case 3, the individual user layer is obtained by

$$\mathbf{y} = \mathbf{H}_{\mathrm{b}}^{-1}\tilde{\mathbf{B}}_{\mathrm{d,MRC}}\big(\mathbf{H}_{\mathrm{d}}\mathbf{x} + \mathbf{n}_{\mathrm{d}}\big)$$
$$= \mathbf{x} + (\tilde{\mathbf{H}}_{\mathrm{d}}^{\mathrm{H}}\mathbf{H}_{\mathrm{d}})^{-1}\tilde{\mathbf{H}}_{\mathrm{d}}^{\mathrm{H}}\mathbf{n}_{\mathrm{d}}, \tag{7.12}$$

where there is no mutual interference left. We show in Appendix B that the SINR for the k-th element of $\mathbf{y}$ in Eq. (7.12) can be approximated by

$$\widetilde{\mathrm{SINR}}_{\mathrm{case\,3},k} \approx \frac{\rho^2}{[\mathbf{\Gamma}]_{k,k} + \big((N - K)\varepsilon^2 + N\varepsilon^4\,\mathrm{Tr}[\mathbf{\Gamma}]\big)[\mathbf{\Gamma}^2]_{k,k}}. \tag{7.13}$$

When $\varepsilon^2 = 0$, both Eq. (7.11) and (7.13) are equal to Eq. (7.8) as the CEE-free case.

Fig. 7.5 compares the SINR CDFs of the MRC scheme regarding the three cases, respectively. To validate the theoretical approximation of the per-user-layer SINR in Eqs. (7.11) and (7.13), the results with simulated CEEs are also presented. The arrow-marked gap between cases 2 and 3 implies the potential performance improvement that can be achieved in BBU regarding existing CEE in RRU. The gap between case 1 and case 3 indicates the performance degradation due to the CEE in RRU.

Specifically, Fig. 7.5a simulates the three cases with the estimation SNR $= 1/\varepsilon^2 = 3\,\mathrm{dB}$. For case 2 (the dashed line and triangular markers), the theoretical approximation of Eq. (7.11) matches with the simulated results at the 50-th percentile SINR, while the simulated CEEs yield a wider SINR distribution than the theoretical approximation in Eq. (7.11), due to neglecting higher order terms of Taylor expansion. For case 3, the theoretical approximation
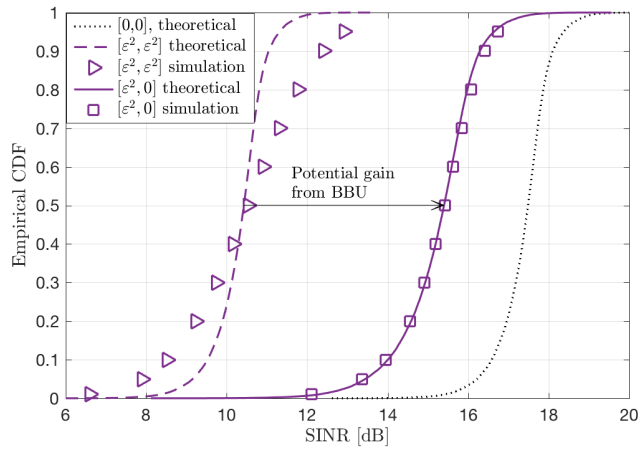
(a) CDF regarding estimation SNR $1/\varepsilon^2 = 3\,\text{dB}$
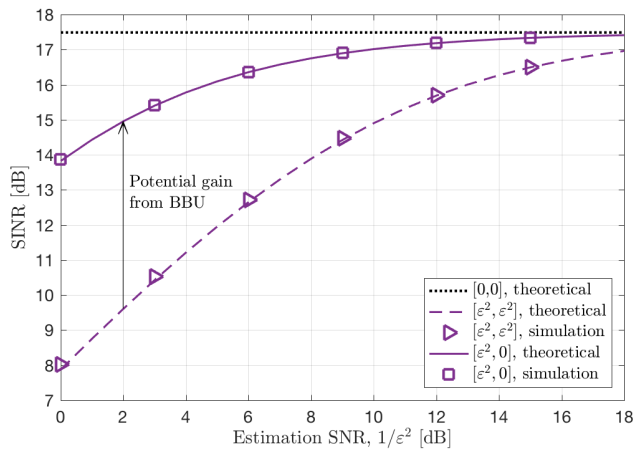
(b) 50th percentile of CDF

Fig. 7.5: Exemplification of the advantageous functional split that makes use of BBU resources to improve the SINR performance given different estimating accuracy in RRU. The CDFs are calculated considering $N = 64$, $K = 8$, and input SNR $\rho^2 = 0\,\text{dB}$.

in Eq. (7.13) matches well with the simulation results. The ε^2 value can be lowered for example when estimating with more reference signals or with more advanced techniques. To show the related trend, Fig. 7.5b compares the three cases concerning decreasing ε^2 (equivalently increasing $1/\varepsilon^2$) values. The empirical CDFs regarding each ε^2 is calculated and the SINRs corresponding to the 50-th percentile values are extracted to plot the curves in Fig. 7.5b. The gain from BBU implementing better channel estimation is specially evident when the estimation SNR in RRU is limited, *i.e.,* when ε^2 is high.
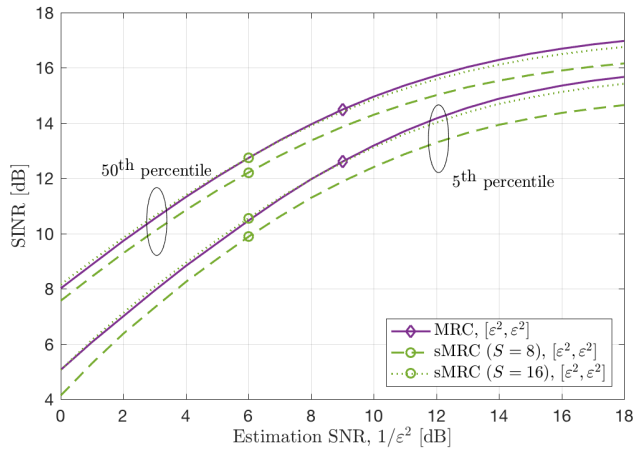
7.4.2   sMRC Scheme

One of the advantages of implementing the sMRC scheme is to exclude the channel coefficients dominated by CEEs. But if the number of selected directions S is set to be too small so that some of the informative channel components are zeroed out, it is equivalent to increasing the CEE, which in turn degrades the performance.

Fig. 7.6 compares the sMRC performance (circle-marked) to the MRC performance (diamond-marked) with different S and ε^2 values. The 50-th and 5-th percentile SINR values are plotted for each arrangement to show the median and edge results. When the estimation SNR in RRU is low (*i.e.,* ε^2 is high), selecting a small subset of directions in the sMRC approach can slightly improve the performance compared to the MRC case by excluding some weak directions. When the estimation SNR is high, the additional selection step of the sMRC scheme degrades the performance compared to the MRC scheme because the former zeros out the directions that contribute positively to the coherent channel gain. But the degradation is negligible as long as sufficient channel information is selected, *e.g.,* $S = 16$ in our case.

Since the selected directions for each user are decided based on the channel power, we also investigate the preferred power portion contained in the selection. Concerning our simulated channel, $S = 8$ corresponds to a mean value of 65% of the channel power, while $S = 16$ corresponds to a mean value of 80% of the channel power. Fig. 7.6 suggests that selecting the strongest directions summing up to 80% of channel power for each user achieves a good balance in capturing sufficient channel information and containing smaller amount of CEEs.

7.4.3   DS Scheme

For the DS scheme, CEE contained in $\tilde{\mathbf{H}}_\mathrm{d}$ may lead to an non-optimal selection of direction subset instead of the one from Eq. (7.6), which impairs the performance.

(a) Case 2: BBU uses the same erroneous channel estimation as in RRU.
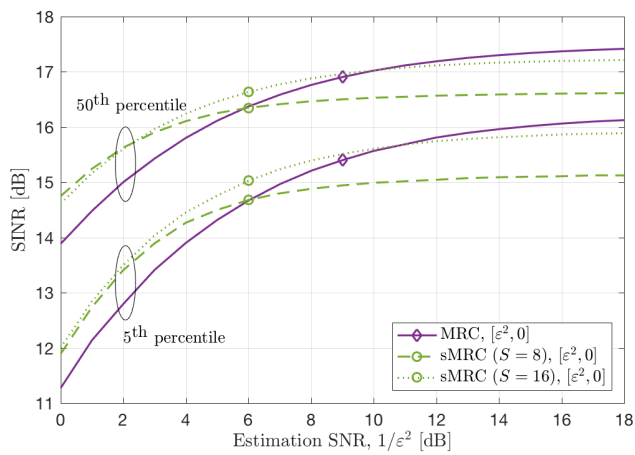
(b) Case 3: BBU knows the true beam-domain channel $\mathbf{H}_\mathrm{b}$.

Fig. 7.6: Comparison between the sMRC and MRC schemes with different estimating accuracy in RRU. Two selected percentile values are presented, considering $N = 64$, $K = 8$, and input SNR $\rho^2 = 0$ dB.

(a) Case 2: BBU uses the same erroneous channel estimation as in RRU.

(b) Case 3: BBU knows the true beam-domain channel $\mathbf{H}_\mathrm{b}$.

Fig. 7.7: Comparison between the DS and MRC schemes with different estimating accuracy in RRU. Two selected percentile values are presented, when $N = 64$, $K = 8$, and input SNR $\rho^2 = 0\,\mathrm{dB}$.

Again, regarding the DS scheme, the 50-th and 5-th percentile SINR values are plotted in Fig. 7.7 for cases 2 and 3, respectively. In case 2 (Fig. 7.7a), dimension reduction with DS yields a large performanc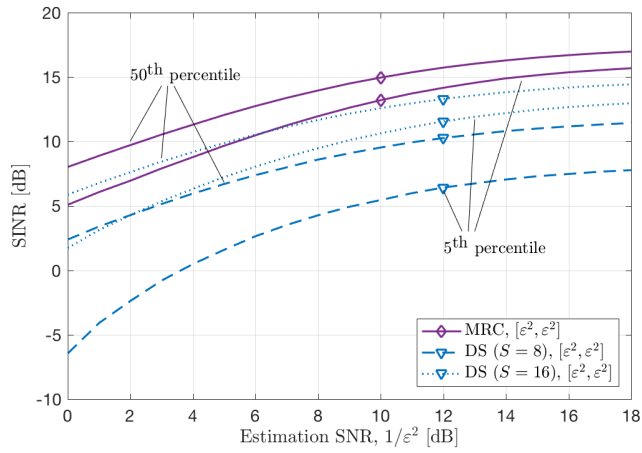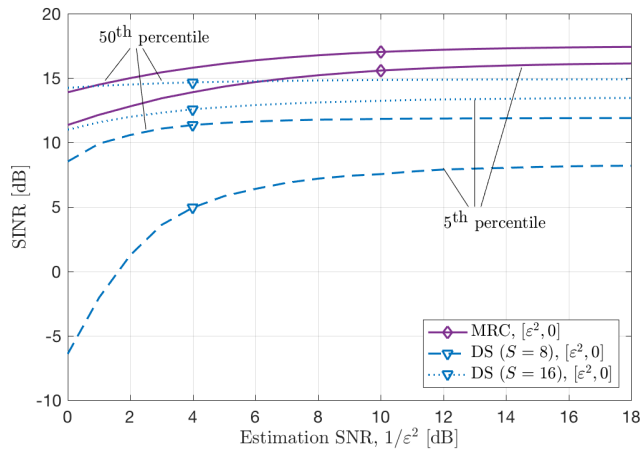e degradation compared to that with the MRC scheme, even if $S = 16$ directions are selected which doubles the amount of the FH streams compared to MRC. For case 3, a similar trend is observed except for that the performance degradation of the DS method is less than in case 2 when a larger selection number (*e.g.*, $S = 16$) is targeted. The reason is that the generated $\mathbf{H}_\text{b}$ from the DS method is composed by rows of the true channel which is known to BBU in case 3. The DS method in a decremental order will become more sensitive to the CEE in the later steps of removing rows. In other words, the fewer rows to remove, the less CEE sensitive it will be, and the more true channel coefficients can be accessed by BBU. As a comparison, the $\mathbf{H}_\text{b}$ from the MRC approach always contains the mismatched beamformer $\tilde{\mathbf{B}}_{\text{d,MRC}} = \hat{\mathbf{H}}_\text{d}^\text{H}$, which degrades the coherent channel gain. This causes that, for low estimation SNR, the MRC approach may perform slightly worse than the DS method with $S = 16$ in Fig. 7.7b.

7.5 Conclusion

To reduce the FH load for C-RAN architecture especially when massive MIMO is considered, this paper proposes to split the MIMO processing between RRU and BBU in the uplink direction. This split strategy firstly reduces signal dimension in RRU by beamforming per user layer, *e.g.*, using MRC, and then conducts interference cancellation between user layers in BBU. The evaluation is done based on ZF equalization. Compared with an existing split having all MIMO processing in RRU which achieves the same amount of dimension reduction in RRU, the new scheme benefits the system with reduced RRU complexity without degrading performances. Specifically among the three investigated dimension reduction schemes, the DS scheme is straightforward but compromises performance. The two MRC-based schemes (MRC and sMRC) achieve the best balance in the sense of reducing the FH streams to the number of MIMO user layers, while achieving high post-processing performance with modest complexity in RRU. When the channel features "sparsity" in direction domain, the sMRC approach performs close to the performance of the MRC scheme, while further reducing the RRU complexity. Especially with large channel estimation errors, sMRC can even achieve slightly better performance.

Appendix A

This section derives the relation between $\mathrm{Tr}\left[(\mathbf{H}_\mathrm{d}^\mathrm{H}\mathbf{H}_\mathrm{d})^{-1}\right]$ and $\mathrm{Tr}\left[(\mathbf{H}_\mathrm{b}^\mathrm{H}\mathbf{H}_\mathrm{b})^{-1}\right]$, where $\mathbf{H}_\mathrm{b}$ is composed by S selected rows of $\mathbf{H}_\mathrm{d}$.

For the convenience of formulation, define $\mathbf{R}\{\mathbf{A}\}$ as a matrix based on the argument $\mathbf{A}$ as $\mathbf{R}\{\mathbf{A}\} = \mathbf{A}^\mathrm{H}\mathbf{A}$. Let $\bar{\mathbf{H}}_0 = \mathbf{H}_\mathrm{d}$ denote an initialized channel matrix from which $N - S$ rows/directions will be removed. Also, let $\bar{\mathbf{H}}_l$ denote the matrix after deleting l rows from $\bar{\mathbf{H}}_0$, and $\bar{\mathbf{H}}_{l(j)}$ specifies that the j-th row of $\bar{\mathbf{H}}_{l-1}$ is eliminated to get the $\bar{\mathbf{H}}_l$. Starting with deleting the j-th row $\mathbf{h}_j^\mathrm{T}$ from $\bar{\mathbf{H}}_0$, the $\mathbf{R}\{\mathbf{H}_{1(j)}\}$ becomes a rank-1 down-date of $\mathbf{R}\{\bar{\mathbf{H}}_0\}$ due to

$$\mathbf{R}\{\mathbf{H}_{1(j)}\} = \mathbf{R}\{\bar{\mathbf{H}}_0\} - \mathbf{h}_j^*\mathbf{h}_j^\mathrm{T},$$

where $*$ denotes complex conjugate. Based on the Sherman-Morrison formula, the trace of its inverse becomes

$$\mathrm{Tr}[\mathbf{R}^{-1}\{\bar{\mathbf{H}}_{1(j)}\}] = \mathrm{Tr}[\mathbf{R}^{-1}\{\bar{\mathbf{H}}_0\}] + \frac{\mathbf{h}_j^\mathrm{T}(\mathbf{R}^{-1}\{\bar{\mathbf{H}}_0\})^2\mathbf{h}_j^*}{1 - \mathbf{h}_j^\mathrm{T}\mathbf{R}^{-1}\{\bar{\mathbf{H}}_0\}\mathbf{h}_j^*}$$

$$= \mathrm{Tr}[\mathbf{R}^{-1}\{\bar{\mathbf{H}}_0\}] + \frac{[\mathbf{R}\{\bar{\mathbf{H}}_0^\dagger\}]_{j,j}}{1 - [\bar{\mathbf{H}}_0\bar{\mathbf{H}}_0^\dagger]_{j,j}}.$$

When $N - S$ rows are deleted from $\bar{\mathbf{H}}_0$ one by one, the objective function in Eq. (7.4) can be expanded accordingly as

$$\mathrm{Tr}[\mathbf{R}^{-1}\{\mathbf{H}_\mathrm{b}\}] = \mathrm{Tr}[\mathbf{R}^{-1}\{\bar{\mathbf{H}}_{N-S}\}]$$

$$= \mathrm{Tr}[\mathbf{R}^{-1}\{\bar{\mathbf{H}}_0\}] + \sum_{l=1}^{N-S} \beta_{l-1},$$

for

$$\beta_l = \frac{[\mathbf{R}\{\bar{\mathbf{H}}_l^\dagger\}]_{j_l,j_l}}{1 - [\bar{\mathbf{H}}_l\bar{\mathbf{H}}_l^\dagger]_{j_l,j_l}},$$

where j_l denotes the row index which is deleted from $\bar{\mathbf{H}}_l$ to yield $\bar{\mathbf{H}}_{l+1}$. The pseudo-inverse $\bar{\mathbf{H}}_{l+1}^\dagger$ can be updated from $\bar{\mathbf{H}}_l$ using the rank-1 down-date to avoid calculating matrix inverse for every l.

Appendix B

Here we derive the post-processing SINR for the split MRC-ZF structure when the CEE in RRU is denoted as $\boldsymbol{\Delta}$ whose entries are *i.i.d.* zero-mean Gaussian

with a power of ε^2 and the CSI in BBU is perfect. Accordingly, the receive signal is interference-free with an equivalent additive noise as

$$\mathbf{n}_{\mathrm{b}} = (\tilde{\mathbf{H}}_{\mathrm{d}}^{\mathrm{H}}\mathbf{H}_{\mathrm{d}})^{-1}\tilde{\mathbf{H}}_{\mathrm{d}}^{\mathrm{H}}\mathbf{n}_{\mathrm{d}}.$$

Use the linear term of Taylor expansion to approximate the above matrix inverse term as

$$
\begin{aligned}
(\tilde{\mathbf{H}}_{\mathrm{d}}^{\mathrm{H}}\mathbf{H}_{\mathrm{d}})^{-1} &= (\mathbf{H}_{\mathrm{d}}^{\mathrm{H}}\mathbf{H}_{\mathrm{d}} + \boldsymbol{\Delta}^{\mathrm{H}}\mathbf{H}_{\mathrm{d}})^{-1} \\
&\approx (\mathbf{H}_{\mathrm{d}}^{\mathrm{H}}\mathbf{H}_{\mathrm{d}})^{-1}\big(\mathbf{I}_K - \boldsymbol{\Delta}^{\mathrm{H}}\mathbf{H}_{\mathrm{d}}(\mathbf{H}_{\mathrm{d}}^{\mathrm{H}}\mathbf{H}_{\mathrm{d}})^{-1}\big).
\end{aligned}
$$

For brevity, let $\boldsymbol{\Gamma} = (\mathbf{H}_{\mathrm{d}}^{\mathrm{H}}\mathbf{H}_{\mathrm{d}})^{-1}$. The covariance of the equivalent noise becomes

$$
\begin{aligned}
\mathrm{E}\big[\mathbf{n}_{\mathrm{b}}\mathbf{n}_{\mathrm{b}}^{\mathrm{H}}\big] &= \mathrm{E}\big[(\tilde{\mathbf{H}}_{\mathrm{d}}^{\mathrm{H}}\mathbf{H}_{\mathrm{d}})^{-1}\tilde{\mathbf{H}}_{\mathrm{d}}^{\mathrm{H}}\mathbf{n}_{\mathrm{d}}\mathbf{n}_{\mathrm{d}}^{\mathrm{H}}\tilde{\mathbf{H}}_{\mathrm{d}}(\tilde{\mathbf{H}}_{\mathrm{d}}^{\mathrm{H}}\mathbf{H}_{\mathrm{d}})^{-1}\big] \\
&= \sigma^2\mathrm{E}\Big[\boldsymbol{\Gamma}\big(\mathbf{H}_{\mathrm{d}}^{\mathrm{H}} + \boldsymbol{\Delta}^{\mathrm{H}} - \boldsymbol{\Delta}^{\mathrm{H}}\mathbf{H}_{\mathrm{d}}\boldsymbol{\Gamma}\mathbf{H}_{\mathrm{d}}^{\mathrm{H}} - \boldsymbol{\Delta}^{\mathrm{H}}\mathbf{H}_{\mathrm{d}}\boldsymbol{\Gamma}\boldsymbol{\Delta}^{\mathrm{H}}\big) \\
&\qquad \big(\mathbf{H}_{\mathrm{d}} + \boldsymbol{\Delta} - \mathbf{H}_{\mathrm{d}}\boldsymbol{\Gamma}\mathbf{H}_{\mathrm{d}}^{\mathrm{H}}\boldsymbol{\Delta} - \boldsymbol{\Delta}\boldsymbol{\Gamma}\mathbf{H}_{\mathrm{d}}^{\mathrm{H}}\boldsymbol{\Delta}\big)\boldsymbol{\Gamma}\Big] \\
&= \sigma^2\boldsymbol{\Gamma}\Big(\boldsymbol{\Gamma}^{-1} - \mathbf{H}_{\mathrm{d}}^{\mathrm{H}}\mathrm{E}\big[\boldsymbol{\Delta}\boldsymbol{\Gamma}\mathbf{H}_{\mathrm{d}}^{\mathrm{H}}\boldsymbol{\Delta}\big] + \mathrm{E}\big[\boldsymbol{\Delta}^{\mathrm{H}}\boldsymbol{\Delta}\big] - \mathrm{E}\big[\boldsymbol{\Delta}^{\mathrm{H}}\mathbf{H}_{\mathrm{d}}\boldsymbol{\Gamma}\mathbf{H}_{\mathrm{d}}^{\mathrm{H}}\boldsymbol{\Delta}\big] \\
&\quad - \mathrm{E}\big[\boldsymbol{\Delta}^{\mathrm{H}}\boldsymbol{\Delta}\boldsymbol{\Gamma}\mathbf{H}_{\mathrm{d}}^{\mathrm{H}}\boldsymbol{\Delta}\big] - \mathrm{E}\big[\boldsymbol{\Delta}^{\mathrm{H}}\mathbf{H}_{\mathrm{d}}\boldsymbol{\Gamma}\mathbf{H}_{\mathrm{d}}^{\mathrm{H}}\boldsymbol{\Delta}\big] + \mathrm{E}\big[\boldsymbol{\Delta}^{\mathrm{H}}\mathbf{H}_{\mathrm{d}}\boldsymbol{\Gamma}\mathbf{H}_{\mathrm{d}}^{\mathrm{H}}\boldsymbol{\Delta}\big] \\
&\quad + \mathrm{E}\big[\boldsymbol{\Delta}^{\mathrm{H}}\mathbf{H}_{\mathrm{d}}\boldsymbol{\Gamma}\mathbf{H}_{\mathrm{d}}^{\mathrm{H}}\boldsymbol{\Delta}\boldsymbol{\Gamma}\mathbf{H}_{\mathrm{d}}^{\mathrm{H}}\boldsymbol{\Delta}\big] - \mathrm{E}\big[\boldsymbol{\Delta}^{\mathrm{H}}\mathbf{H}_{\mathrm{d}}\boldsymbol{\Gamma}\boldsymbol{\Delta}^{\mathrm{H}}\big] - \mathrm{E}\big[\boldsymbol{\Delta}^{\mathrm{H}}\mathbf{H}_{\mathrm{d}}\boldsymbol{\Gamma}\boldsymbol{\Delta}^{\mathrm{H}}\boldsymbol{\Delta}\big] \\
&\quad + \mathrm{E}\big[\boldsymbol{\Delta}^{\mathrm{H}}\mathbf{H}_{\mathrm{d}}\boldsymbol{\Gamma}\boldsymbol{\Delta}^{\mathrm{H}}\mathbf{H}_{\mathrm{d}}\boldsymbol{\Gamma}\mathbf{H}_{\mathrm{d}}^{\mathrm{H}}\boldsymbol{\Delta}\big] + \mathrm{E}\big[\boldsymbol{\Delta}^{\mathrm{H}}\mathbf{H}_{\mathrm{d}}\boldsymbol{\Gamma}\boldsymbol{\Delta}^{\mathrm{H}}\boldsymbol{\Delta}\boldsymbol{\Gamma}\mathbf{H}_{\mathrm{d}}^{\mathrm{H}}\boldsymbol{\Delta}\big]\Big)\boldsymbol{\Gamma} \\
&= \sigma^2\boldsymbol{\Gamma}\big(\boldsymbol{\Gamma}^{-1} - \mathbf{0} + N\varepsilon^2\mathbf{I}_K - K\varepsilon^2\mathbf{I}_K - \mathbf{0} - K\varepsilon^2\mathbf{I}_K + K\varepsilon^2\mathbf{I}_K + \mathbf{0} - \mathbf{0} \\
&\quad - \mathbf{0} + \mathbf{0} + N(\varepsilon^2)^2\,\mathrm{Tr}[\boldsymbol{\Gamma}]\mathbf{I}_K\big)\boldsymbol{\Gamma} \\
&= \sigma^2\big(\boldsymbol{\Gamma} + (N - K)\varepsilon^2\boldsymbol{\Gamma}^2 + N\varepsilon^4\,\mathrm{Tr}[\boldsymbol{\Gamma}]\boldsymbol{\Gamma}^2\big)
\end{aligned}
$$

Accordingly, the the k-th SINR can be written as

$$
\begin{aligned}
\widetilde{\mathrm{SINR}}_{\mathrm{MRC\text{-}ZF},k} &= \frac{\mathrm{E}\big[\mathbf{x}\mathbf{x}^{\mathrm{H}}\big]_{k,k}}{\mathrm{E}\big[\mathbf{n}_{\mathrm{b}}\mathbf{n}_{\mathrm{b}}^{\mathrm{H}}\big]_{k,k}} \\
&= \frac{\rho^2}{[\boldsymbol{\Gamma}]_{k,k} + \big((N - K)\varepsilon^2 + N\varepsilon^4\,\mathrm{Tr}[\boldsymbol{\Gamma}]\big)[\boldsymbol{\Gamma}^2]_{k,k}}.
\end{aligned}
$$

References

[1] V. Jungnickel, K. Manolakis, W. Zirwas, B. Panzner, V. Braun, M. Lossow, M. Sternad, R. Apelfrojd and T. Svensson, "The Role of Small Cells, Coordinated Multipoint, and Massive MIMO in 5G," in *IEEE Communications Magazine*, vol. 52, no. 5, pp. 44-51, May 2014.

[2] "Common Public Radio Interface (CPRI); Interface Specification V7.0," October 2015. [Online]. Available: http://www.cpri.info/downloads/CPRI_v_7_0_2015-10-09.pdf

[3] 3GPP, "Technical Specification Group Radio Access Network: Study on New Radio Access Technology: Radio Access Architecture and Interfaces (Release 14)," 3rd Generation Partnership Project (3GPP), TR 38.801, March 2017.

[4] E. G. Larsson, O. Edfors, F. Tufvesson and T. L. Marzetta, "Massive MIMO for Next Generation Wireless Systems," in *IEEE Communications Magazine*, vol. 52, no. 2, pp. 186-195, February 2014.

[5] D. Gesbert, M. Kountouris, R. W. Heath Jr., C.-B. Chae and T. Sälzer, "Shifting the MIMO Paradigm," in *IEEE Signal Processing Magazine*, vol. 24, no. 5, pp. 36-46, September 2007.

[6] T. Pfeiffer, "Next Generation Mobile Fronthaul and Midhaul Architectures [Invited]," in *IEEE/OSA Journal of Optical Communications and Networking*, vol. 7, no. 11, pp. B38-B45, November 2015.

[7] D. Samardzija, J. Pastalan, M. MacDonald, S. Walker and R. Valenzuela, "Compressed Transport of Baseband Signals in Radio Access Networks," in *IEEE Transactions on Wireless Communications*, vol. 11, no. 9, pp. 3216-3225, September 2012.

[8] M. Peng, C. Wang, V. Lau and H. V. Poor, "Fronthaul-Constrained Cloud Radio Access Networks: Insights and Challenges," in *IEEE Wireless Communications*, vol. 22, no. 2, pp. 152-160, April 2015.

[9] L. Ramalho, M. N. Fonseca, A. Klautau, C. Lu, M. Berg, E. Trojer and S. Höst, "An LPC-Based Fronthaul Compression Scheme," in *IEEE Communications Letters*, vol. 21, no. 2, pp. 318-321, February 2017.

[10] H. Niu, C. Li, A. Papathanassiou and G. Wu, "RAN Architecture Options and Performance for 5G Network Evolution," in *Proc. 2014 IEEE Wireless Communications and Networking Conference Workshops (WCNCW)*, Istanbul, 2014, pp. 294-298.

[11] J. Bartelt, P. Rost, D. Wubben, J. Lessmann, B. Melis and G. Fettweis, "Fronthaul and Backhaul Requirements of Flexibly Centralized Radio Access Networks," in *IEEE Wireless Communications*, vol. 22, no. 5, pp. 105-111, October 2015.

[12] G. Mountaser, M. L. Rosas, T. Mahmoodi and M. Dohler, "On the Feasibility of MAC and PHY Split in Cloud RAN," in *Proc. 2017 IEEE Wireless Communications and Networking Conference (WCNC)*, San Francisco, CA, 2017, pp. 1-6.

[13] S. Pawar, H. Niu and A. Papathanassiou, "Front-haul Compression Using Scheduling Side Information for Cloud Radio Access Networks," in *Proc. 2015 IEEE Global Communications Conference (GLOBECOM)*, San Diego, CA, 2015, pp. 1-6.

[14] N. Shibata, K. Miyamoto, S. Kuwano, J. Terada and A. Otaka, "System Level Performance of Uplink Transmission in Split-PHY Processing Architecture with Joint Reception for Future Radio Access," in *Proc. 2015 IEEE 26th Annual International Symposium on Personal, Indoor, and Mobile Radio Communications (PIMRC)*, Hong Kong, 2015, pp. 1375-1379.

[15] K. Miyamoto, S. Kuwano, J. Terada and A. Otaka, "Split-PHY Processing Architecture to Realize Base Station Coordination and Transmission Bandwidth Reduction in Mobile Fronthaul," in *Proc. 2015 Optical Fiber Communications Conference and Exhibition (OFC)*, Los Angeles, CA, 2015, pp. 1-3.

[16] P. V. Amadori and C. Masouros, "Low RF-Complexity Millimeter-Wave Beamspace-MIMO Systems by Beam Selection," in *IEEE Transactions on Communications*, vol. 63, no. 6, pp. 2212-2223, June 2015.

[17] A. Sayeed and J. Brady, "Beamspace MIMO for High-Dimensional Multiuser Communication at Millimeter-Wave Frequencies," in *Proc. 2013 IEEE Global Communications Conference (GLOBECOM)*, Atlanta, GA, 2013, pp. 3679-3684.

[18] X. Gao, L. Dai, Z. Chen, Z. Wang and Z. Zhang, "Near-Optimal Beam Selection for Beamspace MmWave Massive MIMO Systems," in *IEEE Communications Letters*, vol. 20, no. 5, pp. 1054-1057, May 2016.

[19] J. Hogan and A. Sayeed, "Beam Selection for Performance-Complexity Optimization in High-Dimensional MIMO Systems," in *Proc. 2016 Annual Conference on Information Science and Systems (CISS)*, Princeton, NJ, 2016, pp. 337-342.

[20] J. Brady, N. Behdad and A. M. Sayeed, "Beamspace MIMO for Millimeter-Wave Communications: System Architecture, Modeling, Analysis, and Measurements," in *IEEE Transactions on Antennas and Propagation*, vol. 61, no. 7, pp. 3814-3827, July 2013.

[21] A. F. Molisch, X. Zhang, S. Y. Kung and J. Zhang, "DFT-based Hybrid Antenna Selection Schemes for Spatially Correlated MIMO Channels," in *Proc. 2003 IEEE 14th Annual International Symposium on Personal, Indoor and Mobile Radio Communications (PIMRC),* 2003, vol. 2, pp. 1119-1123.

[22] T. S. Rappaport, S. Sun, R. Mayzus, H. Zhao, Y. Azar, K. Wang, G. N. Wong, J. K. Schulz, M. Samimi and F. Gutierrez, "Millimeter Wave Mobile Communications for 5G Cellular: It Will Work!," in *IEEE Access*, vol. 1, pp. 335-349, 2013.

[23] B. Hassibi and B. M. Hochwald, "How Much Training is Needed in Multiple-Antenna Wireless Links?," in *IEEE Transactions on Information Theory*, vol. 49, no. 4, pp. 951-963, April 2003.

[24] C. Wang, E. K. S. Au, R. D. Murch, W. H. Mow, R. S. Cheng and V. Lau, "On the Performance of the MIMO Zero-Forcing Receiver in the Presence of Channel Estimation Error," in *IEEE Transactions on Wireless Communications*, vol. 6, no. 3, pp. 805-810, March 2007.